The University of Hull

Interaction of oils with Surfactants

being a thesis submitted for the Degree of Doctor
of Philosophy in the University of Hull

by

Jamie Robert MacNab B. Sc. (Hons)

November 1996

Acknowledgements

I would like to thank my three supervisors, Dr Bernie Binks, Professor Paul Fletcher and Professor Robert Aveyard, for their guidance, support and advice during my PhD. Also many thanks to Dr John Clint of the Surfactant Science Group at the University of Hull for contributing his valued advice.

I am grateful to Unilever Research, Port Sunlight Laboratories, for funding the project, and many thanks also to Drs Abid Khan-Lodhi and Tim Finch for participating in several fruitful discussions during the project.

I also appreciate the help given by Chris Maddison and Marie Betney at Unilever Research for their advice and guidance during my time at Port Sunlight and also thanks to the technical staff of Hull University Chemistry Department.

Finally, many thanks to the other members of the Surfactant Science Research Group for making my time in the group so enjoyable.

Abstract

This thesis is concerned with the interactions of oils with surfactants. The understanding of these interactions is important for a number of practical applications which include perfume delivery in fabric softeners. Both non-ionic surfactants, of the general formula $H(CH_2)_n(OCH_2CH_2)_m$-OH, and ionic surfactants, of the general formula $C_nH_{2n+1}N^+(CH_3)_3Br^-$ were used in the study. Oils of varying polarity were investigated from non-polar alkane oils to moderately polar perfume oils.

Initially, the work of adhesions of the perfume oils with water were studied to establish where these oils 'fitted-in' to a range of oils of varying polarity. It was found that the three perfume oils studied (linalool, cineole and eugenol) all exhibited adhesion properties which were fairly typical of moderately polar oils. In order to obtain the enthalpies and entropies of adhesion of the perfume oils with water the surface tensions and interfacial tensions with water were measured as a function of temperature. The enthalpy of adhesion for linalool with water is consistent with values obtained for the enthalpy of hydration of the hydroxyl group.

The co-surfactant nature of the perfume oils was investigated by tension measurements of their adsorption to the heptane-water interface. Linalool and eugenol show reasonably high surface activity at this interface and could therefore be expected to act as co-surfactants in systems that contain conventional surfactants.

The phase behaviour of the C_8E_5 + water + octane microemulsion system was investigated to determine the effect of adding different concentrations of perfume oil on the size, shape and position of the three phase region. It was found that linalool reduces the size of this

three phase region and also reduces the temperature at which the three phase region occurs. Although not conclusive, this behaviour suggests the system is approaching a tri-critical point.

It is of interest also to understand the adsorption of oils at planar surfactant monolayers and then attempt to relate the adsorption data to bulk phase solubilisation of the oils in micelles. The adsorption at a planar interface was attained by measuring the surface pressure of the oil at different activities. The surface concentration of the oils was then calculated from the Gibbs adsorption equation. By measuring these surface pressures as a function of activities at various temperatures, it was possible to derive the adsorption enthalpies and entropies with use of a form of the Van't Hoff equation. It was found that alkane adsorption increases with decreasing alkane chain length and the isotherms show a greater curvature upwards for the shorter chain length alkanes suggesting that the adsorption becomes more favourable as more alkane is added to the mixed alkane/surfactant film.

Headspace analysis was employed to measure the solubilisation of oils in bulk surfactant solutions. The results obtained with this technique were preliminary although early indications suggest that more alkane oil is solubilised in bulk aggregates with curved monolayers than is adsorbed at planar monolayer interfaces. However, solubilisation of oil in bulk solutions may either be in the curved monolayer or they could form a 'core' of oil inside the aggregate.

INTERACTION OF OILS WITH SURFACTANTS

Contents

Chapter 1

CHAPTER 1

INTRODUCTION

1.1 Introduction and industrial relevance

This thesis is concerned with the interaction of oils of varying polarity with surfactants. This is of fundamental importance in attempting to gain a detailed understanding of adsorption, aggregation and phase behaviour in ternary mixtures of surfactant with oil and water. Systems involving oil, water and surfactant find widespread use in products ranging from floor cleaners to pesticides[1] and yet there currently exists little rational basis for the prediction of the components of an optimum formulation. Part of the reason for this arises from a lack of detailed knowledge, at a molecular level, of the microstructure of surfactant interfaces and the energy of interaction between the different components present at the interface.

The work described in this thesis, which was sponsored by Unilever, Port Sunlight, was initiated by their commercial interest in products such as fabric softeners which contain, *inter alia*, surfactant(s) and a blend of perfume oils. For many such products,

the fragrance and persistence of the perfume oils present are often the major determinant of consumer appeal. It is worth mentioning that, although the majority of current understanding of surfactant + oil + water systems is based on studies of apolar hydrocarbon oils, most oils of commercial interest, including perfume oils, dyes drugs, pesticides, etc., contain polar groups. Although a number of the experiments and methodologies described in this thesis have been restricted to structurally simple hydrocarbon oils, there is a longer term interest in extending this type of study to include more complex oils.

In this first chapter, a brief review of some relevant aspects of liquid surface chemistry and surfactant behaviour is presented together with a discussion of previous work related to the present study.

1.2 Interactions of oils with water

Surfactant adsorption at an oil-water interface can be expected to be dependent on the nature of the oil although little systematic information on this is available in the literature. Before looking at systems with surfactants present, we first discuss the interactions that occur when oils of different polarity are brought into contact with water and other polar phases.

Non-polar oils and water are virtually immiscible. The reason for this is the highly negative hydration entropy of oils, giving a positive contribution to the standard free energy of transfer of oil into water, and making the mixing unfavourable. In contrast, the standard free energy associated with adsorption of oils from vapour to the water interface becomes more negative and favourable as the number of CH_2 groups in the oil increases.[2] This suggests that, despite the insolubility of non-polar oils in water, London dispersion forces of attraction do occur across an interface between CH_2 groups and water molecules. It is of interest therefore, not only to study the interactions of non-polar alkane oils with water but also to use polar oils for which polar interactions may occur in conjunction with dispersion forces. Studies of the interactions of oils with water are presented in Chapter 3.

1.3 Relevant surfactant behaviour

1.3.1 General surfactant structure

The word surfactant is a diminutive form of the phrase SURFace ACTive ageNT. Not only does this show the origin of the word itself, it also sheds some light on the properties of surfactants i.e. they tend to accumulate at surfaces. Surfactants are amphiphilic molecules, which means they consist of two distinct and diverse regions. The molecule can be divided into polar and non-polar parts. Figure 1.1 shows a

schematic representation of a straight chain, single tailed surfactant. The non-polar region, which is hydrophobic, is typically a straight or branched hydrocarbon or fluorocarbon chain. The headgroup is polar and hydrophilic in nature and can be anionic, cationic, non-ionic or zwitterionic.[3]

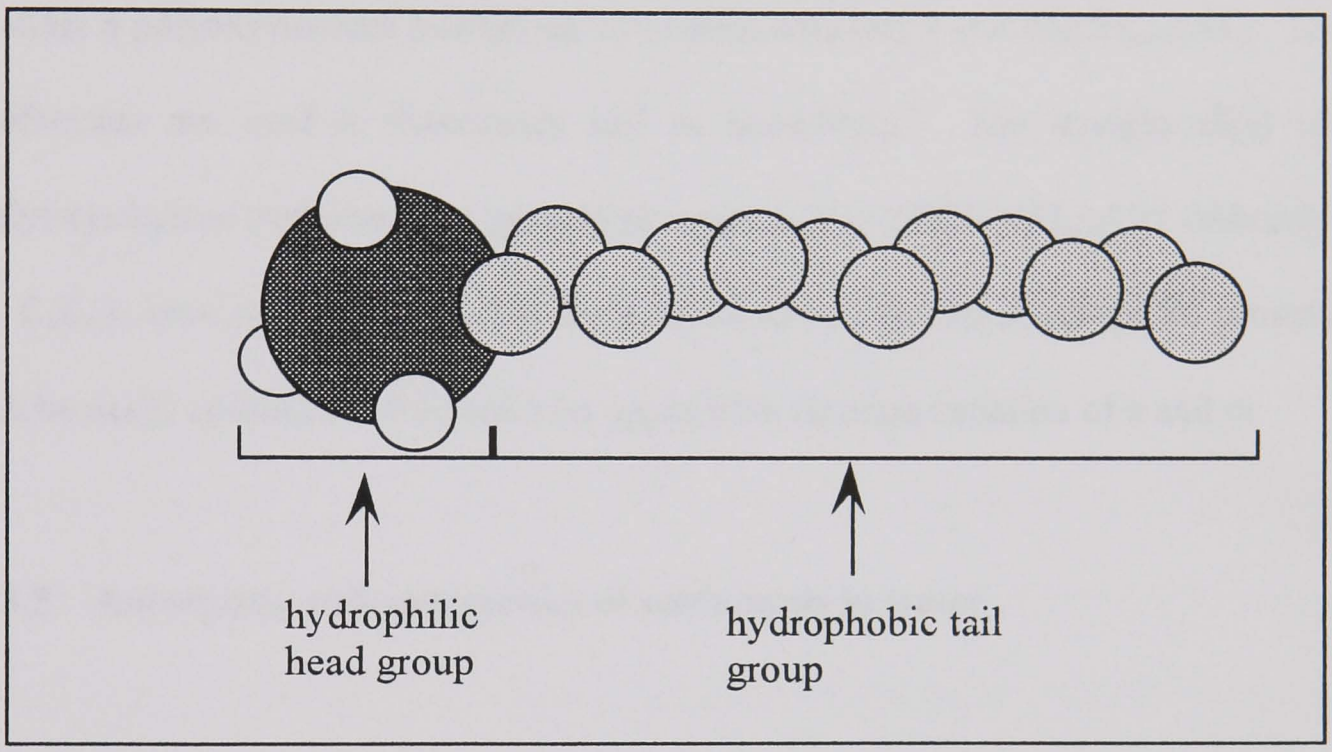

Figure 1.1 Schematic diagram of a surfactant molecule

Anionic surfactants include sulphates and sulphonates and the traditional soaps with the headgroup $-CO_2^-$, which are still used in many cleaning formulations. Cationic headgroups are usually quaternary ammonium or alkyl pyridinium compounds. These surfactants are generally used in fabric and hair conditioners due to the fact that the positive charge on the headgroup has an attraction for negatively charged fibres such as hair and cotton. The zwitterionic surfactants, which are surfactants with both a

positive and negative group present in the headgroup, include betaines and sulphobetaines ($-N^{+}(CH_3)_2CH_2SO_3^{-}$). These surfactants are used in the formulation of baby shampoos and toiletries because they generally have a milder effect on the skin relative to the anionic surfactants. The fourth class, non-ionic surfactants, is the type that has been most studied in this thesis. The vast majority of non-ionic surfactants contain a polyoxyethylene headgroup of general structure ($-(OCH_2CH_2)_mOH$). These surfactants are used in detergency and as emulsifiers.[3] The straight alkyl chain polyoxyethylene surfactants, of general structure $C_nH_{2n+1}(OCH_2CH_2)_mOH$ (abbreviated to C_nE_m), have the advantage that the balance of hydrophobic/hydrophilic properties can be easily optimised for a particular application through variation of n and m.

1.3.2 Adsorption and aggregation of surfactants in water

As we have seen, surfactant molecules are made up of a hydrophobic group and a hydrophilic group. When a single surfactant molecule is added to water, the hydrophilic region is in a medium of similar polarity to itself but the hydrophobic part is not. For this reason, as surfactant is added to water, it tends to distribute itself between the bulk solution and the interface between water and air. At the interface, the tail region either projects into the air at high surface concentrations or lies flat at lower concentrations, the head region remains in the water. This can be seen in figure 1.2.

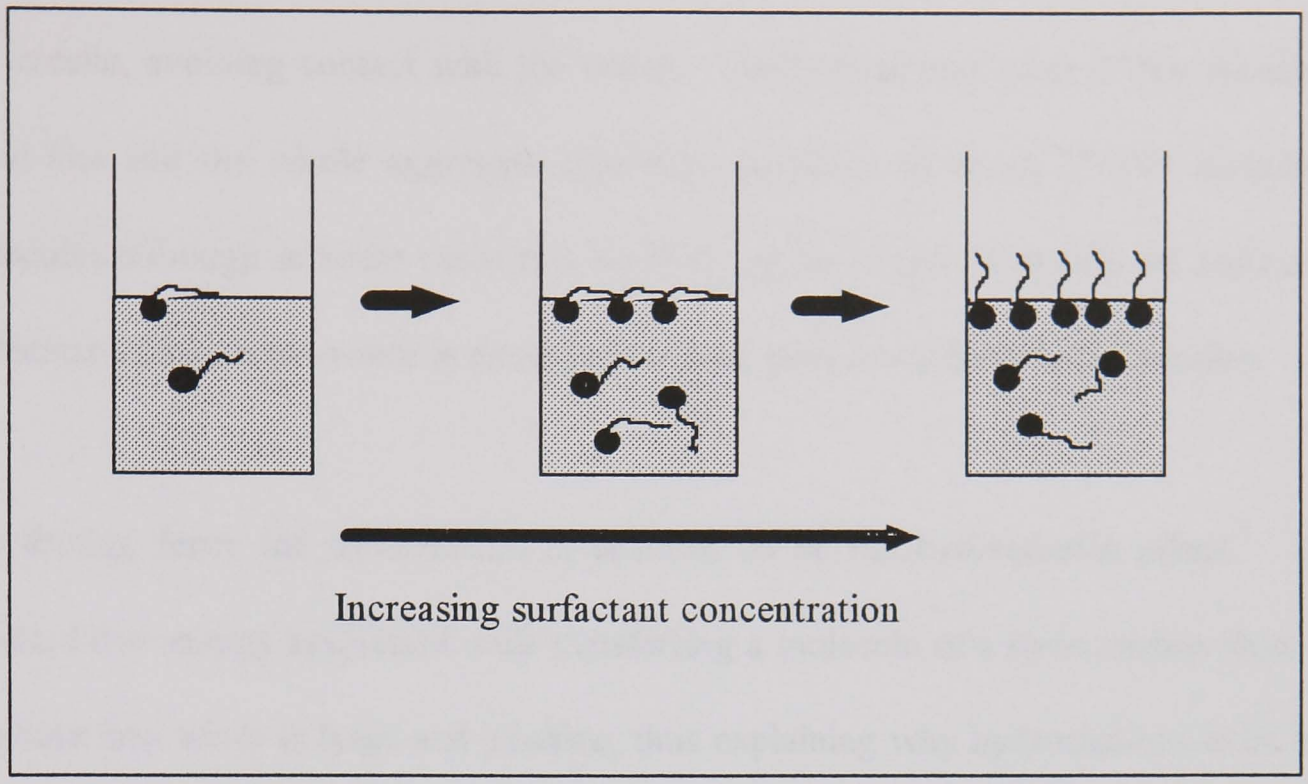

Figure 1.2 Surfactant adsorption at an air/water interface

As more and more surfactant is added to the water, the interface eventually becomes saturated with surfactant. Upon further addition of surfactant, it eventually becomes energetically more favourable for the surfactant to form micellar aggregates in the bulk water rather than adsorb at the interface. The concentration at which this happens is called the critical micelle concentration (cmc). In the micellar aggregates, the surfactant again arranges itself in such a way so that the surfactant tails' contact with water is minimised.

It was Hartley[4] in 1936 who first described micelles as they are understood today. Micelles are commonly spherical aggregates (although they can be rod or disc like at higher concentrations) of surfactant which form in the bulk water with the heads on the outside of the sphere in contact with water and the tails locked away in the core of

the micelle, avoiding contact with the water. The hydrocarbon core of the micelle is liquid-like and the whole aggregate typically comprises of about 50-100 surfactant molecules although in some cases this number can be larger. Virtually all additional surfactant added to the water in excess of the cmc goes towards forming micelles.

The driving force for micellisation is believed to be the hydrophobic effect.[5] The standard free energy associated with transferring a molecule of a hydrocarbon from an oil phase into water is large and positive, thus explaining why hydrocarbons have low solubilities in water. This large and positive value would be expected to be also found for hydrocarbon tails of surfactants in water and thus explain the driving force for micellisation. The problem with this simple interpretation arises when the free energy is split into contributions from both enthalpy, which is generally small at 25°C, and entropy, which, at 25°C, is surprisingly large and negative.[3] It is the loss of the ordering of the water as the surfactant tail is incorporated into a micelle that contributes to the driving force for micellisation. Over the past fifty years there have been several suggestions to interpret the hydrophobic effect[6,7,8] and recently work has been carried out to analyse micellisation in a range of polar solvents.[9,10]. It is fair to say that the hydrophobic effect in micelle forming systems is complex and involves both enthalpic and entropic contributions as well as the particular hydrogen bonding capabilities of water.[3]

When the critical micelle concentration is reached in a surfactant + water system, a number of physical properties show an abrupt change in a plot versus surfactant concentration. Figure 1.3 shows a selection of these properties.

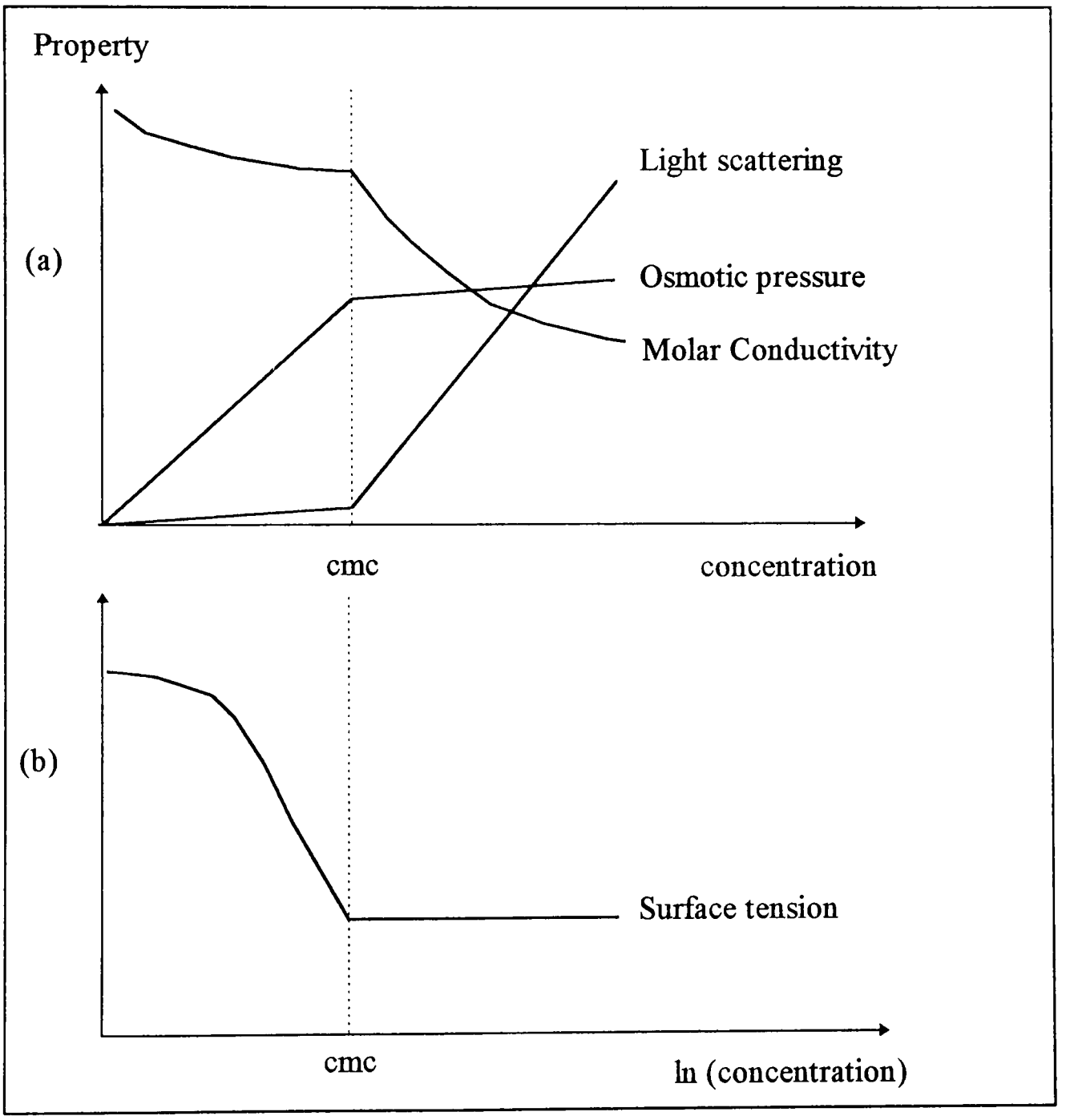

Figure 1.3 Changes in physical properties around the critical micelle concentration

Scattered light intensity increases as the concentration of surfactant is increased and shows a steep rise after the cmc due to the relatively large size of the aggregates present after the cmc when compared to the monomers which are present prior to the cmc.

Surface tension, at concentrations less than the cmc, is reduced as more surfactant is adsorbed at the interface. At concentrations in excess of the cmc, the surface tension remains approximately constant because the aggregates are not surface active. This is the method by which most critical micelle concentrations are determined. The Gibbs adsorption equation (1.1) can be utilised to give the concentration of surfactant at the interface or surface excess concentration (Γ) from figure 1.3b.

$$\Gamma = -\frac{1}{RT}\frac{d\gamma}{d \ln c} \qquad (1.1)$$

This form of the Gibbs equation assumes that the surfactant solutions are dilute (equating activity with concentration (c)) and it can be seen that as the tension (γ) falls at concentrations below the cmc, the surface excess concentration is positive and adsorption occurs. Chapter 5 gives a more detailed account of the various forms of the Gibbs adsorption equation.

Osmotic pressure shows a break at the cmc due to the fact that it is proportional to the number of particles present in the solution. At concentrations greater than the cmc, the number of particles shows a slower increase than prior to the cmc due to the formation of the micelles.

For ionic surfactants, molar conductivity shows a break at the cmc since a mole of micelled surfactant conducts much less than a mole of surfactant monomers since micelles are relatively large and slow moving.

1.3.3 Adsorption of surfactants at the oil-water interface

In the previous section the adsorption of surfactants at the air-water interface was discussed. In a similar manner, surfactants can adsorb at an oil-water interface. Water and hydrocarbon oil, when placed together will separate into two phases with water on the bottom and the oil on top. When surfactant is added to the system, its state of lowest energy occurs when it straddles the interface with the headgroup in the water phase and the tailgroup in the oil phase. Again, adsorption continues until a critical concentration, now known as the critical microemulsion concentration (cμc) is reached. At this concentration aggregates form in either the water phase, in the oil phase or in a third phase depending on a number of factors (see section 1.3.5)

1.3.4 Structure of microemulsions

Microemulsion droplets are similar in structure to micelles in that they arrange themselves so that the part of the surfactant molecule with a polarity most like the solvent is on the outside of the aggregate and the other is held in the core. Thus, if the aggregates form in the water phase, the headgroups are on the outside and if the aggregates are formed in the hydrocarbon oil, the tailgroups are on the outside. Moreover, if we take the case of aggregates forming in the water, an amount of the oil phase can be taken into the oil-like core of the aggregate. This is known as solubilisation of the oil and the phase in which it occurs is known as a microemulsion phase. The oil continues to be solubilised and the droplet becomes larger until an equilibrium size of aggregate is produced (see section 1.3.5). The radii of the droplets are in the order of nanometres and are dependent on composition.

The equation that relates droplet radius (r_c) to the molar ratio of soluibilised oil or water (dispersed component) and surfactant is

$$r_c = \frac{3V_{dc}}{A_s}\left\{\frac{[\text{dispersed component}]}{[\text{surfactant}] - \text{cmc}}\right\} \qquad (1.2)$$

where A_s is the area per surfactant on the surface of the droplet and V_{dc} is the molar volume of the dispersed component. It can be seen from equation 1.2 that larger

droplets are produced as the amount of dispersed component is increased. The structure of an oil-in-water microemulsion droplet and a water-in-oil microemulsion droplet are shown schematically in figure 1.4. In between these two cases, three phases may exist in which a bicontinuous or lamellar microemulsion phase coexists with excess phases of water and oil (see section 1.3.5).

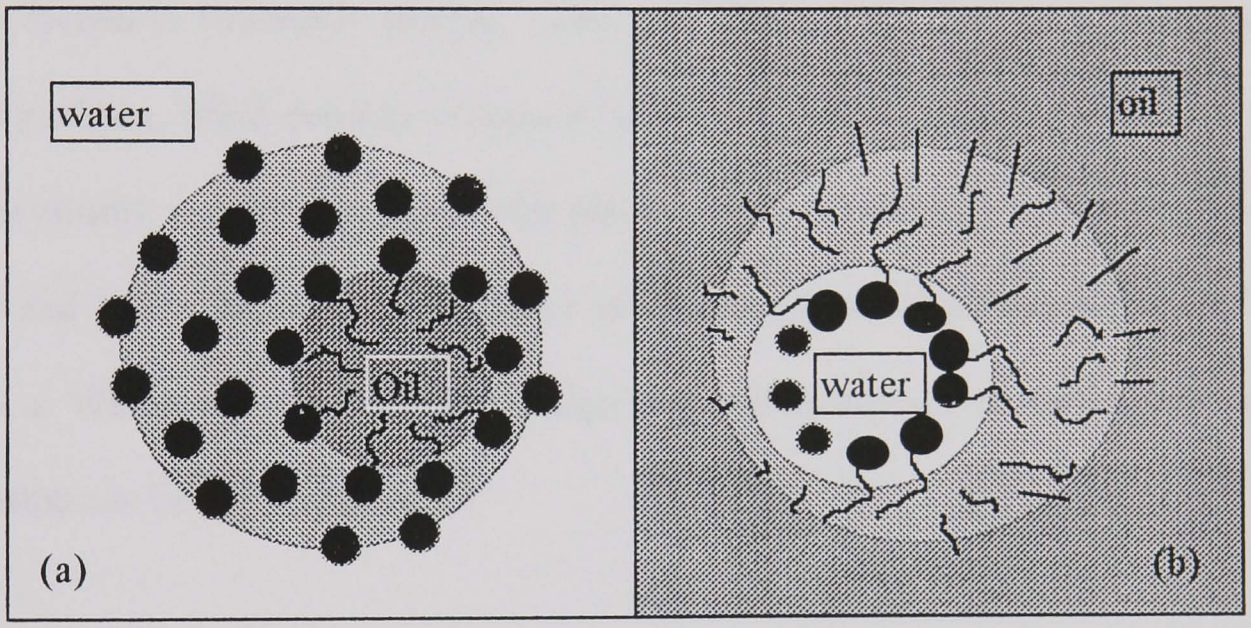

Figure 1.4 **Schematic diagram of (a) an oil-in-water and (b) a water-in-oil microemulsion droplet**

1.3.5 Microemulsion phase inversion and its relation to preferred monolayer curvature

If, in a surfactant + water + oil system containing comparable volumes of oil and water and a concentration of surfactant above the cμc, the aggregates are found in the water and only monomers exist in an excess oil phase, this is a Winsor I microemulsion

system. The aggregate phase, in this case, is an oil in water (O/W) microemulsion and the curvature of the monolayer of surfactant coating the droplets is defined as positive. Alternatively, when the aggregates are found in the oil phase, in equilibrium with excess water, this is a Winsor II system. The aggregate phase is a water in oil (W/O) microemulsion and the monolayer of surfactant around the droplets has negative curvature. In between these two cases the curvature is approximately zero and a three phase system is commonly formed. The third phase can either be a bi-continuous microemulsion, which consists of regions of positive and negative curvature (but zero net curvature), or a lamellar phase with planar arrays of surfactant and alternate layers of oil and water. The other two phases are excess phases of oil and water. This is called a Winsor III system. The progression of monolayer curvature and phase formation can be seen in figure 1.5.

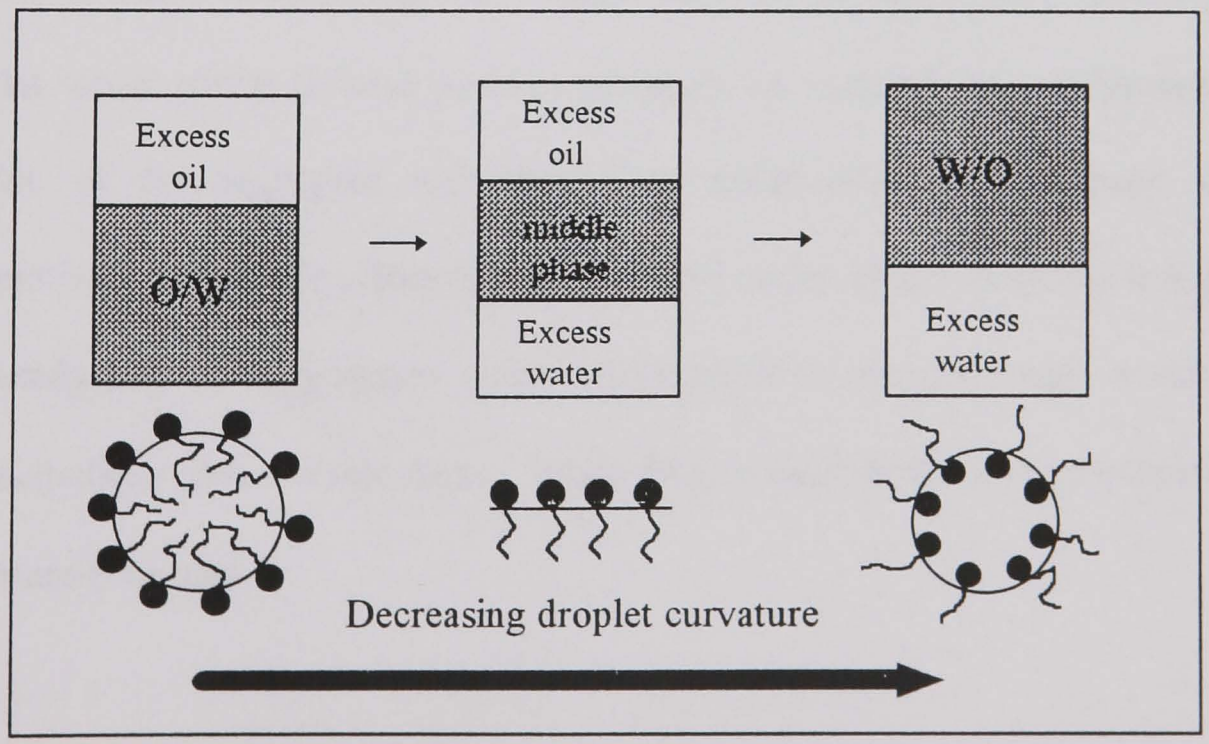

Figure 1.5 Curvature effects in microemulsion formation

The curvature of the monolayers is controlled by geometrical packing considerations of the surfactant molecules. A packing factor, P, can be defined as

$$P = \frac{a_h}{a_c} \qquad (1.3)$$

where a_h is the effective area of the surfactant headgroup and a_c is the effective area of the surfactant tailgroup. In Winsor I and II systems, the system is free to adopt its preferred curvature since the droplets are free to swell or shrink by more or less solubilisation of the excess dispersed phase until the preferred droplet size (and hence preferred monolayer curvature) is attained at equilibrium. Monolayers of high preferred curvature give rise to smaller droplets and lower solubilisation limits, whilst greater solubilisation and larger droplets occur at lower preferred curvature. If $P>1$, the effective area of the headgroup is bigger than the tail region and the microemulsion droplet would prefer to have positive curvature i.e., arrange the headgroups on the outside of the aggregate and thus form oil-in-water microemulsion droplets. Alternatively, if $P<1$, the effective area of the tail region of the surfactant is larger than the headgroup, the aggregates would adopt negative curvature and a water-in-oil microemulsion phase would form. When $P\approx1$, a third phase of approximately zero curvature is formed.

It is possible to produce a change in curvature by affecting the relative sizes of the surfactant headgroup and tailgroup, hence yielding a Winsor progression. If a surfactant + water + oil system is initially a Winsor I microemulsion with aggregates of positive curvature, changing certain parameters of the system can either reduce the effective area of the headgroup or increase the effective area of the tailgroup. This in turn reduces P, reduces curvature and causes the system to move through a progression Winsor I → Winsor III → Winsor II which is known as phase inversion.

Several factors may cause this progression[11,12] and they are surfactant dependent. Changing the surfactant molecular structure changes the effective areas of the headgroup and tailgroup and thus affects curvature. For example, $C_{12}E_5$ has a different phase inversion temperature (the temperature at which the system moves through zero curvature) to $C_{12}E_9$. For non-ionic surfactants of the C_nE_m type, temperature effects are large. At low temperatures, the aggregates form in the water phase (Winsor I). As the temperature is increased it has the effect of dehydrating the headgroup of the surfactant, reducing a_h and P, and thus causing a phase inversion from an oil-in-water system to a water-in-oil system.[13] For ionic surfactants, as the temperature of a water + oil + ionic surfactant system is increased, the preferred curvature becomes more positive. This is possibly mainly due to an increase in counter-ion dissociation from the headgroup which increases the repulsion between the headgroups and increases a_h.[14] This is the opposite behaviour to that observed for non-ionic surfactants. An additional way of changing the curvature of ionic surfactants

is to add an electrolyte to the system. This has the effect of screening the repulsions that exist between the charged headgroups, thus reducing both P and the curvature. For both types of surfactants, increasing the length of the alkane oil chain has the effect of making the curvature more positive. This is due to the fact that long chain length oils penetrate and swell surfactant tails to a lesser degree than short chain length oils.[2] This aspect of the interactions of oils with surfactants will be discussed further throughout this thesis.

Several physical parameters of the microemulsion system change dramatically upon phase inversion. Firstly, if the conductivity of the emulsion formed by shaking the microemulsion and excess phase vigorously is measured, there is a sudden change in conductivity as the phase inversion is reached. O/W emulsions (formed from Winsor I systems) are conducting and W/O emulsions (formed from Winsor II systems) are not conducting. Also, the post cμc interfacial tension (γ_c) between the oil and the water phases and the size of the microemulsion droplets vary as the preferred curvature of the microemulsion droplets is changed. This can be seen in figure 1.6.

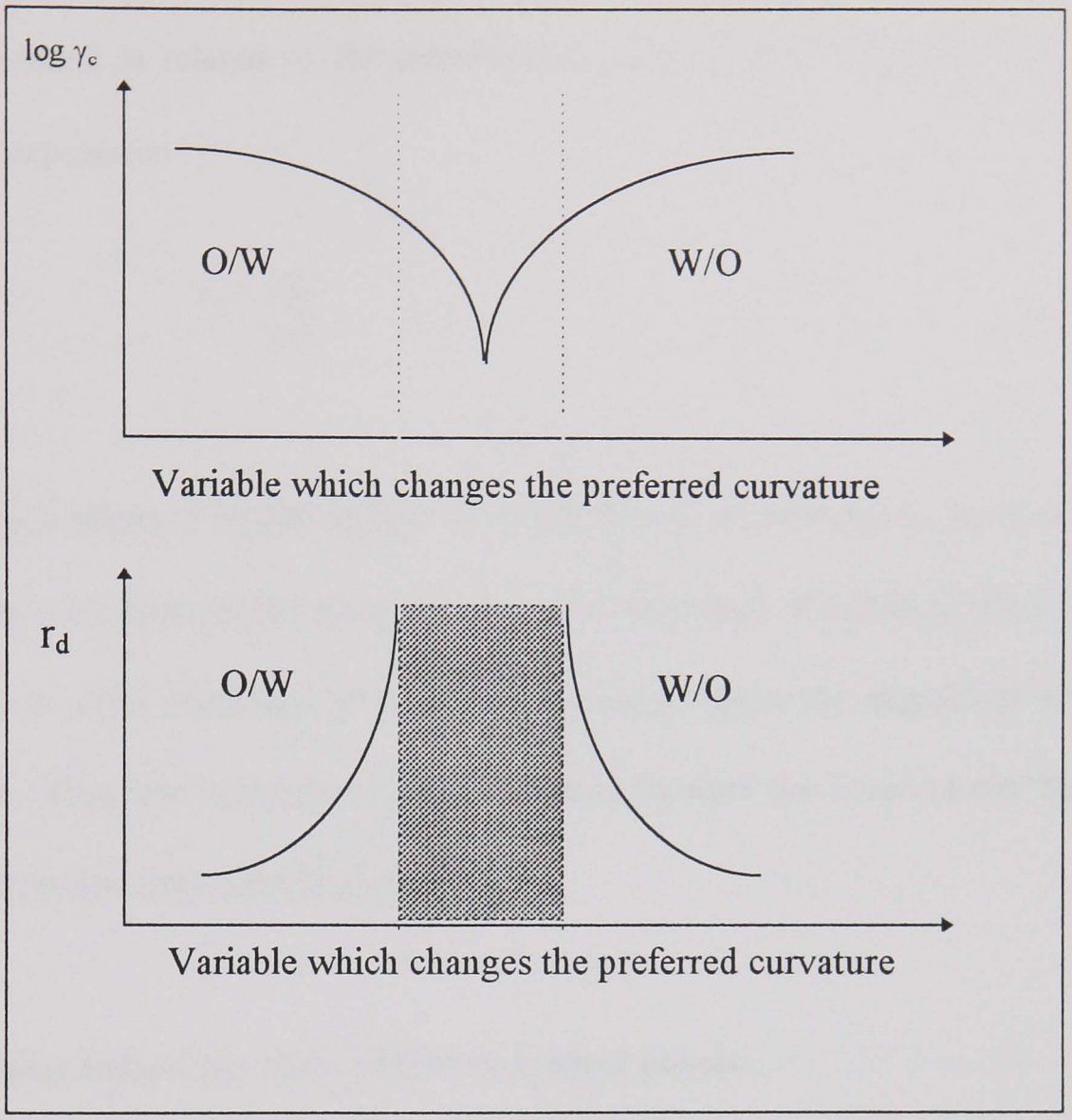

Figure 1.6 Interfacial tension (γ_c) and droplet size (r_d) changes associated with a phase inversion

For non-ionics, as the variable changing the preferred curvature is increased and the packing factor becomes close to unity the curvature decreases and thus the droplet size (r_d) becomes bigger (figure 1.6). This coincides with a drop in interfacial tension and a minimum in interfacial tension occurs at phase inversion. As the variable which is changing the preferred curvature is increased further, the system moves further into the Winsor II region, the curvature becomes more negative, droplets become smaller and the interfacial tension increases once more. The radius (r_d) of the microemulsion

droplets formed is related to the interfacial tension between the phases (γ_c) by the following expression

$$\gamma_c = \frac{2K}{r_d^2} \qquad (1.4)$$

where K is a measure of the rigidity of the surfactant monolayer around the droplet. Work has to be done to the system to bend the monolayer from its preferred natural curvature to zero curvature at a planar interface where the interfacial tension is measured. Thus, the more curved the monolayer around the droplets, the higher the interfacial tension between the phases.

1.3.6 Phase behaviour and relation to critical points

The complete phase behaviour of a ternary water + oil + non-ionic surfactant system can be represented by an upright prism, the base being a Gibbs phase triangle and the ordinate being the temperature.[15] Figure 1.7 shows this prism unfolded so that each of the three sides show a different binary diagram.

Firstly, the water + oil binary region shows that water and oil are almost completely immiscible over the entire temperature range. The immiscibility is shown because if we take, for example, a point in the middle of the binary phase diagram, A, it can be seen that, over the full temperature range, the system remains in a miscibility gap and

would separate into two distinct phases (with compositions corresponding to the ends of the tie line, B and C).

Water + non-ionic surfactant (of the C_nE_m type) binary systems commonly have a miscibilty gap at very low temperatures but as the temperature is increased the two components become miscible. At still higher temperatures, there exists an upper miscibilty gap and the value of the critical point, T_β, lies between the melting point and boiling point of the mixture.[16] The position and shape of this upper miscibility gap depends strongly on the chemical nature of the surfactant; the higher the hydrophobicity, the lower the critical temperature of the miscibilty gap.

The oil + surfactant binary phase diagram shows the situation for a surfactant with a low hydrophilicity which is miscible in the oil at ambient temperatures. The miscibility gap lies below 0°C. As the hydrophilicity is increased, the lower miscibilty gap appears on the phase diagram above 0°C. This miscibility gap has an upper critical temperature denoted T_α which lies, in general, close to the melting point of the mixture.

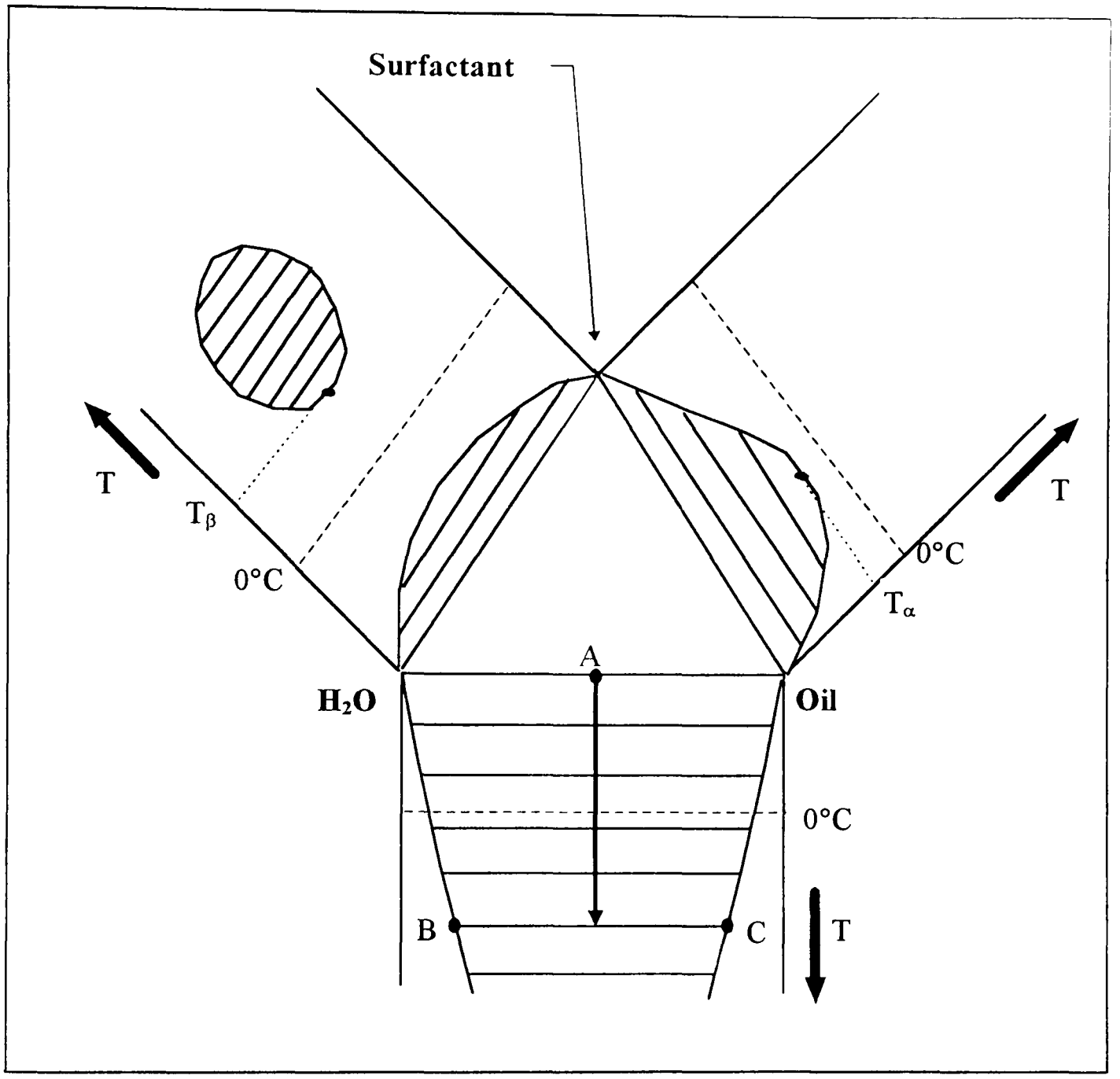

Figure 1.7 **Unfolded phase prism of a ternary water + oil + non-ionic surfactant system**

For a given oil, the position of the two critical temperatures (T_α and T_β) depend on the amphiphilicity of the surfactant and it is the interplay of the miscibility gaps that largely determines the phase behaviour of the ternary system. For C_nE_m surfactants, T_β is generally higher than T_α, and so the surfactant is mainly dissolved in the water phase at

low temperatures. With rising temperature, the influence of the upper loop eventually overcomes that of the oil-surfactant miscibility gap. Thus, the plait point (the point at which the end of the tie lines converge) of the central gap between water and oil moves from the oil-rich towards the water-rich side. The opposite is true as the temperature is reduced from the Winsor II side of the phase prism.[16] The two lines formed by tracing out this movement of the plait point is sigmoidal in nature when shown in relation to temperature (see figure 1.8). The inflection point of this curve indicates the temperature at which the influence of the loop and the oil-surfactant gap compensate each other.

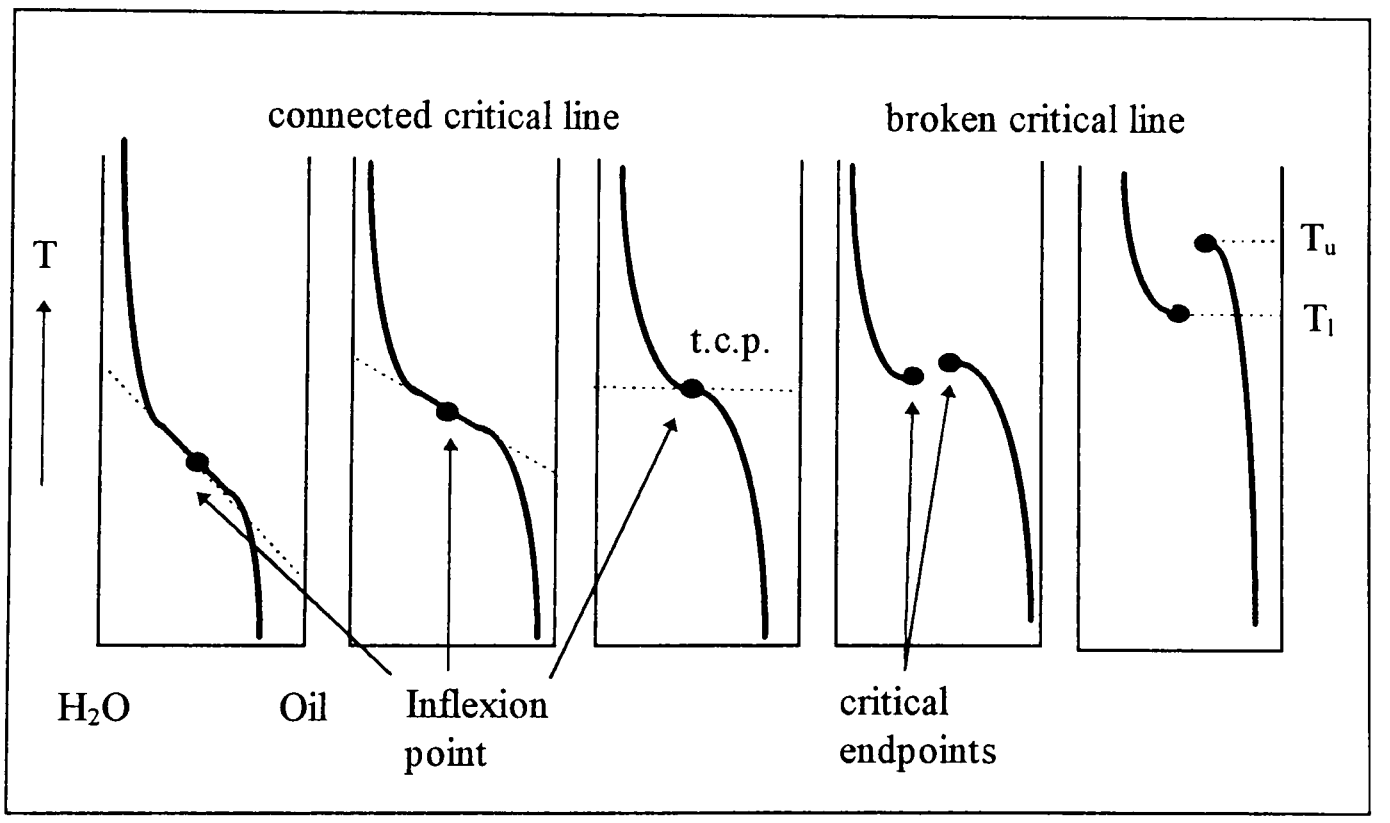

Figure 1.8 Transition from a connected to a broken critical line

As discussed by Kahlweit et al,[16] the critical line that connects the plait points of the central gap within the phase prism, can be looked upon as an elastic spring. If its 'bending tension' is increased, as shown in figure 1.8, the critical line may break at what is known as the tri-critical point (t.c.p.).[17] Figure 1.8 shows the point just before the line breaks as the tangent to the inflection becomes horizontal and then the bending tension becomes too 'strong' and the critical line breaks. Bending tension is increased on the plait point curve by raising the critical point T_α or lowering the critical point T_β (see figure 1.7). This can be accomplished by increasing the chain length of the oil (hence raising T_α) or decreasing the number of headgroups present in the surfactant (hence lowering T_β). With further rising of T_α or lowering of T_β, the two ends of the broken plait point curve move increasingly further apart.

The breaking of the critical line gives rise to the formation of a three-phase body within the phase prism.[18] Systems with a 'broken' critical line, i.e. at a temperature above the t.c.p., thus show a Winsor I microemulsion phase below T_l, a Winsor III microemulsion phase between T_l and T_u, and a Winsor II microemulsion phase above T_u. The three phase body is characterised by its position on the temperature scale as well as its dimensions;

i. Its width $\Delta T = T_u - T_l$

ii. Its mean temperature $T = (T_l + T_u)/2$

iii. Its horizontal extension in the surfactant concentration scale

Close to the tri-critical point, the three phase body is small but with increasing distance from this point, it increases in size and hence so does ΔT.[19]

The most convenient way to view the three phase region is to cut a vertical slice through the phase prism (usually at an oil:water ratio of 1:1 wt%). If this slice is viewed from the oil edge of the prism, the three phase region resembles the body of a fish as seen in figure 1.9.

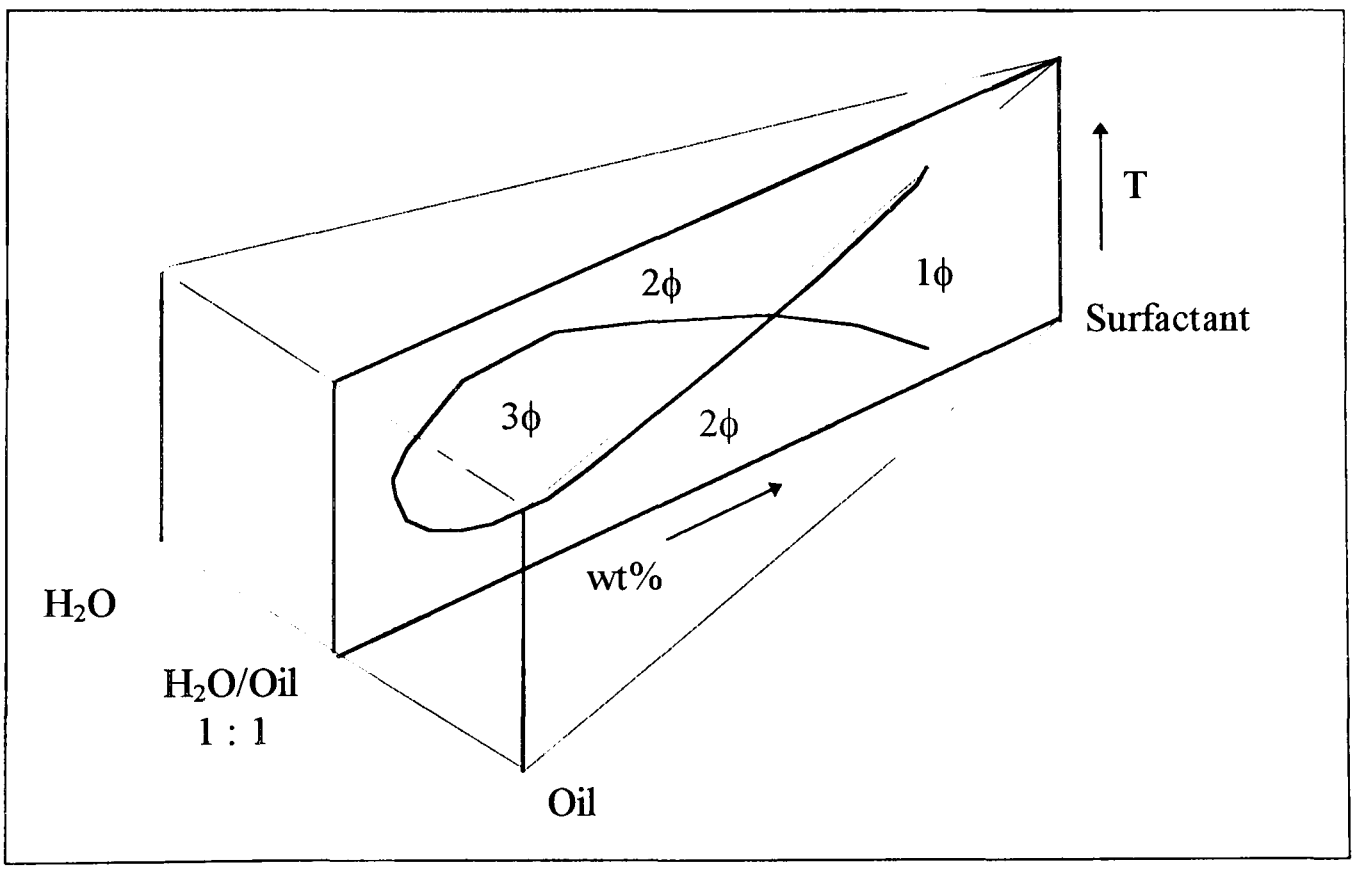

Figure 1.9 Vertical section through the phase prism of a ternary water + oil + nonionic surfactant at water/oil = 1:1 showing the three phase body

The tri-critical point is the point at which the three phase region just disappears. Moving towards a tri-critical point from a system which shows a Winsor III microemulsion phase, reduces the temperature range over which the three-phase body exists and so the variable being changed as the tri-critical point approaches can be said to be destroying the microstructure responsible for the formation of the three phase region.[20]

The third phase can be destroyed either by weakening the amphiphilic strength of the surfactant[21] or, as shown in figure 4.5, the addition of polar oils to such a system can also lead to weaker interactions with the surfactant causing the third phase to disappear.

1.4 Adsorption of oils at the surfactant solution-air interface

1.4.1 Basic phenomenology arising when oil drops are added to aqueous surfactant solution surfaces

The adsorption of oils into surfactant monolayers at solution-air interfaces is in many ways easier to study than the corresponding solubilisation of oils into surfactant micelles and yet the two phenomena are probably related.[22] The interaction of oils with surfactant monolayers can be investigated by monitoring the changes in tension

following the addition of a small quantity of oil to the surface.[23] When a small quantity of oil is added to an aqueous solution surface, it can undergo a number of possibles fates.

Firstly, the oil can produce a thick (on the molecular scale) oil film spread over the surface of the solution. These films give characteristic interference colours making them easily recognisable. For spreading oils, the measured surface tension of the solution falls from the value of the aqueous solution to the sum of the oil-water and the oil-air tensions.

Alternatively, the oil can form stable lenses on the surfactant solution surface. The lenses of bulk oil coexist with a thin mixed film of surfactant and oil molecules which can be either a multilayer[24] or a monolayer. In this case, the tension again falls after oil addition because the tension of the mixed surfactant/oil film is lower than the tension of the pure surfactant monolayer. A fuller account of the spreading behaviour of oils on surfactant solutions can be found in Chapter 5.

1.4.2 Previous surface tension studies

When oil is added to a surfactant monolayer, whether either spreading or forming lenses, it may reduce the tension of the solution. This reduction in tension, denoted as $\Delta\gamma$, is equal to the surface pressure of the oil. When $\Delta\gamma$ is measured as a function of

the activity of the adsorbing species, an adsorption isotherm of surface concentration (Γ) against activity of the adsorbing species can be obtained and used to estimate the thickness of the adsorbed layer (see Chapter 5). The literature already contains information for oils with ionic surfactants studied in this way.[22,23] The alkane chain length dependence of $\Delta\gamma$ values on tri-methyl ammonium bromide (TAB) type ionic surfactants has been studied and squalane has been used to vary the concentration of the adsorbing alkane oil. It was found that $\Delta\gamma$ values for dodecane on a range of surfactants were dependent on the concentration of surfactant below the cmc but were independent of it above the cmc. Using squalane as a diluent oil, measurements were made of $\Delta\gamma$ values as a function of the activity of dodecane for mixed oil drops on ionic surfactant solutions both above and below their cmc. These studies, however, did not allow for the possibility that squalane, although non-adsorbing when pure, could adsorb when added as a mixed oil to the surfactant monolayer. Also, the activity coefficients for alkanes with squalane were not known so, for the $\Delta\gamma$ versus mole fraction of the adsorbing oil graphs obtained in these studies, mole fraction was equated with activity i.e. the activity coefficients were assumed to be effectively 1. This thesis is aimed at furthering the understanding of alkane adsorption onto non-ionic surfactants, investigating the possibilty of squalane adsorption when mixed with the adsorbing oil, and incorporating activity coefficients into the adsorption isotherms.

1.4.3 Previous neutron reflection studies

As well as looking at the effect the oils have on the surface tension of surfactant monolayers, the molecular orientation and position of the oil and surfactant molecules in mixed oil/surfactant films can be determined by using neutron reflection techniques.[25] This method involves determining the intensity of a specularly reflected beam of neutrons as a function of either the angle of incidence or neutron wavelength. Neutron reflection from a deuterated species is of much higher intensity than protonated species. Therefore, by deuterating different components within a system containing a surfactant solution and an oil film, important information concerning the molecular make-up of the interface can be ascertained. There have been studies using ionic surfactants, investigating the change in area per molecule of the surfactant before and after the addition of oil and also analysing where the oil lies in the interface in relation to the surfactant monolayer.[26] This study showed that a mixed monolayer of TTAB (tetradecyl tri-methyl ammonium bromide) and dodecane exists at the aqueous/air interface rather than a multilayer oil film coexisting with a lens. This distinction is not possible with tension measurements alone. For the same system, it was concluded that the area per surfactant at the interface in the mixed film derived from neutron reflection agrees, within experimental error, with that derived from surface tension measurements (52Å^2). It was also shown that the area per surfactant at the interface increases by ~10% upon the addition of the oil. It was also deduced that when the oil is placed onto the surfactant monolayer, it distributes itself unevenly

within the surfactant layer, in such a way that part of the chain of the oil lies outside the surfactant chain region. It can be seen from this that neutron reflection is a useful technique to complement surface tension studies, giving an insight into the actual position and spacing of the molecules at the interface.

1.5 Presentation of this thesis

The overall aim of this study was to increase the understanding of the interactions of oils with surfactants. Both polar and non-polar oils have been studied and the main aspects discussed in each chapter are listed below.

1. Firstly, a study of the interactions of both polar and non-polar oils with water was investigated using work of adhesion and the oils' interfacial tension with water. This is an essential starting point for this study so that before any surfactants are used, a perception of how the polarity of oils affect their adhesion properties with polar phases can be assessed.

2. The cosurfactant properties of the oils were determined to assess their effect at surfaces prior to the use of conventional surfactant systems. This was carried out by investigating the surface activity of the oils from dilute solution in heptane to the heptane-water interface.

3. Following discussion of the cosurfactant nature of the oils, the oils were incorporated into a non-ionic surfactant + hydrocarbon + water system. This determined the effect they have on the phase behaviour of such a system with relation to phase inversion and the position and size of the Winsor III region.

4. Finally, an investigation into the adsorption of the oils into surfactant monolayers at the air-water interface was carried out to derive values for the surface concentrations of oils and thus relate this, if possible, to the solubilisation seen in curved interfaces via the phase behaviour studies and headspace analysis studies.

1.6 References

[1] R. J. Hunter, Foundations of colloid science, Volume 1, Clarendon Press, Oxford, 1986.

[2] D. C. Jones, R. H. Ottewill, J Chem. Soc., 4076, 1955.

[3] J. H. Clint, Surfactant Aggregation, Blackie, Glasgow, 1992.

[4] G. S. Hartley, Aqueous solutions of paraffin chain salts, Hermann & Cie, Paris, 1936

[5] C. Tanford, The hydrophobic effect : Formation of micelles and biological membranes, 2nd edition, Wiley, New York, 1980

[6] R. H. Aranow and L. T. Witten, J. Phys. Chem., **64**, 1643, 1960.

[7] H. S. Frank and M. W. Evans, J. Chem. Phys., **13**, 507, 1945.

[8] K. Shinoda, J. Phys. Chem., **81**, 1300, 1977.

[9] D. F. Evans, Langmuir, **4**, 3, 1988.

[10] A. H. Beesley, D. F. Evans and R. G. Laughlin, J. Phys. Chem., **92**, 791, 1988.

[11] R. Aveyard, B. P. Binks and P. D. I. Fletcher in E. Wyn-Jones and D. Bloor (Eds), Structure, Dynamics and Equilibrium Properties of Colloidal systems, Kluwer, Amsterdam, pg 557, 1990

[12] J. Th. G. Overbeek, Faraday Discuss. Am. Chem. Soc., **65**, 7, 1978.

[13] R. Aveyard, B. P. Binks, T. A. Lawless and J. Mead, J. Chem. Soc. Faraday Trans 1, **81**, 2155, 1985.

[14] R. J. Hunter, Foundations of Colloid Science, Volume II, Clarendon Press, Oxford, 1989.

[15] C. U. Hermann, G. Klar and M. Kahlweit, J. Colloid Inter. Sci., **82**, 6, 1981.

[16] M. Kahlweit and R. Strey in Microemulsion systems, H. L. Rosano and M. Clausse (Eds), Dekker, New York, 1987.

[17] R. B. Griffiths and B. Widom, Phys. Rev., **A8**, 2173, 1973.

[18] M. Kahlweit and R. Strey, Angew. Chem., **24**, 654, 1985.

[19] M. Kahlweit and R. Strey, J. Phys. Chem., **91**, 1553, 1987.

[20] M. Kahlweit, R. Strey and P. Firman, J. Phys. Chem., **90**, 671, 1986.

[21] M. Kahlweit, Ber. Bunsenges. Phys. Chem., **98**, 490, 1994.

[22] R. Aveyard, B. P. Binks, P. Cooper and P. D. I. Fletcher, Adv. Coll. Int. Sci., **33**, 59, 1990.

[23] R. Aveyard, P. Cooper and P. D. I. Fletcher, J. Chem. Soc., Faraday Trans., **86**, 3623, 1990.

[24] H. Kellay, J. Meunier and B. P. Binks, Phys. Rev. Lett., **69**, 1220, 1992.

[25] R. Aveyard, B. P. Binks, P. Cooper, P. D. I. Fletcher and A. Sokolowski, J. Phys. Chem., **96**, 1383, 1992.

[26] J. R. Lu, R. K. Thomas, R. Aveyard, B. P. Binks, P. Cooper, P. D. I. Fletcher and A. Sokolowski, J. Phys. Chem., **96**, 10971, 1992.

Chapter 2

CHAPTER 2

EXPERIMENTAL

All experiments were carried out at 25°C unless otherwise stated.

2.1 Materials

2.1.1 Water

All water used in the study was firstly purified by reverse osmosis and then further treated with a Milli-Q reagent water system. After treatment, water gave a surface tension of 71.9 ± 0.1 mN m^{-1} at 25°C which is in good agreement with literature values,[1] indicating the absence of surface active impurities.

2.1.2 Oils, excluding perfume oils, used in the study

The oils used in this work were purchased from various sources and the alkanes were all at least 99% pure. All the oils were twice passed through an alumina column prior to use to remove all polar impurities. Table 2.1 lists the oils used, their sources and their purities. Measured oil/air tensions of the hydrocarbons agreed with literature values[2] within 0.1mN m^{-1}.

Table 2.1 Table of oils used, their sources and their purities.

Material	Supplier	Purity
Heptane	Fisons	99%
Octane	Fluka	>99.5%
Nonane	Fluka	>99%
Decane	Fluka	>99%
Undecane	Aldrich	>99%
Dodecane	Aldrich	>99%
Tridecane	Aldrich	>99%
Tetradecane	Aldrich	>99%
Pentadecane	Aldrich	>99%
Hexadecane	B.D.H.	>99%
Di-iso nonyl phthalate	Fluka	Technical grade
Squalane	B.D.H.	99%

2.1.3 Perfume oils used in the study

The perfume or polar oils which have been used in this study had to satisfy a number of criteria before they would be acceptable for the purposes of a fundamental study of the phase behaviour and associated surface chemistry. The criteria were

1. The oils must have densities different from that of water by at least 0.1 g cm^{-3}. This density difference is required to facilitate the measurement of interfacial tension and to aid phase separation of oil + water mixtures.

2. The oils must be as pure as possible.

3. The oils must be available comercially at a reasonable cost.

After examining a wide range of moderately polar oils, the most suitable choices for detailed study were found to be linalool, linalyl acetate, eugenol, cineole and limonene.[3,4] These oils were twice passed through an alumina column prior to use in order to remove all polar impurities. The structure of these oils can be seen in figure 2.1.

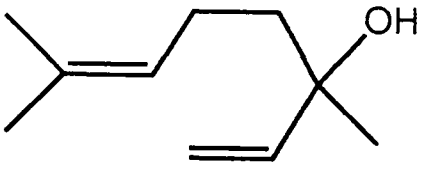

Linalool

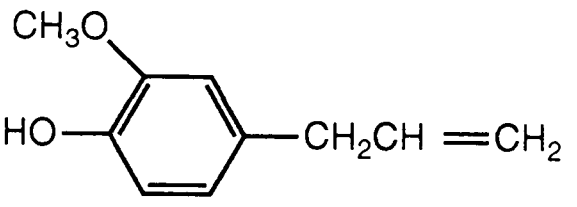

Eugenol

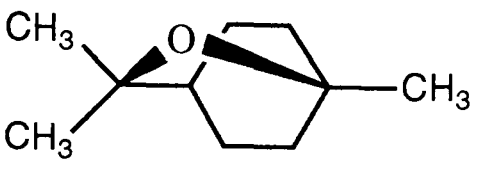

Cineole

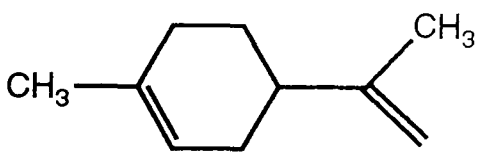

Limonene

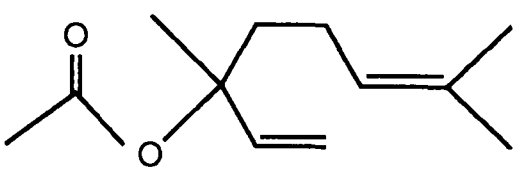

Linalyl acetate

Figure 2.1 Molecular structure of the perfume oils

Table 2.2 Table of perfume oils used, their sources and their purities.

Material	Supplier	Purity
Linalool	Fluka	97%
Eugenol	Fluka	>99%
Cineole	Fluka	99%
Linalyl acetate	Quest	-
Limonene	Quest	-

2.1.4 Non-ionic surfactants

The non-ionic surfactants used in the study, all of the alkyl polyoxyethylene glycol ether type (C_nE_m), were obtained from various sources. They have the following general structure.

$$C_nH_{2n+1}(OCH_2CH_2)_mOH$$

All surfactants from Nikko showed only a single detectable GC peak in the manufacturer's analysis. Surfactants purchased from Fluka and Bachem had a purity of at least 97%. The purity of the samples was further tested by comparison of the measured cloud points of an aqueous sample of the surfactant with literature values.[5]

A summary of the non-ionic surfactants used can be seen in Table 2.3. The values obtained agreed with literature within 0.3°C.

Table 2.3 Summary of the non-ionic surfactants used, their sources and measured and literature cloud points (for 1 wt% solutions in water).

Surfactant	Source	Measured cloud point (°C)	Literature cloud point (°C)
C_8E_3	Bachem	11.5	11.6
C_8E_5	Bachem	63.6	63.9
$C_{12}E_5$	Nikko	31.7	32.0
$C_{12}E_7$	Nikko	66.8	67.0
$C_{12}E_9$	Fluka	Undetermined	88.0
$C_{10}E_7$	Fluka	75.8	75.8
$C_{14}E_7$	Nikko	57.3	57.6

2.1.5 Ionic surfactants

The ionic surfactants used in the study were all of the alkyl trimethyl ammonium bromide (TABs) type. These surfactants have the general formula

$$C_nH_{2n+1}N^+(CH_3)_3Br^-$$

All the ionic surfactants used in the study were at least 98% pure and no further purification was carried out in the laboratory.

Table 2.4 Table to show the ionic surfactants used in the work, their sources and their purities.

Surfactant	Source	Purity
DoTAB (n=12)	Sigma	99%
TTAB (n=14)	Sigma	99%
CTAB (n=16)	B.D.H.	98%

2.2 Preparation of glassware

All glassware was washed thoroughly in chromic acid, rinsed twice with distilled water and then twice with ultrapure milli-Q water. The glassware was dried using a clean oven.

2.3 Visual Experimental methods

2.3.1 Spreading behaviour of oils on surfactant solutions

The spreading behaviour of oils on surfactant solutions was studied by using a teflon dish contained within a thermostatted glass vessel with a thermostatted lid and a teflon bung, through which the oil was introduced with a syringe (figure 2.2). All the apparatus was cleaned, prior to use, by using chromic acid and distilled water in the usual way.

The procedure to investigate spreading behaviour was, firstly, to fill the teflon dish, housed in the open thermostatted vessel, with the surfactant solution. The lid of the glass vessel was then replaced and the apparatus was allowed to thermostat for about 15 minutes. The oil (≈50 μl) was then added to the surface of the surfactant solution by using a 100μl syringe inserted through the small hole in the teflon bung. The apparatus was illuminated , from behind, by a lamp. It was then ascertained wether the oil formed distinct circular lenses on the surfactant solution or patches of film showing interference colours.

Figure 2.2 **Apparatus used to visually observe the spreading behaviour of oils on surfactant solutions**

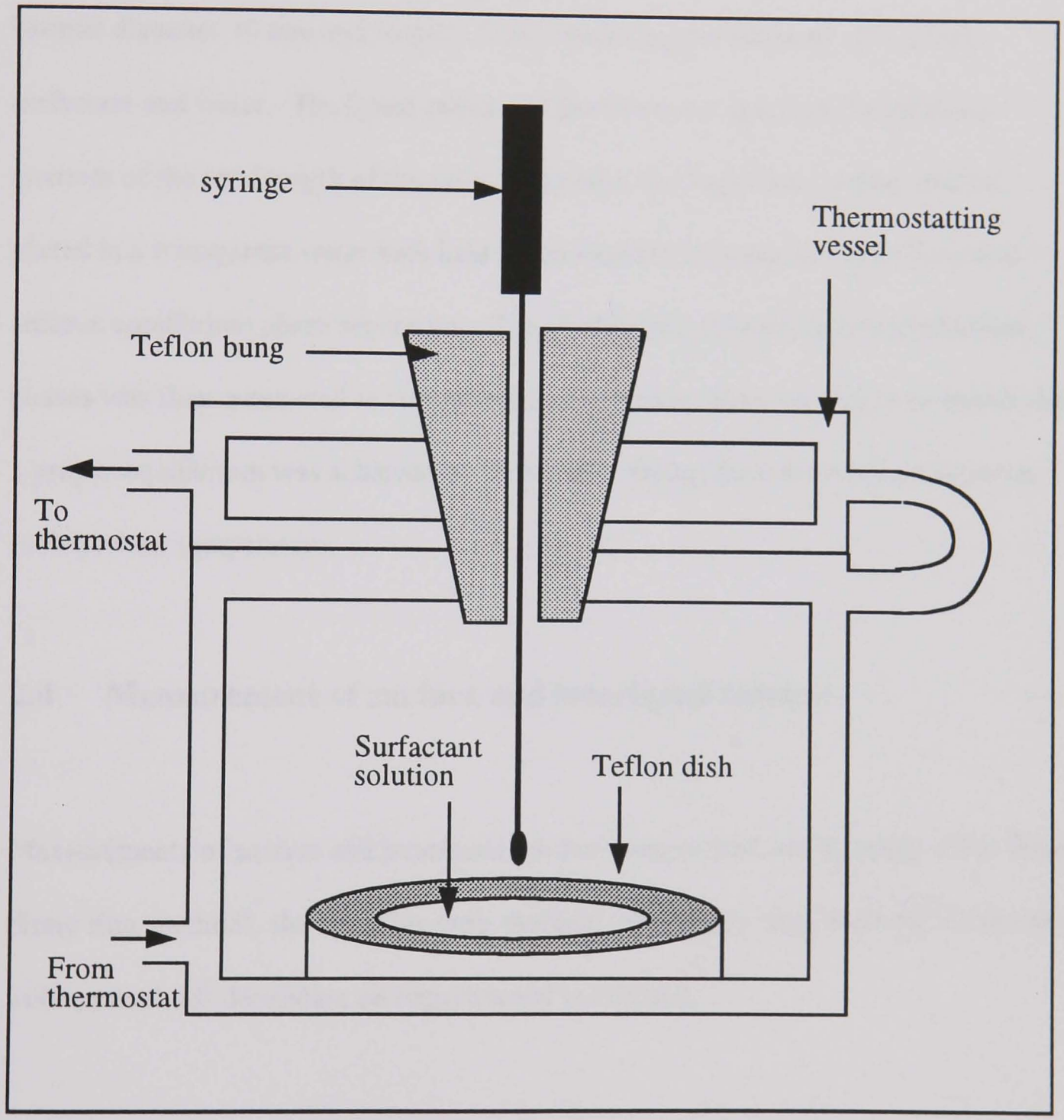

2.3.2 Phase behaviour observations

The phase behaviour work in the study was carried out by preparing sealed tubes, of internal diameter 10 mm and length 15 cm, containing the required ratio of oil, surfactant and water. The liquid content of the tubes was generally about three-quarters of the total length of the tubes. The tube was then flame sealed, shaken, placed in a transparent water bath held at the required temperature and allowed to achieve equilibrium phase separation. The number and volumes of the equilibrium phases was then monitored at various set temperatures. Care was taken to ensure that a proper equilibrium was achieved by thoroughly mixing the tube contents between each new set temperature.

2.4 Measurement of surface and interfacial tension

Measurements of surface and interfacial tension were carried out by using either the du Nouy ring method[6], the spinning drop method[7], the sessile drop method[8] or the drop volume method[9] depending on experimental conditions.

2.4.1 The du Nouy ring method

The du Nouy ring method was used for measuring surface tensions greater than 5 mN m^{-1}.

The du Nouy ring tensiometer used (a Kruss K10 instrument) consists of a platinum/iridium alloy ring and a glass sample container which are housed within a glass thermostatting vessel. The ring is lowered into the liquid being measured and is, first manually, and then automatically withdrawn from the sample. The force on the ring increases as it is pulled from the solution until it reaches a maximum. At this point, the contact angle of the solution with the ring is zero and the direction of the force arising from the tensions is vertical (figure 2.3). This maximum pull is then used to calculate the surface tension of the sample. Further raising of the ring eventually causes the lamella to break. This is also shown in figure 2.3. The Kruss K10 instrument uses a servo control motor to hold the ring at maximum force.

Harkins and Jordan[10] showed that the surface tension, γ, of a solution is given by equation 2.1

$$\gamma = \frac{mgF}{4\pi R} \qquad (2.1)$$

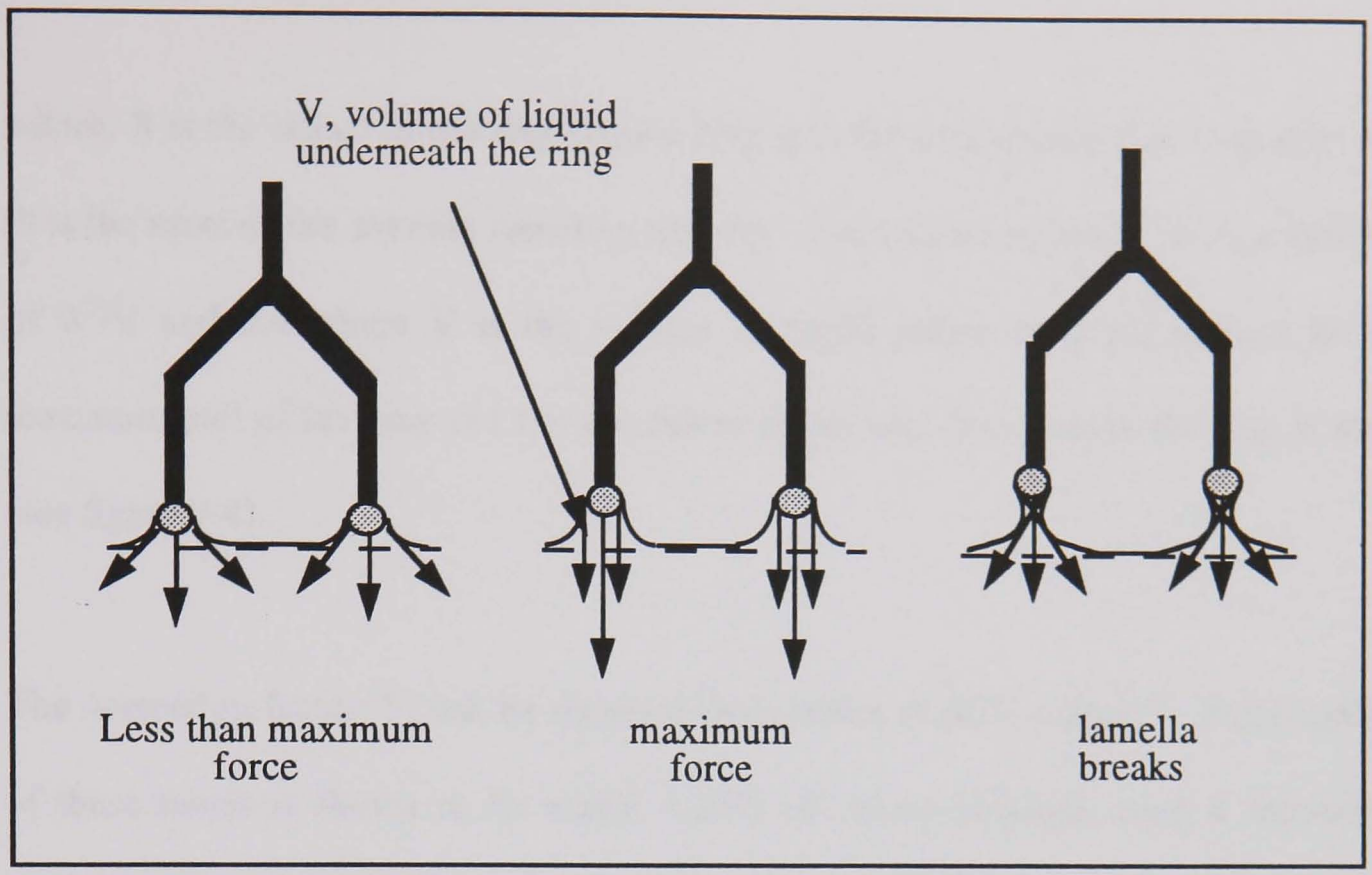

Figure 2.3 Cross-sectional view of the Du Nouy ring showing the different stages of measurement

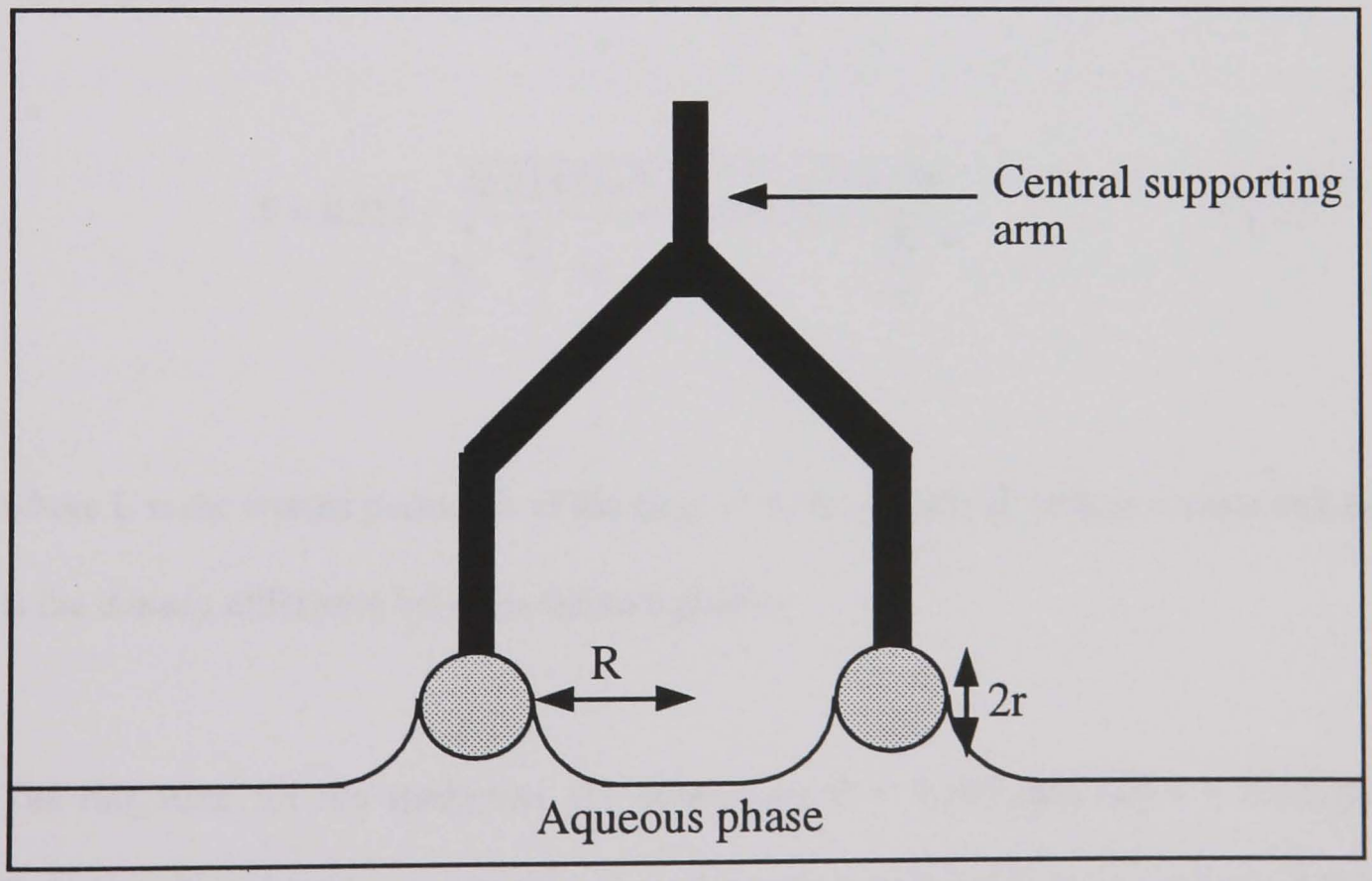

Figure 2.4 Schematic diagram of the ring

where, R is the radius of the ring (figure 2.4), g is the acceleration due to gravity and m is the mass of the solution raised by the ring. The correction factor, F, is a function of R^3/V and R/r where V is the volume of liquid pulled from the surface by the maximum pull of the ring and r is the radius of the wire from which the ring is made (see figure 2.4).

The correction factor, F, can be obtained from tables of R^3/V values.[10] The accuracy of these tables is shown to be within 0.25% of values obtained using a theoretical consideration of meniscus shapes[11]. Zuidema and Waters[12] extended the work of Harkins and Jordan to include measurements of tensions below 25 mN m^{-1}. Their equation for the correction factor is given below.

$$F = 0.725 + \sqrt{\frac{0.01425\gamma^*}{\frac{L^2}{4}\Delta\rho} + 0.04532 - \frac{1.679}{\frac{R}{r}}} \qquad (2.2)$$

where L is the wetted perimeter of the ring, γ^* is the measured surface tension and $\Delta\rho$ is the density difference between the two phases.

The ring used for the study had the dimensions R = 9.545 mm and r = 0.185mm. Before each measurement, the ring was cleaned by immersing in chromic acid for a few minutes, rinsed with high purity water then heated in a blue bunsen burner flame

until it glowed red. The sample dish was cleaned by immersing it in chromic acid for a period of half an hour, followed by rinsing with high purity water and finally left to dry in a clean oven.

The tensiometer was calibrated using high purity water for which the tension was 71.9 mN m^{-1} at 25°C. The calibration, adjusted using internal potentiometers, was checked every week. Measured tensions were usually reproducible to ± 0.1 mN m^{-1}.

The following procedure was used to measure the decrease in tension when a small oil drop was added to a surfactant solution. Firstly, the tension of the surfactant solution was measured in the normal way and then a 20μl drop of the alkane oil mixture was then added, by means of a microsyringe, down the inside wall of the sample container onto the surface of the solution. The alkane drops were thus kept close to the wall of the container and well away from the ring. Filter paper was soaked in the particular alkane mixture being investigated and placed around the edge of the sample container. This filled the atmosphere within the glass thermostatting vessel with the alkane vapour and prevented evaporation of the oil lens which had been added to the surface. A measurement was then made in the manner described for pure surfactant solutions.

2.4.2 The spinning drop method

The spinning drop technique was developed during the 1940's by Vonnegut[7] and is particularly suitable for measuring low interfacial tensions (10^{-4} - 5 mN m^{-1}), a range in which the other methods described in this chapter fail. Figure 2.5 shows a schematic diagram of a spinning drop apparatus. The instrument consists of a rapidly rotating horizontal glass capillary tube encased within a thermostatting oil chamber. As it revolves, the capillary tube is illuminated by a stroboscopic light source and is viewed through a travelling microscope.

The technique involves injecting a drop of the lighter of the two phases into the spinning capillary containing the more dense phase. An equilibrium of forces is then established between the centripetal force which acts to elongate the drop along the axis of rotation, and the interfacial tension force which tries to minimise the surface area between the two phases. The equilibrium drop diameter achieved is a function of the angular velocity of the spinning capillary, the interfacial tension and the density difference between the two phases as described by the equation due to Vonnegut.

$$\gamma = \left(\frac{\omega^2 c^3 \Delta\rho}{4}\right)\left(1+\frac{2c}{3D}\right) \qquad (2.3)$$

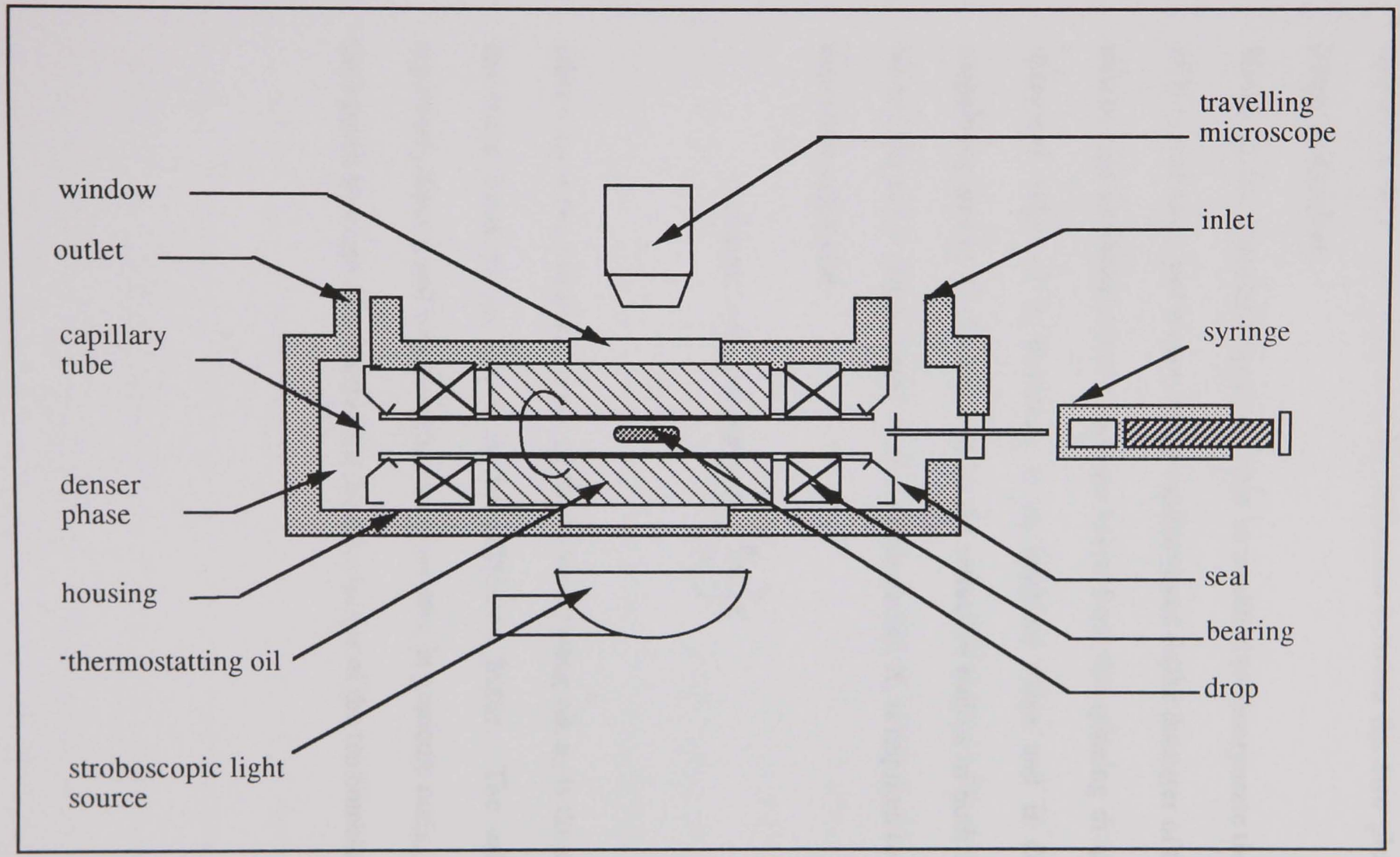

Figure 2.5 Schematic diagram of the spinning drop tensiometer

where γ is the interfacial tension, ω is the angular velocity, c is the radius of the cylindrical drop, $\Delta\rho$ is the density difference between the two phases and D is the length of the drop.

However, the Vonnegut equation must be modified to incorporate the measured values of N (revolutions per minute of the capillary) and d (the diameter of the drop formed in microscope graticule units) which are taken from the spinning drop apparatus. This measured value of d, however, is an apparent value and is determined by the magnifying power of the lens and by the refractive indices of both the thermostatting oil and the more dense phase. A conversion factor, X, is required to obtain c from the measured value of d.

$$c(\text{metres}) = d(\text{graticule units})\left(\frac{n_{oil}}{n_2}\right)X \qquad (2.4)$$

where n_{oil} is the refractive index of the thermostatting oil, n_2 is the refractive index of the more dense phase and X is the calibration factor. The calibration factor is seperately determined by measuring the diameters, in graticule units, of syringe needles (of known absolute diameter) using the microscope of the tensiometer.[13]

By collecting all the conversion factors into a single factor, A, which is specific to the particular lens and machine that is used, equation 2.3 can be expressed as

$$\gamma = AN^2 d^3 \left(\frac{n_{oil}}{n_2} \right)^3 \Delta\rho \qquad (2.5)$$

Equation 2.5 is valid only for drops whose axial ratio (length/diameter) exceeds approximately 5. The Kruss spinning drop tensiometer (site 04) was used to measure the interfacial tension between surfactant solutions and alkane oils in this study. The surfactant solution, being the denser of the two phases, was placed into the capillary tube by allowing it to drain from a resevoir. A drop of the oil phase was then injected into the capillary through the septum by using a 100µl syringe and was brought into the viewing area by adjusting the angle of tilt of the tensiometer and by allowing more of the dense phase through the capillary tube. The drop dimensions were altered by increasing or decreasing the revolutions per minute shown on the front panel. The diameter of the drop formed was then determined by viewing the drop through the travelling microscope, aligning the zero mark on the graticule with the top of the drop and moving the cross hairs into line with the lower edge of the drop. The diameter of the drop was monitored over a period of time until it became constant. The speed of rotation, N was noted and equation 2.5 was used to calculate the interfacial tension. For any particular measurement, different rotation speeds were used which gave

different drop diameters but the same interfacial tension. Tensions acquired by the spinning drop method were accurate to ±10%.

2.4.3 The drop volume technique

The drop volume technique was used to measure both surface and interfacial tensions. The drop volume apparatus, which was built in the laboratory, can be seen in figure 2.6, and consists of a stainless steel tip, A, of radius 2.494±0.002mm (measured by a micrometer screw gauge), in conjunction with an Agla syringe, B, and a micrometer screw gauge, C. The syringe was housed in a glass tube, D, which contained the less dense phase (air for surface tension measurements). The apparatus was immersed into a water bath which was thermostatted to the required temperature. The apparatus was kept as free from vibration as possible.

The procedure used for tension measurement was as follows. The more dense phase was placed into the Agla syringe and the apparatus was allowed to thermostatt for half an hour. The reading on the micrometer screw gauge was noted. By turning the micrometer screw gauge, the Agla syringe expelled a little of the more dense phase which eventually, with more turning, formed into a drop hanging from the stainless steel tip. The later stages of forming the drop were carried out over a longer time, of the order of one minute. Once the drop has detached from the tip, the reading on the

Figure 2.6 Schematic diagram of the drop volume apparatus

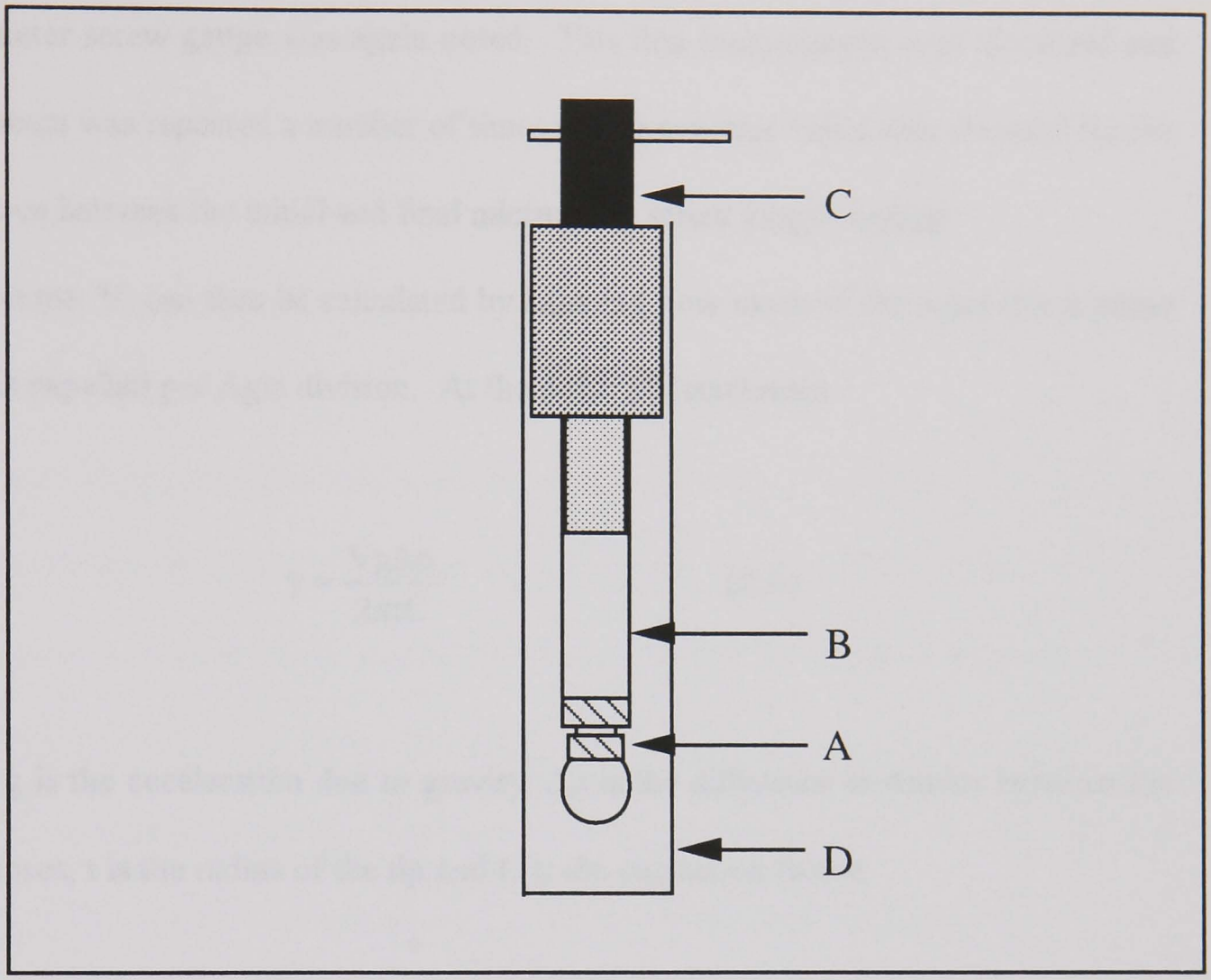

Figure 2.7 Cross-section of the detachment of a drop from the drop volume apparatus

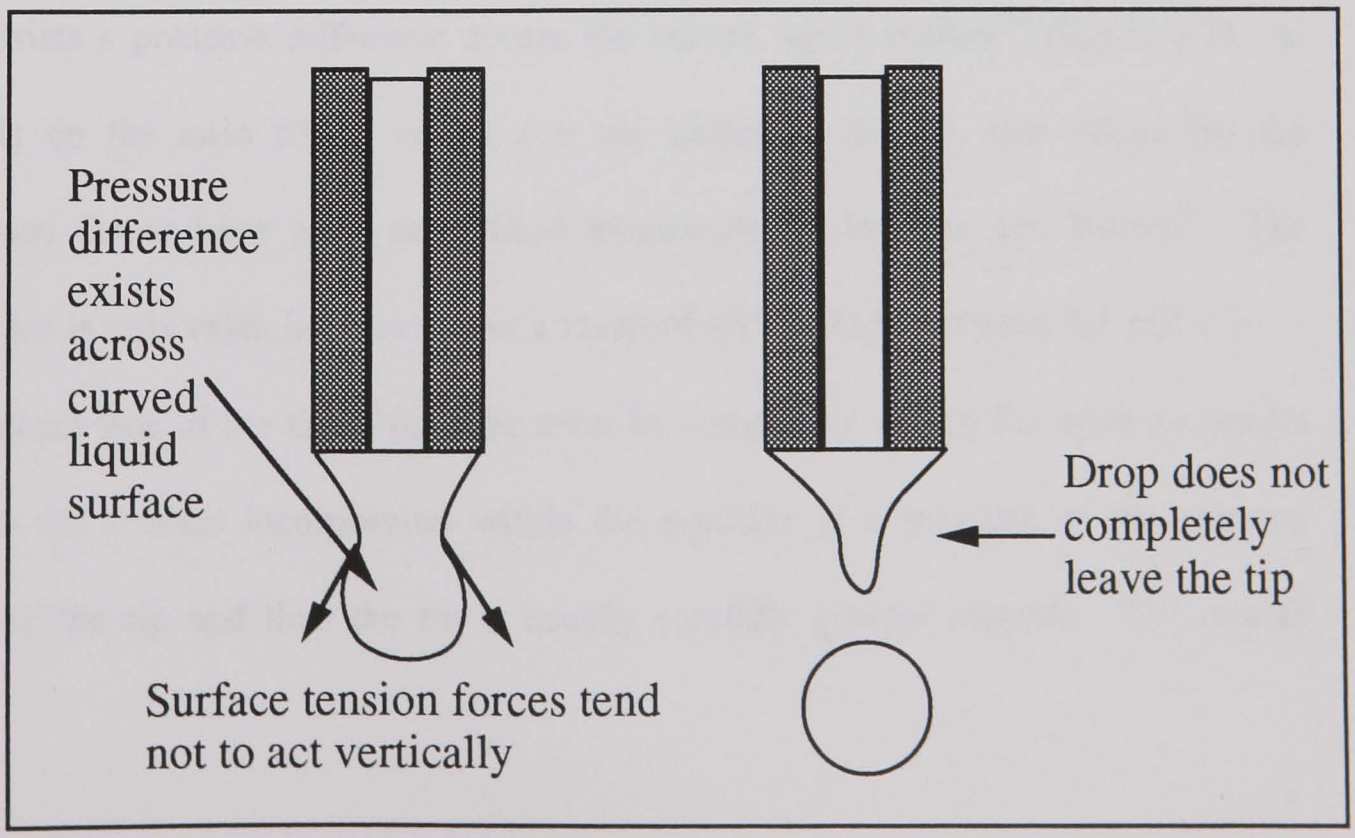

micrometer screw gauge was again noted. This first measurement was discarded and the process was repeated a number of times until a constant value was obtained for the difference between the initial and final micrometer screw gauge reading.

The volume, V, can then be calculated by knowing how much of the more dense phase phase is expelled per Agla division. At the point of detachment

$$\gamma = \frac{Vg\Delta\rho}{2\pi tC} \qquad (2.6)$$

where g is the acceleration due to gravity, $\Delta\rho$ is the difference in density between the two phases, t is the radius of the tip and C is the correction factor.

The correction factor is required because on detachment of the drop, the drop does not completely leave the tip, the surface tension forces are seldom exactly vertical and there exists a pressure difference across the curved liquid surface[14] (figure 2.7). C depends on the ratio $r/V^{1/3}$, where r is the radius of the tip, and values for the correction factor have been determined empirically by Harkins and Brown[9]. The correction is only valid, however, over a range of $r/V^{1/3}$ values between 0.4 and 1.2.

The bottom face of the tip of the tube must be completely wetted for accurate results because the r value incorporated within the equation is a measure of the *external* radius of the tip and thus the tip is usually carefully ground smooth. The overall

reproducibility of the tension values determined by this method was found to be ± 0.2 mN m^{-1}.

2.4.4 The sessile drop technique

The sessile drop technique was used for interfacial tensions between phases which have closely matching densities. The shape of a liquid drop which is lying on a flat surface with a contact angle of 180° is determined by the equilibrium between the action of the gravitational field, which has the tendancy to flatten the drop, and the action of the interfacial tension which tends to make the drop spherical or to create the smallest surface area[15]. The interfacial tension is obtained from the equation

$$\gamma = \frac{\Delta\rho g Z^2 C_{180}}{4} \qquad (2.7)$$

where $\Delta\rho$ is the difference in density between the two phases, g is the acceleration due to gravity, Z is the height of the drop and C_{180} is a correction factor according to Padday and Pitt.[8] A schematic diagram of a sessile drop forming a contact angle of 180° with a solid surface is shown in figure 2.8. A horizontal glass platform, A, was placed into a large, clean glass vessel containing the lighter of the two phases being studied, B. A drop of the more dense phase, C, was formed on the surface of the

Figure 2.8 Schematic diagram of the sessile drop apparatus

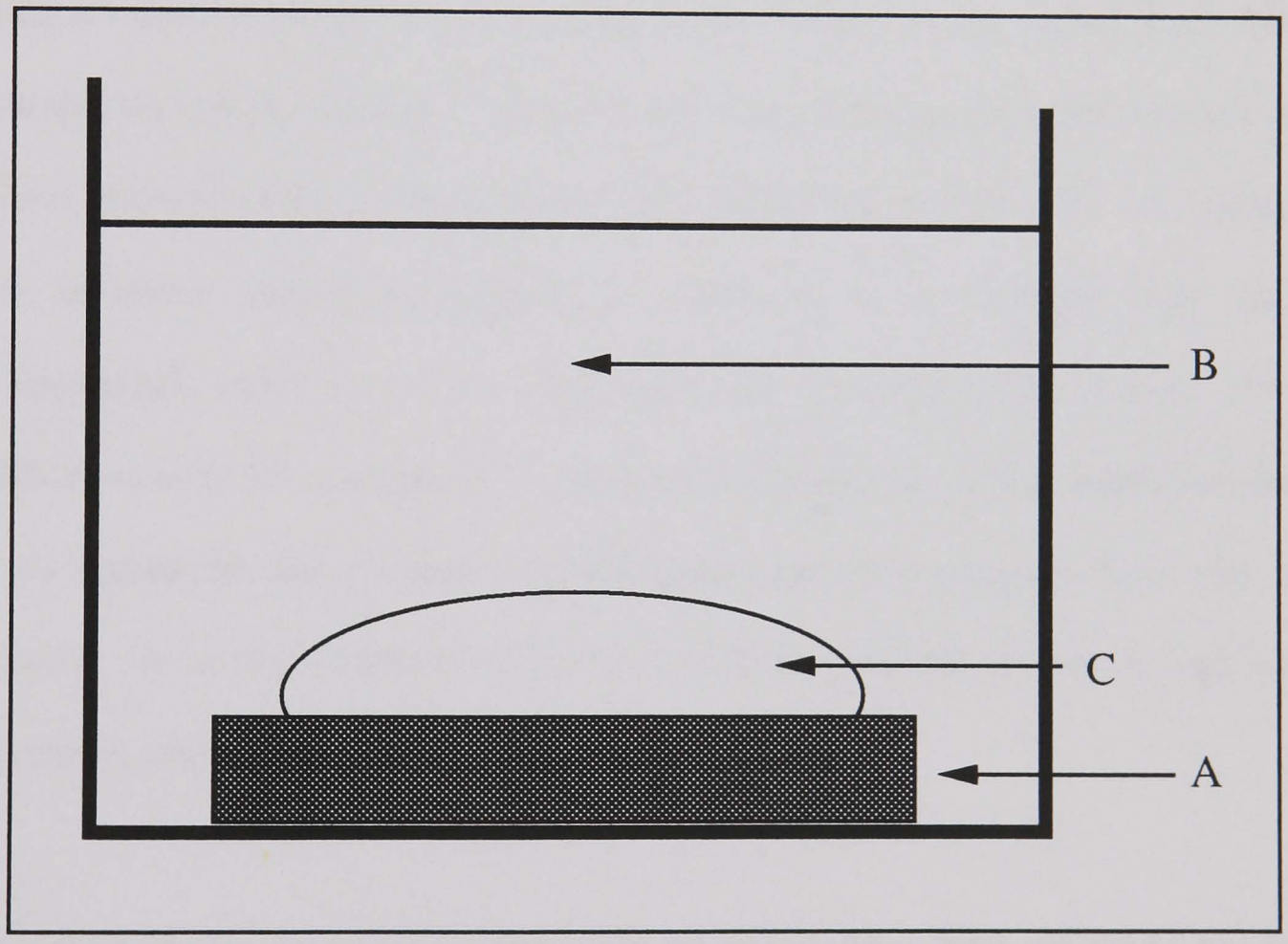

platform and its volume increased until a maximum drop height was reached. The height of the drop was measured with a micrometer connected to a needle, the point of which was viewed through a travelling microscope. The reader is referred to literature[16] for a more in-depth account of the sessile drop method.

2.5 Headspace analysis

Headspace analysis by gas chromatography is the analysis of the vapour phase that exists above a volatile solution. A schematic diagram of the apparatus that was used at Unilever Research, Port Sunlight Laboratories, can be seen in figure 2.9. A Tekmar 7000 automatic headspace analyser is connected to a Finnegan Mat Gas Chromatograph, which in turn feeds information into the computer for analysis. The computer controls the sampling of the headspace, the injection of the sample into the gas chromatograph and processes the subsequent gas chromatograph trace that is produced. Up to twelve sample vessels can be left to equilibrate and run through the apparatus at any one session.

The instrument was set up to determine the oil content of a fixed volume (1 ml) of vapour above an equilibrated liquid sample (1 ml) at a fixed temperature. The volumes of the liquid and the vapour space (21 ml) were kept constant and a schematic diagram of the vessels used can be seen in figure 2.10. The vessel, along with up to twelve others, was placed into the thermostatted headspace analyser and allowed to

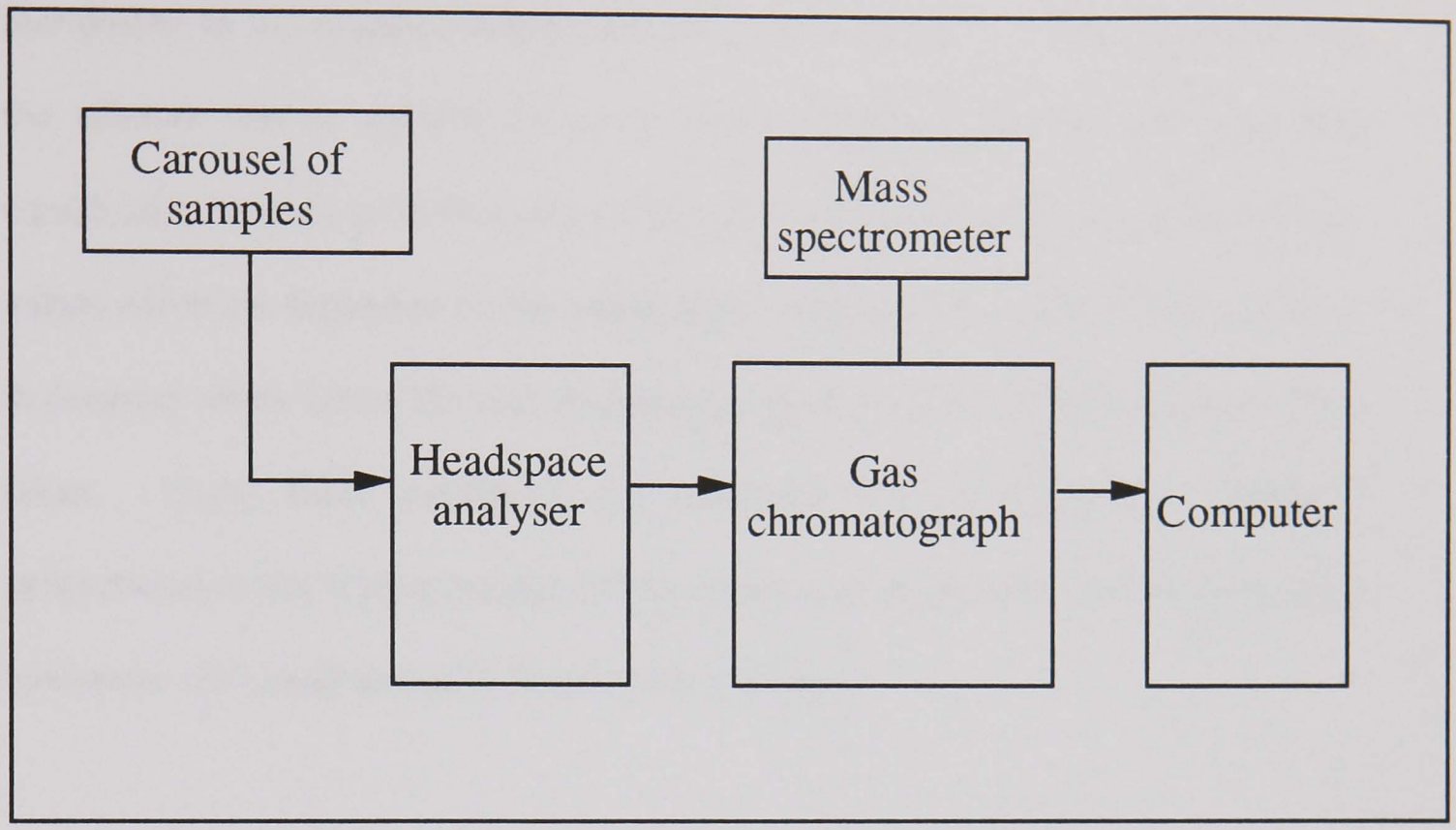

Figure 2.9 Schematic representation of the G.C. Headspace apparatus

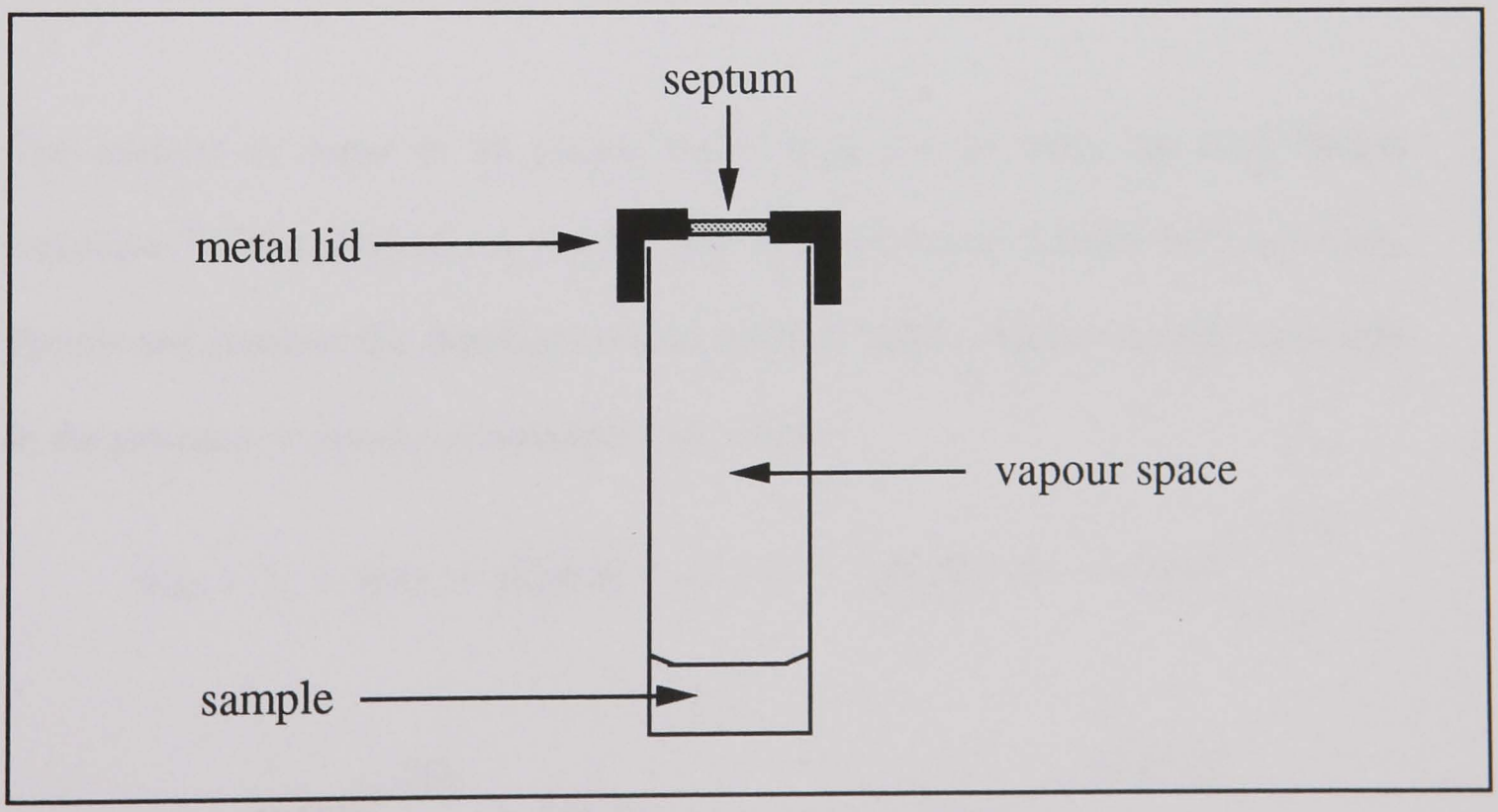

Figure 2.10 Schematic diagram of the vessels used in headspace analysis

thermostatt to the required temperature for at least one hour. After thermostatting, the solution can be agitated for up to thirty minutes. The injection time, loop equilibration time, loop fill time and vial pressurisation time need to be set to optimum values which are dependent on the nature of the sample. The Tekmar 7000 has a built in program which allows the user to determine these prior to any measurements being taken. Under these conditions, the measured detector peak area should be proportional to the vapour pressure of the component of interest. The applications of headspace G.C. analysis can be found in the literature.[17]

2.6 Analytical determinations

2.6.1 Determination of the water content of oil phases

The analysis of water in oil phases was carried out by using the Karl Fischer technique.[18] This method requires the use of a Baird and Tatlock AF3 automatic titrator and involves the chemical reaction between iodine, sulphur dioxide and water in the presence of anhydrous methanol and pyridine.

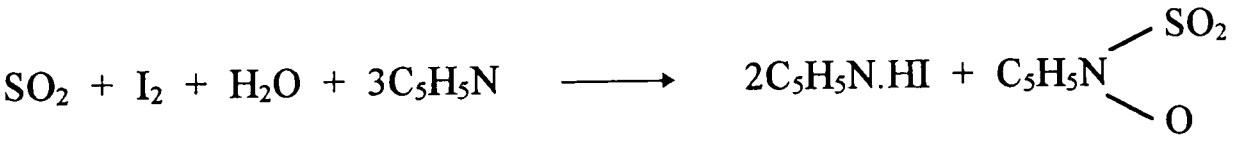

The sample was mixed with a moisture free solvent (methanol) and titrated against Karl Fischer reagent. The endpoint was determined electrochemically.

Calibration was carried out prior to any measurements using pure water to ascertain the particular characteristics of the peristaltic pump used to dispense the reagent. Known weights of the oil phase were then added to the reaction vessel and a digital readout of the milligrams of water present was obtained. The process was repeated at least three times for each sample.

2.7 Additional experimental techniques

2.7.1 Conductivity measurements

The conductivity of emulsions were measured using a Jenway PCM3 digital conductivity meter. The oil and water phases of the microemulsion were stirred and shaken until an emulsion was formed. Measurements of conductivity were then taken once the reading had stabilised.

2.7.2 Density measurements

Densities were measured using a Paar DMA 55 densimeter with a Haake F3-C water thermostatt to control the temperature. The measurements were accurate to ±0.0001 g cm^{-3}.

2.7.3 Refractive index measurements

A thermostatted Abbe refractometer and sodium lamp were used to measure the refractive indices of the thermostatting oil used in the spinning drop tensiometer. Measurements were accurate to ±0.0001.

2.8 Vapour adsorption apparatus

Adsorption isotherms obtained in Chapters 5 and 6 were carried out using a vapour adsorption train after isotherms completed using the addition of lenses to surfactant solutions was discovered to have an unexpected time dependence. The apparatus was built in the laboratory[19] from a design developed at The University of Bristol[20]. A schematic diagram of the vapour train can be seen in figure 2.11. Nitrogen gas flows through the equipment and acts as a carrier gas for the oil being studied. The nitrogen first flows through bubblers which contain the pure oil under investigation. This part

of the equipment is at the highest temperature, higher than the experimental temperature. The saturated nitrogen gas then flows through two glass spirals which are accurately thermostatted. The temperature of these spirals when compared to the experimental temperature determines the activity of the adsorbing oil. When the temperature around the spirals is equal to the experimental temperature, the activity of the adsorbing oil is unity. Activities below unity are obtained by varying the temperature of the spirals between 0°C and the experimental temperature and are calculated using the Antoine equation from constants available in the literature.[21] The vapour then flows through a spiral thermostatted at the experimental temperature and finally to the experimental vessel.

The vapour enters the experimental vessel close to the liquid surface being studied. The tension of the solution is then measured using a du-Nouy ring attached to a Precisa 125A balance which is capable of measuring to 4 decimal places.

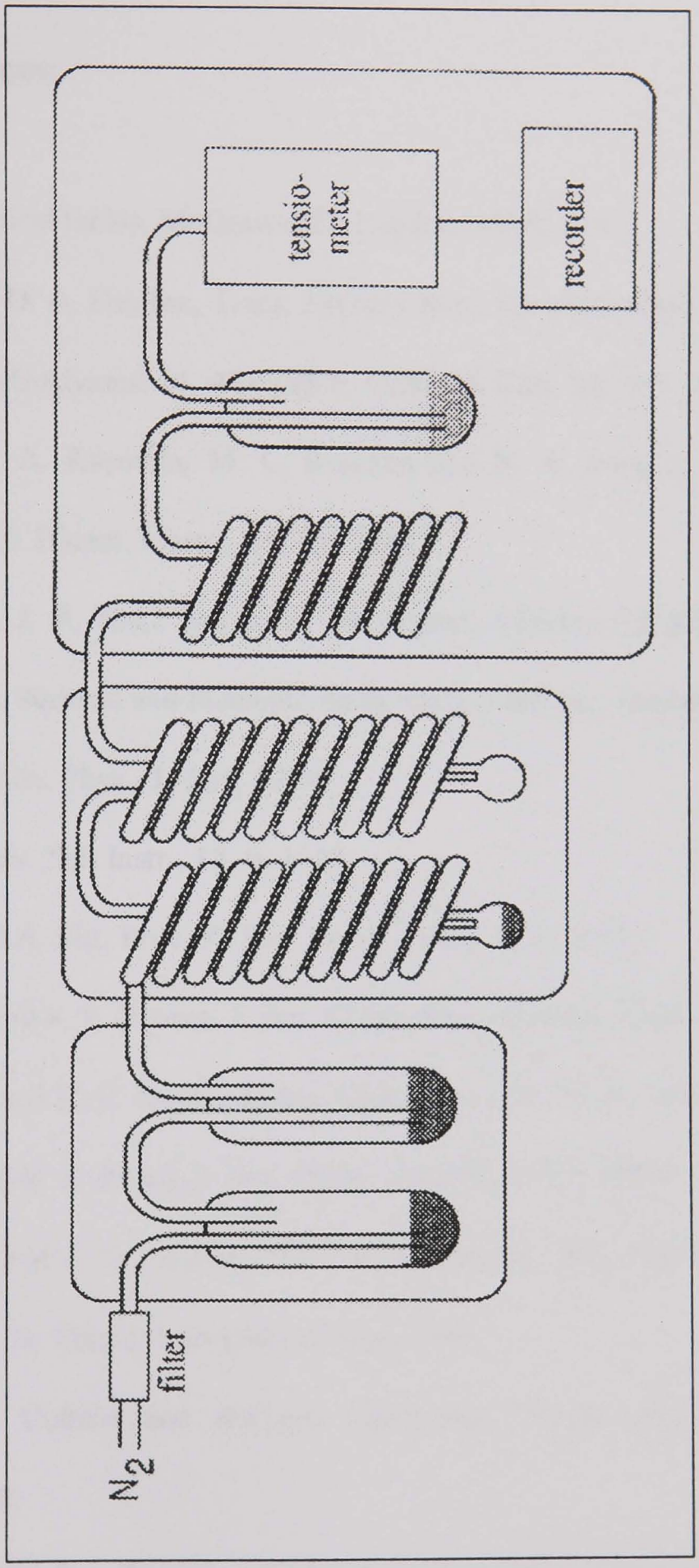

Figure 2.11 Schematic diagram of the vapour adsorption train

2.9 References

[1] International critical tables, McGraw-Hill, London, 1928, **4**, 447.

[2] R. Aveyard and D. A. Haydon, Trans. Faraday Soc., **61**, 2255, 1965.

[3] Y. Tokuoka, H. Uchiyama, M. Abe and K. Ogino, J. Coll. Int. Sci., **152**, 402, 1992.

[4] L. Keneipp, K. A. Korowin, M. L. Brannon and N. A. Peppas, Proceed. Intern. Symp. Control Rel. Bioact. Matter, **15**, 89, 1988.

[5] N. M. Van Os, J. R. Haak and L. A. M. Rupert, Physico-Chemical Properties of Selected Cationic, Anionic and Nonionic Surfactants, Elsevier, Amsterdam, 1993.

[6] L. du Nouy, J. Gen. Phys., **1**, 521, 1919.

[7] B. Vonnegut, Rev. Sci. Instr., **13**, 6, 1942.

[8] J. F. Padday and A. Pitt, Proc. R. Soc. Lond., **A329**, 421, 1972.

[9] W. D. Harkins and F. E. Brown, J. Am. Chem. Soc., **41**, 499, 1919.

[10] W. D. Harkins and H. F. Jordan, J. Am. Chem. Soc., **52**, 1751, 1930.

[11] B. B. Freud and H. Z. Freud, J. Am. Chem. Soc., **52**, 1772, 1930.

[12] H. H. Zuidema and G. W. Waters, Ind. Eng. Chem., **13**, 312, 1941.

[13] B. P. Binks, Ph D. Thesis, University of Hull, 1986.

[14] D. J. Shaw, Colloid and Surface Chemistry, Fourth edition, Butterworth-Heinemannn, 1992.

[15] R. S. Burdon, Surface Tension and the Spreading of Liquids, Chapter 2, C.U.P., Cambridge, 1949.

[16] Paul Kingston, Ph D. Thesis, University of Hull, unpublished

[17] B. Kolb (Ed), Applied Headspace Gas Chromatography, Chapter 1, Heydon & Son, Bristol, 1980.

[18] K. Fischer, Angew. Chem., **48**, 394, 1935.

[19] R. Aveyard, B. P. Binks, D. Crichton and P. D. I. F. Fletcher, unpublished work.

[20] F. Hauxwell, PhD Thesis, University of Bristol, 1969.

[21] R. C. Wilhoit, Handbook of Vapour Pressures and Heats of Vapourisation of Hydrocarbons and Related Compounds, Evans Press, 1971.

Chapter 3

CHAPTER 3

WORK OF ADHESION BETWEEN OILS + WATER AND SURFACE ACTIVITY OF THE PERFUME OILS AT THE HEPTANE-WATER INTERFACE

3.1 Introduction

Interactions between perfume oils and surfactants are important in a number of practical applications which include perfume delivery systems in fabric softeners. Perfume oils of relevance are generally moderately polar water-insoluble species such as limonene, eugenol, cineole, linalyl acetate and linalool (the oils used in this study). In this chapter, prior to the study of surfactant containing systems, the work of adhesion between these perfume oils and water was studied with a view to deriving the enthalpies and entropies of adhesion which offer information about the relative polarity of these oils and some insight into the nature of the oil-water interface in the case of oil species of moderate polarity.

It is also of importance to assess the surface activity[1,2] of the perfume (polar) oils prior to any work being carried out in the presence of surfactants to evaluate their ability to act as cosurfactants. This was done here by studying the variation in interfacial tension of a heptane-water interface, as the perfume oil was added, by using drop volume tensiometry.

3.2 Introduction to the uses of perfume oils and some relevant background information

The perfume oils used in this work have a number of applications which can be seen in the literature.[3] A brief overview of their uses and fragrant properties is contained below.

Limonene is a colourless liquid with a fresh, light and sweet citrusy odour which bears a strong resemblance to orange peel oil. It is used extensively in perfume compositions, particularly in fragrances for household products and is one of the most inexpensive perfume materials. Limonene is produced by the redistillation of citrus oil obtained from sweet orange.

Linalool is also a colourless liquid and has a light and refreshing, floral wood odour. Linalool is used extensively in perfume compositions of almost all types and price

levels and has now grown above the million pound a year mark for production. It is used frequently in blueberry, lemon, lime and other fruit formulations and is produced by isolation from Bois de Rose oil although several synthetic methods of preparation can be utilised.[3]

Linalyl acetate has a very similar molecular structure to that of linalool (see figure 2.1) and is produced naturally by isolation from Bois de Rose oil although, as with linalool, there are several synthetic methods available.[3] It has a sweet floral-fruity odour and is used as an additive to perfume compositions which are rich in Bergamot or Lavender.

Cineole or eucalyptol is the most widely distributed perfume of those used in this study. Because of its refreshing, eucalyptus-like odour, it is extensively used in medicinal odours for soaps and household products as well as in all types of preparations for oral hygiene such as breath-sprays, mouth washes and cough lozenges.

Eugenol is a colourless or very pale yellow oily liquid. It's powerful, spicy, sharp odour makes it ideal for use in incense, oriental fragrances and other spicy compositions. Eugenol is prepared by isolation from clove leaf oil.

3.3 Temperature dependence of the density, surface tension and interfacial tension with water of the perfume oils

Very little information concerning the perfume oils used in the study was available in the literature. The densities of the perfume oils and how they varied with temperature are required for tension measurements. This work was carried out by using the Paar densimeter and the results are shown in figure 3.1.

Figure 3.2 shows the temperature dependence of the solubility of water within the perfume oils measured with the use of the Karl Fischer apparatus. Due to the polar nature of the perfume oils it was expected that the solubilities would be significant. However, for all temperatures studied the solubilities were sufficiently low to be disregarded in this work.

3.4 Quantifying the interactions between water and oils

Surfactant adsorption at an oil-water interface can be expected to depend on the nature of the oil, although little systematic information on this is available in the literature. Polar oils are expected to interact more strongly with interfacial water than non-polar oils such as alkanes[4].

Figure 3.1 Density versus Temperature for the Perfume Oils

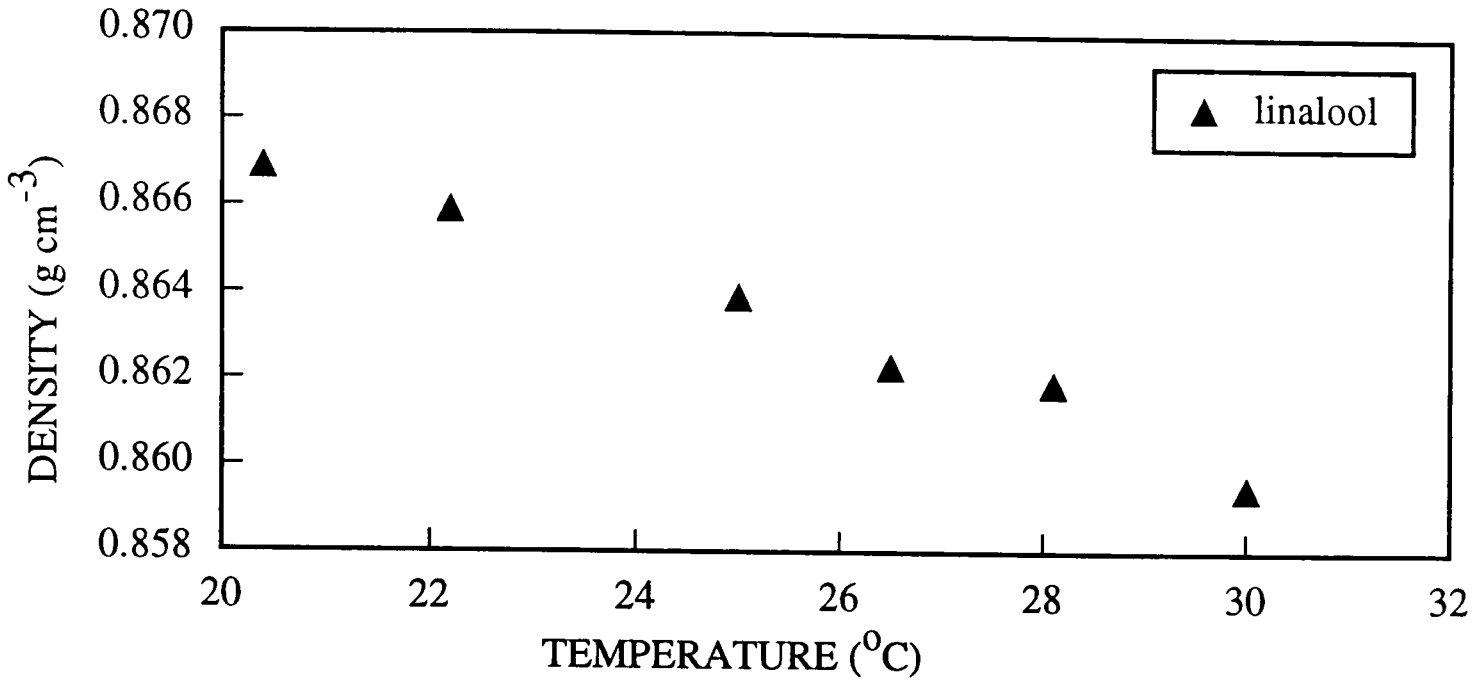

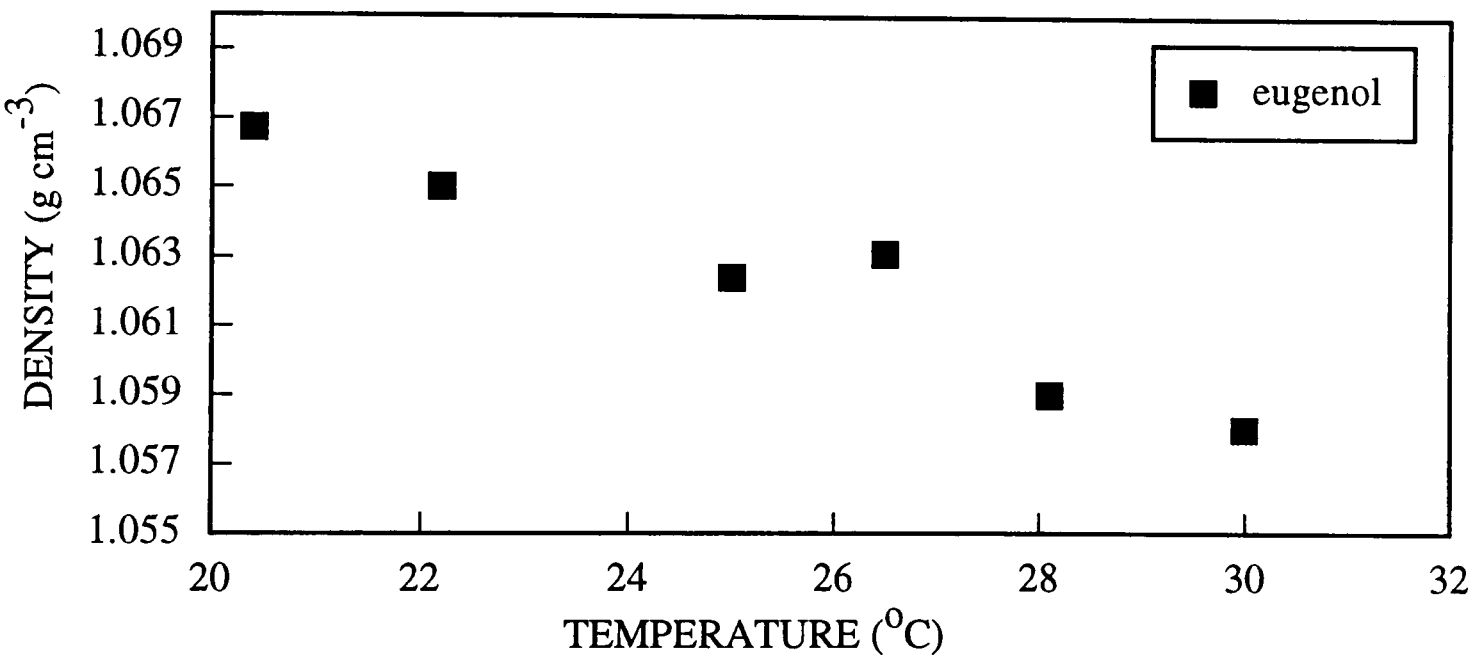

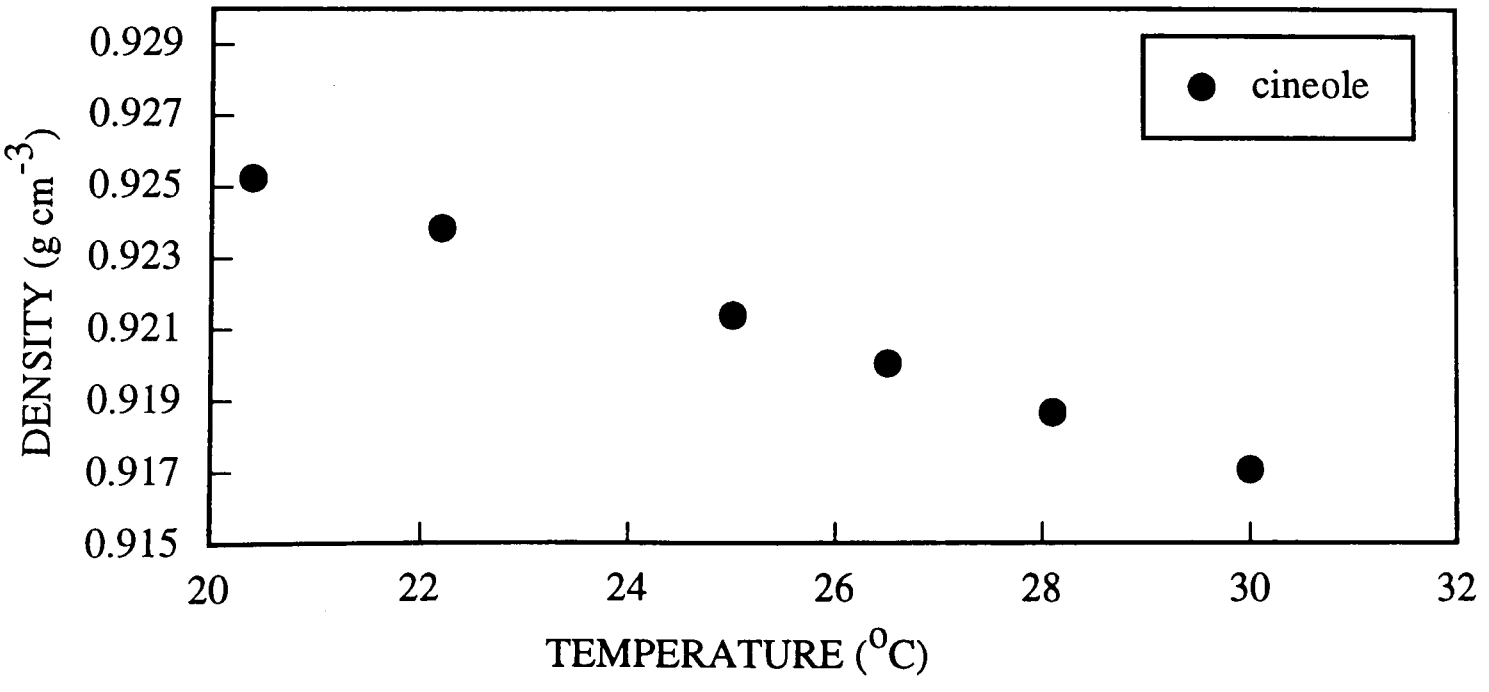

Figure 3.2 Solubility of water in the oil phase versus temperature for 3 of the perfume oils

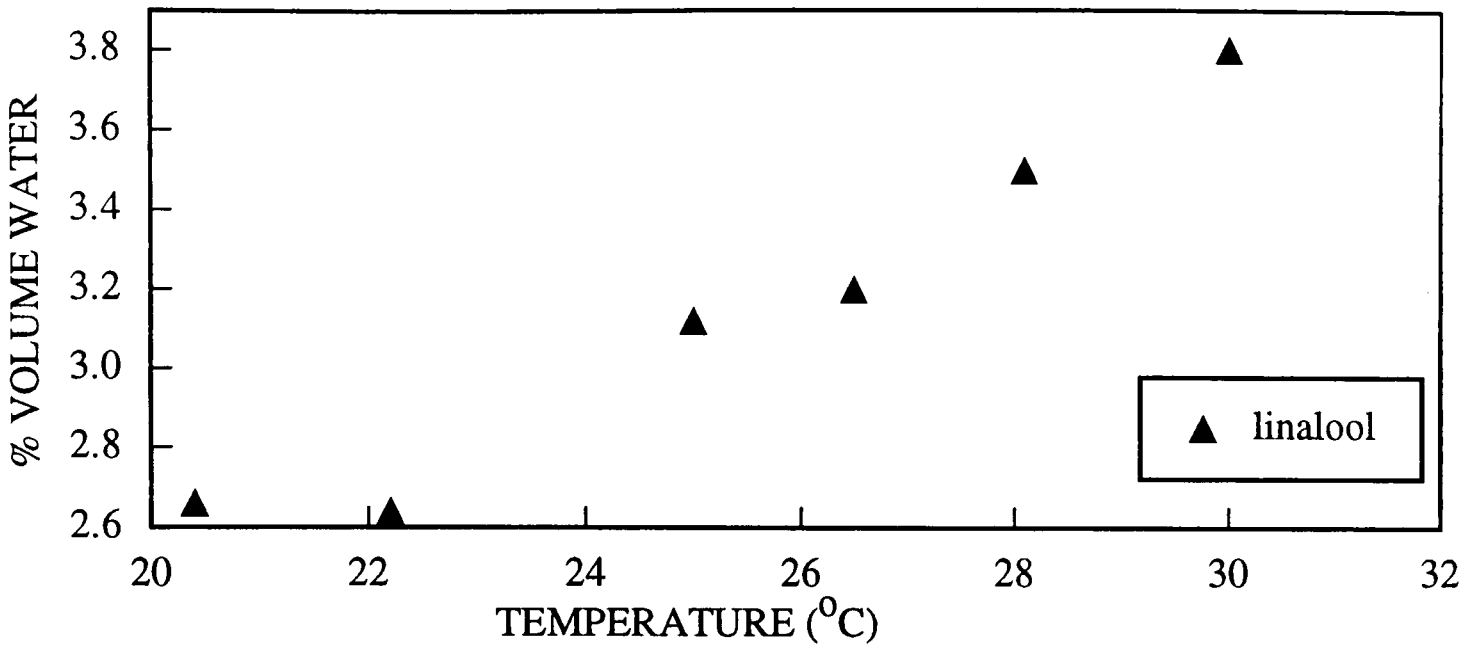

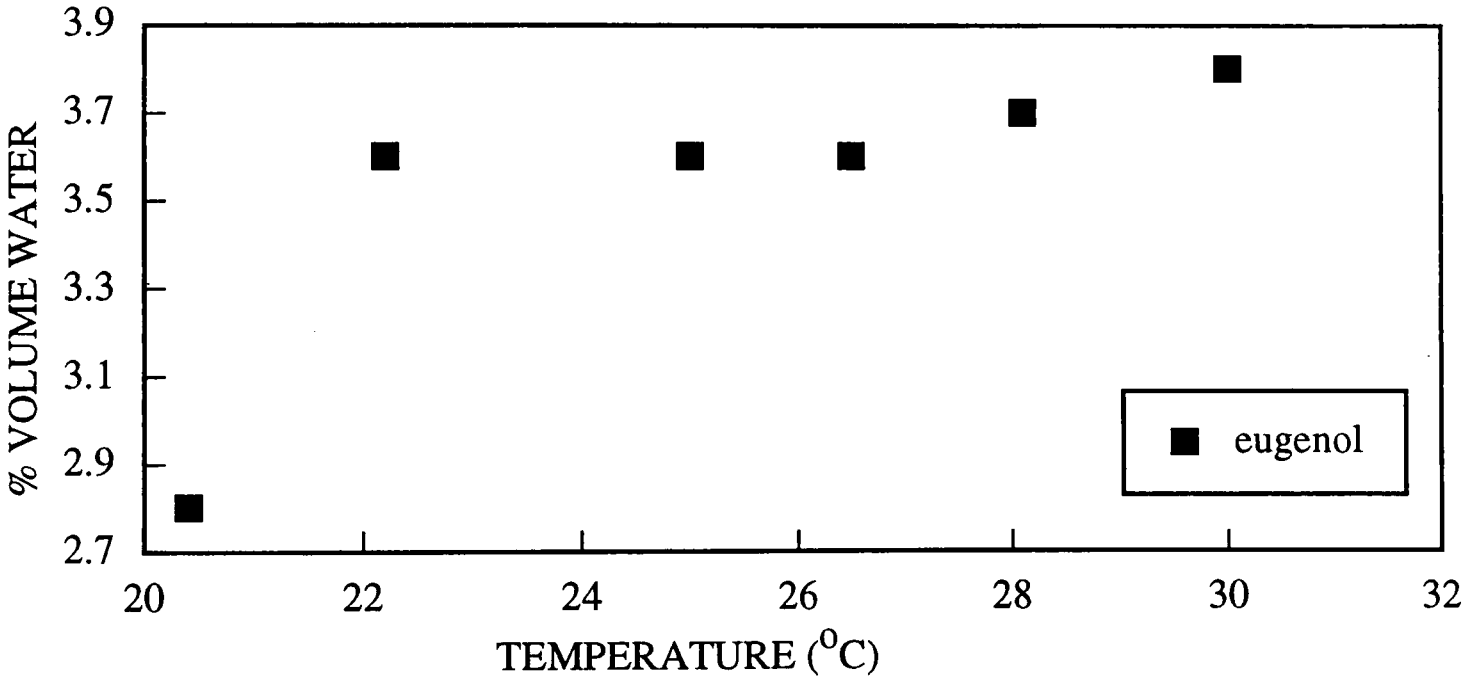

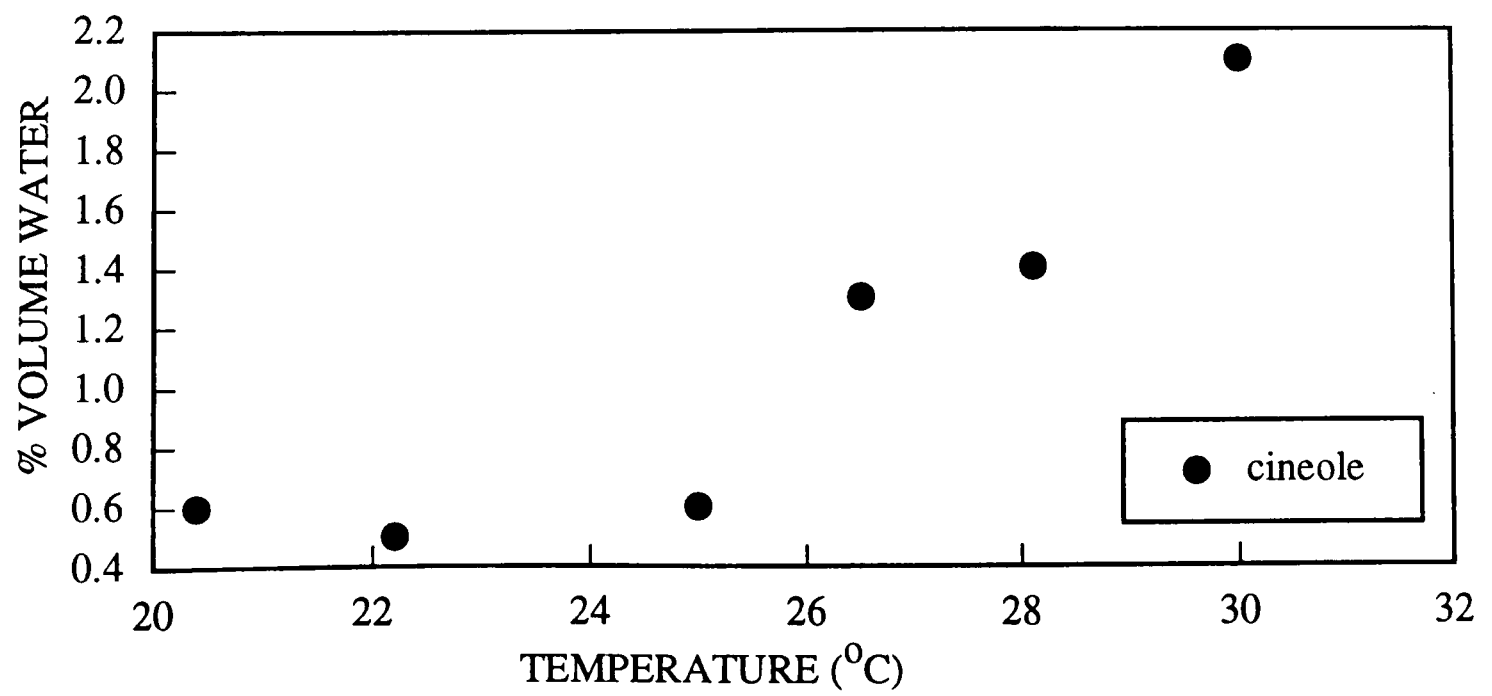

The strength of the interaction can be quantified in terms of the reversible work of adhesion, W_A, existing between the two liquids. If we suppose that a column of liquid α with unit cross sectional area is resting on a similar column of liquid β, giving unit area of $\alpha\beta$ interface with an interfacial tension $\gamma_{\alpha\beta}$ (figure 3.3 shows a schematic diagram representing the mechanics involved in the work of adhesion[5]), the reversible work required to part the two columns, so as to form unit surface areas of α and β (the work of adhesion), is given by the Dupré equation[6]

$$W_A^{\alpha\beta} = \gamma_\alpha + \gamma_\beta - \gamma_{\alpha\beta} \qquad (3.1)$$

It is found that the work of adhesion between water and oil increases as the polarity of the oil increases. Since surfactant adsorption at the polar oil-water interface requires the displacement of the oil from the interface, it is expected that an increased work of adhesion should lead to a decrease in the surface activity of the surfactant that is present. Any reduced tendancy for surfactant adsorption or competitive adsorption by the oil will obviously have consequences for solubilisation and phase behaviour in oil + water + surfactant systems.

Figure 3.3 **Schematic diagram representing the mechanics of work of adhesion**

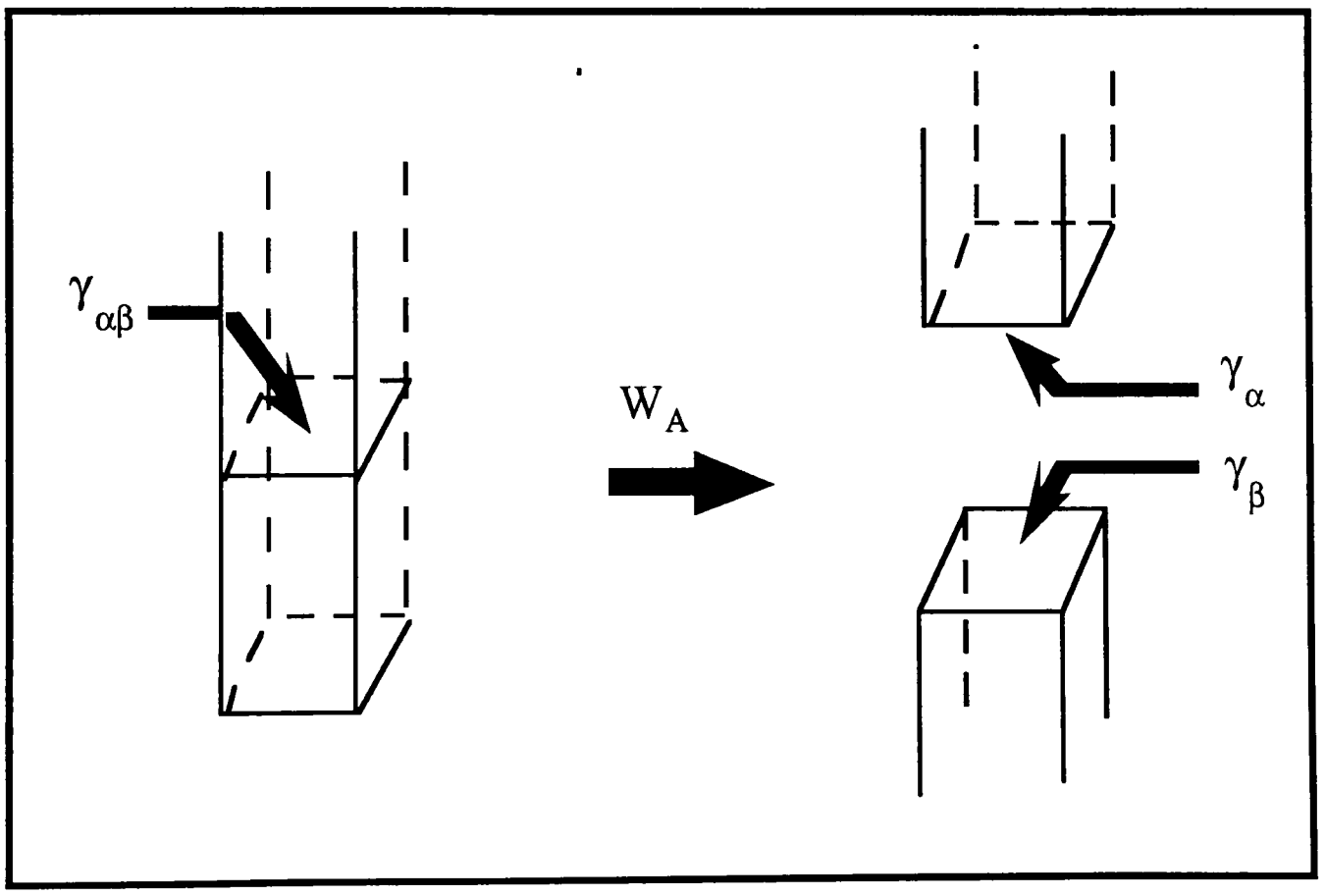

3.5 Work of adhesion between oils and a polar phase as a measure of the polarity of the oil

3.5.1 Changes in work of adhesion associated with varying the polarity of the oils

The aim of this stage of the study was to investigate where typical perfume oils 'fitted in' to a range of oils as judged by the work of adhesion between the oils and a range of polar solvents, including water. The work of adhesion between a range of oils of varying polarities and either water or glycerol was measured. Figure 3.4 shows the data obtained in the form of a plot of work of adhesion against interfacial tension between the two liquids. The tensions were measured by the drop volume technique or, for closely density matched liquids, by the sessile drop technique. The two data sets shown approximately follow two parallel lines of slopes close to -1. It can be seen from the results that an increase in the polarity of a liquid causes the work of adhesion to increase and the interfacial tension with either water or glycerol to decrease. From the intercepts of the plots with the y-axis (102 and 92 mJ m^{-2} for water and glycerol respectively) and by inspection of the definition of work of adhesion, it can be seen that the data for a series of oils with either water or glycerol is expected to follow a linear dependence with slope -1 if the oil-air tension is equal to 30 mN m^{-1}. The difference in intercepts between the glycerol plot and the water plot arises since the water-air and glycerol-air tensions are 72 and 63 mN m^{-1} respectively. Deviations

Figure 3.4 Work of Adhesion versus Interfacial Tension for oil/water and oil/glycerol systems at 25^{0}C

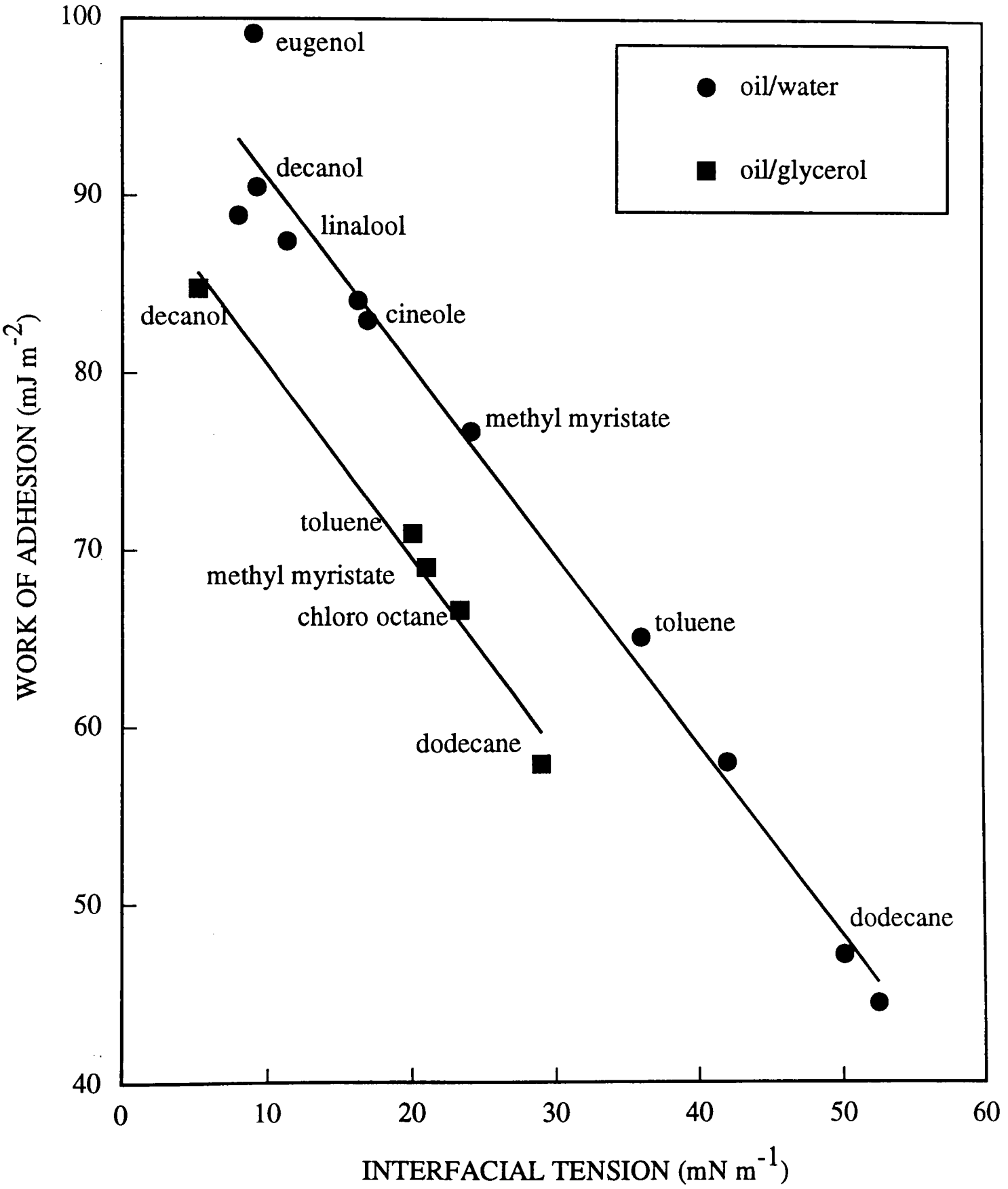

from linearity are associated with oils which have a surface tension which is different to 30 mN m^{-1}. From the study, it was shown that eugenol is one such oil, with a surface tension of 36 mN m^{-1}.

3.5.2 Changes in work of adhesion associated with varying the polar phase

Figure 3.5 is a similar plot to that seen in figure 3.4 but in this case only two oil phases are studied in combination with a range of polar phases. It can be seen from figure 3.5 that the work of adhesion is almost invariant with interfacial tension, staying constant at about 68 mN m^{-1} for toluene and 57 mN m^{-1} for dodecane.

The difference in these values arises partly from the difference in tension values for dodecane-air (24.9 mN m^{-1}) and toluene-air (27.9 mN m^{-1}) but mainly from differences in the oil-polar liquid tensions for the two oils. The reason for the consistent value for work of adhesion for these oils is due to the fact that any variation in surface tension of the polar liquids is generally accompanied by an equal change (within 5 mN m^{-1} or so) in the interfacial tension with either dodecane or toluene. The exception being water where the interfacial tension with dodecane shows a much larger variation than the surface tension value, giving a reduced value for work of adhesion.

Figure 3.5 **Work of Adhesion versus Interfacial Tension for dodecane/polar phase and toluene/polar phase systems at 25^0C**

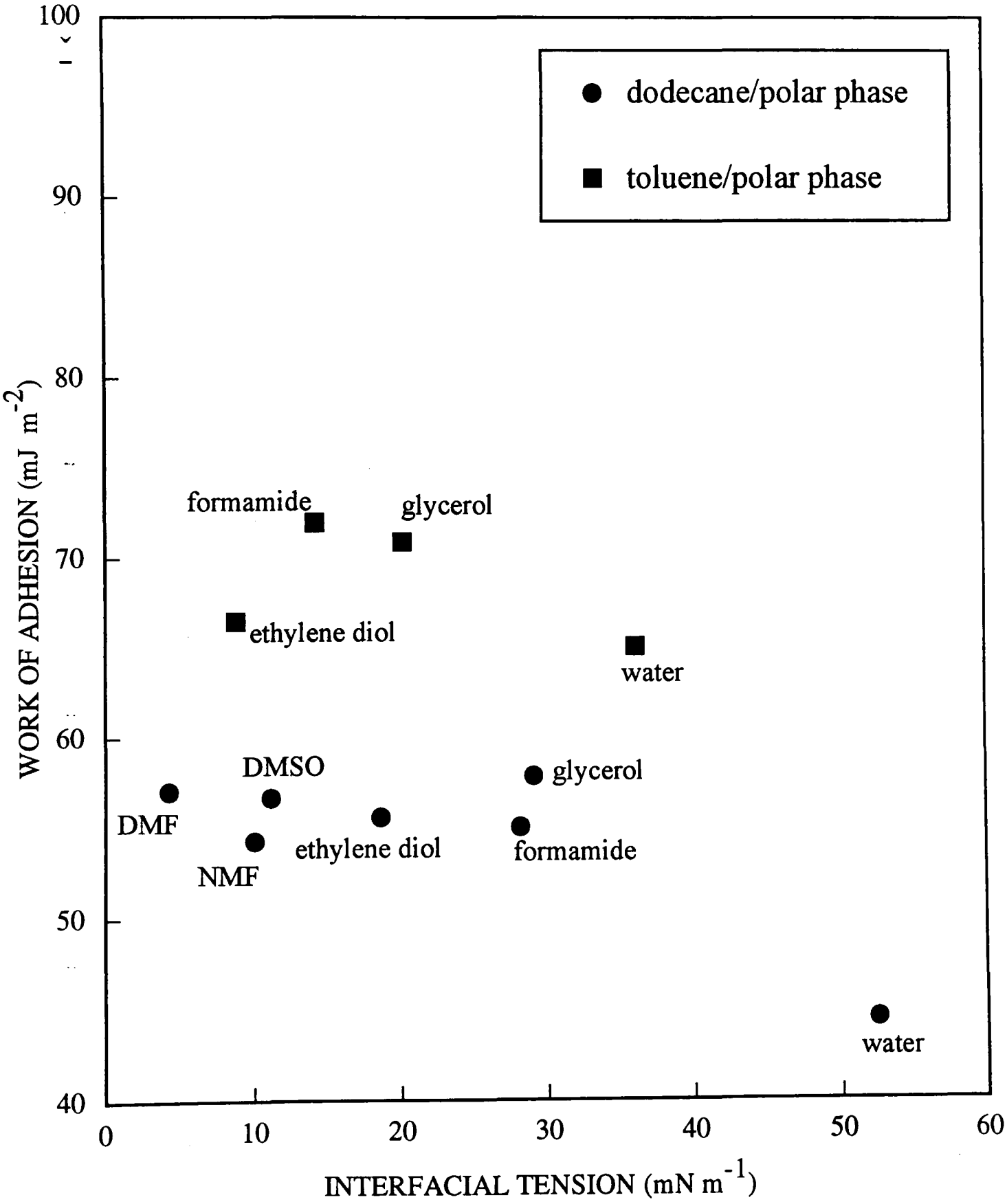

The results of this section show that the perfume oils 'fit in' as polar oils on a work of adhesion versus interfacial tension graph. With the exception of eugenol, they lie along a straight line of slope -1.

3.6 Temperature dependence of work of adhesion for the polar oils with water

Figures 3.6 and 3.7 show the temperature dependence of surface tension and interfacial tension with water for three of the perfume oils measured by the drop volume technique. It follows from the definition of work of adhesion in the Dupré equation, that the rate of change of work of adhesion with temperature can be expressed as

$$dW_A/dT = d\gamma_{oil}/dT + d\gamma_{water}/dT - d\gamma_{oil\text{-}water}/dT \qquad (3.2)$$

and it can be seen from figures 3.6 and 3.7 that, over a narrow temperature range, the various tensions studied decrease linearly with increasing temperature and thus the temperature dependence of work of adhesion can be represented by an equation of the form

$$W_A = A - BT \qquad (3.3)$$

Figure 3.6 Surface tension versus temperature for three of the perfume oils

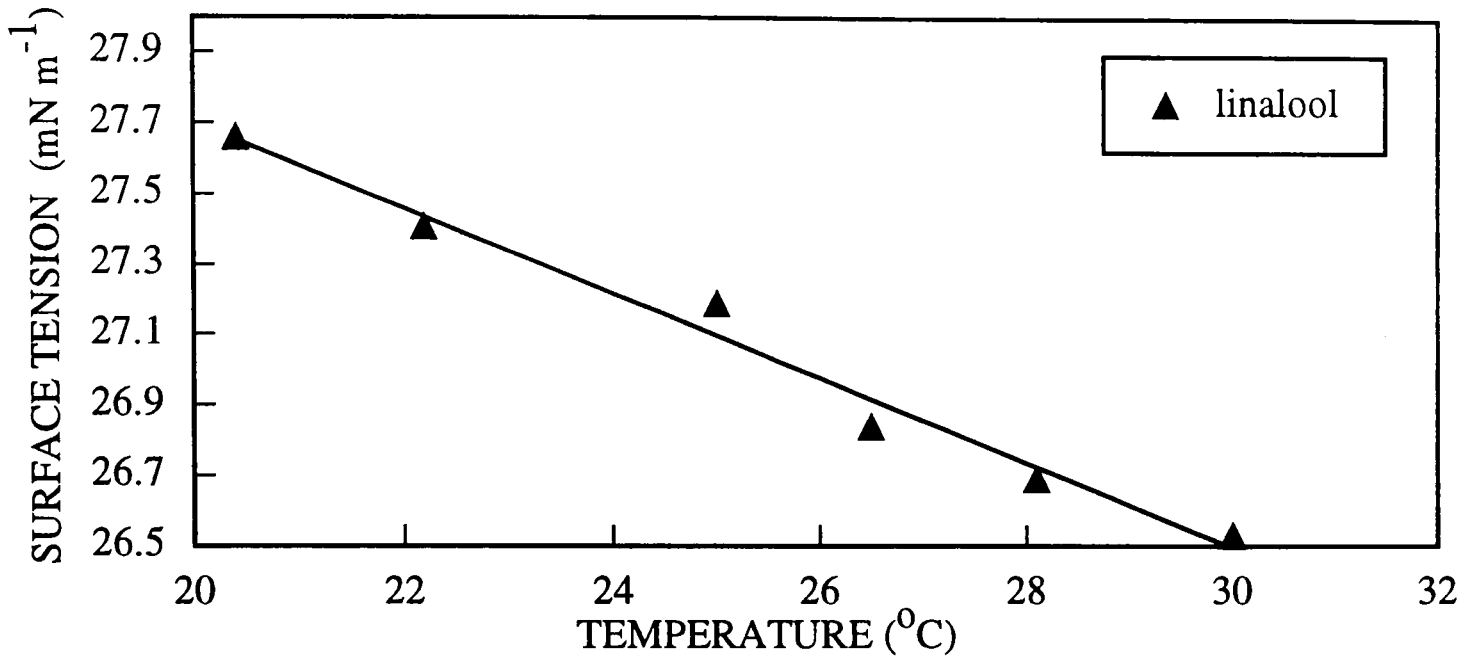

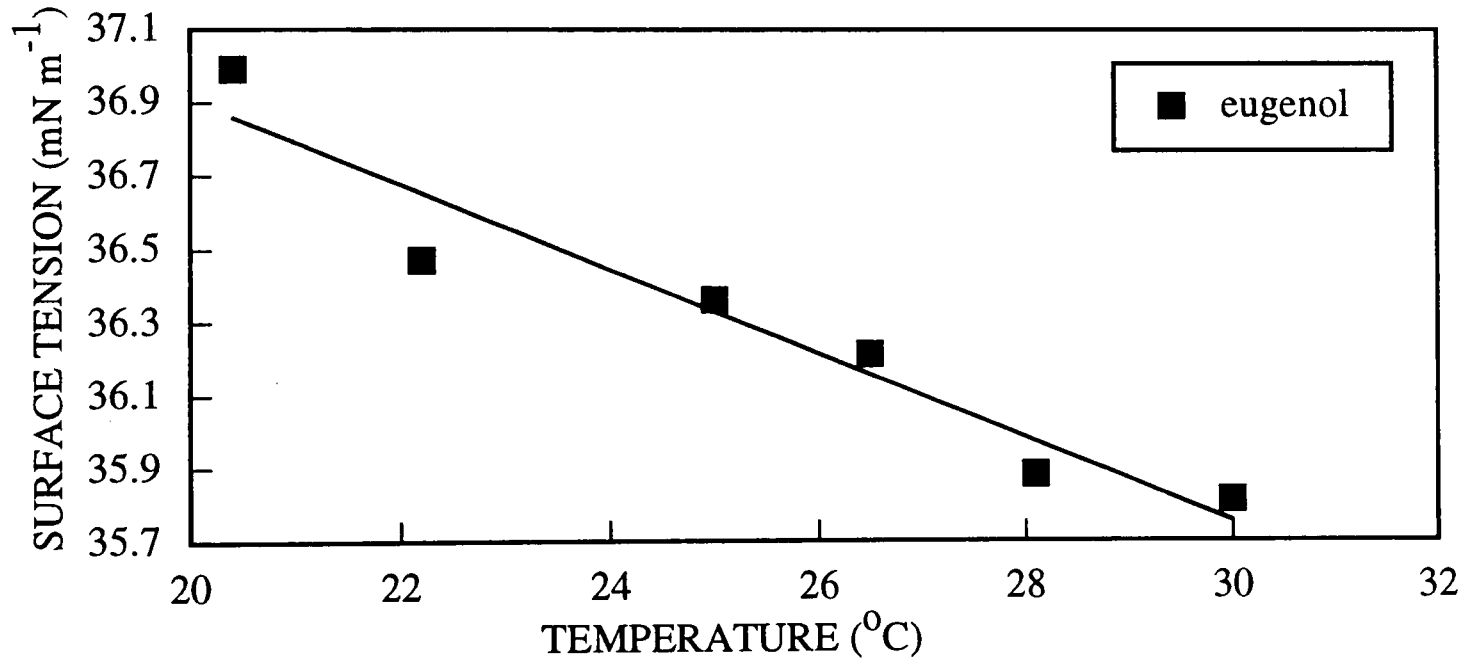

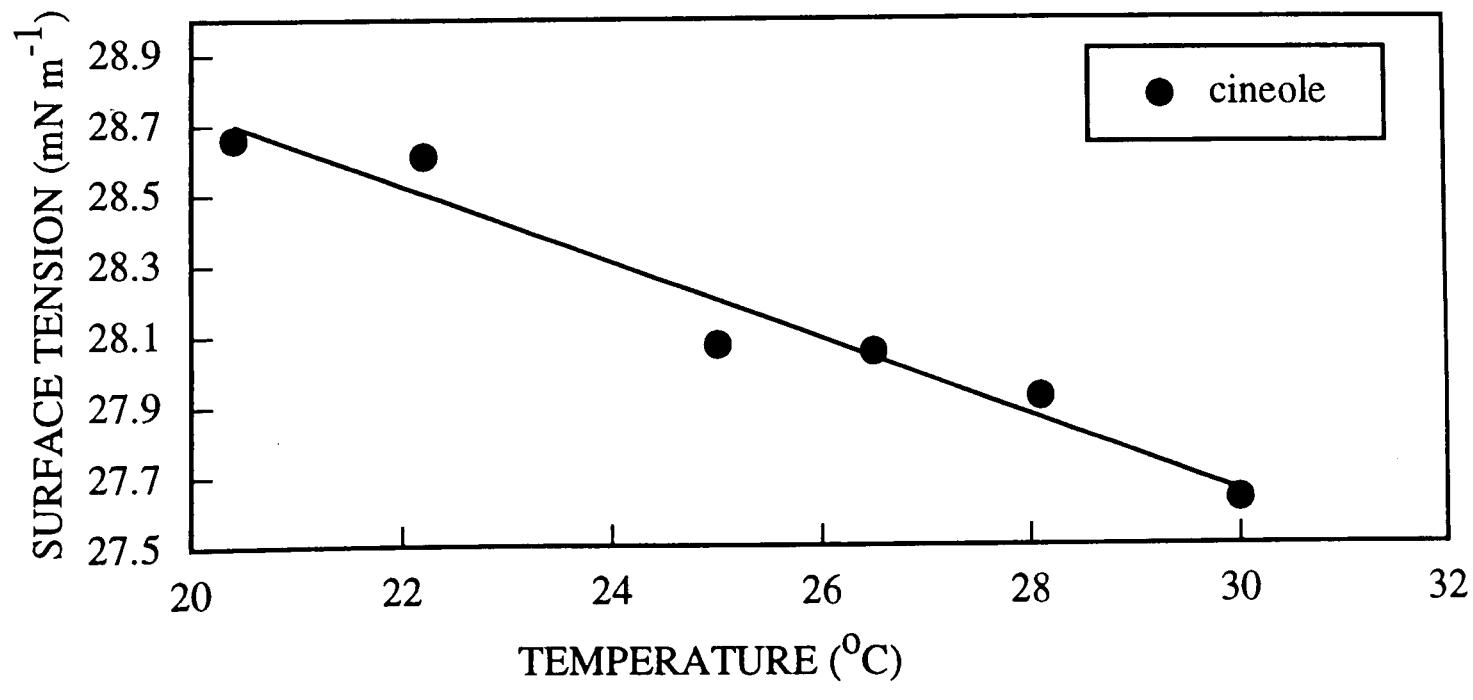

Figure 3.7 **Interfacial tension with water versus temperature for three of the perfume oils**

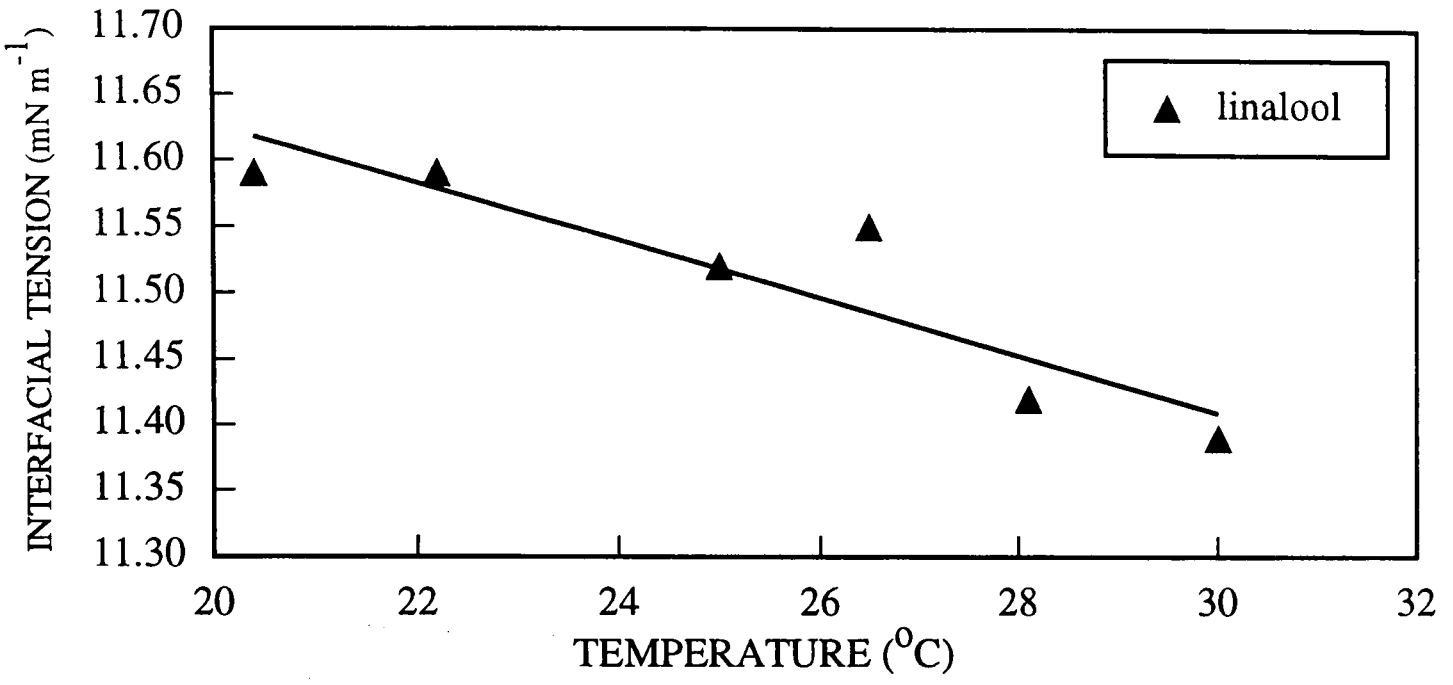

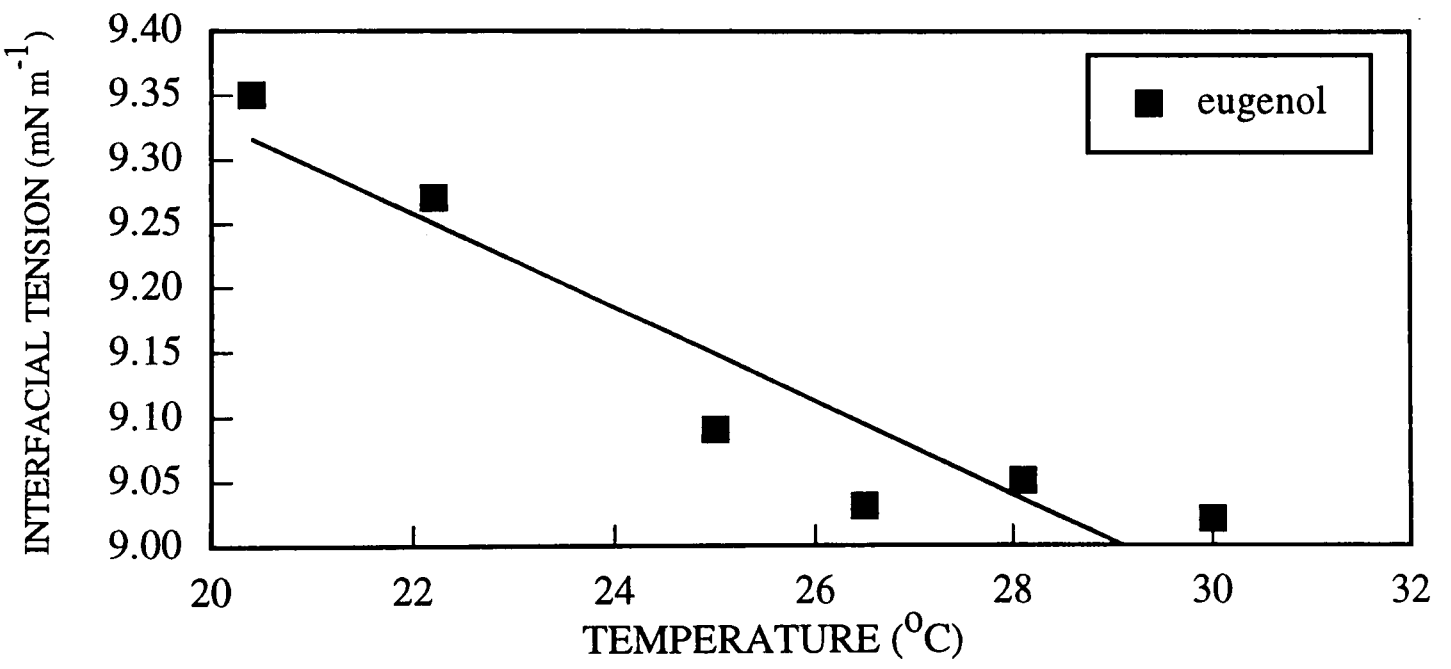

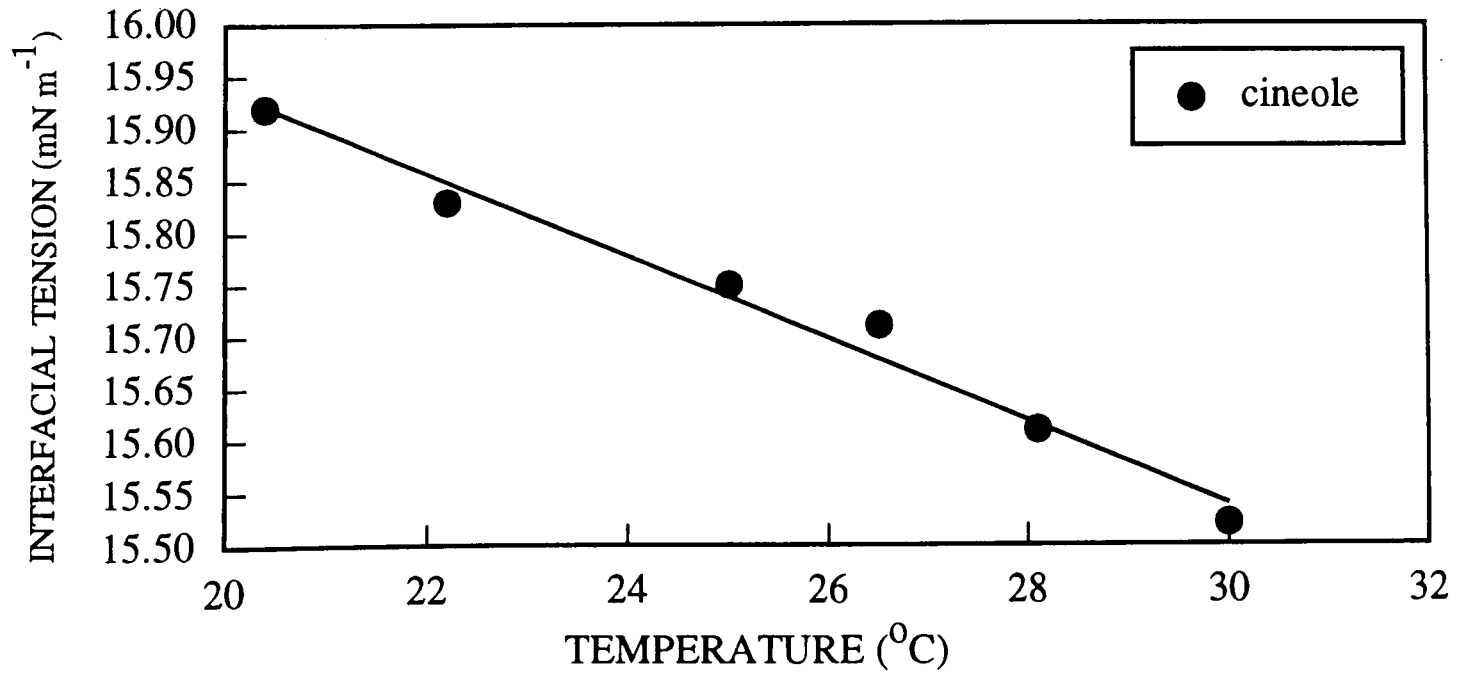

where T is the temperature in Kelvin. This can then be compared to an equation of the form $\Delta G = \Delta H - T\Delta S$ and thus the constants A and -B can be equated with the enthalpy and entropy of separating unit area of the liquid interfaces.

The slopes of the plots shown in figures 3.6 and 3.7 and the derived values of the enthalpies and entropies of adhesion are collected together in table 3.1.

Table 3.1 Values of the gradients for the tension graphs and the derived enthalpies and entropies of adhesion.

Oil	$d\gamma_{oil}/dT$ (mN m^{-1} $°C^{-1}$)	$d\gamma_{oil\text{-}water}/dT$ (mN m^{-1} $°C^{-1}$)	A (mJ m^{-2})	-B (mJ m^{-2} K^{-1})
Linalool	-0.12±0.02	-0.02±0.01	164±10	0.26±0.03
Eugenol	-0.12±0.02	-0.04±0.01	171±10	0.24±0.03
Cineole	-0.11±0.02	-0.04±0.01	153±10	0.23±0.03

3.6.1 Comparing enthalpies of adhesion with values available in the literature

The enthalpies of adhesion for the polar oils are comparable with the values for a range of methyl esters of alkanoic acids of chain lengths varying from six to fourteen with water (162 mJ m^{-2})[7] and for decanol-water (183 mJ m^{-2})[7], due to the presence of attractive interactions of the polar groups across the interface. The values are considerably higher than for alkane-water interfaces for which the value is 92 mJ m^{-2}.[7] The three values measured for the polar oils are within the experimental error of each

other but the ranking order observed (eugenol>linalool>cineole) seems intuitively reasonable in terms of the polar groups present in each molecule. That is, an hydroxy and methoxy group in eugenol, a hydroxy group in linalool and a cyclic ether linkage in cineole.

3.6.2 Area per linalool molecule at the oil-water interface

The enthalpy of adhesion for linalool can be used to derive a crude estimate of the area per linalool molecule at the oil-water interface. It is assumed here that the enthalpy of adhesion is mainly associated with the transfer of the hydroxyl group from the oil phase to an aqueous environment when adsorbed at the interface. It is known that the enthalpy per mole of hydroxy transferred is approximately 31 kJ mol^{-1}.[4] Similar values are measured either for partitioning of short chain alcohols between dilute solution in alkanes and water or for the enthalpy of adsorption of octanol from dilute solution in dodecane to the oil-water interface.[4]

Assuming that this value of 31 kJ mol^{-1} applies to the case of adhesion of linalool to water (although linalool might be expected to give a lower value due to hydrogen bonding with other linalool molecules in the bulk oil), then the measured enthalpy of adhesion per unit area (E_{ad}, in units of mJ m^{-2}) can be used to estimate the average area per linalool molecule at the oil-water interface. The relevant equation is

$$A = 310/6.02\ E_{ad} \qquad (3.4)$$

where A is the area per molecule (units of nm^2 $molecule^{-1}$) and E_d is in mJ m^{-2}. This treatment yields an approximate area per linalool molecule of 0.31 nm^2, slightly higher than the value estimated for a straight chained alcohol (octanol at the dodecane water interface gives 0.24 nm^2 by applying the Volmer surface equation of state to the interface)[4]. The value obtained for linalool seems reasonable when compared to the octanol value due to the extra bulkiness associated with the linalool molecule. It can thus be seen that the adhesion studies can provide some insight into the nature of the polar oils at the oil-water interface.

3.7 Adsorption of the perfume oils to the heptane-water interface

3.7.1 Adsorption from dilute solution in heptane to the heptane-water interface

To assess the surface activity and possible co-surfactant behaviour of the polar oils, their adsorption at the heptane-water interface was investigated by using drop volume tensiometry.[8] In order to apply the Gibbs adsorption equation[9] to estimate the surface concentration of the oils, the variation of interfacial tension with polar oil activity in one of the bulk phases is required. Experimentally, the variation of tension with initial polar oil concentration in the heptane phase was measured. The problem then arises that the concentration in the heptane phase, upon equilibration with the water phase,

may not be the same as the initial concentration due to partitioning of the perfume oil into the aqueous phase.

The extent of this partitioning into the water phase was estimated by making interfacial tension measurements at different heptane-water volume ratios. In this way, it was expected that, if partitioning occurred, decreasing interfacial tensions would be obtained for increasing volume ratios of oil:water. Differing volume ratios of water and heptane containing a constant concentration of polar oil were shaken together to achieve an equilibrium distribution of the polar oil between the two phases at 25°C and the interfacial tension between the phases was determined. The results for linalool and eugenol are shown in figure 3.8. It can be seen that, for eugenol, the interfacial tension is independent of the volume fraction of the two phases indicating that no significant partitioning of eugenol into the water phase occurs. Hence, the initial concentration of eugenol can be equated with the equilibrium concentration. For linalool, however, the interfacial tension is reduced as the volume ratio (oil:water) is increased up to a volume ratio of 10:1, suggesting a significant degree of partitioning into the water phase. Above volume ratios of 10:1, the interfacial tension remains constant. It is therefore evident that, for linalool, volume ratios higher than 10:1 must be used to enable the equilibrium oil phase concentration to be equated with the initial

Figure 3.8 **Interfacial Tension of a Heptane/water system versus O/W volume/volume ratio for Eugenol and Linalool at constant initial concentration in the oil phase**

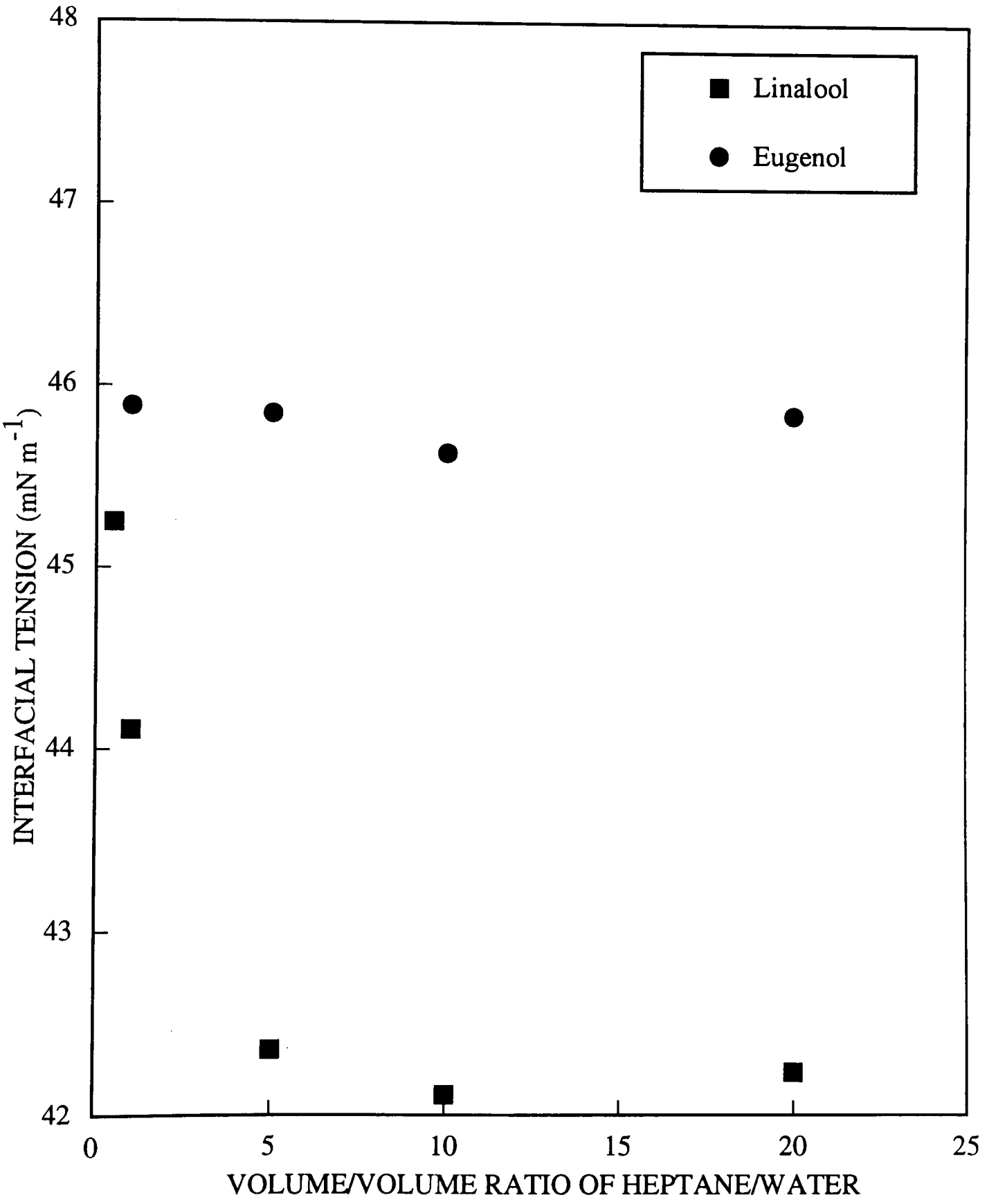

value. Figure 3.9 shows plots of how the interfacial tension of a heptane-water interface varies as the concentration of linalool in the heptane is increased for different volume ratios. The plots do not overlay because of the partitioning effects, but for both volume ratios, the interfacial tension decreases as more linalool is added to the heptane suggesting that linalool is surface active. It is also clear that the same is true for eugenol as can be seen in figure 3.10 although in this case no difference in adsorption is observed at different volume ratios due to the lack of partitioning to the aqueous phase.

3.7.2 Calculation of the partition coefficient of linalool between heptane and water

Figure 3.9 can be used to obtain the partition coefficient for linalool between the heptane and water at an oil water ratio of 1:1. This is carried out by measuring the interfacial tension of both ratios of oil water at different concentrations of linalool. A horizontal line is then drawn from the value obtained for the 1:1 ratio until it reaches the 20:1 oil:water ratio curve at a lower concentration of linalool. This is the actual concentration of linalool in the aqueous phase and thus the partition coefficient can be calculated. Figure 3.11 shows a plot of the concentration of linalool in the aqueous phase against the concentration of linalool in the heptane phase. It can be seen that the plot is not linear, therefore the partition coefficient is not constant across the entire concentration range and the linalool solutions are behaving non-ideally. At a low

Figure 3.9 **Interfacial Tension of a Heptane/water system versus ln[Linalool] for 1:20 and 1:1 oil:water volume/volume ratio**

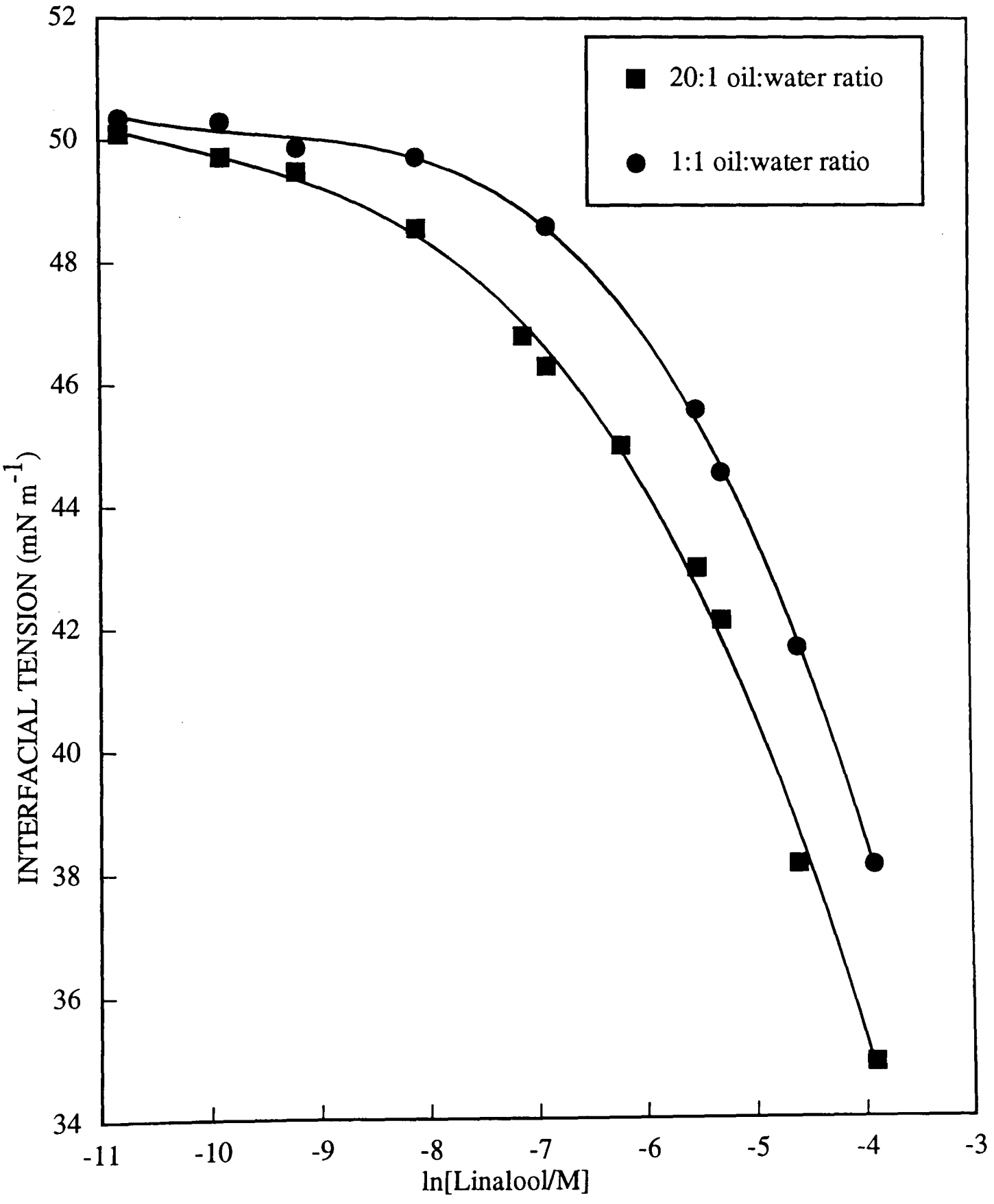

Figure 3.10 **Interfacial Tension of a Heptane/water system versus $\ln[\text{Eugenol}]_{oil}$ ($\ln[\text{Eugenol}]_{initial}=\ln[\text{Eugenol}]_{eq}$ since no variation with O/W volume/volume ratio)**

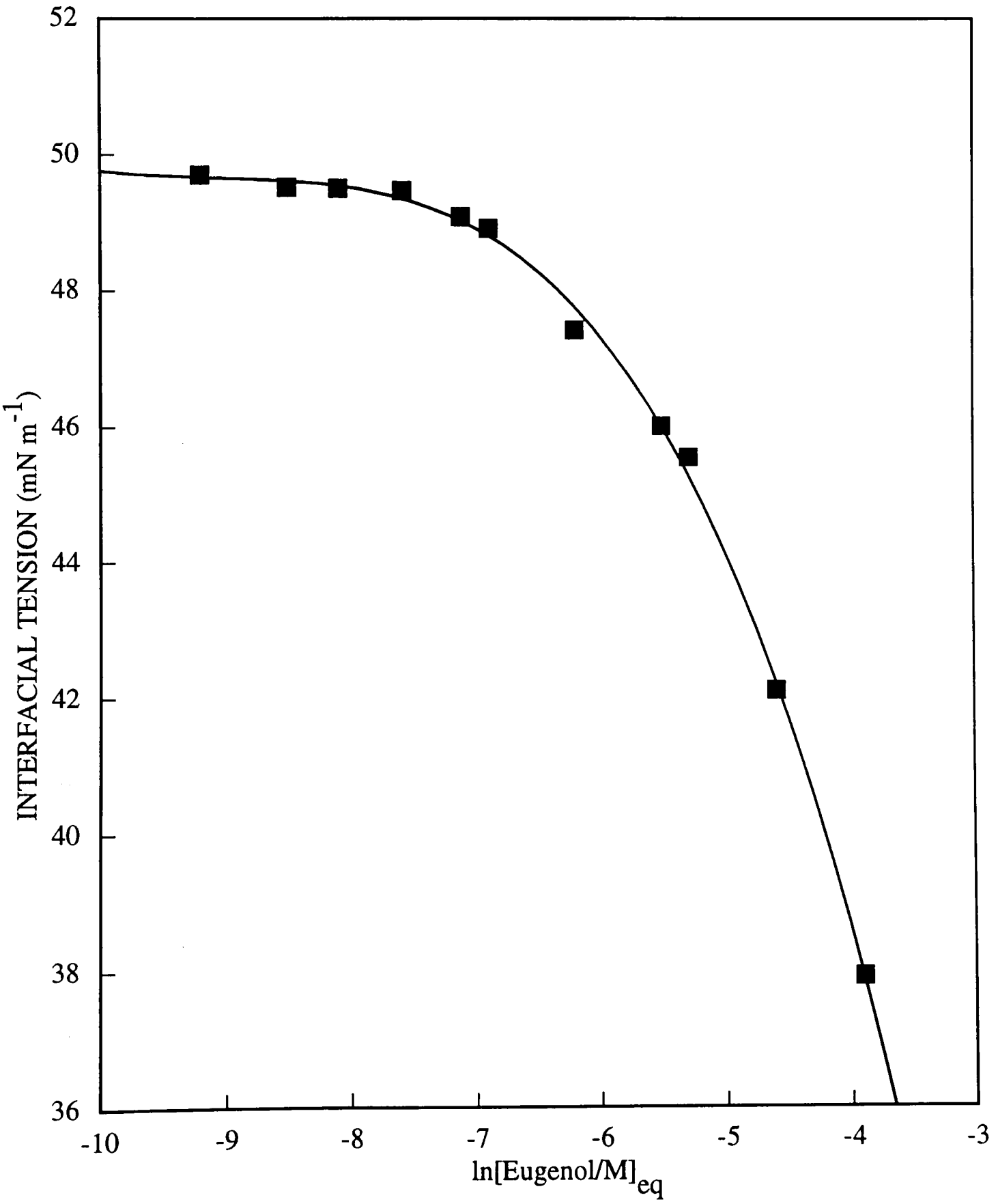

Figure 3.11 **Concentration of linalool present in the aqueous phase against concentration of linalool present in the heptane phase at 1:1 oil:water volume ratio**

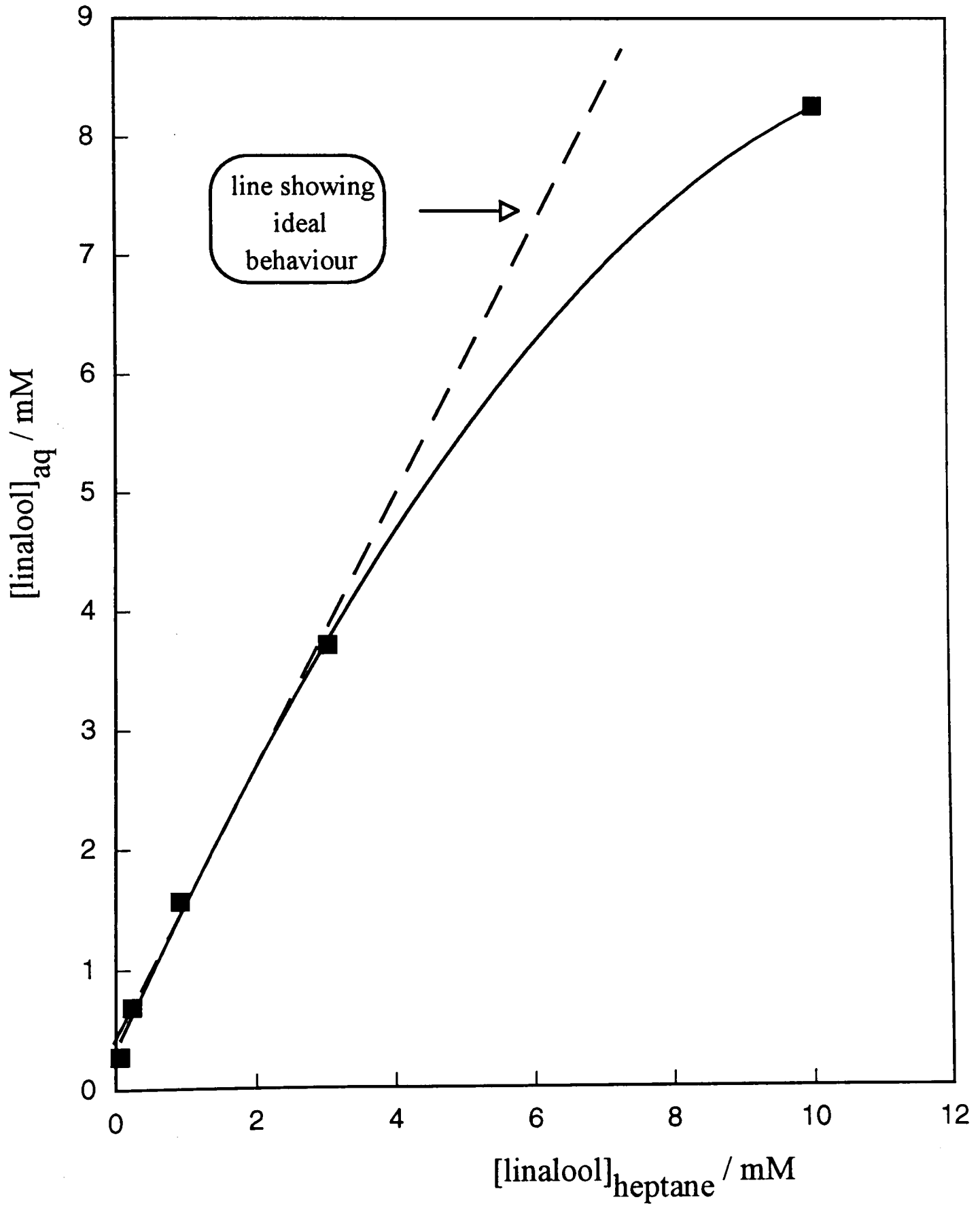

concentration of linalool in heptane (1mM), the partition coefficient (P), defined in equation 3.5, has a value of 1.56. At a higher concentration (9mM), it has a value of 0.88.

$$P = \frac{[\text{linalool}]_{\text{water}}}{[\text{linalool}]_{\text{heptane}}} \qquad (3.5)$$

3.7.3 The application of surface equation of states to the perfume oils adsorption to the heptane/water interface

The surface pressure (Π), in mN m^{-1}, which is the difference between the interfacial tension before addition of the perfume oil and the interfacial tension at a particular concentration of perfume oil can be plotted against the area per perfume oil molecule (A) in $Å^2$. Equation 3.6 shows the surface equation of state for the relationship between Π and A for an adsorbed oil film behaving as an ideal 2-dimensional gas.

$$\Pi A = kT \qquad (3.6)$$

Using figures 3.9 and 3.10, the form of the Gibb's equation shown in equation 1.1 and the fact that the area per molecule at the interface is the reciprocal of the surface excess concentration (Γ), the area per molecule at different concentrations of

adsorbing perfume oil can be determined. It has already been shown that linalool behaves non-ideally with respect to partition coefficients (especially at higher concentrations) and so assuming concentration can be equated with activity, as shown in equation 1.1, is not strictly correct. However, since activity coefficients are not available for these systems, it is a neccesary assumption. This data allows the surface equation of state of the film to be compared with various models. The ideal surface equation of state (equation 3.6) doesn't allow for interactions between adsorbing molecules nor does it account for the physical size of the molecules. The Volmer equation is a modified form of equation 3.6 which allows for the finite size of the adsorbing molecules by incorporating a term A_0 (the excluded area) but still makes no account for the interactions between adsorbing molecules. This can be seen in equation 3.7.

$$\Pi(A-A_0) = kT \qquad (3.7)$$

Figure 3.12 shows the surface pressure versus area per molecule plots for eugenol and linalool at the heptane-water interface. A Volmer plot has been fitted to both sets of data giving excluded area terms for eugenol and linalool of 24 $Å^2$ and 48 $Å^2$ respectively. Also shown is the plot relating to the ideal surface equation of state. It can be seen from figure 3.12 that the data observed for perfume oils does not fit precisely to a Volmer plot and at lower surface pressures they are forming expanded films (giving a higher area per molecule than the Volmer plot). This discrepency could

Figure 3.12 **Surface pressure versus area per molecule for the perfume oils adsorbing at the heptane/water interface**

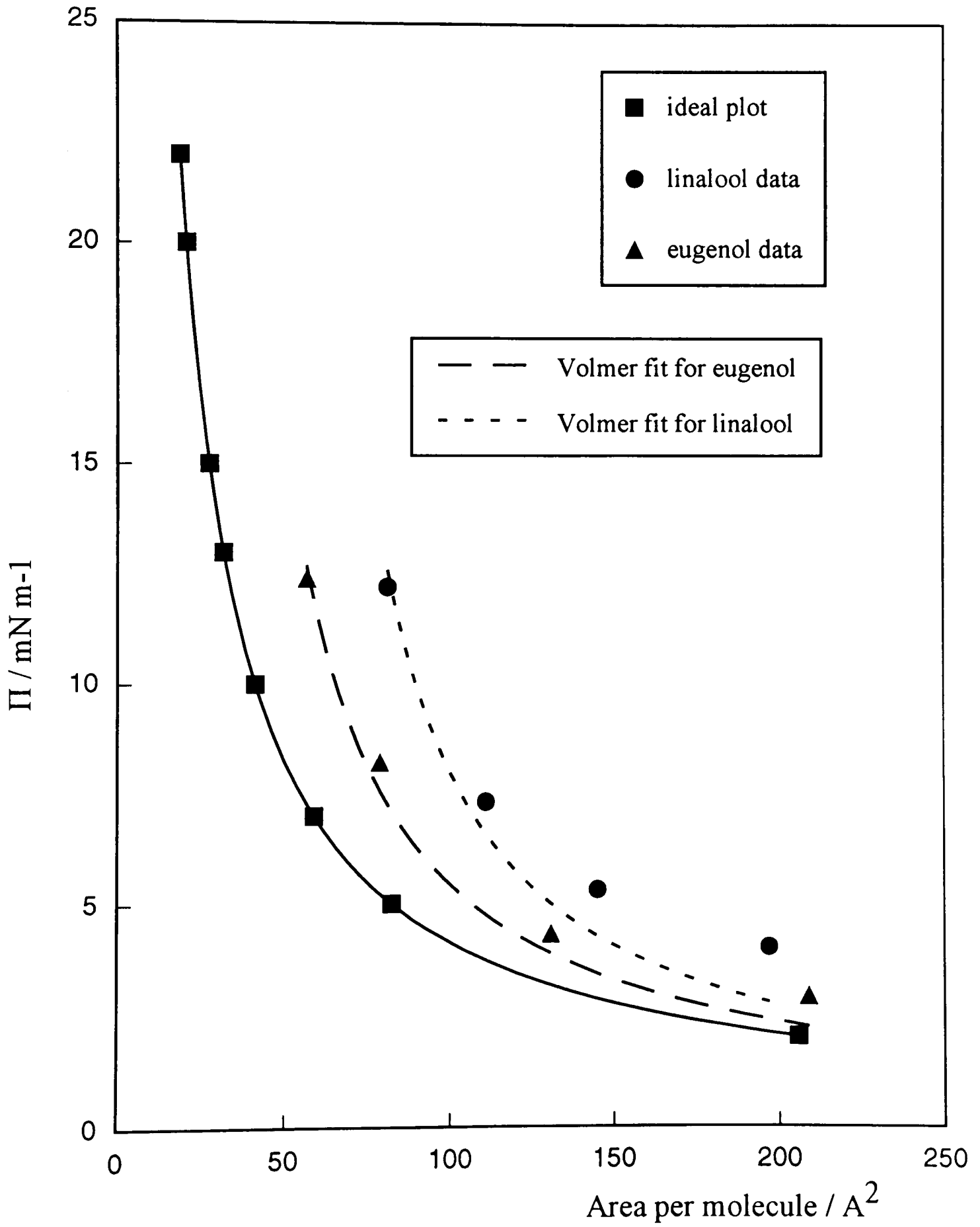

be due to the A_0 value changing during adsorption. At low surface pressures the A_0 value may be relitively high as the molecules can lie flat against the interface. As the surface pressure is increased, the molecules may be forced into a more vertical orientation and the A_0 value decreases.

3.8 Conclusions

The work in this chapter has provided the basis required for further detailed studies into the perfume oils and the conclusions can be summarised as follows.

1. The three perfume oils studied in this chapter show liquid adhesion properties which are fairly typical of moderately polar oils. In particular, the enthalpy of adhesion for linalool with water is consistent with typical values for the enthalpy of hydration of the hydroxyl group when account is taken of the surface area occupied per linalool molecule.

2. Linalool and eugenol show reasonably high surface activity at the heptane-water interface. On this basis, one might expect these molecules to operate to some extent as co-surfactants in systems containing surfactants. The measurements show that linalool (but not eugenol) partitions to a significant extent into water from heptane solution.

3.9 References

[1] R. Aveyard and B. J. Briscoe, J. Chem. Soc. Faraday Trans. 1, **68**, 478, 1972.

[2] J. J. Jasper and B. L. Houseman, J. Phys. Chem., **67**, 1548, 1963.

[3] S. Arctander, Perfume and flavour chemicals, New Jersey, 1969.

[4] R. Aveyard and D. A. Haydon, An Introduction to the Principles of Surface Chemistry, Cambridge University Press, 1973.

[5] R. Aveyard, 'Adsorption at the air liquid, liquid liquid and solid liquid interfaces' in Surfactants, Th. F. Tadros (Ed), Academic Press, pg 153, 1982.

[6] R. Aveyard and S. M. Saleem, J. Chem. Soc. Faraday Trans. 1, **73**, 896, 1977.

[7] R. Aveyard, B. J. Briscoe and J. Chapman, J. Chem. Soc. Faraday Trans. 1, **68**, 10, 1972.

[8] B. J. Briscoe, Ph.D Thesis, University of Hull, 1970.

[9] J. W. Gibbs, Scientific papers, **1**, 219, 1906.

Chapter 4

CHAPTER 4

PHASE BEHAVIOUR OF MIXTURES CONTAINING SURFACTANT + WATER + OCTANE + POLAR OILS

4.1 Introduction

This chapter is concerned with the phase behaviour of mixtures containing octane + water + non-ionic surfactant (C_8E_5 or C_8E_3) + perfume oil (linalool, eugenol or cineole). Initially, the manner in which the perfume oils affect the phase inversion temperatures of emulsions containing C_8E_3 or C_8E_5 + water + octane was studied to ascertain the best system with which to investigate the phase behaviour more fully. 'fish diagrams' were then determined for this system at varying concentrations of perfume oil to investigate the size and shape changes of the three phase region. This chapter contains certain notation which are current in the literature[1] and a table of these can be seen in figure 4.1.

Figure 4.1 Table of notations used.

A signifies water

B signifies perfume oil

B' signifies alkane oil

C signifies non-ionic surfactant

E signifies electrolyte

Symbol	Definition (all fractions in mass %)
α	$\frac{B + B'}{A + B + B' + E}$
β	$\frac{B}{B + B'}$
γ	$\frac{C}{A + B + B' + C + E}$
ε	$\frac{E}{A + E}$

4.2 The effect of added polar oils on the phase inversion temperature of water + octane + non-ionic surfactant systems

Both C_8E_3 and C_8E_5 surfactants were used in this section to determine how substitution of a linear alkane oil by a moderately polar oil affected the phase inversion temperature of the octane + water + surfactant system. The conductivity of the emulsion formed by homogenising a multiphase microemulsion system was used to determine the phase inversion temperature of the system due to the fact that oil in water emulsions are highly conducting whereas water in oil emulsions conduct only weakly.[2] For non-ionic surfactants, temperature can be used as a variable to change the preferred monolayer curvature, forcing an inversion from positive to negative curvature.

A typical plot of emulsion conductivity versus temperature can be seen in figure 4.2. For this system, phase inversion occurs at 12°C, inside the three phase region. The effect of perfume oil addition on the phase inversion temperatures of two non-ionic surfactant (C_8E_5 and C_8E_3) systems was studied using three of the perfume oils (cineole, eugenol and linalool) at various concentrations (values of β). The results can be seen in figures 4.3 and 4.4. Replacement of octane by any of the three oils reduces the phase inversion temperatures of both the surfactants. The effect becomes more pronounced as the concentration of the perfume oil is increased. This implies that the

Figure 4.2 A typical conductivity versus temperature plot

α = 50 wt %, β = 2 wt % (cineole), γ = 5 wt % (C_8E_3)
ε = 0.0544 wt % (NaCl).

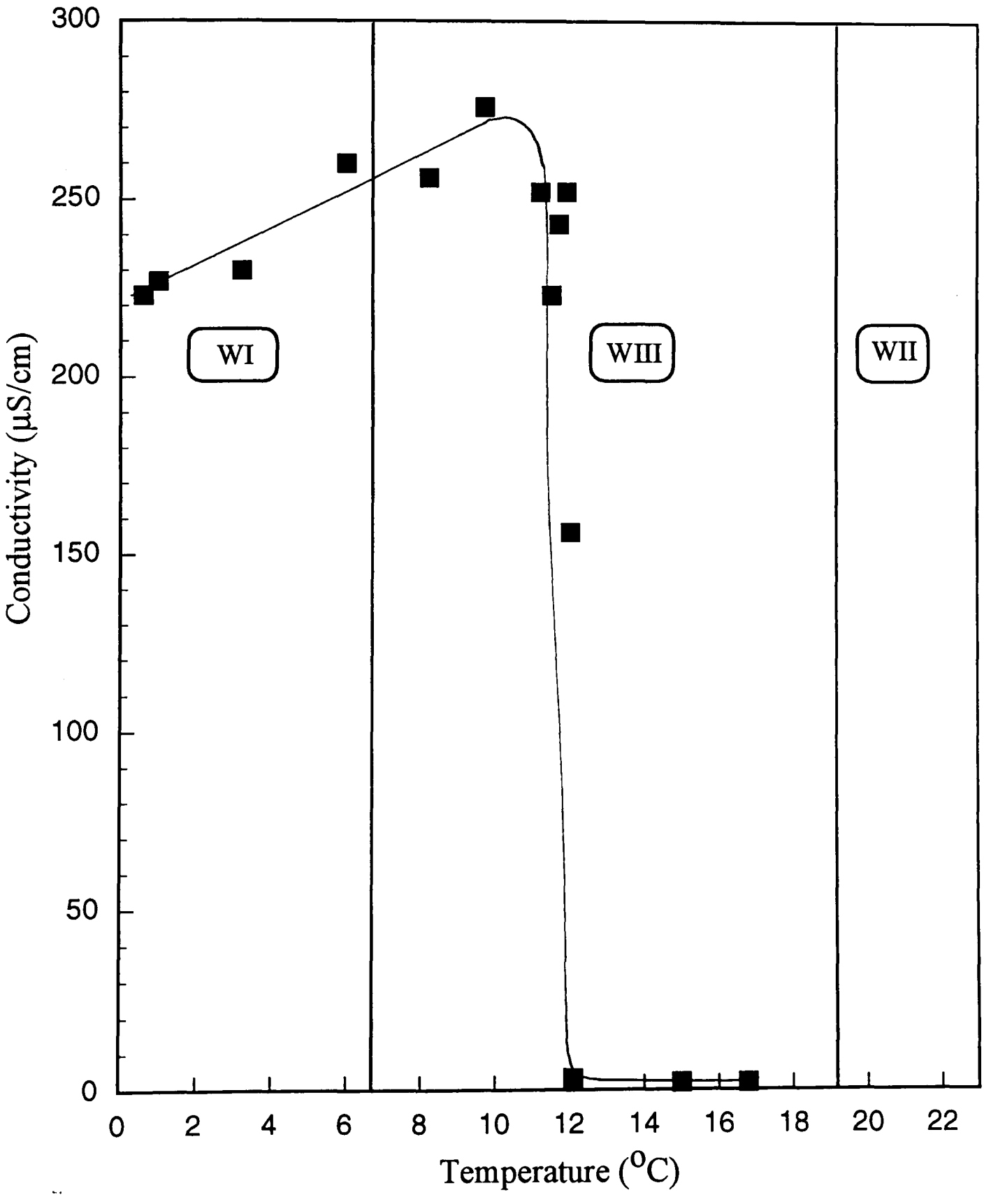

Figure 4.3 **Phase inversion temperature versus β for the three polar oils with C_8E_3 as surfactant**
($\alpha = 50$ wt %, $\gamma = 5$ wt %)

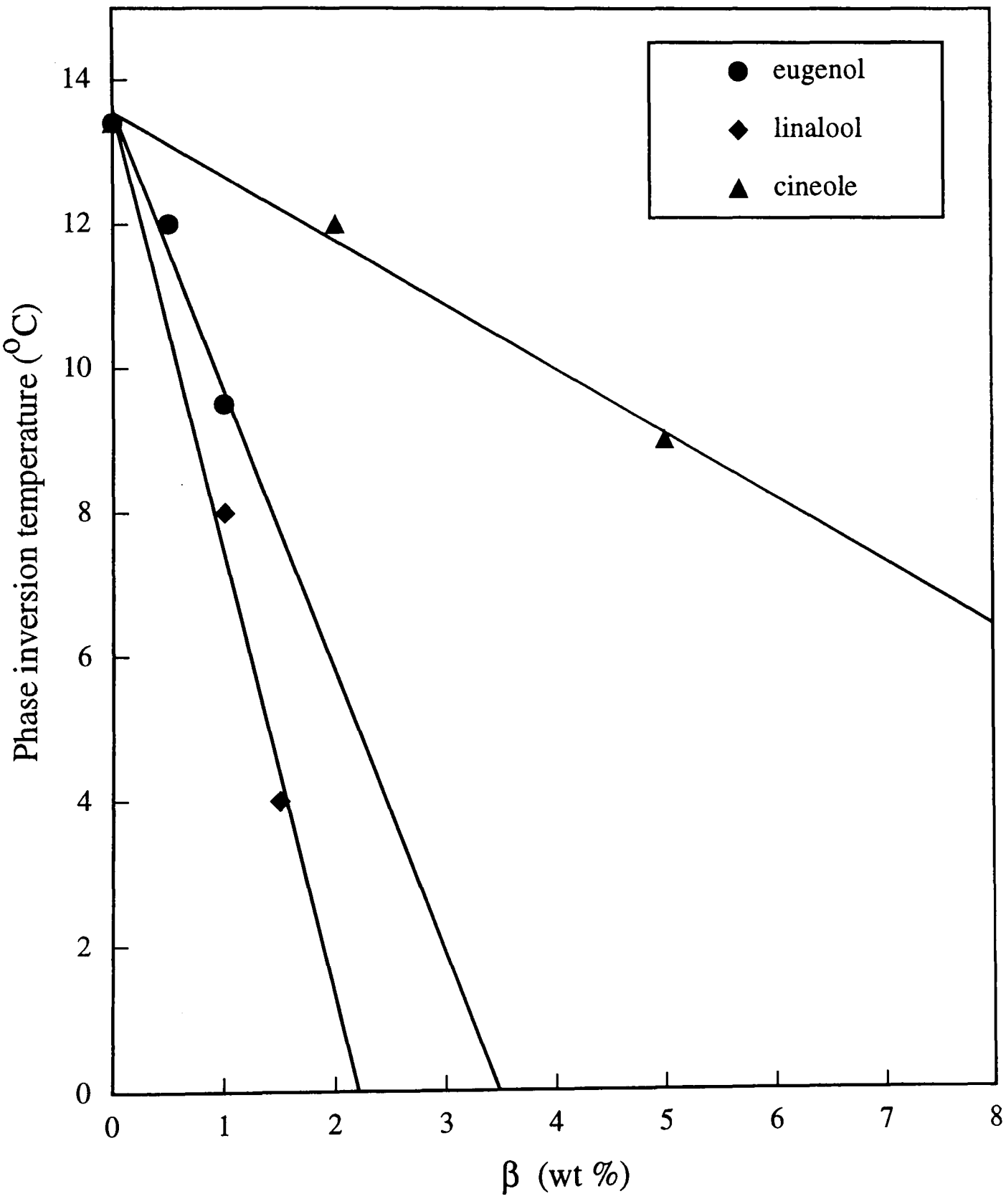

Figure 4.4 **Phase inversion temperature versus β for the three polar oils with C_8E_5 as surfactant**
(α = 50 wt %, γ = 5 wt %)

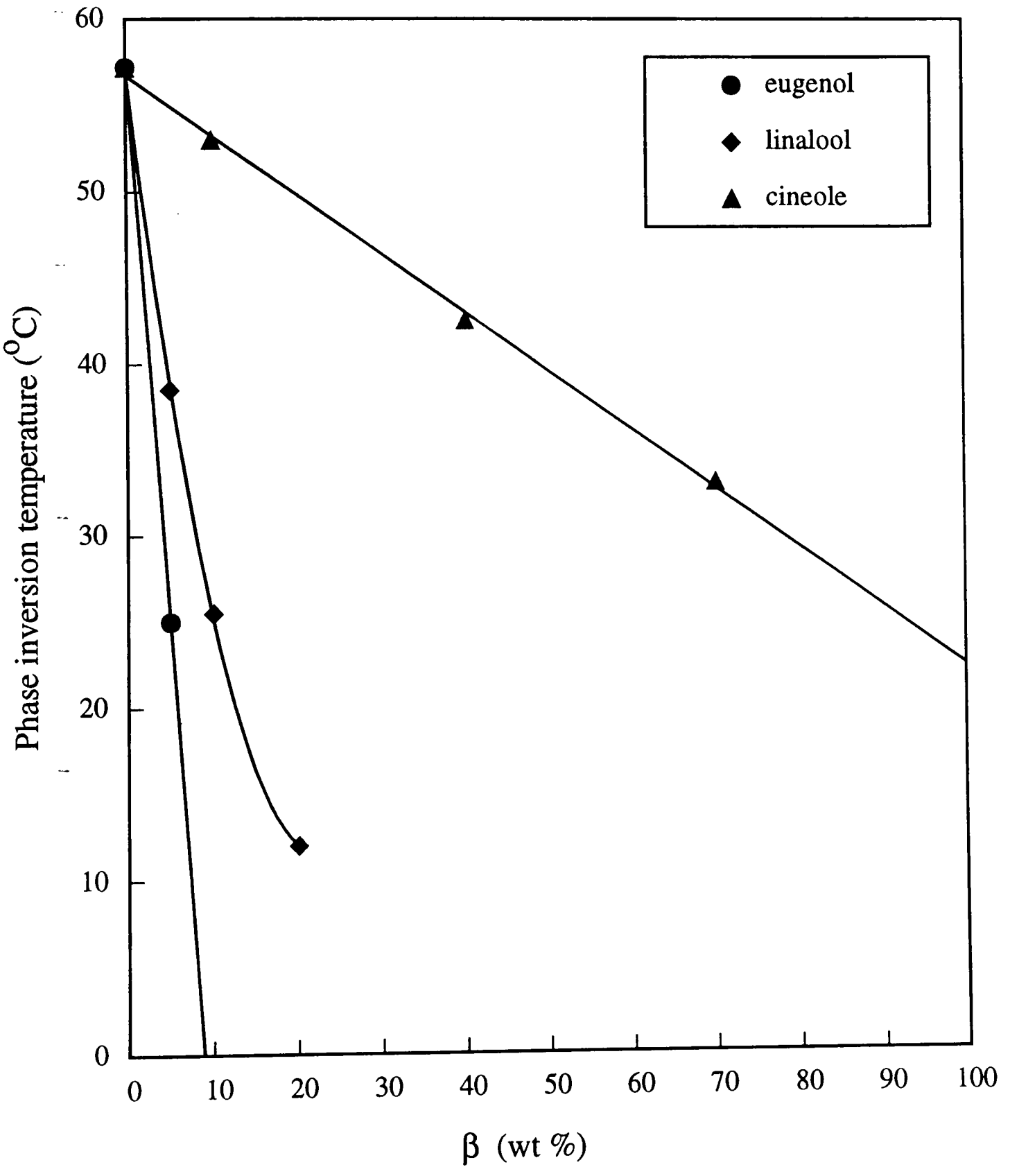

perfume oils penetrate and swell the surfactant tails more readily than the alkane oil, causing a change to negative preferred monolayer curvature at a lower temperature. Knowing this information, it is now possible to select a viable microemulsion system to trace the three phase body or 'fish' diagram as perfume oil is added to the alkane oil phase over a reasonably wide range of β.[3] C_8E_5 was selected as the surfactant to use since only small concentrations of the perfume oils reduce the phase inversion temperature of C_8E_3 to 0°C.

4.3 Tracing the three phase body of the water + octane + C_8E_5 system with increasing polar oil content

4.3.1 Representing the three phase region as a 'fish' diagram

The aim of this section of the study was to investigate the effect of substituting an alkane with a polar or perfume oil, in this case linalool, on the temperature range and extent of the three phase region with a view to locating the tri-critical point of the system.[4] For each 'fish' diagram, tubes were prepared at constant α and β values but at a range of different γ values (figure 4.1 gives an explanation of the different symbols involved). The progression from Winsor I through Winsor III to Winsor II microemulsion systems was then studied as the temperature was increased. Figure 4.5 shows the 'fish' diagrams produced at different concentrations of perfume oil (data

Figure 4.5 **Temperature versus γ (wt % of C_8E_5) for linalool in octane (α = 50 wt %) at various values of β**

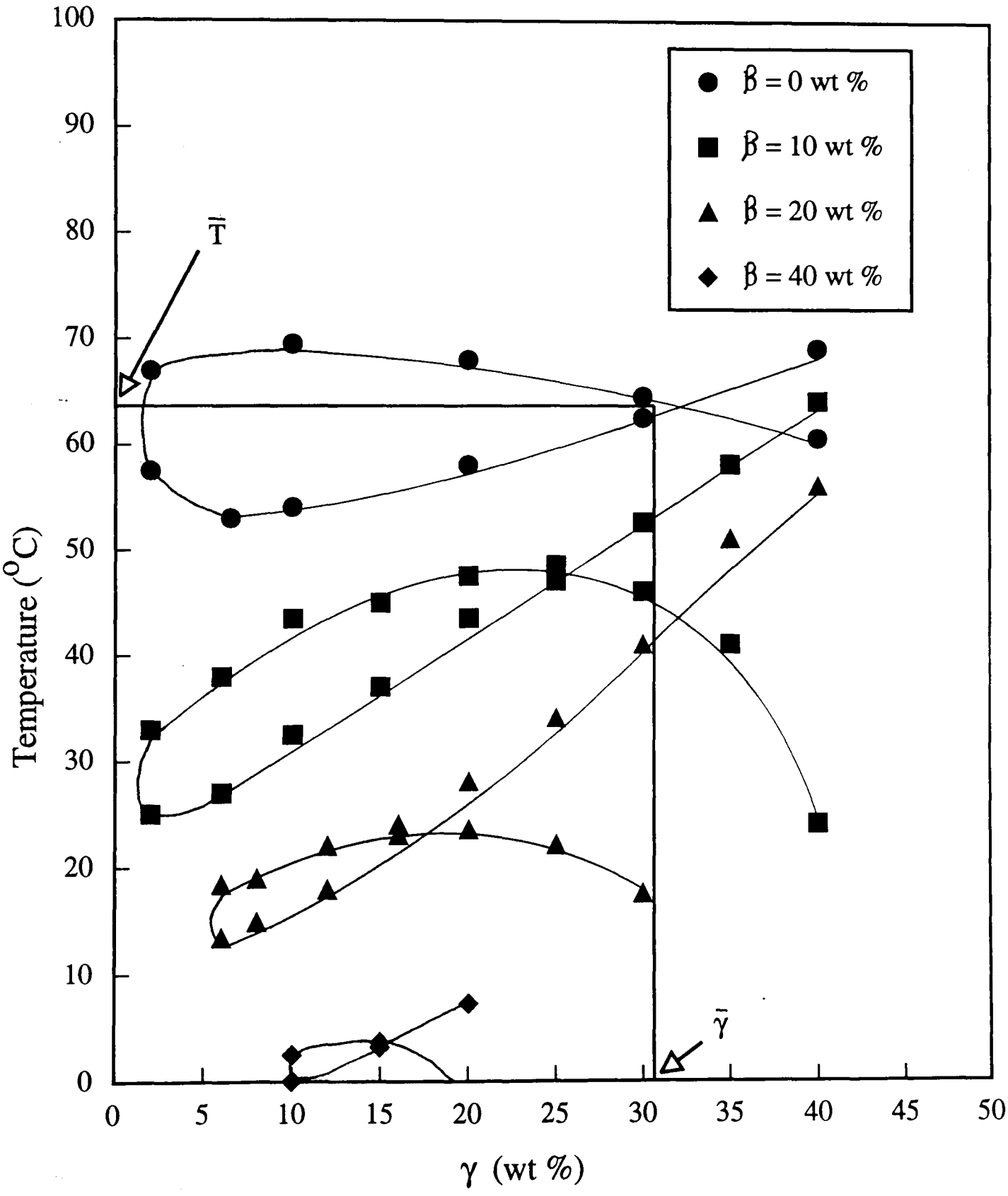

was also produced for β = 16 wt% but is omitted for clarity). It can be seen from this figure that as the concentration of the perfume oil is increased, the three phase region becomes progressively smaller and is found at lower temperatures. By analogy with other systems, this implies that the polar oil destroys the microstructure of the bicontinuous phase.[5] However, the tri-critical point of this system (when the three phase region just disappears) is located at a temperature below 0°C because the three phase region is still present at β = 40 wt% at a temperature close to zero.

4.3.2 Variations of $\bar{T}$, $\bar{\gamma}$, critical aggregation concentration and extent of the three phase region with increasing polar oil content

The $\bar{T}$ values of the fish diagrams (the temperature at which the three phase region joins the one phase region) decreases as the amount of perfume oil is increased, which is to be expected from the decrease in phase inversion temperatures with perfume oil concentration. Figure 4.5 also shows that $\bar{\gamma}$ values decrease with increasing β values. This is the minimum amount of surfactant required to produce a single phase system. It is a measure of the efficiency of the surfactant. It can also be seen in figure 4.5 that, with the exception of the 'fish' with no polar oil present, the three phase region slopes from high values of β to low values of β. This is due to the assumption that the polar oils can be treated purely as oils and not as surfactants i.e. they affect β but have no effect on γ. However, the dilute adsorption study (chapter 3), showed that these oils

do adsorb at interfaces, so increasing the amount of perfume oil present in the oil phase not only increases the polarity of the oil phase, but also changes the composition of the monolayer surrounding the droplets which alters the position of the three phase region for a particular surfactant concentration.

A number of other plots can be extracted from the fish diagrams. Firstly, a plot of $\bar{\gamma}$ versus β is useful to ascertain exactly how the efficiency of the surfactant is affected by the addition of perfume oil. The value of $\bar{\gamma}$ should reach a minimum at the tri-critical point and the variation in figure 4.6 is consistent with the idea that the system moves towards a tri-critical point as the concentration of perfume oil is increased. Figure 4.7 shows a similar plot of $\bar{T}$ versus β and it can be seen that $\bar{T}$ varies almost linearly with increasing concentration of perfume oil. Figure 4.5 shows that as well as the value of $\bar{\gamma}$ decreasing with increasing perfume oil content, the critical aggregation concentration (the 'nose' of the 'fish') increases. Therefore a higher concentration of surfactant is required before aggregates are formed, suggesting that the oil phase, water phase and surfactant are becoming more alike. This infers that the system is moving towards a tri-critical point because at this point all three phases are exactly the same.

By studying one particular γ value on figure 4.5, the extent of the three phase region in the temperature axis can be derived at fixed surfactant concentration and constant

Figure 4.6 $\bar{\gamma}$ **versus** β **(wt %) for linalool in octane** ($\alpha = 50$ wt %)

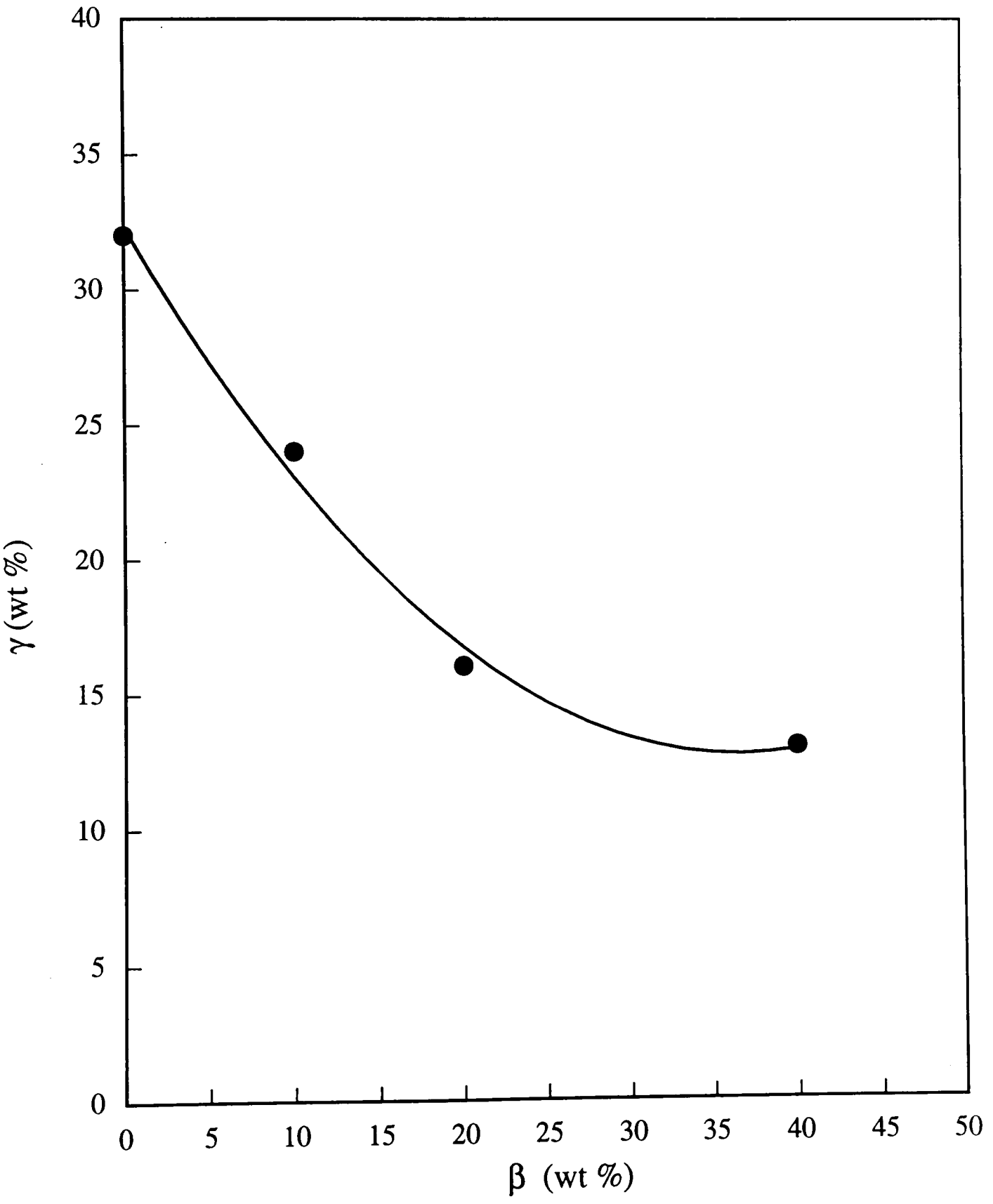

Figure 4.7 $\bar{T}$ **versus** β **(wt %) for linalool in octane** (α = 50 wt %)

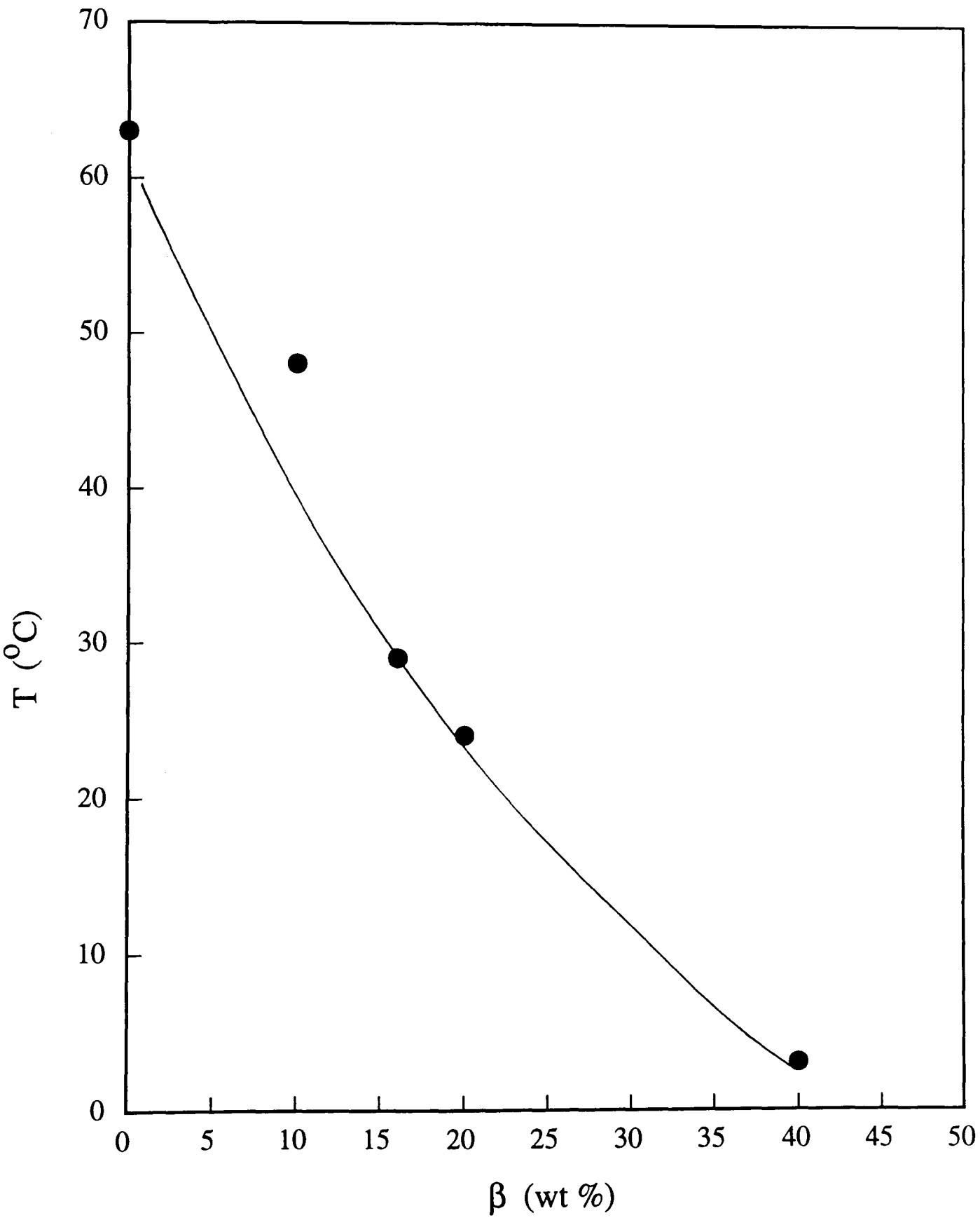

oil/water ratio (α). Figure 4.8 shows the reduction in size of the three phase region as the perfume oil concentration is increased.

4.3.3 Phase volume variations with temperature

The volumes of the individual phases shown within the tubes were investigated as a function of temperature. Figures 4.9-4.11 show examples of such figures. In figure 4.9, where γ = 10 wt%, initially, at low temperatures, a Winsor I type microemulsion exists. This is deduced because the meniscus between the two phases is almost 60% from the base of the total length of liquid in the tube, suggesting that oil has been solubilised in the water. As the temperature is increased, a second meniscus appears from the base of the tube and a Winsor III system arises. By knowing the volume of each constituent, it is possible to calculate how much oil has been solubilised in the middle microemulsion phase. When the three phase region first appears, at a temperature of 32°C, it contains 0.6cm^3 of the oil and 1.5cm^3 of the water for 0.37g of surfactant. Just before the three phase region disappears, at a temperature of 42°C, it contains 2.1cm^3 of oil and 0.3cm^3 of water for 0.37g of surfactant. At higher temperatures, a Winsor II microemulsion system is formed with the meniscus lying at 33% of the total height of the tube contents.

Figure 4.8 **ΔT (extent of three phase region) versus β (wt %) for linalool in octane (α = 50 wt %), showing the disappearance of the three phase region. (γ = 8 wt %)**

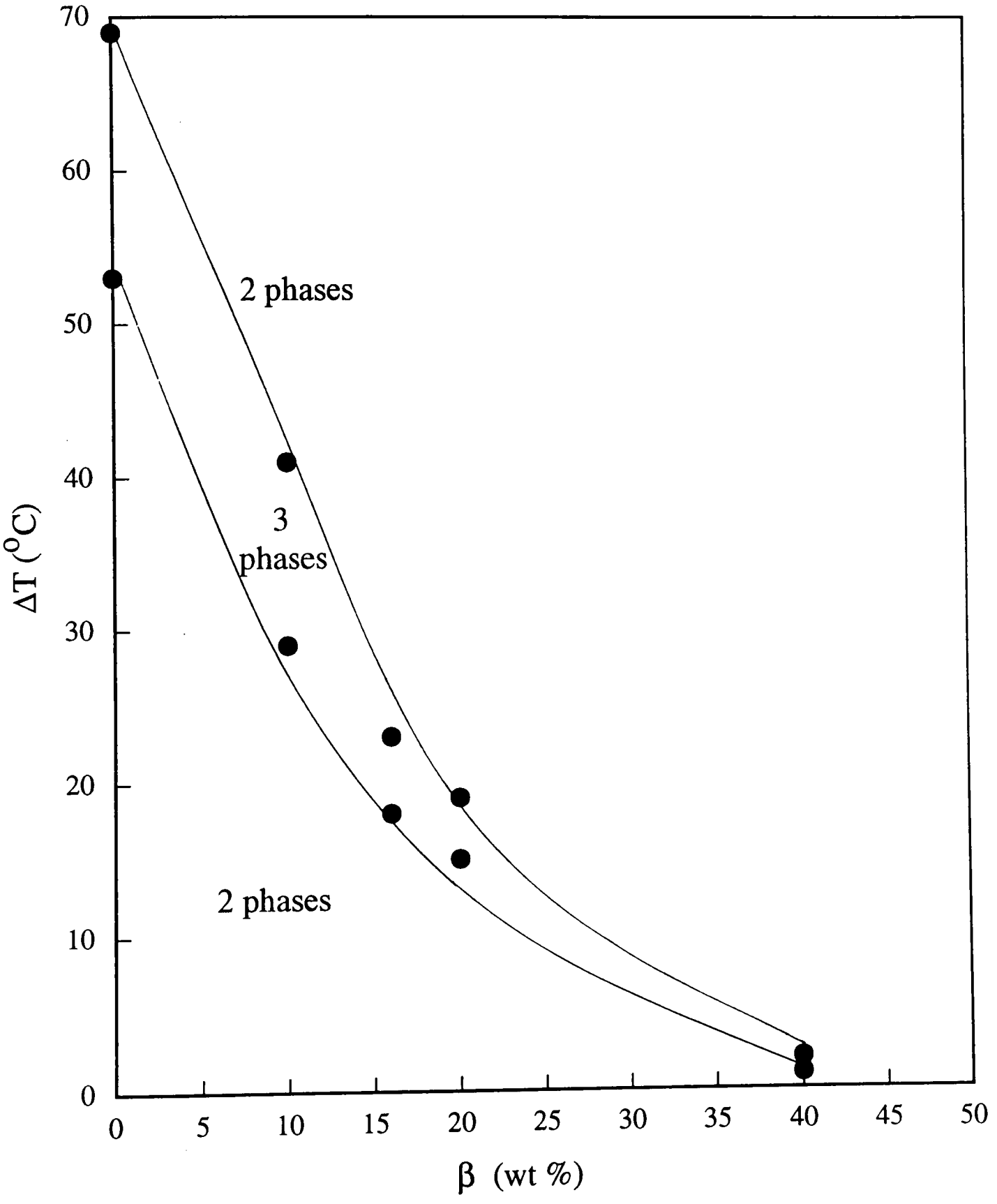

Figure 4.9 **Percentage phase volumes versus temperature for linalool in octane with C_8E_5 as surfactant**
(α = 50 wt %, β = 10 wt %, γ = 10 wt %)

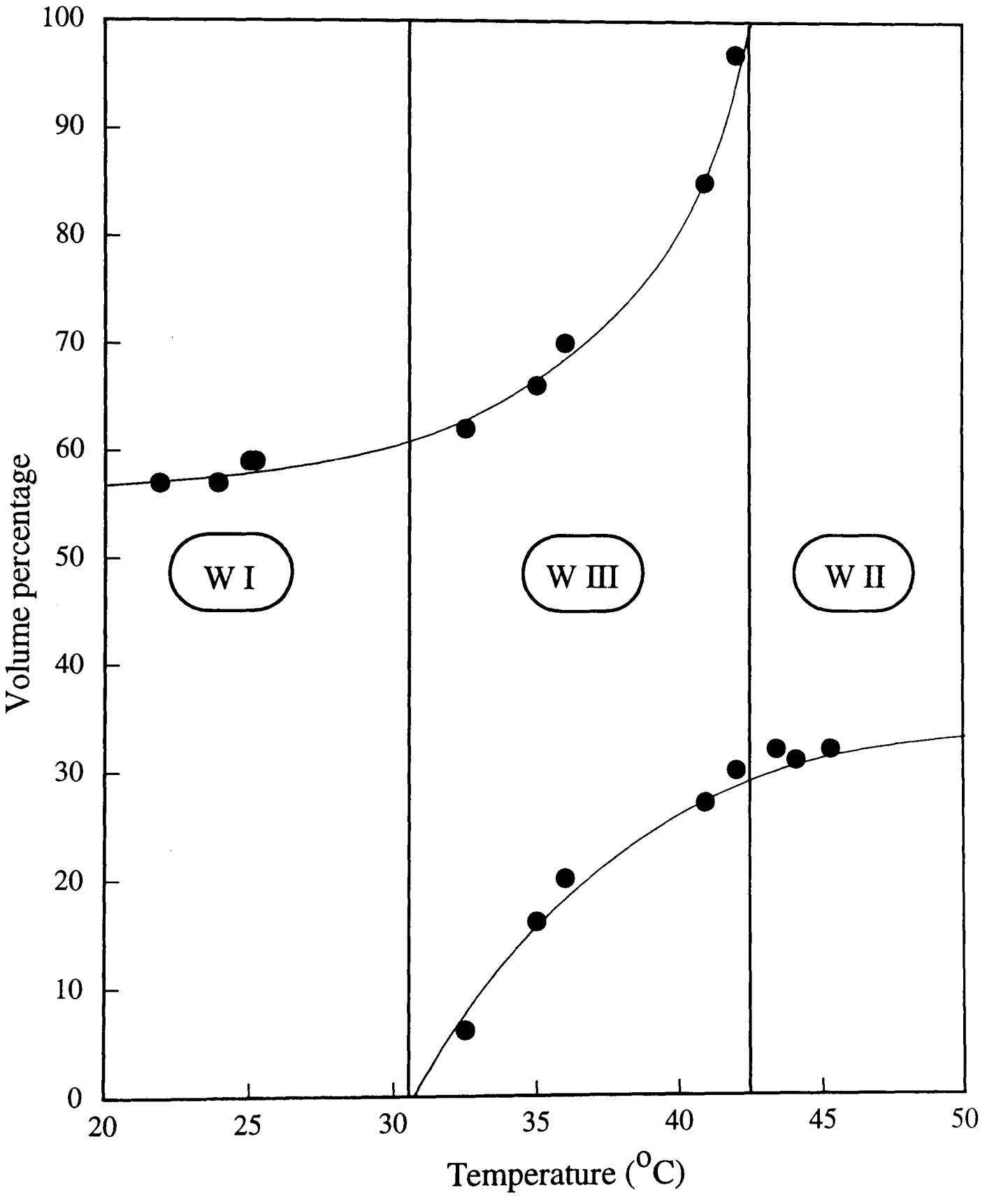

Figure 4.10 shows a similar diagram, but now γ = 20wt% so the amount of solubilisation of the excess phase would be expected to increase. It can be seen that at low temperatures, again a Winsor I microemulsion system is present as the meniscus is now found 65% of the way up the tube. At the temperature where three phases first exist, the middle phase contains 1.7cm^3 of oil and 1.5cm^3 of water for 0.75g of surfactant. Figure 4.10 shows the size of the three phase region becoming smaller as the γ value becomes closer to the tail of the fish. At higher temperatures, a Winsor II microemulsion system exists giving solubilisation of water into the oil phase.

Figure 4.11 is the final phase volume diagram where γ = 30wt% which lies in the tail region of the β = 10wt% fish diagram so a one phase region exists in place of the previous three phase regions. As expected, due to the increase in surfactant concentration, solubilisation of the oil is increased in the Winsor I region of the diagram (the meniscus lies at 75% along the tube). A one phase region exists between the temperatures 46°C and 52°C, where the only meniscus is the air-liquid meniscus. Throughout this region, there is complete solubilisation of one phase in the other. A Winsor II system exists after the one phase region with a high degree of solubilisation (the meniscus lies at 20% of the total tube length).

Figure 4.10 **Percentage phase volumes versus temperature for linalool in octane with C_8E_5 as surfactant**

(α = 50 wt %, β = 10 wt %, γ = 20 wt %)

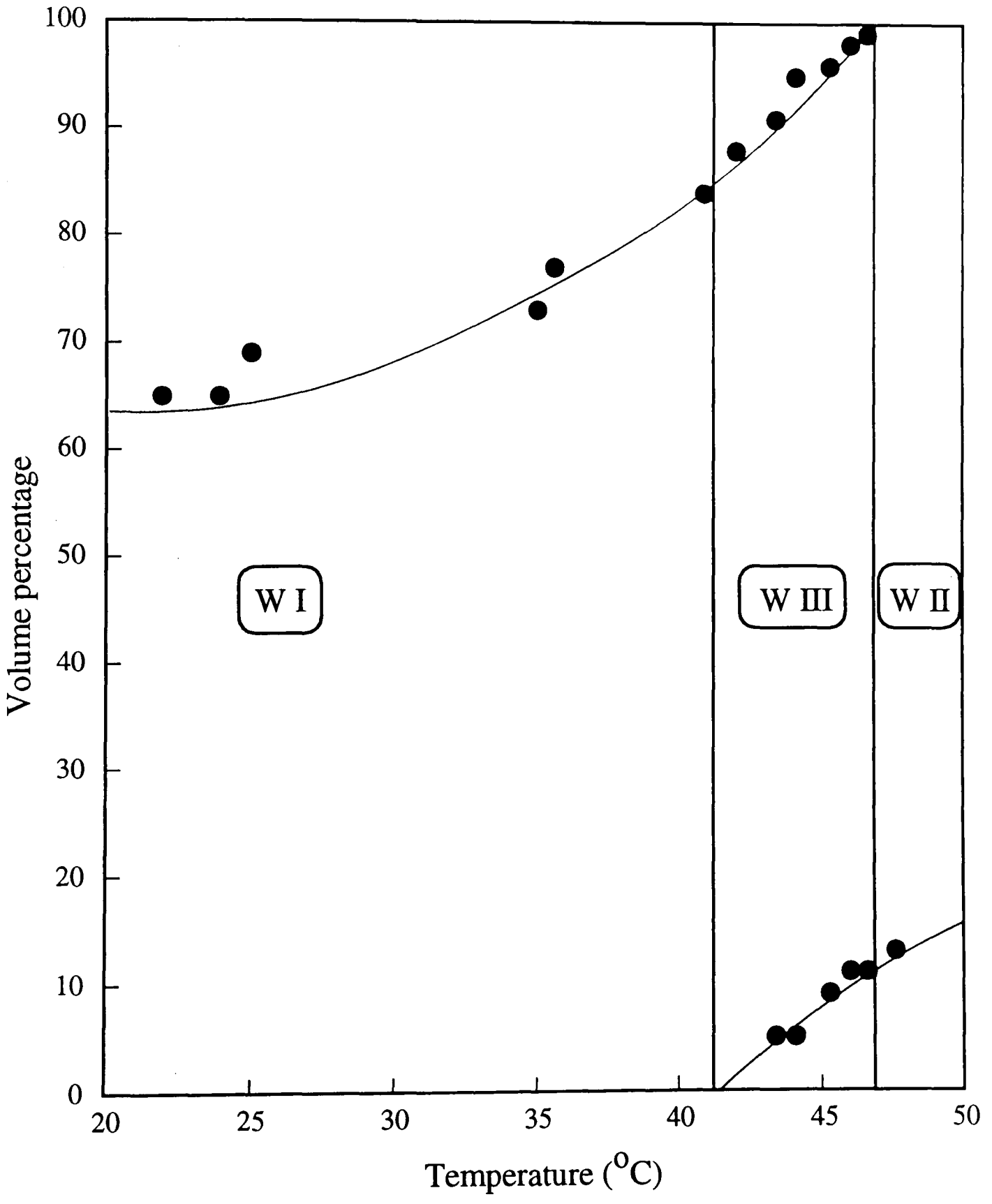

Figure 4.11 **Percentage phase volumes versus temperature for linalool in octane with C_8E_5 as surfactant**

(α = 50 wt %, β = 10 wt %, γ = 30 wt %)

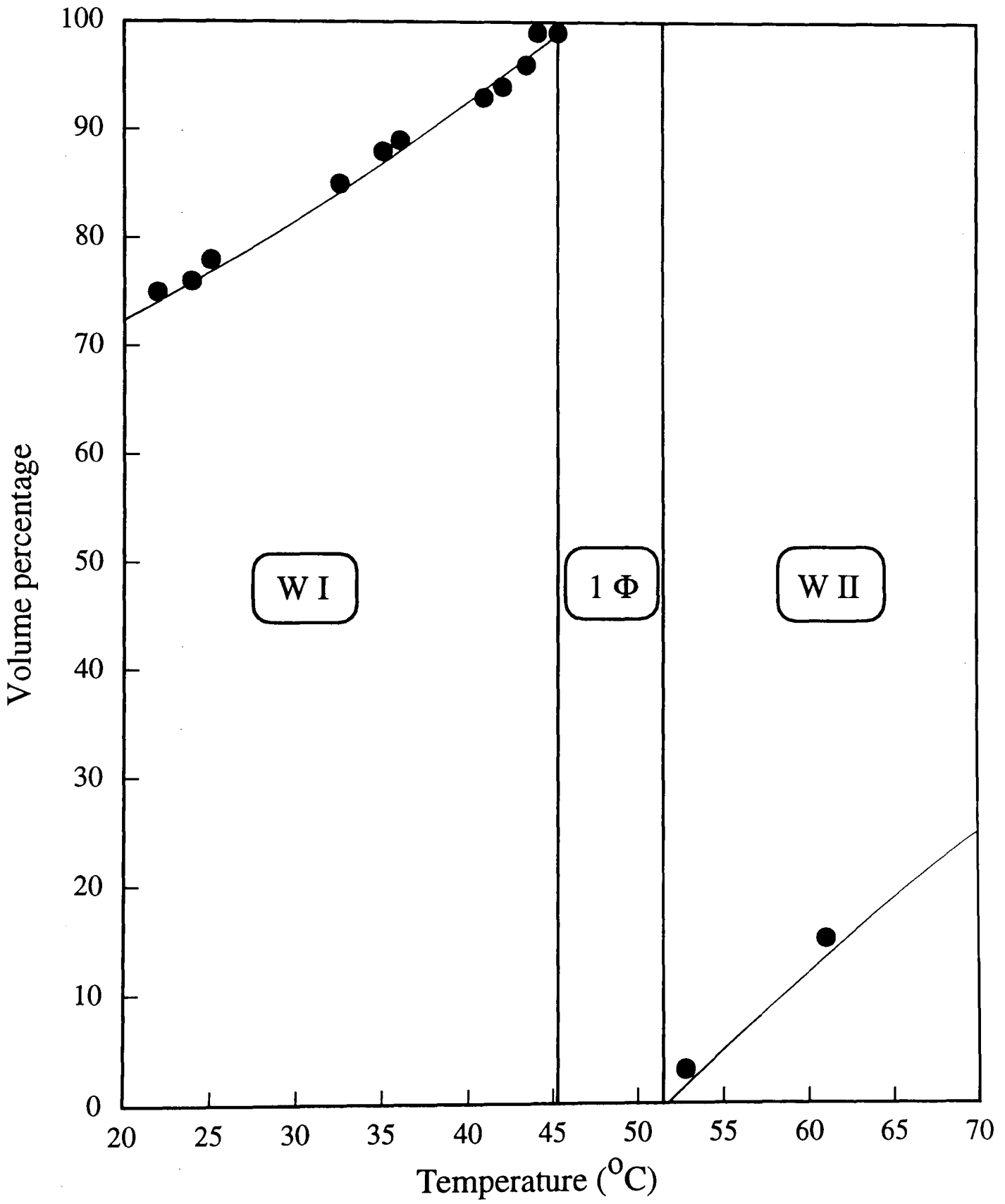

4.4 Conclusions

The phase behaviour of the linalool + octane + water + C_8E_5 system studied in this chapter gave the following conclusions.

1. All three perfume oils studied in this chapter reduce the phase inversion temperature of systems containing non-ionic surfactants (C_8E_5 and C_8E_3). As the concentration of perfume oil is increased the phase inversion temperature is further reduced, suggesting that the perfume oils penetrate and swell the tailgroups of the surfactant to a greater extent than the alkane oils.

2. Linalool reduces the size of the three phase region observed for a water + octane + C_8E_5 microemulsion system, reduces ΔT, $\bar{\gamma}$ and increases the critical aggregation concentration in a manner which is consistent with the approach to a tri-critical point. However, the tri-critical point of the system was not found as it lies at temperatures below 0°C.

4.5 References

[1] M. Kahlweit and R. Strey in Microemulsion Systems, H. L. Rosano and M. Clausse (Eds), Dekker, New York, 1987.

[2] R. Aveyard, B. P. Binks, P. D. I. Fletcher, X. Ye and J. R. Lu in Emulsions - A fundamental and practical approach, J. Sjöblom (Ed), Kluwer, Dordrecht, The Netherlands.

[3] M. Kahlweit, R. Strey and P. Firman, J. Phys. Chem., **90**, 671, 1986.

[4] R. Strey and M. Jonsromer, J. Phys. Chem., **96**, 4537, 1992.

[5] F. Lichterfeld, T. Schmeling and R. Strey, J. Phys. Chem., **90**, 5762, 1986.

Chapter 5

CHAPTER 5

ADSORPTION OF OILS INTO NON-IONIC SURFACTANT MONOLAYERS

5.1 Introduction

An oil which has been added to the surface of an aqueous surfactant solution can either spread to form a continuous oil film over the surface or form discrete lenses. The tendency of an oil to spread is related to the three tensions which are present in the system and the equilibrium spreading coefficient of an oil on an aqueous phase ($S_{ow}(eq)$) is defined as

$$S_{ow}(eq) = \gamma_{aw} - \gamma_{ao} - \gamma_{ow} \qquad (5.1)$$

where γ_{aw}, γ_{ao} and γ_{ow} are the *equilibrium* air-aqueous solution, air-oil and oil-aqueous solution tensions respectively. It is important that equilibrium values are taken for these tensions because it will be seen later in the chapter that the equilibrium air-

aqueous solution tension (when the oil has been added to the solution) is appreciably different to the initial tension (before the addition of oil). The equilibrium spreading coefficient is negative for lens forming oils and zero for spreading oils. The value of the spreading coefficient at equilibrium cannot be positive.[1]

In a system where the equilibrium spreading coefficient is zero, the addition of a small quantity of oil to the surface will cause the tension to fall from that of the aqueous solution to that of the composite film including both the surfactant monolayer and the oil film. If a small quantity of oil is present, a thin film will exist across the surfactant monolayer and a degree of interaction will be present between the oil-aqueous solution and air-oil interfaces. For film thicknesses less than approximately 100nm, these interactions may be sufficient to cause the resulting tension to be different from the sum of the bulk phase tensions ($\gamma_{ao} + \gamma_{ow}$). Upon the addition of further oil, the film of oil will thicken and the measured tension will approach the sum ($\gamma_{ao} + \gamma_{ow}$). Film excess tensions which arise from colloidal interactions across thin films have been found to be of the order of 0.01 mN m^{-1} for films with a thickness of a few nanometres.[2] It is therefore expected that for spreading oils which show interference colours (thickness > 100 nm) that the composite film tension will be equal to the sum ($\gamma_{ao} + \gamma_{ow}$) within the experimental errors of the tension determinations reported here ($\pm$0.1-0.2 mN m^{-1}).

In the case where a lens is formed on the aqueous solution, the lens coexists with a mixed film of oil and surfactant. This mixed film can either be a monolayer or a multilayer. A multilayer in equilibrium with a lens of oil has been observed for alkanes on solution of sodium bis(2-ethylhexyl) sulfosuccinate (AOT).[3,4] The case in which a lens coexists with a mixed monolayer of oil and surfactant has already been investigated using apolar oils on ionic surfactant solutions. The amount of oil present in the mixed monolayer was estimated using the decrease in surface tension of the surfactant solution once the oil has been added ($\Delta\gamma$).[5,6]

In this way, important fundamental information can be obtained about the interaction of oils with surfactant monolayers. Studies to date, however, have been restricted to ionic surfactants where the surfactants do not partition into the apolar oil phase. Any study into the equivalent solubilisation of these oils into non-ionic surfactants must first address the problem of partitioning of the non-ionic surfactant into the added oil lens.[7] The partitioning that occurs[8,9] would cause severe problems to the measurement of surface tension decrease due to the oil. This chapter is concerned with how problems associated with surfactant partitioning can be overcome and how, because of this, the adsorption and spreading behaviour of the alkane oils on non-ionic surfactants can be studied.

5.2 Avoiding measurement artefacts caused by non-ionic surfactants

In order to prevent surfactant partitioning from the aqueous phase into the oil phase whilst studying non-ionic surfactants, it is necessary that the oil + water + surfactant mixture forms a Winsor I two-phase system at equilibrium. In this way, no surfactant aggregates will partition into the oil phase (see chapter 1). The work was therefore carried out with surfactant + oil combinations which had phase inversion temperatures (values of which are given in table 5.1) sufficiently higher than the temperature of the measurements (usually 25°C).

This precaution only stops the surfactant aggregates partitioning into the oil. It is also necessary to consider the partitioning of the surfactant monomers. In alkane oil + water two phase systems, monomers of non-ionic surfactants of the C_nE_m type, generally distribute strongly in favour of the oil. From this, a Winsor I system can be defined as consisting of an aqueous phase containing both aggregates and monomers of concentration cmc_{water}, in equilibrium with an oil phase which contains surfactant monomers at a concentration which is given by the product of the cmc_{water} and the partition coefficient and is known as c*. Values of both cmc_{water} and c* for the surfactants studied are shown in table 5.1. It is assumed, therefore, that once a drop of pure alkane oil has been added to the surface of a surfactant solution that the

surfactant partitions into the oil drop until reaching the concentration c* at equilibrium. Thus it is necessary that this concentration is present in the oil before it is added to the surface.

5.3 Preliminary measurements of $\Delta\gamma$ using pure alkane oils

Oil adsorption should cause the surfactant solution surface tension to decrease by an amount $\Delta\gamma$ which is equal to the surface pressure of the adsorbed oil film. In preliminary measurements, pure alkane oil drops were added to the surface of the surfactant solution and the drop in tension was recorded. At low concentrations of surfactant in the aqueous phase (just in excess of the cmc_{water}) it was commonly observed that the tension *increased* on the addition of oil (i.e. a negative value of $\Delta\gamma$). This was thought to be due to the depletion of surfactant from the aqueous phase into the oil phase which then takes the aqueous phase concentration below cmc_{water} and results in a tension increase.

Figure 5.1 shows how the surface tension of a $C_{12}E_7$ surfactant solution (γ_{aw}) varies with aqueous phase surfactant concentration (above cmc_{water}) without added dodecane, with pure dodecane lenses and with dodecane lenses containing 0.15 wt% of the surfactant (c* for this combination of oil and surfactant). When pure dodecane is

Table 5.1 Summary of phase inversion temperature (PIT)[10,11,12,13] values and critical aggregation concentrations (at 25°C) for the surfactant + oil systems (c*)[14,15] and the surfactant + water systems (cmc_{water}).[10,16]

surfactant	alkane chain length	cmc_{water}/mM	c^*_{oil}/wt%	PIT/°C
$C_{12}E_5$	7	0.064	1.29	29
	8		1.13	32
γ_{aw} (no oil)	9		1.01	35
29.8 mN m^{-1}	10		0.91	38
at 6.4 mM	11		0.81	40
	12		0.76	43
	13		0.70	44
	14		0.65	46
	16		0.57	50
$C_{12}E_7$	7	0.050	0.26	58
	8		0.22	61
γ_{aw} (no oil)	9		0.20	64
32.5 mN m^{-1}	10		0.18	66
at 5.0 mM	11		0.16	68
	12		0.15	71
	13		0.14	74
	14		0.13	76
	16		0.11	81
$C_{12}E_9$	7	0.10	0.043	72
	8		0.038	75
γ_{aw} (no oil)	9		0.034	77
34.8 mN m^{-1}	10		0.030	79
at 1.0 mM	11		0.028	82
	12		0.025	84
	13		0.023	86
	14		0.022	89
	16		0.019	94
$C_{10}E_7$	7-16	0.95	0.3 used for all alkanes	>60 used for all alkanes
γ_{aw} (no oil) 33.8 mN m^{-1} at 9.5 mM				
$C_{14}E_7$	7-16	0.0095	0.3 used for all alkanes	>40 used for all alkanes
γ_{aw} (no oil) 33.3 mN m^{-1} at 0.95 mM				

Figure 5.1 Variation of γ_{aw} with aqueous phase concentration of $C_{12}E_7$. The curves refer to (i) the absence of added oil, (ii) the addition of pure dodecane and (iii) the addition of dodecane containing 0.15 wt% $C_{12}E_7$, equal to c^*_{oil}

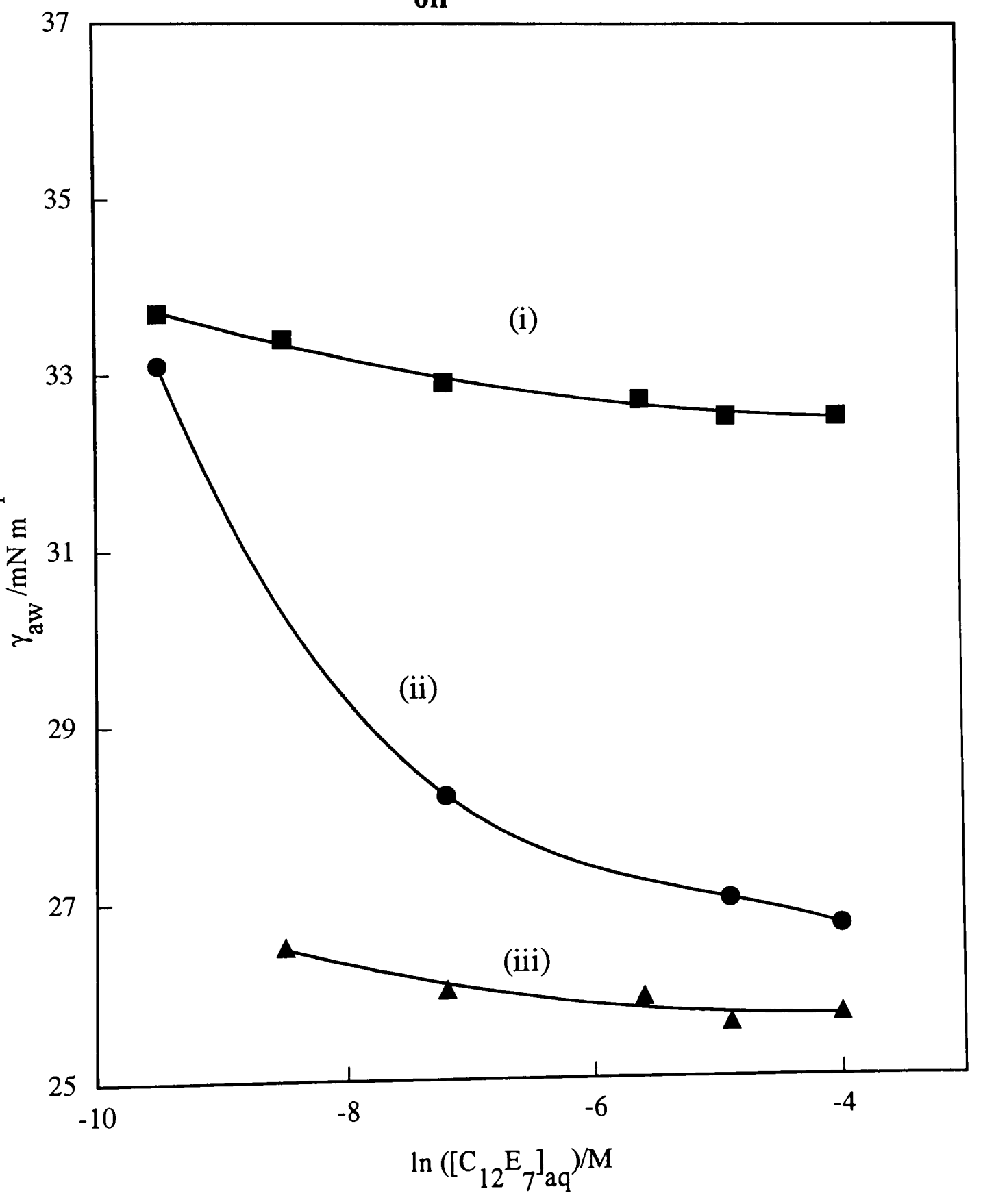

added, the difference between the pure surfactant solution graph and that for dodecane addition, $\Delta\gamma$, increases with increasing aqueous phase concentration. This is consistent with the theory that depletion occurs into the oil phase because higher aqueous phase concentrations are likely to lessen the effect of low $\Delta\gamma$'s due to the fact that the amount partitioning into the oil phase is a lower proportion of the total amount present in the aqueous phase. Figure 5.1 also shows that incorporating a surfactant concentration equal to c* in the dodecane lens prevents the large variations in $\Delta\gamma$ as the aqueous phase concentration is varied.

5.4 Measurement of surface tension to obtain c* values

It was possible to obtain c* values for certain oil and surfactant combinations to verify values available in the literature. Figures 5.2 and 5.3 show the results of experiments in which drops of alkanes containing different concentrations of surfactant were placed on aqueous phases containing surfactant concentrations in excess of cmc_{water}. It was expected that as the concentration of surfactant in the oil phase is increased, the measured tension should decrease until the concentration c* was present. Above which, the tension should remain constant. This behaviour was observed for all the surfactants and oils used. It can be seen from figures 5.2 and 5.3 that the c*s obtained by this method are in good agreement from those obtained from literature.[14,15] It was sometimes necessary to extrapolate the data available in literature to attain values for

Figure 5.2 Variation of γ_{aw} in the presence of added dodecane with oil phase surfactant concentration at 25°C. The curves refer to $C_{12}E_5$ (▲), $C_{12}E_7$ (●) and $C_{12}E_9$ (■). The aqueous phase surfactant concentrations were fixed at 1.5 times cmc_{water}

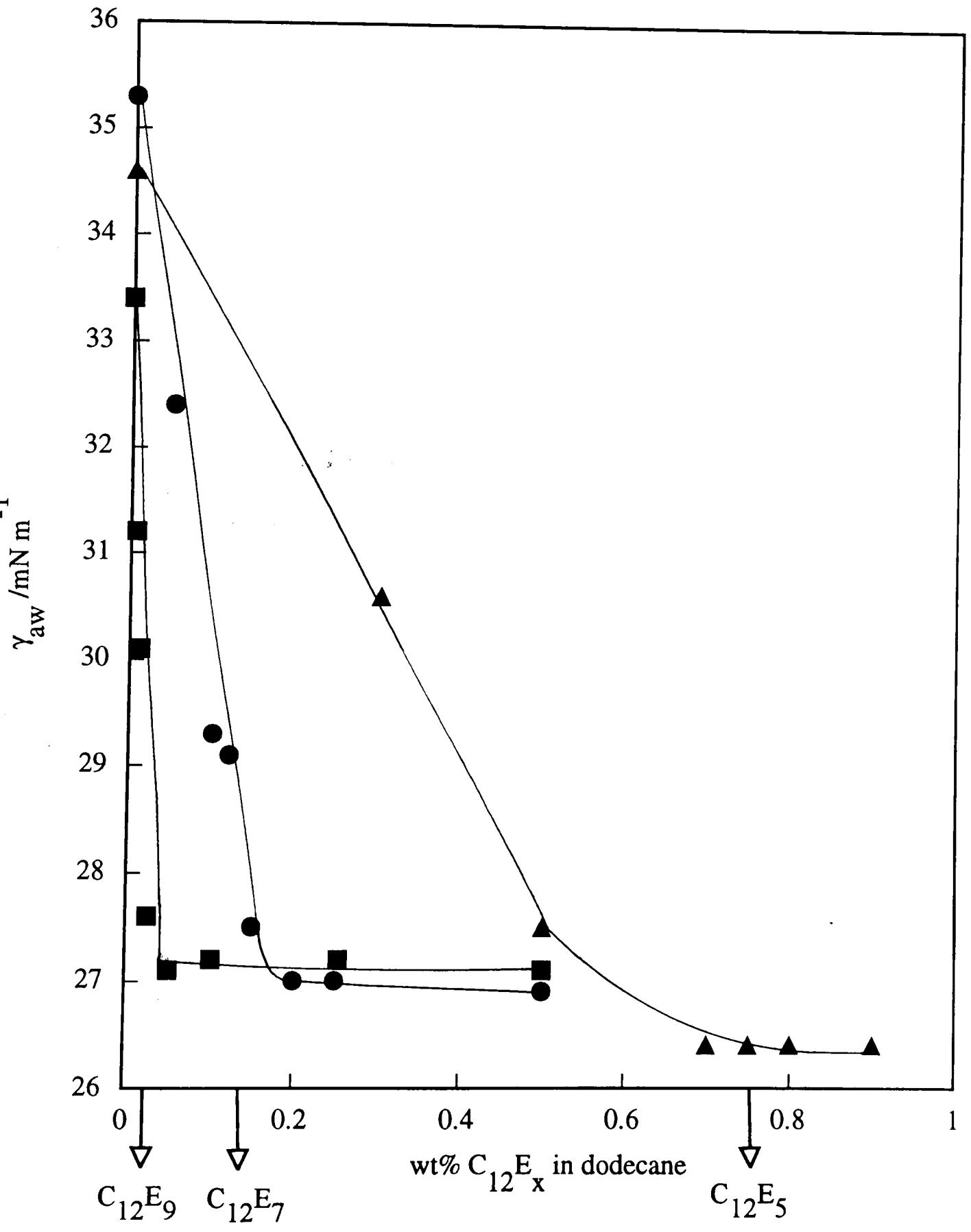

Figure 5.3 **(a) Variation of γ_{aw} in the presence of added dodecane with oil phase surfactant concentration. (b) Variation of γ_{aw} in the presence of added oil with oil phase concentration of $C_{10}E_7$. All measured at 25°C. All aqueous phase concentrations of surfactant were fixed at 1.5 times cmc_{water}.**

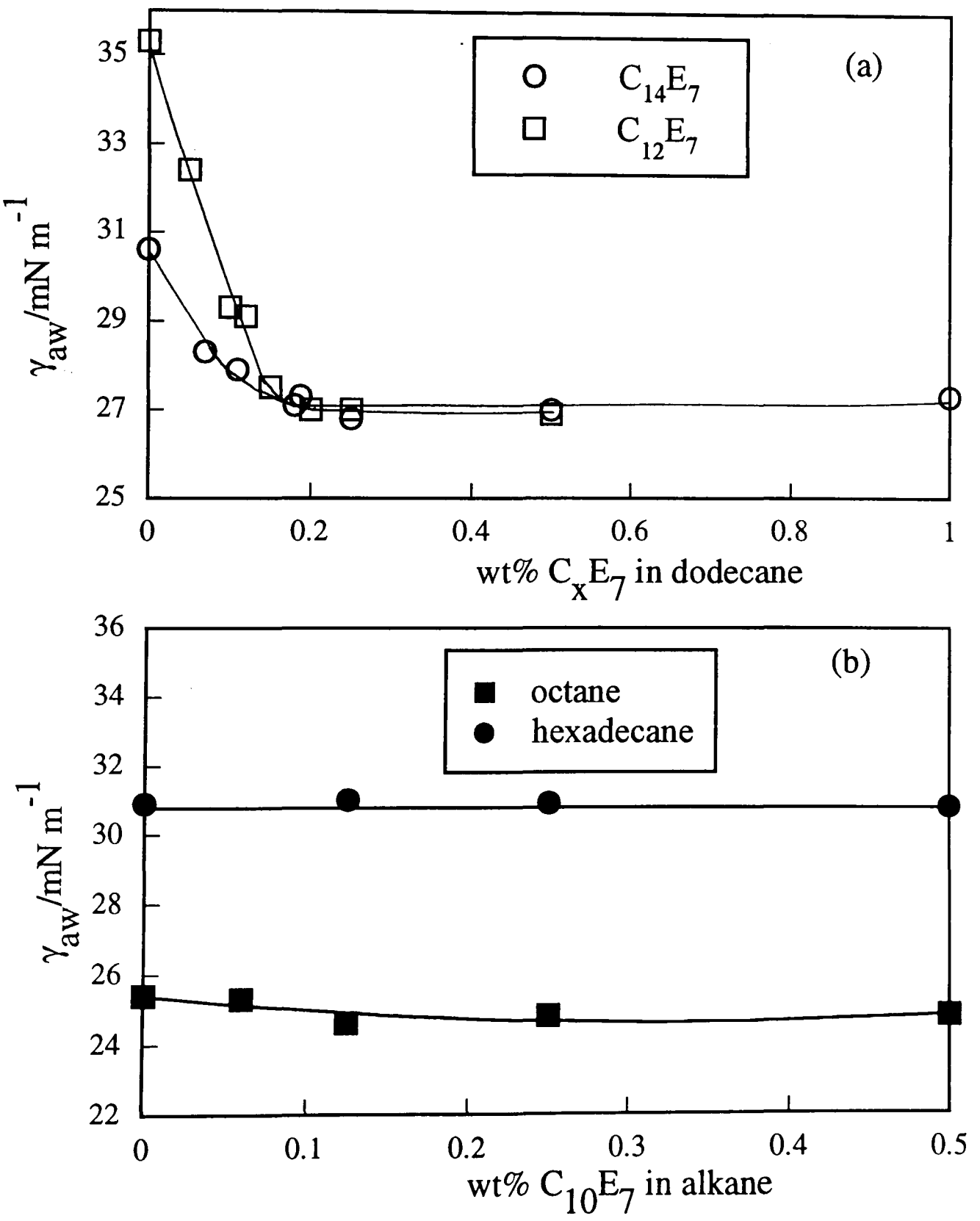

c*s for surfactant and oil combinations which were unavailable in the literature. It has been shown that c* values for different alkanes with one particular surfactant are independent of the chain length of the oil when c* is expressed in mole fraction.[14] In this way, extrapolations are possible to obtain c* values for all chain length oils for a particular surfactant. The partitioning hypothesis seems intuitively reasonable because of the agreement between literature values and those obtained by figures 5.2 and 5.3. Figure 5.3 shows this type of graph for systems in which the surfactant tail group chain length and the alkane chain length are varied. Figure 5.3a, showing data for dodecane with $C_{14}E_7$ and $C_{12}E_7$, are of a similar shape to those of figure 5.2 showing clearly the c* value. Figure 5.3b, showing data for octane and hexadecane on $C_{10}E_7$ solutions, show little variation in surface tension as the oil phase concentration is increased. This is probably a consequence of the high concentration of aqueous phase surfactant used for $C_{10}E_7$ (see table 5.1). Figure 5.1 has already shown that at higher aqueous phase concentrations, the partitioning effect has less of a consequence on the tension measurement. From the study so far, it can be ascertained that monomeric partitioning of the surfactant from the aqueous phase into the oil phase can be halted by ensuring that (i) the oil phase surfactant concentration is equal to or greater than c* and (ii) the aqueous phase concentration is equal to or greater than cmc_{water}.

It is worth noting, however, that the true $\Delta\gamma$(max) values obtained refer to alkane oil drops with an activity of unity. Incorporation of too much surfactant or associated water in the oil lens may reduce the activity significantly from unity. For systems

studied in this chapter, the maximum surfactant concentration in the oil lens is 1.3 wt% (less than 1 mol %) and hence there is little reduction in the activity of the oil.

5.5 Spreading behaviour of oils on aqueous solutions of C_nE_m surfactants

Once the alkane oil, containing c* of surfactant, is added to the surface of the solution, the first consideration is its spreading behaviour. This was observed using the spreading behaviour apparatus described in section 2.3.1. The oil drops generally spread initially on the surfactant solution, after which, non-spreading oils retract into visible circular stable lenses. Oils that were classified as spreading never produced stable lenses but instead gave irregular patches of spread film seen as patches showing interference colours. Table 5.2 summarizes the visual observations for the various systems. When lenses are formed, they are generally very flat. This, combined with the fact that the oils spread initially, makes it very difficult to be completely certain of the equilibrium spreading behaviour of oils on a particular surfactant, particularly for the oil chain lengths close to the apparent transition from spreading to non-spreading.

Table 5.2 **Summary of the spreading observations at 25°C for the surfactant + oil systems.**

surfactant	oil chain length	oil spreads ?
$C_{12}E_5$	7	yes
	8	no
	9	no
	10	no
$C_{12}E_7$	7	no
	8	no
	9	no
	10	no
$C_{12}E_9$	8	yes
	9	yes
	10	yes
	11	no
$C_{10}E_7$	11	yes
	12	yes
	13	no
	14	no
$C_{14}E_7$	8	yes
	9	yes
	10	no
	11	no
	12	no

Despite the uncertainty in the exact value of the oil chain length corrresponding to the transition, it can be seen that the alkane chain length at which the transition from equilibrium spreading behaviour to nonspreading occurs is affected by the nature of the surfactant, i.e. the transition occurs between chain lengths 7 and 8 for $C_{12}E_5$, between 10 and 11 for $C_{12}E_9$, between 12 and 13 for $C_{10}E_7$ and between 9 and 10 for $C_{14}E_7$.

The spreading transitions of linear alkanes on aqueous solutions of C_nE_m surfactants can be compared with their spreading behaviour on pure water and on solutions of some ionic surfactants at concentrations above cmc_{water}. For pure water, the transition from spreading to non-spreading behaviour has been reported to occur at alkane chain lengths between 6 and 7 at 24.5°C,[17] between 7 and 8 at 15°C,[18] and between 6 and 7 for a range of temperatures.[19] At room temperature, the spreading transition was found to be between alkane chain lengths of 9 and 10 for aqueous solutions of alkyltrimethylammonium bromides with chain lengths of 10, 12 and 16 carbon atoms.[20] The presence of surfactant monolayers generally increases the tendency of alkanes to spread (i.e. the transition moves to higher alkane chain lengths).

The magnitudes of the spreading coefficients can now be discussed in light of the visually observed spreading behaviour. Equation 5.1 defined the *equilibrium* spreading coefficient in terms of the equilibrium tensions. An *initial* spreading coefficient (S_{ow}(init)) can also be defined.

$$S_{ow}(\text{init}) = \gamma_{aw}(\text{no oil}) - \gamma_{ao} - \gamma_{ow} \qquad (5.2)$$

where γ_{ao} and γ_{ow} have the same meaning as before but γ_{aw}(no oil) is the tension of the aqueous surfactant solution in the absence of oil and this initial (i.e. non-equilibrium) value of the spreading coefficient can be positive. The following data concerning the spreading coefficients of alkane oils on surfactant solutions was carried out using the

Vapour Adsorption Train discussed in section 2.9 after the lens addition technique was discovered to have an unexpected time dependence. Figure 5.4 shows the variation of both $S_{ow}(eq)$ and $S_{ow}(init)$ with alkane chain length for both $C_{12}E_7$ and $C_{12}E_5$. It can be seen that the initial spreading coefficients are positive but that the equilibrium values drop to roughly zero. The visual observation that oil drops generally spread initially on the surfactant monolayers is consistent with the positive initial spreading coefficients and the fact that all equilibrium spreading coefficients are zero (most are ± 0.5 mN m^{-1} of zero) means that they cannot be used reliably to predict spreading behaviour. Table 5.3 summarizes the tensions involved and the spreading coefficients for various oils on various surfactants. It is concluded, therefore, that all the surfactant/oil combinations investigated here are rather close to spreading at equilibrium, an observation that is consistent with the formation of rather flat oil lenses.

Inspection of equations 5.1 and 5.2 shows that the tension decrease following the addition of the oil to the surface ($\Delta\gamma$) is the difference between the initial and equilibrium spreading coefficients. In the case of spreading oils, $S_{ow}(eq)$ is zero and hence $\Delta\gamma$ is equal to $S_{ow}(init)$. For non-spreading oils, $\Delta\gamma$ is greater than $S_{ow}(init)$ by an amount equal to $S_{ow}(eq)$. However, as has been shown in figure 5.4 and table 5.3, the equilibrium spreading coefficient for non-spreading oils are generally close to zero and hence, $\Delta\gamma$ values are close to $S_{ow}(init)$ values. This signifies that the addition of oil to a

Figure 5.4 **Variation of S_{ow}(init) (□) and S_{ow}(eq) (○) with alkane chain length for (a) $C_{12}E_7$ and (b) $C_{12}E_5$.**

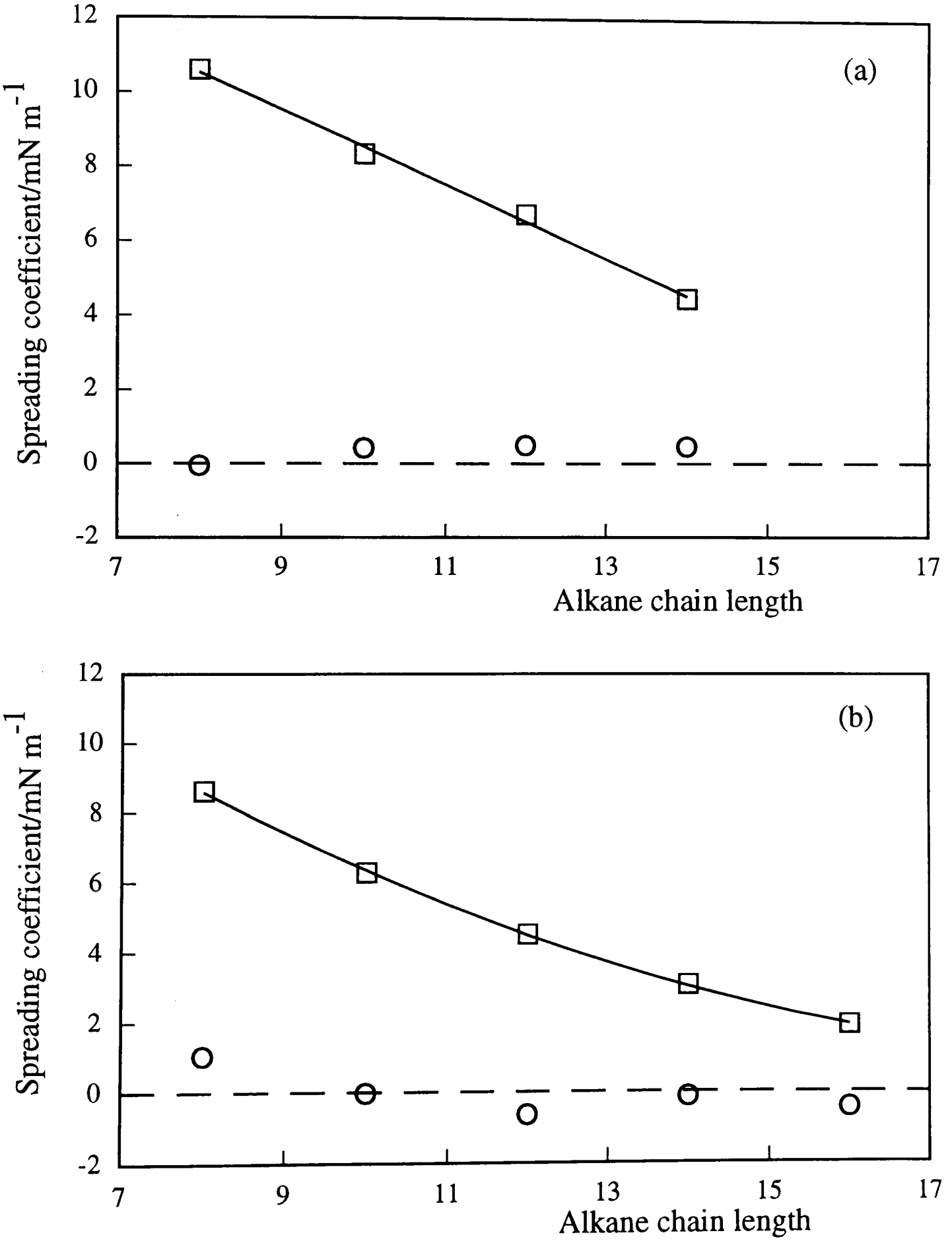

surfactant solution generally reduces the air-water tension to a value very close to the sum of γ_{ow} plus γ_{oa}.

Table 5.3 Equilibrium air/water, air/oil and oil/water tensions and equilibrium spreading coefficients (in mN m^{-1}) at 25°C for octane and hexadecane with the various nonionic surfactants.

surfactant	oil chain length	γ_{aw}	γ_{ao}	γ_{ow}	$S_{ow}(eq)$
$C_{12}E_5$	10	23.5	23.4	0.16	-0.06
	16	27.45	27.0	0.90	-0.45
$C_{12}E_7$	8	22.02	21.3	0.77	-0.05
	14	27.56	26.12	0.98	0.46
$C_{12}E_9$	8	22.8	21.3	1.34	0.2
	16	28.2	27.0	1.52	-0.3
$C_{14}E_7$	8	22.0	21.3	0.52	0.2
	16	27.9	27.0	0.80	0.1

5.6 Surface tension and the extent of oil adsorption onto surfactant monolayers.

The values of $\Delta\gamma$ for the adsorption of a range of spreading and non-spreading alkanes are shown in figures 5.5 and 5.6. Data for sodium dodecyl sulphate (SDS) and

Figure 5.5 **Variation of $\Delta\gamma$(max) for the addition of pure alkane with alkane chain length for C_{12} tailgroup surfactants with different headgroups with aqueous phase surfactant concentrations in excess of cmc_{water} at 25°C.**

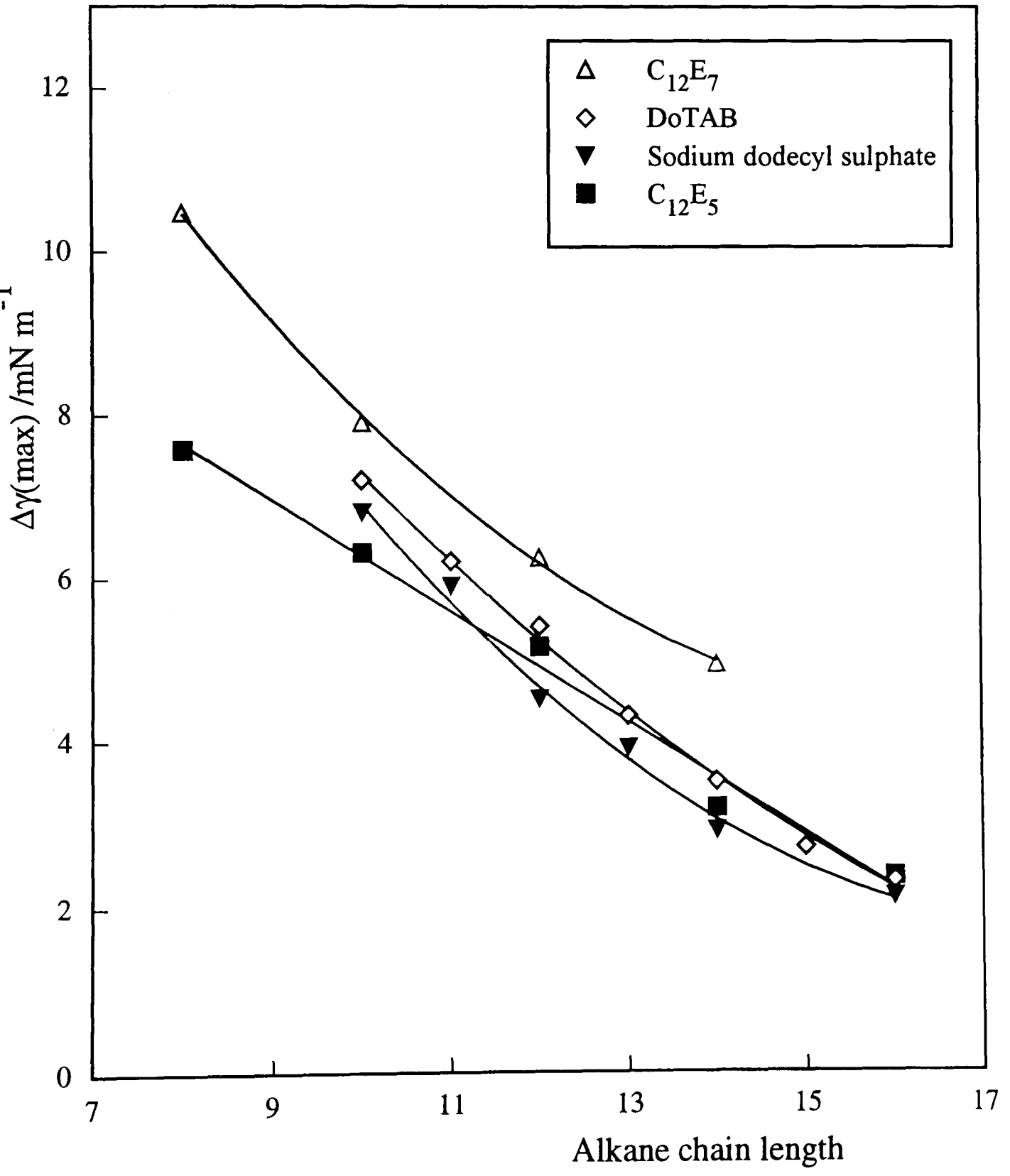

Figure 5.6 **Variation of $\Delta\gamma$(max) for the addition of pure alkane with alkane chain length for C_nE_7 surfactants and two cationic surfactants at surfactant concentrations in excess of cmc_{water} at 25°C. Filled symbols refer to spreading oils and unfilled symbols refer to non-spreading oils**

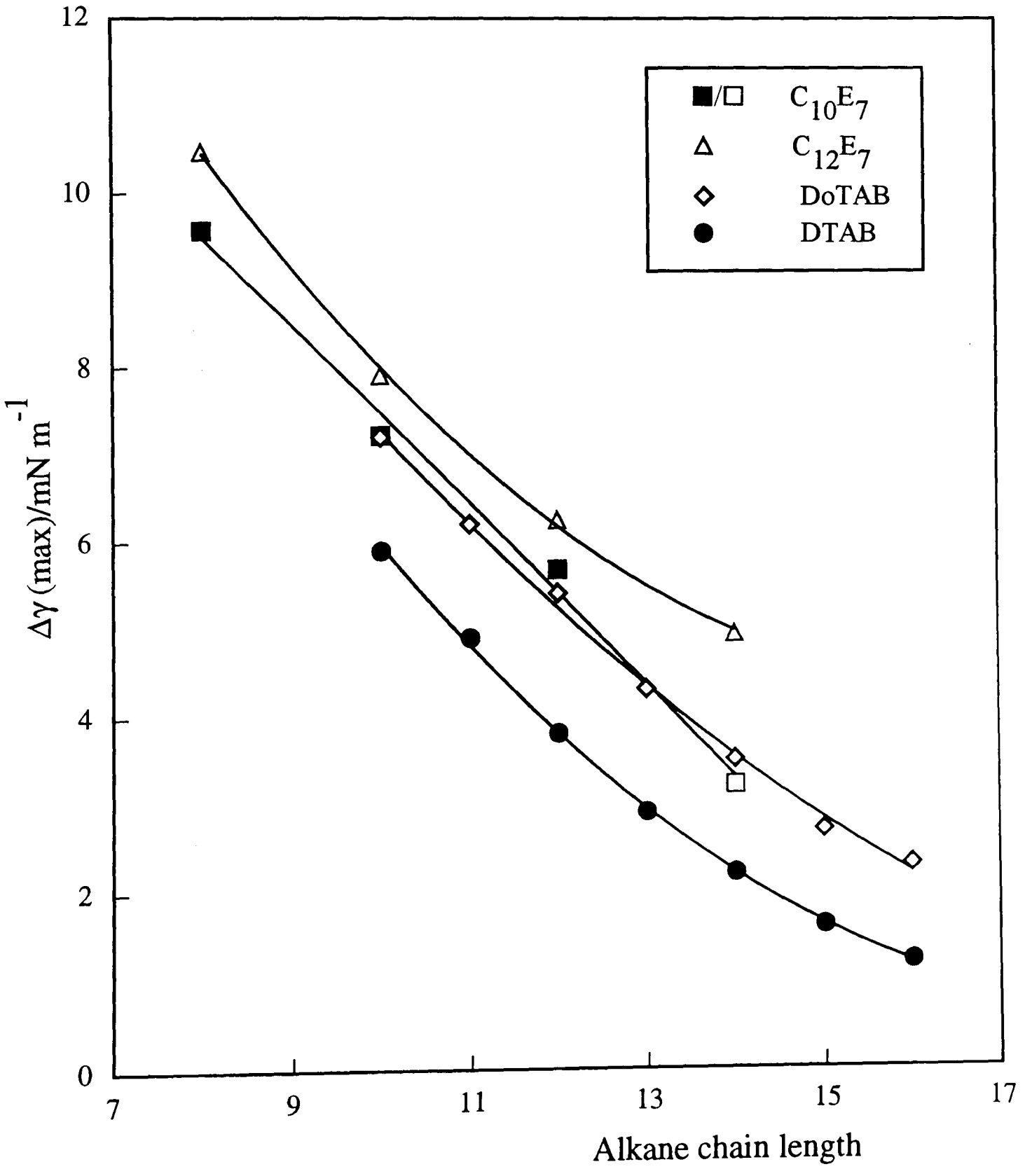

dodecyltrimethylammonium bromide (taken from reference 6) are also shown in figure 5.5 to allow comparison of the different headgroups. Figure 5.6 shows a comparison of results for surfactants of different chain lengths. For the non-ionics, $\Delta\gamma$ for a particular alkane increases with increasing headgroup and tailgroup.

We now consider how tension measurements can be used to estimate the extent of adsorption of oil onto the surfactant monolayers. At a constant temperature, the tension change is related to surface excess concentrations (Γ_i for species i) and changes in chemical potential ($d\mu_i$ for species i) according to the Gibbs adsorption isotherm.

$$-d\gamma = \sum_i \Gamma_i d\mu_i \qquad (5.3)$$

It is thus necessary to measure the variation in tension as a function of chemical potential of the adsorbing species (keeping the chemical potential of all other species constant) to obtain the surface concentration of the adsorbing oil. The initial method chosen to vary the chemical potential of the adsorbing oil was to add to the surface drops of the adsorbing oil mixed with a non-adsorbing diluent oil over a range of activities. The Gibbs equation can then be reconsidered for a system containing water (w), surfactant (s), diluent oil (do) and adsorbing oil (ao) in which the mixed monolayer of surfactant plus adsorbing oil is in equilibrium with lenses of bulk mixed oil. For such a system, the Gibbs equation becomes:

$$-d\gamma = \Gamma_w d\mu_w + \Gamma_s d\mu_s + \Gamma_{ao} d\mu_{ao} + \Gamma_{do} d\mu_{do} \qquad (5.4)$$

We assume that the addition of the oil mixture to the solution surface causes negligible change to the chemical potentials of either water or surfactant. This is certainly justifiable for water in which the alkanes are virtually insoluble. For the surfactant, the aqueous phase cmc values for $C_{12}E_5$ have been found to be almost identical for solutions both in the absence and in the presence of alkane oils[9] and thus $d\mu_s$ is likely to be zero. Noting that $-d\gamma = d\Delta\gamma$ it can be said,

$$d\Delta\gamma = \Gamma_{ao} d\mu_{ao} + \Gamma_{do} d\mu_{do} \qquad (5.5)$$

For a mixed oil drop containing a mole fraction x_{ao} of adsorbing oil and x_{do} of diluent oil, from the Gibbs-Duhem equation we obtain $d\mu_{do} = -(x_{ao}/x_{do})d\mu_{ao}$ and hence,

$$d\Delta\gamma = \{\Gamma_{ao} - (x_{ao}/x_{do})\Gamma_{do}\} d\mu_{ao} \qquad (5.6)$$

Substituting $d\mu_i = kT\ d\ln a_i$, where k is the Boltzmann constant, T is the absolute temperature and a_i is the activity of species i, yields

$$(d\Delta\gamma/d\ln a_{ao}) = kT\{\Gamma_{ao} - (x_{ao}/x_{do})\Gamma_{do}\} \qquad (5.7)$$

It can be seen from equation 5.7 that the surface concentration of the adsorbing oil Γ_{ao} can be obtained from measurements of $\Delta\gamma$ as a function of the adsorbing oil activity, a_{ao} (which is a product of the activity coefficient and mole fraction), only if Γ_{do} is zero i.e., the diluent oil does not adsorb in its own right. Equation 5.7 then becomes

$$(d\Delta\gamma/d \ln a_{ao}) = kT \Gamma_{ao} \qquad (5.8)$$

To check for adsorption of the diluent oil, a drop of the pure diluent oil was added to the surfactant solution surface. Diluent oils showing a zero $\Delta\gamma$ are presumed not to adsorb when added as the pure oil. However, a zero $\Delta\gamma$ for the pure diluent oil does not guarantee that no adsorption takes place when the diluent oil is mixed with the adsorbing oil.

In order to check the validity of equation 5.8, the adsorption of dodecane onto aqueous solutions of $C_{12}E_5$ was examined using both squalane and dinonyl phthalate (DNP) as diluent oil. The activity coefficients for dodecane with both the diluent oils were obtained from literature[21] where possible, or, in most cases, activity coefficients were calculated using the equations and extrapolations of the parameters given in reference 21 For dodecane, the activity coefficients, with which the pure adsorbing oil would have an activity of 1, range from 0.83 (at $x_{dodecane} = 0$) to 1 in squalane mixtures, and from 1.62 (at $x_{dodecane} = 0$) to 1 in DNP mixtures. Figure 5.7a shows the variation

of $\Delta\gamma$ with mole fraction of dodecane and figure 5.7b shows the plot with the mole fractions corrected for non-ideality of the mixtures. The activity coefficients corrections cause the curves for squalane and DNP to collapse to a common line. This result strongly suggests that neither squalane nor DNP adsorb to any significant extent across the entire mole fraction range with dodecane. In theory, it is possible that both squalane and DNP adsorb to the same extent across the mole fraction range but this seems highly unlikely in view of their different polarities.

5.7 Adsorption isotherms for alkanes on C_nE_m solutions

Figure 5.8 shows the variation of $\Delta\gamma$ with mole fraction activity for octane and hexadecane in mixtures with squalane on $C_{12}E_7$ monolayers. It can be seen that pure squalane does adsorb in this case i.e. $\Delta\gamma$ for pure squalane is greater than zero. The non-zero $\Delta\gamma$ value for pure squalane means that equation 5.8 cannot be used to estimate the surface concentration of the alkanes on $C_{12}E_7$ monolayers. However, figure 5.8 does show that hexadecane has a near linear variation of $\Delta\gamma$ with activity whereas the data for octane curves strongly upwards, suggesting much stronger adsorption in the case of octane. It was thus important to determine the $\Delta\gamma$ values for pure squalane on all the potential surfactants for investigation. The values obtained can be seen in table 5.4

Figure 5.7 **Variation of $\Delta\gamma$ with (a) mole fraction and (b) mole fraction activity of dodecane for the addition of mixtures with squalane (●) or DNP (■).**

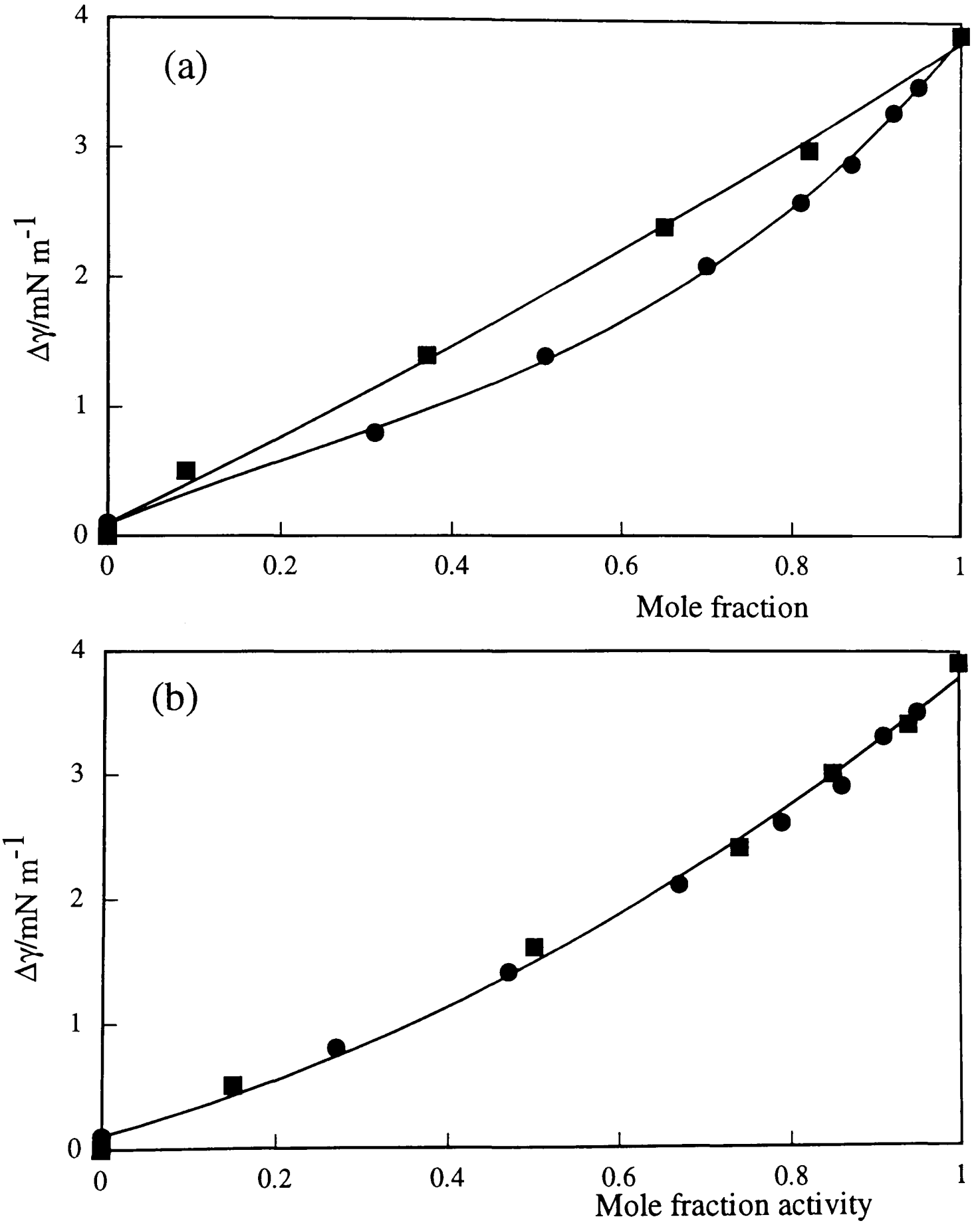

Figure 5.8 **Variation of $\Delta\gamma$ with mole fraction activity of octane (■) and hexadecane (●) for the addition of alkane/squalane mixtures on solutions of $C_{12}E_7$ (5mM).**

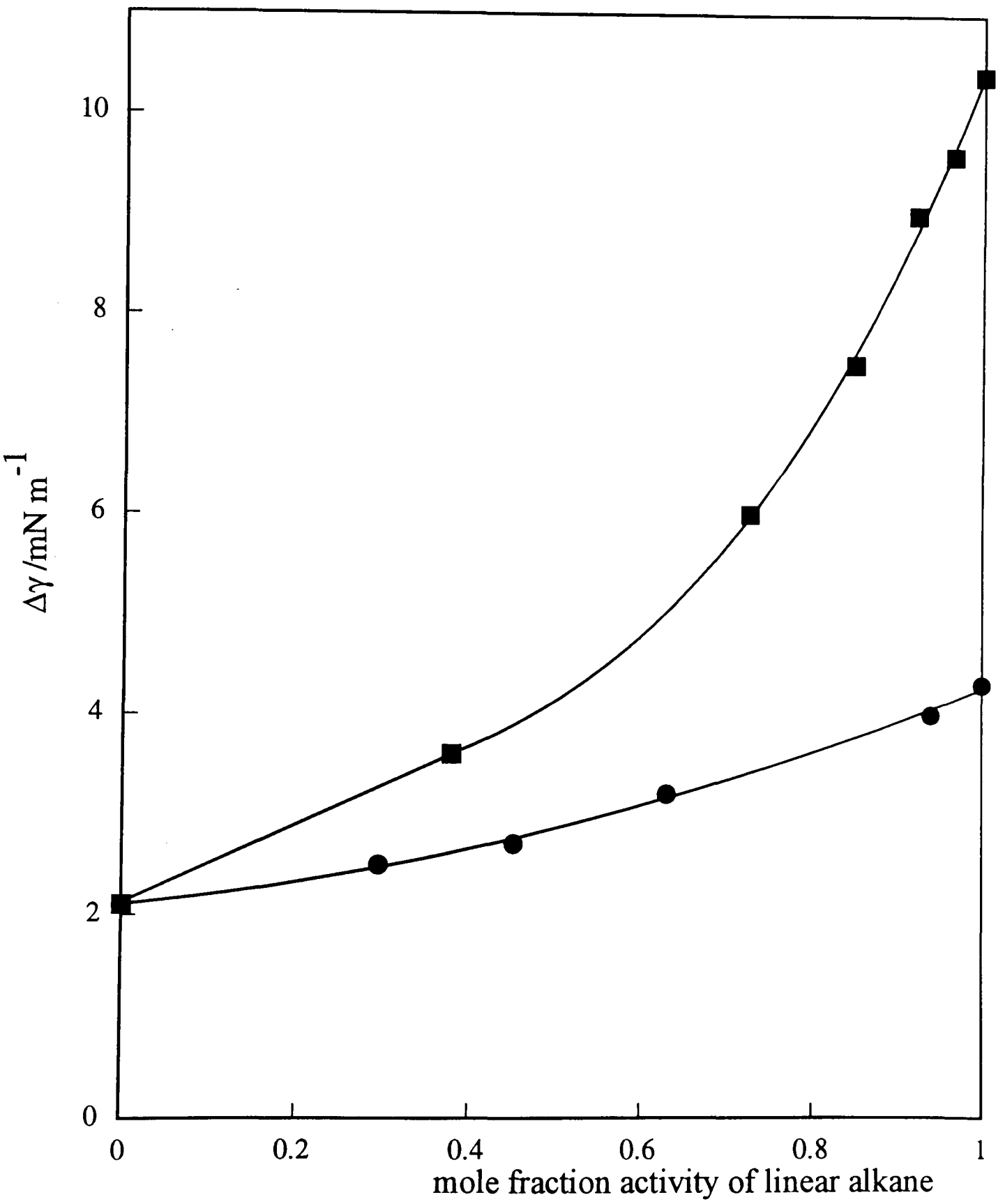

Table 5.4 **Values of $\Delta\gamma$ obtained for pure squalane oil drops on various surfactants.**

Surfactant	$\Delta\gamma$ (mN m^{-1})
$C_{12}E_5$	0.1
$C_{12}E_7$	2.1
$C_{12}E_9$	2.5
$C_{10}E_7$	0.1
$C_{14}E_7$	2.5

The only surfactants which showed negligible adsorption of pure squalane were $C_{12}E_5$ and $C_{10}E_7$ and it is with these two that the detailed adsorption studies were carried out.

5.7.1 Adsorption of alkanes onto $C_{12}E_5$ solutions.

The remaining data in this chapter was derived from the Vapour Adsorption Train apparatus built at the University, a description of which can be seen in section 2.9. Plots of $\Delta\gamma$ versus activity for (in decreasing order) octane, decane, dodecane, tetradecane and hexadecane on $C_{12}E_5$ monolayers are presented in figure 5.9. When the oil spreading behaviour was studied visually, all these oils, at all mole fraction activities appeared to behave as non-spreading oils. The polynomial fits associated with each of

Figure 5.9 **Variation of $\Delta\gamma$ with mole fraction activity for the addition of alkanes on solutions of $C_{12}E_5$ (6.4 mM) at 25°C.**

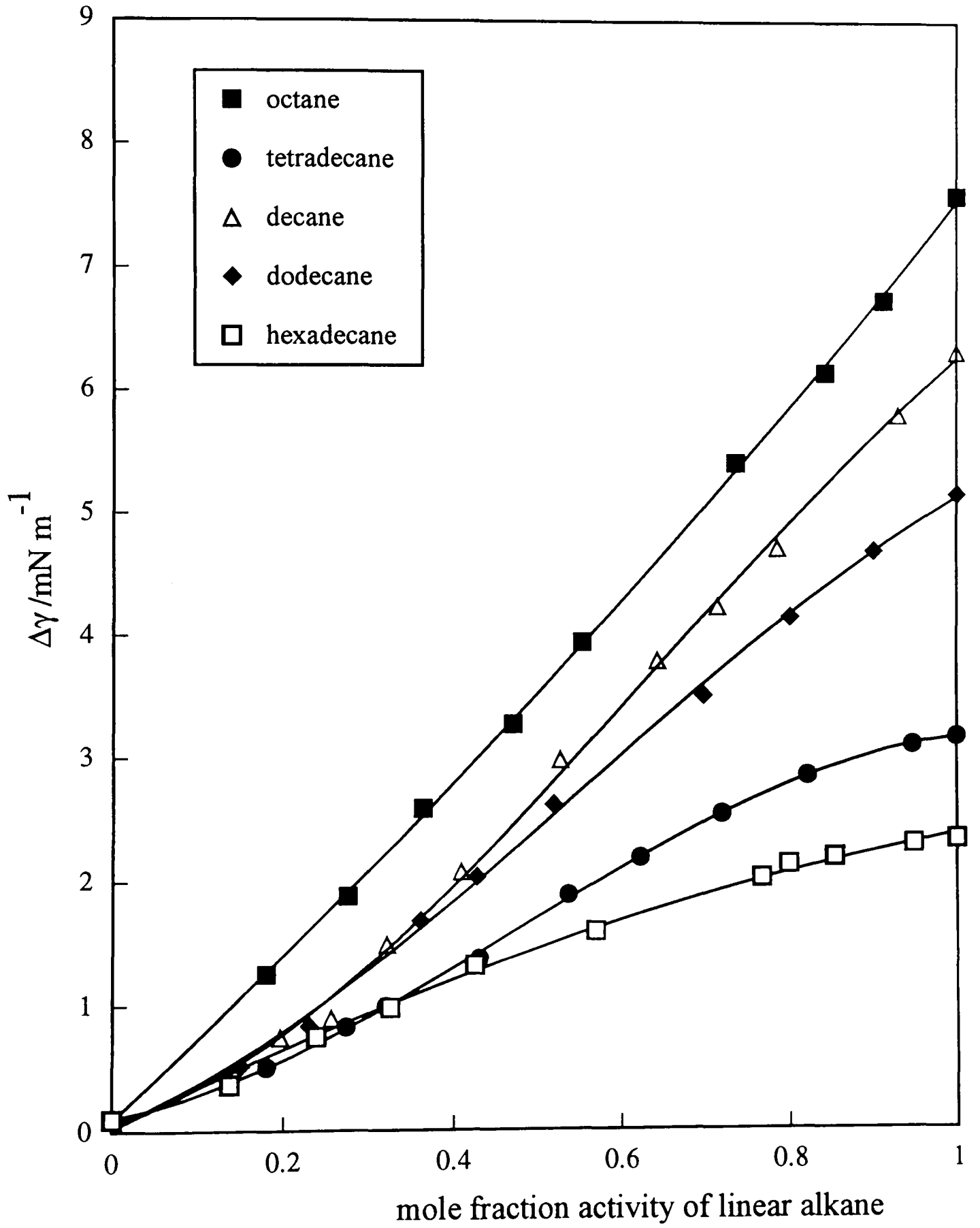

the oils in figure 5.9 can be seen in Appendix 1. Differentiation of the polynomial fitting functions then yield Γ_{ao} as a function of the activity of the adsorbing oil.

A plot of the surface concentrations of the oils as a function of activity on solutions of $C_{12}E_5$ is shown in figure 5.10. As has been seen for both planar air-water surfactant monolayers[6] and for curved monolayers coating microemulsion droplets[8], alkane adsorption increases with decreasing alkane chain length. From figure 5.10, it can be seen that all the adsorption isotherms are almost linear with a slight increase in curvature at the lower chain length oils. The increasing curvature of the isotherms is consistent with an increase in adsorption with increasing alkane content of the mixed alkane/surfactant film. For $C_{12}E_5$, the maximum adsorption observed corresponds to roughly 2 molecules nm^{-2} (for octane). Since the minimum cross-sectional area of an alkyl chain is approximately 0.2 nm^2 and the surfactant contributes approximately 2 alkyl chains per nm^2,[9] it can be said that this result ties in with the fact that these oils do not appear to spread macroscopically (as judged visually) and are lenses in equilibrium with a mixed monolayer. This is in agreement with the adsorption of dodecane on monolayers of alkyltrimethylammonium bromide surfactants with chain lengths of 12, 14 and 16. They give approximately linear plots of $\Delta\gamma$ versus activity and the mixed films have been shown to be monolayers.[22,23] The shapes of the adsorption isotherms for alkanes on surfactant monolayers are highly dependent on the molecular structure of the surfactant.

The adsorption data shown in figure 5.10 are represented in terms of the equivalent thickness of the adsorbed film in figure 5.11. The value for equivalent thickness is

Figure 5.10 **Adsorption isotherms for alkanes on aqueous solutions of $C_{12}E_5$ at 25^0C.**

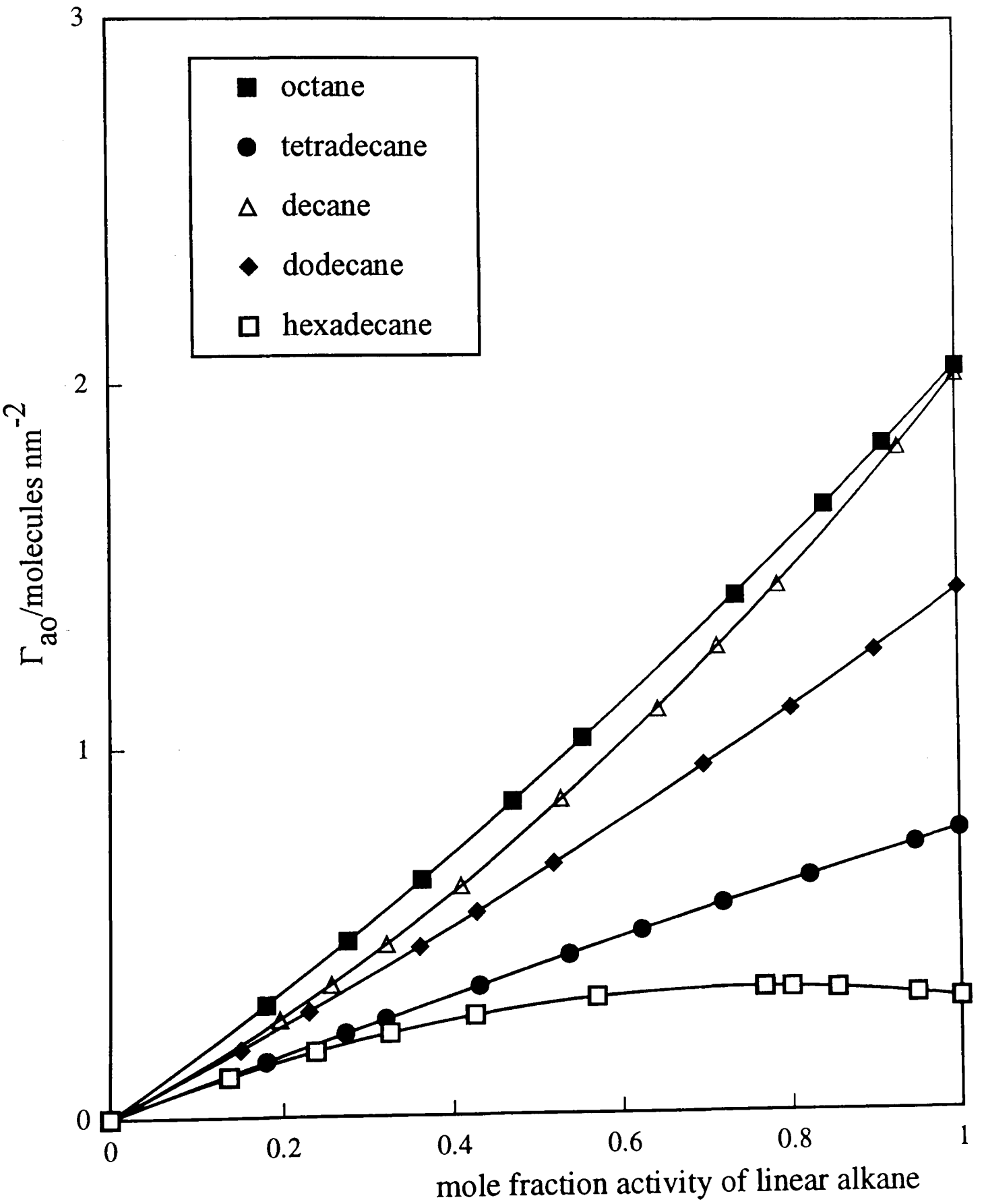

Figure 5.11 **Oil film thickness versus activity of adsorbing alkane on $C_{12}E_5$ (6.4 mM) at 25^0C.**

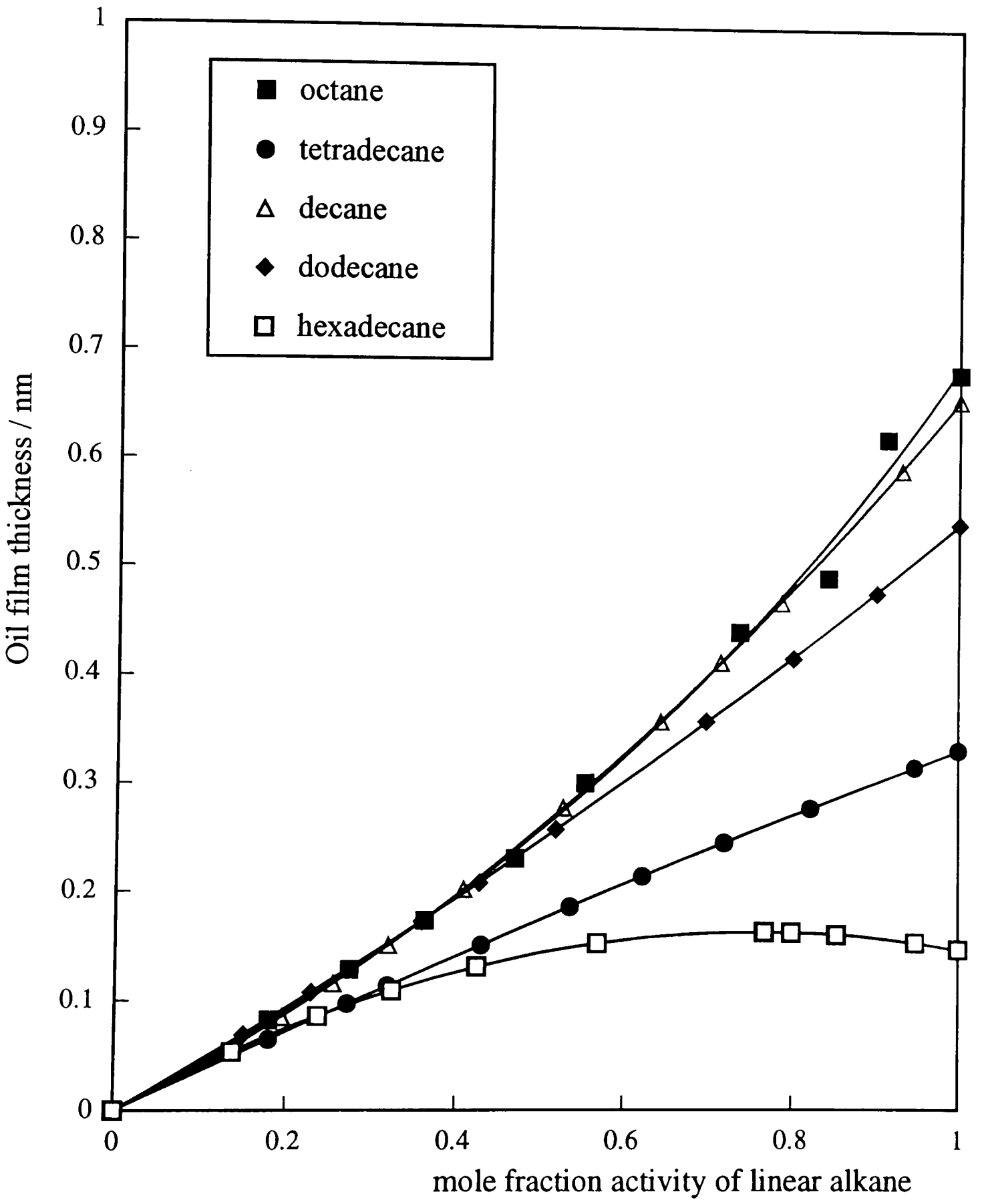

achieved by multiplying Γ_{ao} by the molecular volume of the oil in bulk liquid. This value corresponds to the volume of alkane that is adsorbed per unit area and increases with decreasing alkane chain length. The equivalent thicknesses of the oils obtained for $C_{12}E_5$ monolayers range from 0 to 0.70 nm. This is consistent with the fact that these oils were found not to spread by visual observation. Spreading oils showing interference colours would give film thicknesses in excess of 100 nm.

5.7.2 Adsorption of alkanes onto $C_{10}E_7$ solutions.

For alkanes added to $C_{10}E_7$ solutions, the transition from spreading to non-spreading behaviour is judged visually to occur between dodecane and tridecane. Plots of $\Delta\gamma$ versus oil activity for a range of alkanes spanning this transition can be seen in figure 5.12. Tetradecane, a non-spreading oil, shows approximately linear behaviour whereas the plot for dodecane, a spreading oil, is slightly curved. However, there does not appear to be a clear correlation between the linearity of the plot and the spreading behaviour since figure 5.9 shows a range of non-spreading oils with plots that are slightly curved.

The adsorption isotherms for both spreading and non-spreading alkanes on $C_{10}E_7$ solutions are compared in figures 5.12, 5.13 and 5.14 which show the adsorption data in terms of $\Delta\gamma$, Γ_{ao} and equivalent oil film thickness, respectively. The curvature of the

Figure 5.12 **Variation of $\Delta\gamma$ with mole fraction activity for the addition of alkanes on solutions of $C_{10}E_7$ (9.5 mM) at 25°C.**

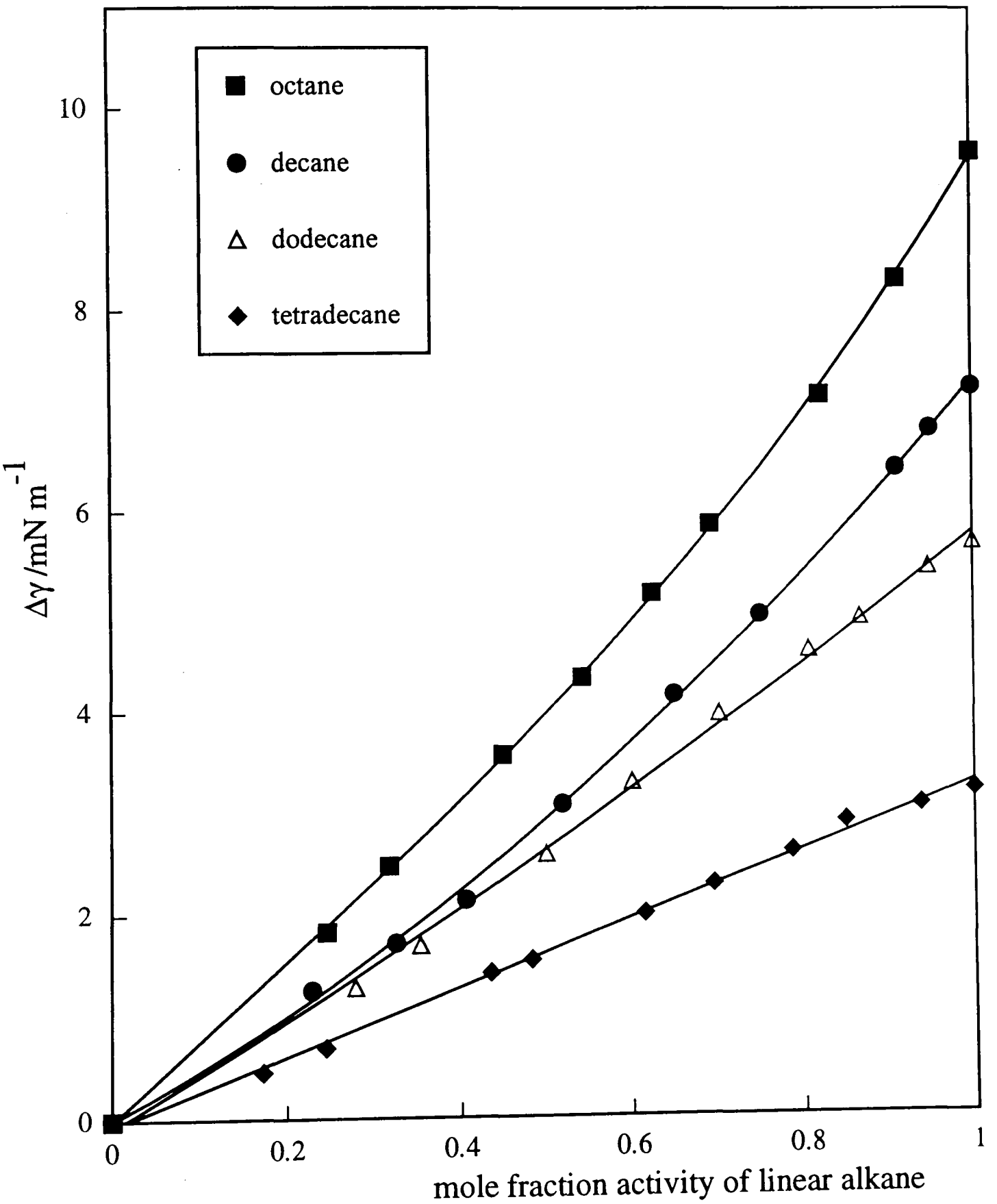

Figure 5.13 **Adsorption isotherms for alkanes on solutions of $C_{10}E_7$ (9.5 mM). Inset shows a comparison of adsorption data for octane on different surfaces at 25°C.**

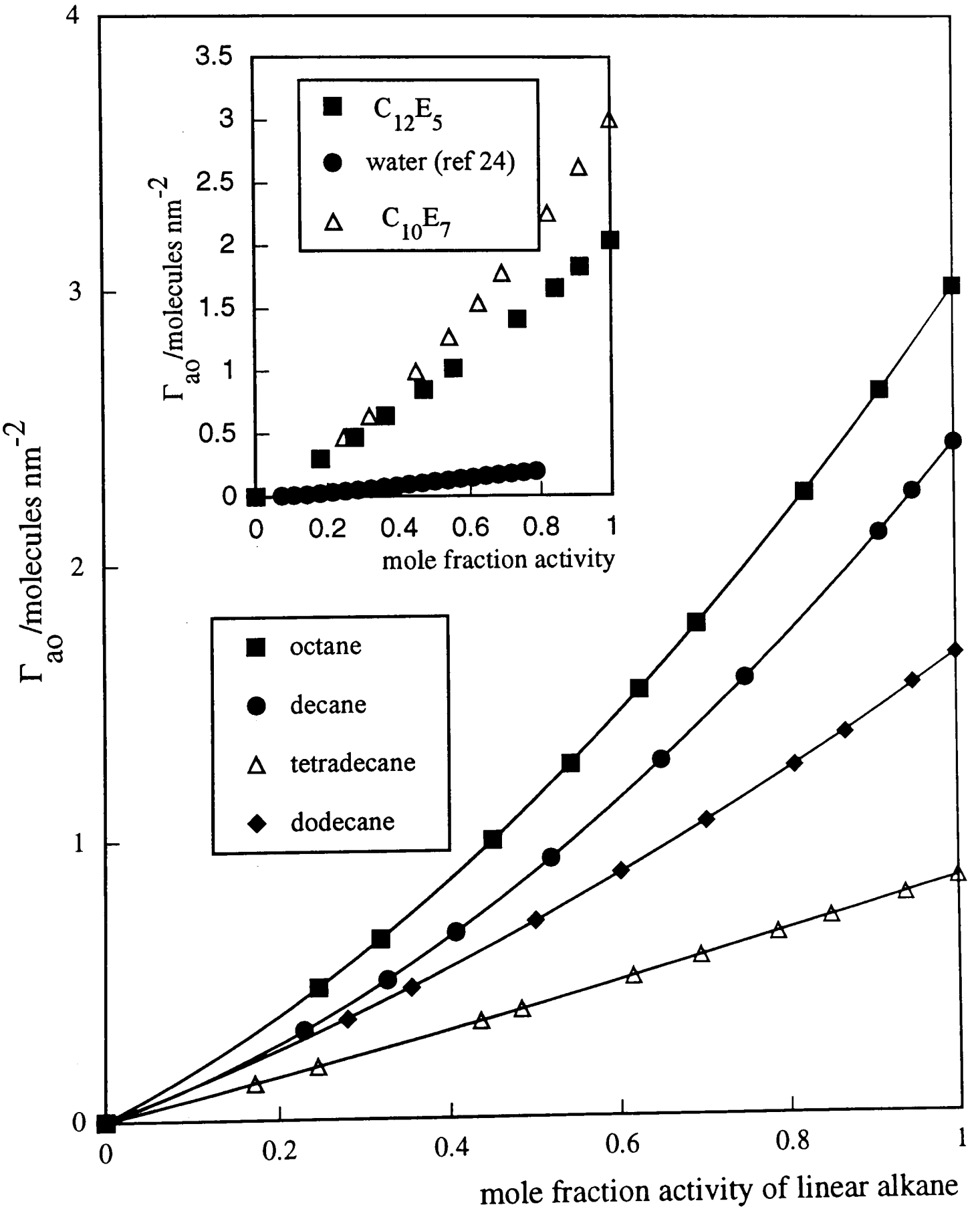

Figure 5.14 **Oil film thickness versus activity of adsorbing alkane on $C_{10}E_7$ (9.5 mM) at 25°C.**

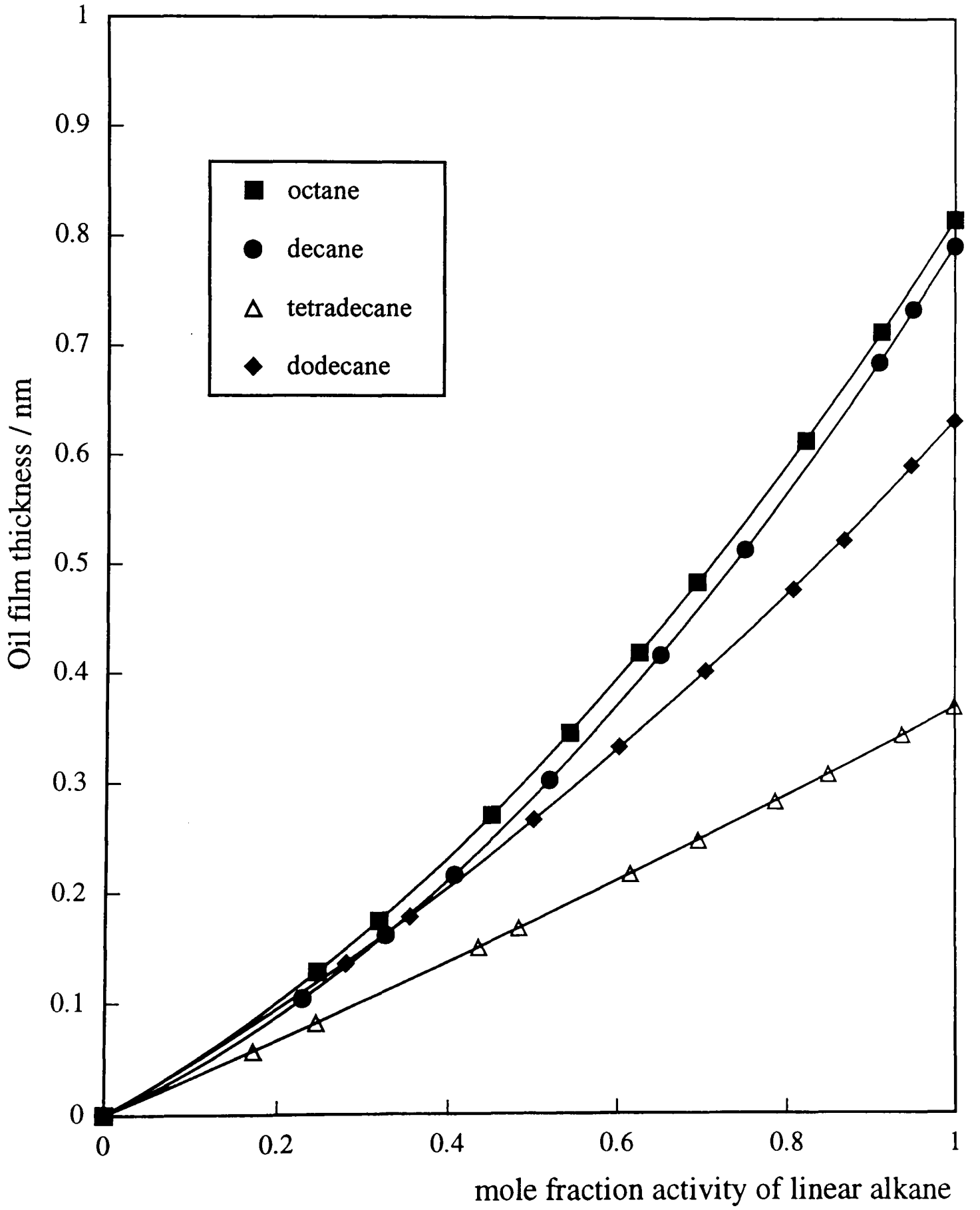

adsorption plots increases slightly with decreasing alkane chain length. The inset plot in figure 5.13 shows a comparison of the adsorption of octane on pure water[24]. on $C_{12}E_5$ solutions and on $C_{10}E_7$ solutions. Octane spreads on $C_{10}E_7$ but forms lenses on water and on $C_{12}E_5$ solutions. It can be seen that the adsorption isotherm is strongly affected by the presence and the nature of the surfactant monolayer.

In the cases where the pure adsorbing oil shows spreading behaviour it is possible to speculate concerning the meaning of the maximum values of Γ_{ao}. Oils which are visually observed to spread and produce interference colours should form film thicknesses of the order of 100 nm. From the data obtained in figures 5.12 to 5.14, thicknesses were obtained which were two orders of magnitude less than this. The measured air-water tension in the presence of oil will decrease with increasing oil film thickness as adsorption increases with increasing activity of the oil. However, at oil film thicknesses greater than a few molecular diameters, the film disjoining pressure is likely to be very small and hence, the tension decrease with further thickening of the oil film is expected to become negligible relative to the precision of the tension measurements. If this argument is correct, the maximum value of Γ_{ao} for spreading oils provides a measure of the amount of surface perturbed oil associated with the *oil-water interface* which exists in the presence of a spread film of the pure oil.

Figure 5.14 shows the thicknesses obtained from the surface concentration measurements in figure 5.13. The spreading oils (octane, decane and dodecane) show

maximum thicknesses ranging from 0.3 to 0.8 nm. and again, as with $C_{12}E_5$ monolayers, the thickness of the oil layer associated with the oil-water interface increases with decreasing alkane chain length. Tetradecane, which is a non-spreading oil on $C_{10}E_7$, shows a lower thickness of 0.4 nm. It is worth noting, however, that the thicknesses reported in figure 5.14 are the contributions from the adsorbed alkane only. The actual thickness of the surface region would include a contribution from the surfactant monolayer.

5.8 Fitting the data to Aranovich adsorption isotherms

The data shown in figures 5.10 and 5.13 appear to be of the type III B.E.T. isotherms. However, the data cannot be fitted to this type of isotherm. A reasonable fit has been found with an adsorption isotherm which has been proposed by Aranovich and Donohue.[25,26,27] The equation has the general form as shown in equation 5.9

$$\Gamma = \frac{Ax}{\left[(1 + Bx)(1-x)^{d}\right]} \qquad (5.9)$$

and is valid for isotherms of types II and III in the IUPAC classification scheme.[28,29] In the equation, x is the activity of the adsorbing species, Γ is the amount of adsorbing species adsorbed at activity x, d is a parameter representing the curvature of the

isotherm (d=0 fits a linear isotherm which is the case for Henry's law, see figure 5.15a) and A and B are constants. As described in reference 26, it is possible to derive an isotherm from equatio 5.9 which is appropriate for the adsorption of oils onto aqueous solutions (a weakly attractive surface). This equation is shown below.

$$\Pi = a_m kT \frac{\left[1-(1-x)^{1-d}\right]}{(1-d)} \qquad (5.10)$$

where Π is the surface pressure ($\Delta\gamma$) of the adsorbing oil at activity x, k is Boltzmann's constant, T is the temperature and a_m is the extrapolation of the Henry's law region of the plot to unit activity of the adsorbing oil (see figure 5.15a). It can be seen that the maximum surface pressure (Π_{max}) when x is unity, is thus related to these parameters according to,

$$\Pi_{max} = \frac{a_m kT}{(1-d)} \qquad (5.11)$$

and rearranging this gives,

$$a_m = \frac{\Pi_{max}(1-d)}{kT} \qquad (5.12)$$

It can be seen from equation 5.12 that when d=0, $a_m = \Pi_{max}/kT$, which is the adsorption obeying Henry's law. Substituting equation 5.12 into equation 5.10, gives

$$\Pi = \Pi_{max}\left[1-(1-x)^{1-d}\right] \qquad (5.13)$$

Equations 5.12 and 5.13 can be used to fit plots of $\Delta\gamma$ (Π) versus x to yield values for d, a measure of the deviation from Henry's law of the isotherm at higher activities (values are always between 0 and 1) and a_m, the extrapolation of the Henry's law region of the graph which may be interpreted as the maximum surface concentration of oil adsorbed in the surfactant monolayer region (see figure 5.15b). Figure 5.16 shows typical fits for alkanes on $C_{12}E_5$ and figure 5.17 shows the Aranovich fits for alkanes on $C_{10}E_7$. In general, the Aranovich adsorption isotherm fits the longer chain length alkanes adsorption better than the adsorption of the shorter chain lengths. Table 5.5 shows all the d values and a_m values for the adsorption of the alkane oils on $C_{12}E_5$ and $C_{10}E_7$ surfactants and figure 5.18 shows this data plotted as a function of alkane chain length.

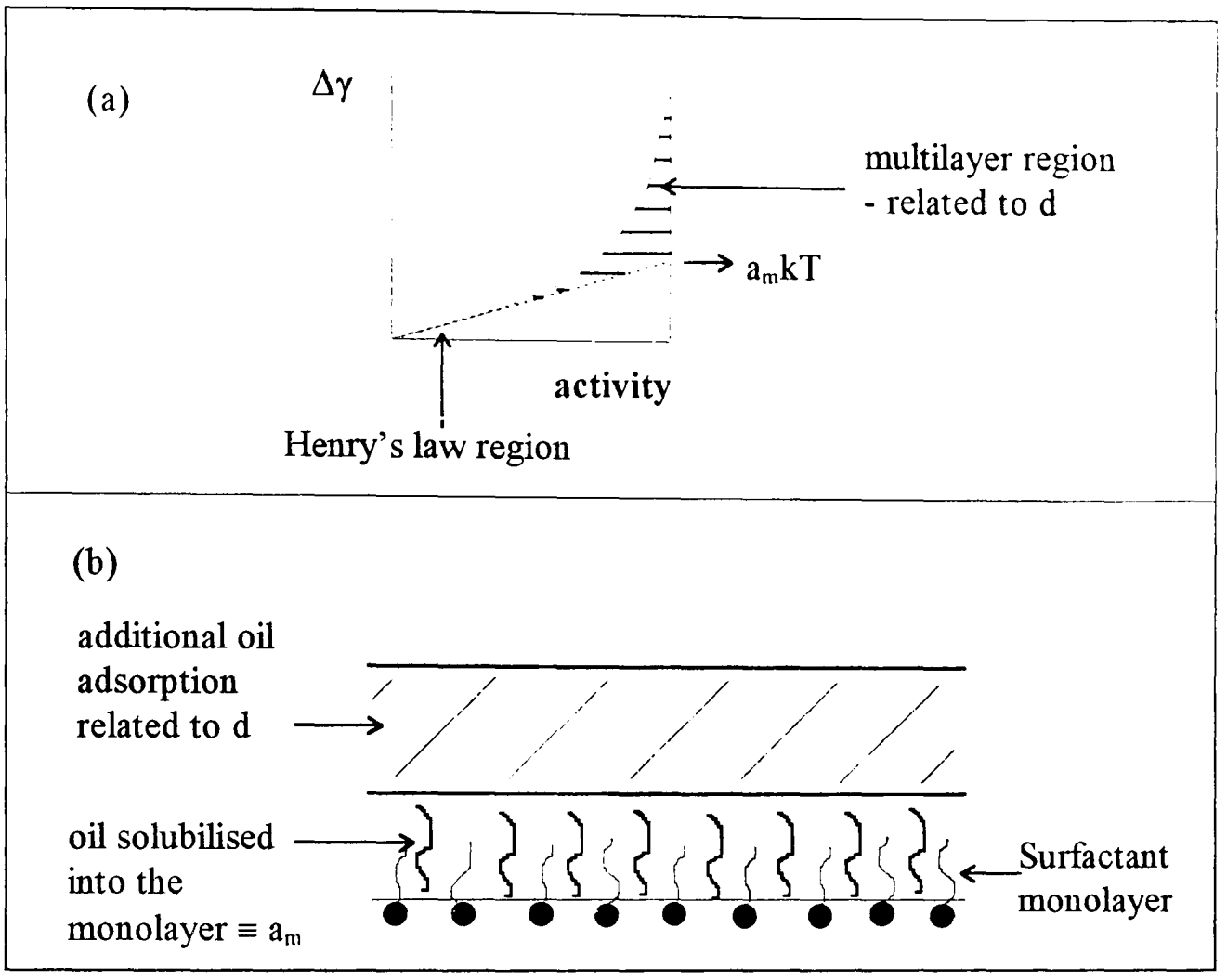

Figure 5.15 (a) Schematic diagram of an adsorption isotherm showing how d and a_m relate to the shape of the isotherm. (b) Schematic diagram showing the adsorption of a monolayer of oil which is equivalent to the value a_m and multilayer adsorption which is related to d.

Figure 5.16 **Aranovich fit to the data obtained for alkanes adsorption onto a $C_{12}E_5$ monolayer at the air-water interface at 25°C.**

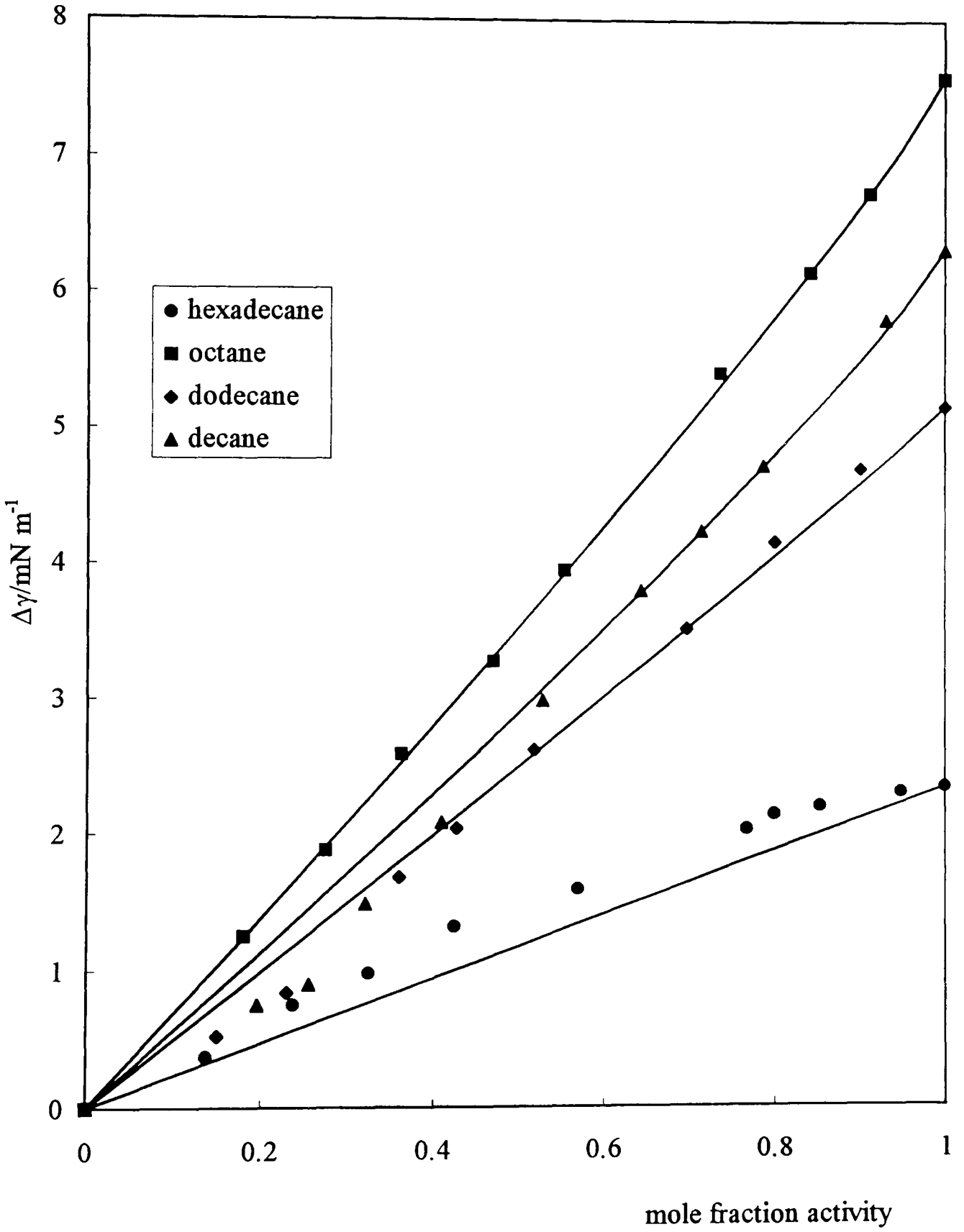

Figure 5.17 **Aranovich fit to the data obtained for alkanes adsorption onto a $C_{10}E_7$ monolayer at the air-water interface at 25°C.**

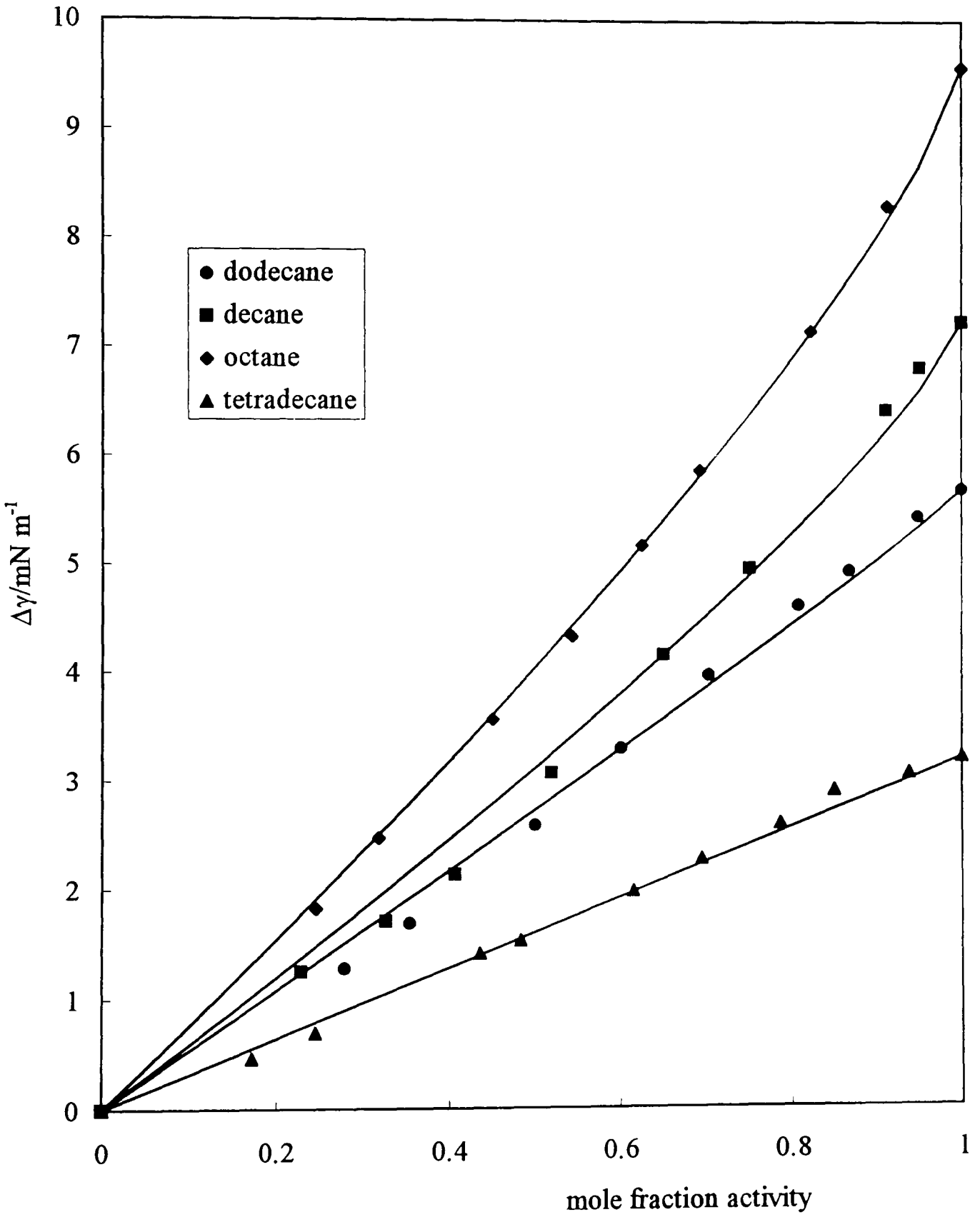

Figure 5.18 **Values of d and a_m versus alkane chain length for $C_{12}E_5$ and $C_{10}E_7$ calculated from the Aranovich adsorption isotherm**

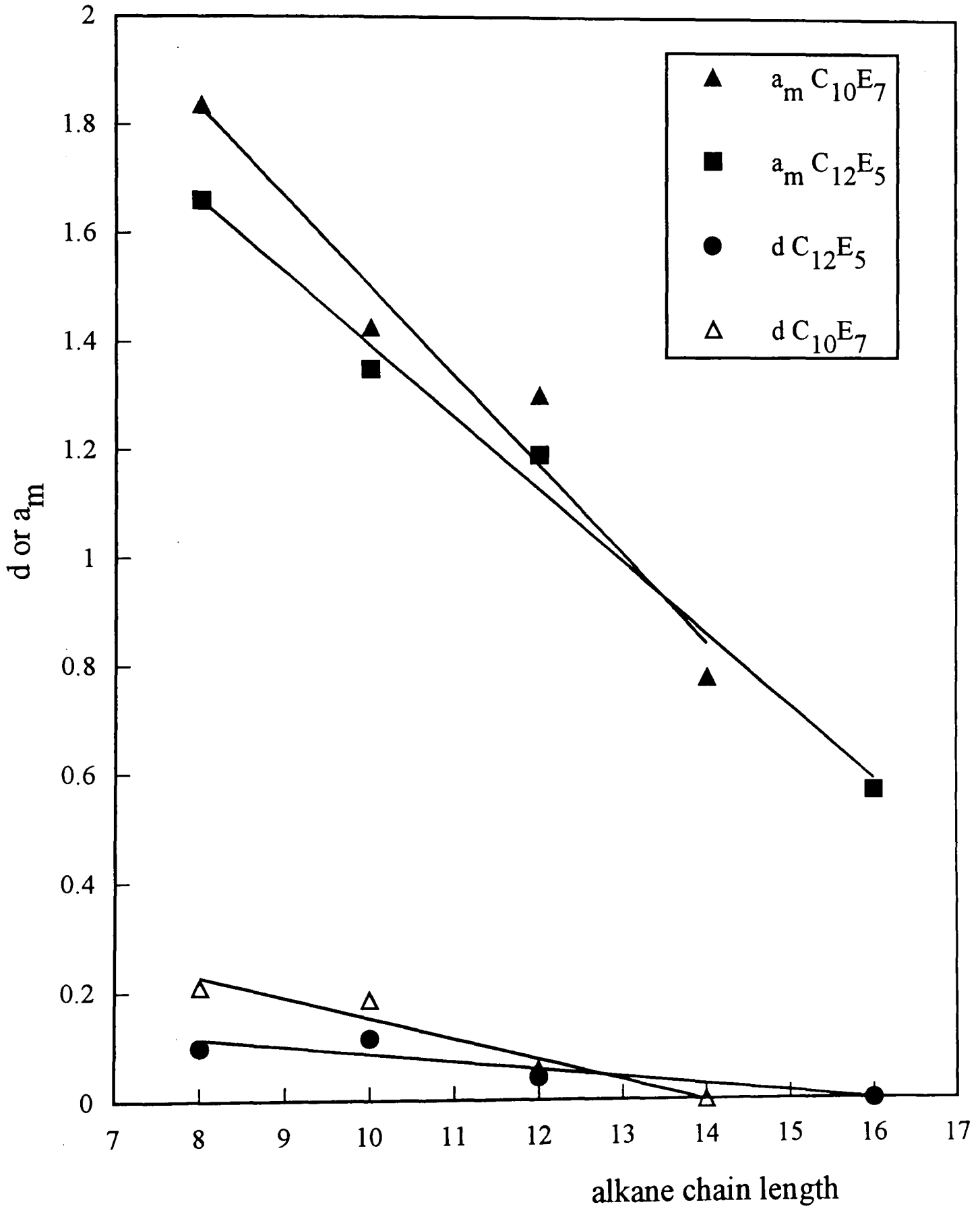

Table 5.5 Values of d and a_m for alkane adsorption onto monolayers of $C_{12}E_5$ and $C_{10}E_7$ calculated from the Aranovich equation of state.

Surfactant	Alkane	d	a_m (molecules nm^{-2})
$C_{12}E_5$	octane	0.098	1.66
	decane	0.114	1.35
	dodecane	0.042	1.19
	hexadecane	0	0.57
$C_{10}E_7$	octane	0.21	1.837
	decane	0.186	1.427
	dodecane	0.055	1.301
	tetradecane	0	0.779

It can be seen from table 5.5 that for the non-ionic surfactants studied in this chapter, both d and a_m tend to decrease with increasing alkane chain length, suggesting that the amount of adsorbing oil in the monolayer decreases with chain length. Also, the extent of multilayer formation decreases with increasing alkane chain length.

5.9 Oil adsorption into surfactant monolayers at the oil-water interface

This chapter has primarily been concerned with oil adsorption from liquid mixtures into monolayers at the air-water surface. However, oil adsorption for oil mixtures which spread on surfactant solutions may be an indication of the amount of oil associated with the surfactant monolayer at the oil-water interface. Since equation 5.8 is valid for the oil-water interface as well as for the air-water interface with oil lenses, measurement of the oil-water tension at fixed surfactant concentration with varying oil composition should yield the adsorption of an oil relative to that of the diluent used. If the adsorption of the diluent oil is zero at the oil-water interface, the surface concentration of the adsorbing oil is given directly by equation 5.8, and the value may be comparable to those obtained from spreading oils at the air-water interface.

Figure 5.19 shows the variation of the oil-water interfacial tension with oil composition for the water + $C_{12}E_5$ + dodecane system with either squalane or DNP as the diluent oil (a non-spreading system at the air-water interface). Large differences between squalane and DNP as diluent oils are seen in figure 5.19 suggesting that adsorption of one or both of these diluent oils *does* occur at the oil-water interface. Figure 5.20 shows the corresponding relative adsorption isotherms at the oil-water interface together with the isotherm for dodecane on $C_{12}E_5$ at the air-water interface. The curves

Figure 5.19 **Oil-water tension, γ_{ow}, versus mole fraction activity for dodecane mixtures with either DNP(●) or squalane(■) with $C_{12}E_5$ (6.4mM, 100xcmc) solution at 25°C.**

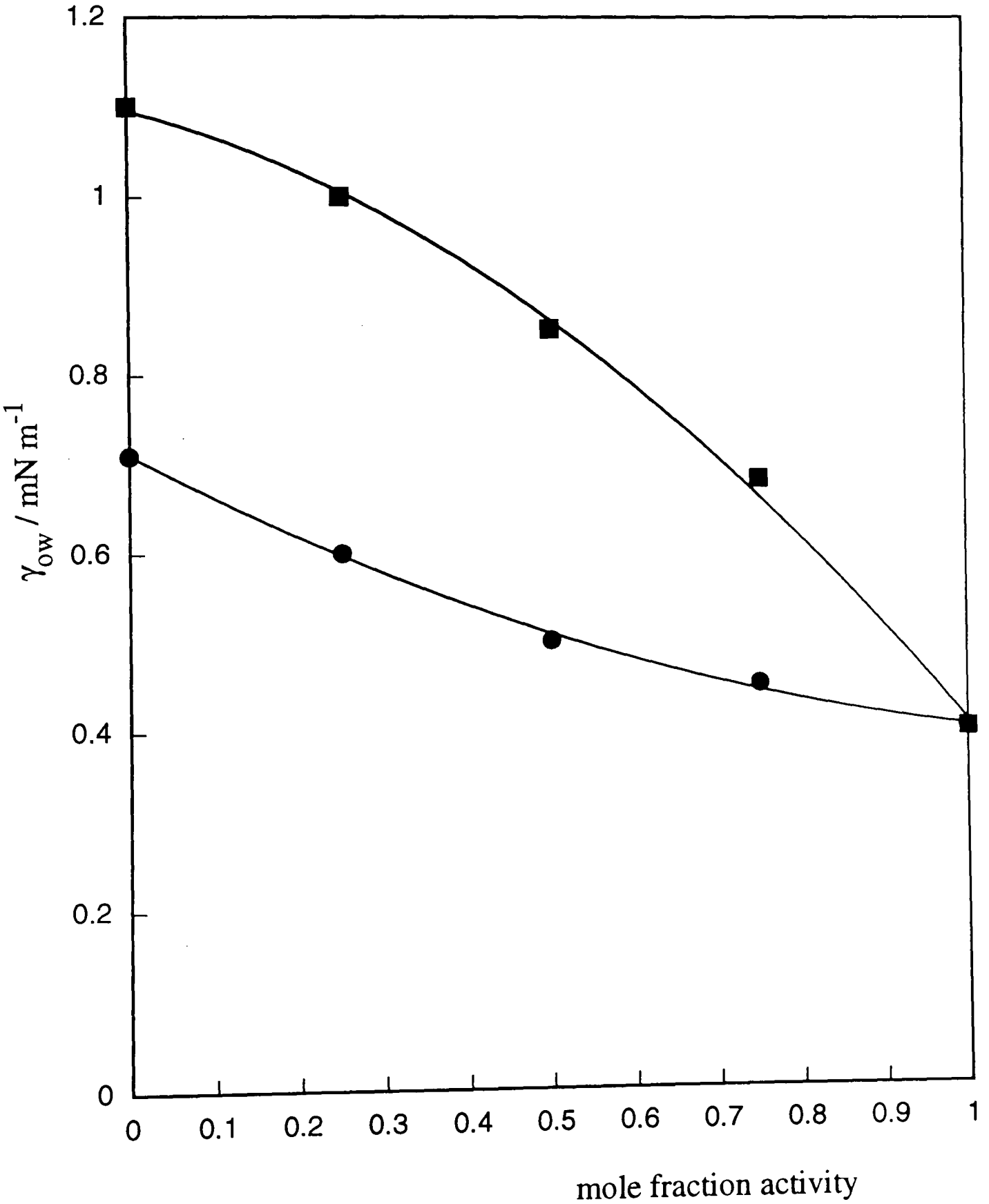

Figure 5.20 **Surface excess concentrations at the oil/water interface versus mole fraction activity for dodecane/diluent oil mixtures with $C_{12}E_5$ (6.4mM, 100xcmc) solution at 25°C.**

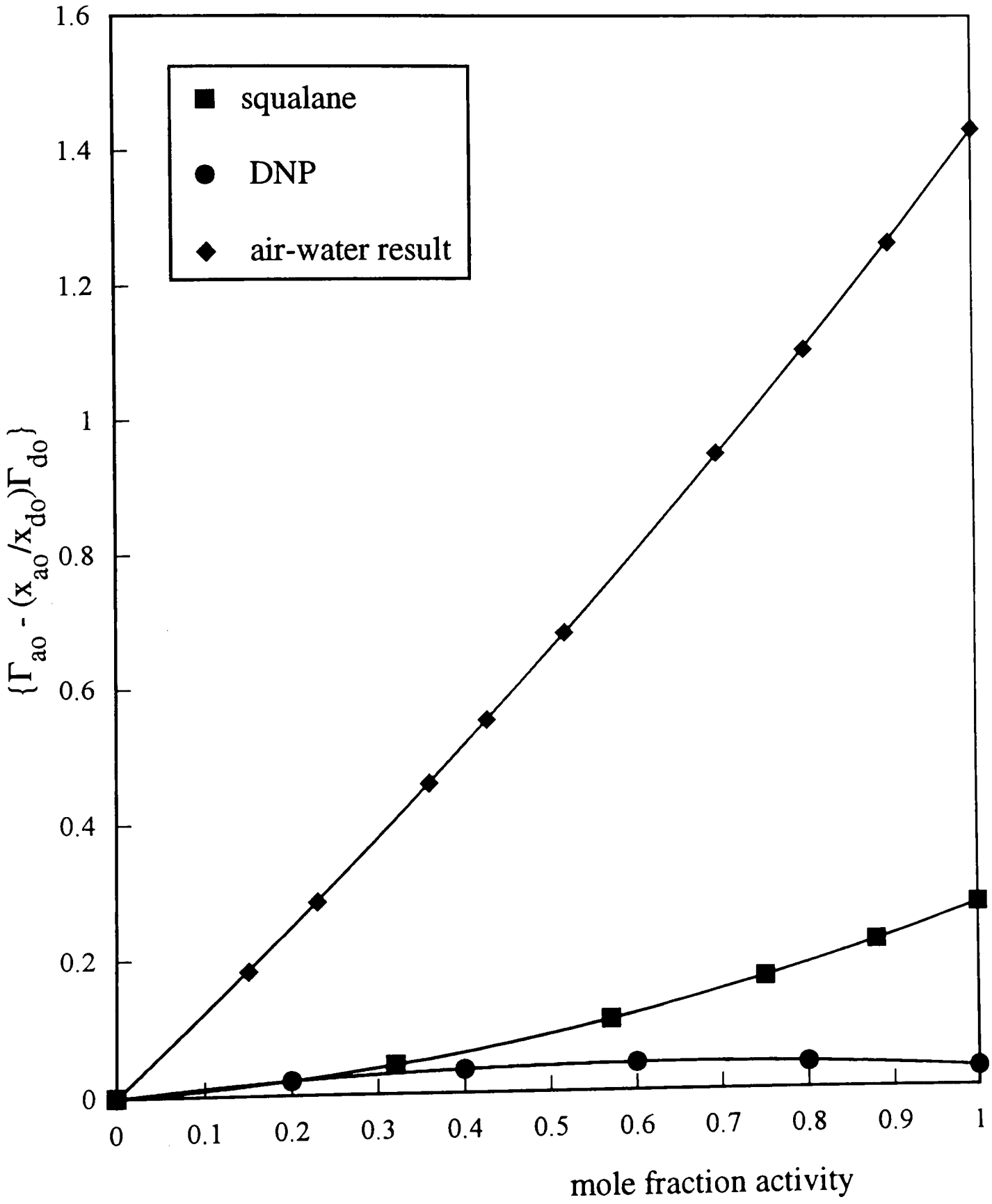

for both squalane and DNP dilution lie well below that for the air-water interface.

The tension data and isotherms for octane on $C_{10}E_7$ (which is a spreading system) are shown in figures 5.21 and 5.22. As for the previous system, the isotherms for the two diluent oils are different indicating that the adsorptions of one or both of these oils are not zero across the full composition range. The relative surface concentrations at the oil-water interface are compared with the surface concentrations measured at the air-water interface in figure 5.22. For this spreading oil system, the curve for the air-water interface again lies above both the curves for the oil-water interface.

This preliminary study into the investigation of oil penetration into surfactant monolayers at the oil-water interface indicates that it is not possible to determine the absolute surface concentration of dodecane alone. Only the relative adsorption of dodecane in the mixed oil system i.e. $\{\Gamma_{ao} - (x_{ao}/x_{do})\Gamma_{do}\}$ can be measured and this is found to be different to the absolute surface concentration probably because of significant adsorption of the diluent oil used. However, the oil-water interface is different to the air-water interface because of the fact that the diluent oil is necessarily close to the interfacial region. Hence, the surface excess concentration of the diluent oil, even for cases where it doesn't adsorb, will still affect the overall surface excess concentration value. If the diluent oil stays out of the interface, Γ_{do} will be finite but negative.

Figure 5.21 **Oil-water tension, γ_{ow}, versus mole fraction activity for octane mixtures with either DNP(●) or squalane(■) with $C_{10}E_7$ (9.5mM, 10xcmc) solution at 25°C.**

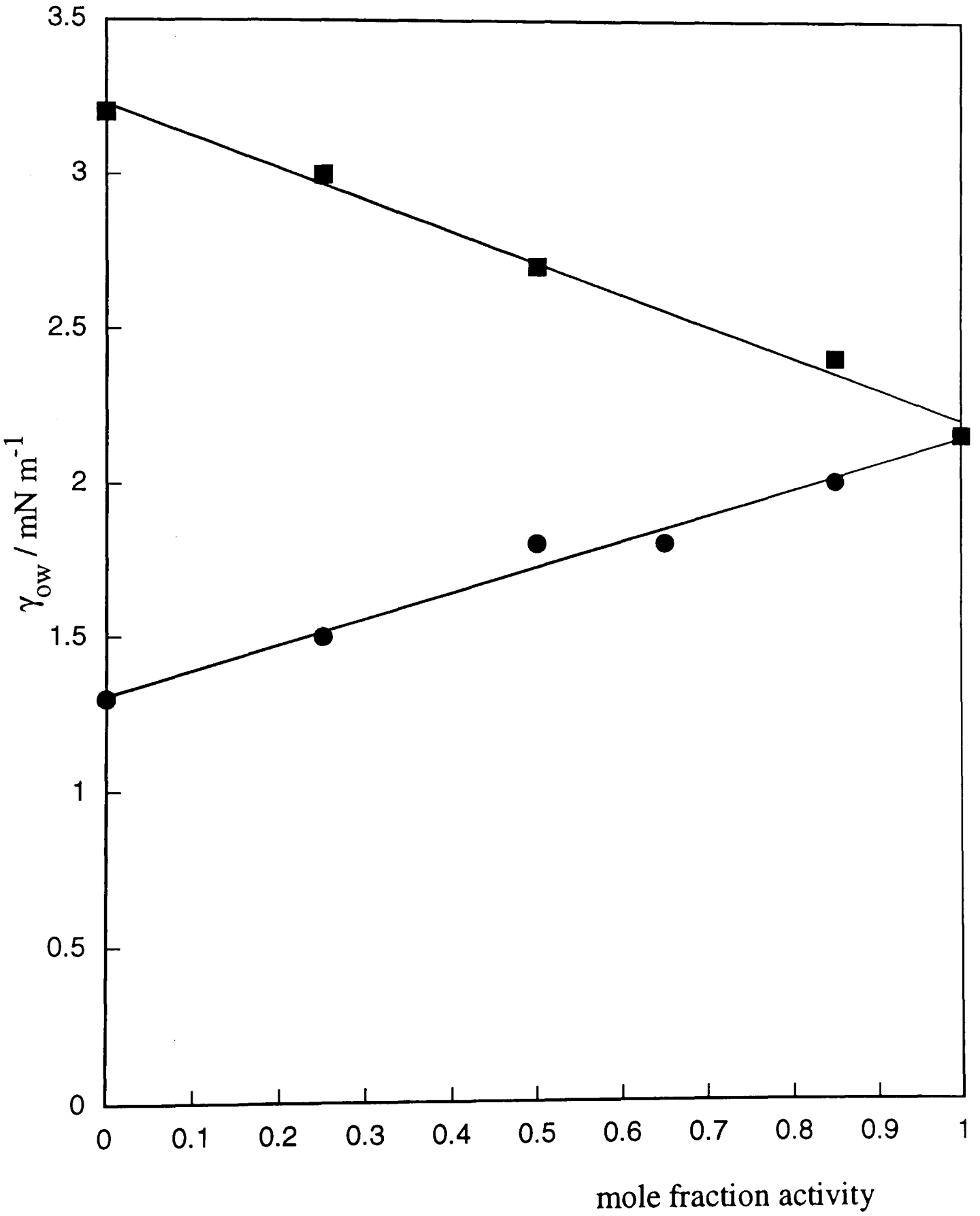

Figure 5.22 **Surface excess concentration at the oil/water interface versus mole fraction activity for octane/diluent oil mixtures with $C_{10}E_7$ (9.5mM, 10xcmc) solution at 25°C.**

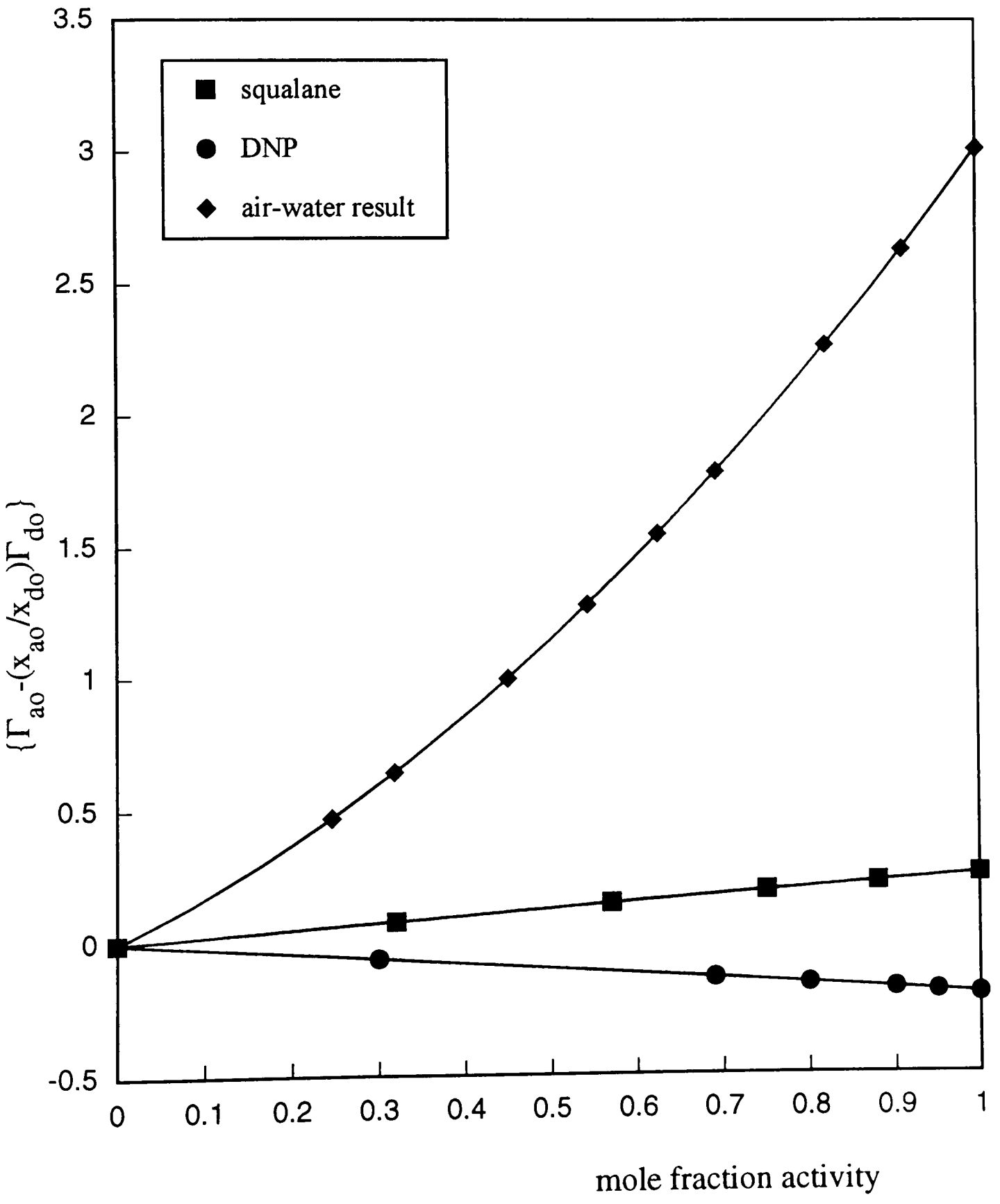

5.10 Conclusions

From the work carried out in this chapter, it is now possible to conclude,

1. The tension changes caused by oil lens addition onto the surfaces of aqueous solutions of non-ionic surfactants can be measured reliably so long as proper allowance is made for the partitioning of surfactant into the added oil.

2. The alkane chain length at which the transition from spreading to non-spreading occurs is affected by the nature of the surfactant.

3. The equilibrium spreading coefficients for all systems investigated are all roughly zero. This is true for systems which have been judged both spreading and non-spreading by visual observations.

4. Total alkane adsorption increases with decreasing alkane chain length. The isotherms show a greater curvature upwards for the shorter chain length alkanes signifying that the adsorption becomes more favourable as more alkane is added to the mixed surfactant/alkane film.

5. The adsorption isotherms for spreading oils yield information about the amount of 'surface perturbed' oil associated with the oil-water interface region.

6. The adsorption of the alkanes onto the non-ionic surfactant monolayers studied fit the Aranowich adsorptin isotherm, yielding a_m and d values which decrease with increasing alkane chain length.

7. In contrast to their lack of adsorption at the air-water interface, squalane and DNP do adsorb significantly (either positively or negatively) and to different extents into the surfactant monolayer at an oil-water interface. This has the consequence that only the relative adsorption of mixed oils can be determined at the oil-water interface using the method described here.

5.11 References

[1] J. S. Rowlinson, B. Widom, Molecular theory of capillarity, International Series of Monographs on Chemistry 8, Oxford University Press, Oxford, 1989, p 216.

[2] V. Bergeron, M. E. Fagan, C. J. Radke, Langmuir, **9**, 1704, 1993.

[3] H. Kellay, J. Meunier, B. P. Binks, Phys. Rev. Lett., **69**, 1220, 1992.

[4] H. Kellay, B. P. Binks, Y. Hendrikx, L. T. Lee and J. Meunier, J. Adv. Colloid Interface Sci., **49**, 85, 1994.

[5] R. Aveyard, P. Cooper and P. D. I. Fletcher, J. Chem. Soc. Faraday Communications, **86**, 211, 1990.

[6] R. Aveyard, P. Cooper and P. D. I. Fletcher, J. Chem. Soc. Faraday Trans., **86**, 3623, 1990.

[7] R. Aveyard, B. P. Binks, P. D. I. Fletcher and J. R. MacNab, Langmuir, **11**, 2515, 1995.

[8] R. Aveyard, B. P. Binks and P. D. I. Fletcher, Langmuir, **5**, 1210, 1989.

[9] R. Aveyard, B. P. Binks, S. Clark and P. D. I. Fletcher, J. Chem. Soc. Faraday Trans., **86**, 3111, 1990.

[10] N. M. van Os, J. R. Haak and L. A. M. Rupert, Physico-Chemical Properties of selected Anionic, Cationic and Nonionic Surfactants, Elsevier, Amsterdam, 1993.

[11] H. Kunieda and K. Shinoda, J. Dispersion Sci. Technol., **3**, 233, 1982.

[12] H. Kunieda and K. Shinoda, J. Colloid Interface Sci., **107**, 107, 1985.

[13] M. Kahlweit, R. Strey and P. Firman, J. Phys. Chem., 90, 671, 1986.

[14] R. Aveyard, B. P. Binks, P. D. I. Fletcher and X. Ye, J. Chem. Tech. Biotechnol., **54**, 231, 1992.

[15] K. Shinoda, M. Fukada and A. Carlsson, Langmuir, **6**, 334, 1990.

[16] M. J. Rosen, Surfactant and Interfacial Phenomena, 2nd Edition, Wiley, New York, 1989.

[17] R. E. Johnson Jr. and R. H. Dettre, J. Colloid Interface Sci., **21**, 610, 1966.

[18] F. Hauxwell and R. H. Ottewill, J. Colloid Interface Sci., **34**, 473, 1970.

[19] T. Takii and Y. H. Mori, J. Colloid Interface Sci., **161**, 31, 1993.

[20] P. A. Cooper, PhD Thesis, University of Hull, 1991, pg 122.

[21] A. J. Ashworth and D. H. Everett, Faraday Society Trans., **56**, 1609, 1960.

[22] J. R. Lu, R. K. Thomas, R. Aveyard, B. P. Binks, P. D. I. Fletcher and A. Sokolowski and J. Penfold, J. Phys. Chem., **96**, 10971, 1992.

[23] J. R. Lu, R. K. Thomas, B. P. Binks, P. D. I. Fletcher and J. Penfold, J. Phys. Chem., in press

[24] F. Hauxwell, PhD Thesis, University of Bristol, 1969.

[25] G. L. Aranovich, J. Coll. Int. Sci., **141**, 30, 1991.

[26] G. L. Aranovich and M. D. Donohue, J. Coll. Int. Sci., **175**, 492, 1995.

[27] G. L. Aranovich and M. D. Donohue, J. Coll. Int. Sci., **173**, 515, 1995.

[28] K. S. W. Sing, D. H. Everett, R. A. W. Haul, L. Moscou, R. A. Pierotti, J. Rouquerol and T. Siemieniewska, Pure Appl. Chem., **57**, 613, 1985.

[29] K. S. W. Sing, Carbon, **32**, 1311, 1994.

Chapter 6

CHAPTER 6

TEMPERATURE DEPENDENCE OF THE ADSORPTION OF OILS INTO SURFACTANT MONOLAYERS

6.1 Introduction

This chapter is concerned with the temperature dependence of the adsorption of dodecane onto solutions of two surfactants; a non-ionic surfactant ($C_{12}E_5$) and an ionic surfactant (DoTAB). The interest in this work arises from the opposite temperature dependence of microemulsion phase inversion for water + oil systems containing ionic and non-ionic surfactants. It is known that at low temperatures, non-ionic surfactant aggregation in such a system occurs in the water phase producing a Winsor I system consisting of an oil-in-water (o/w) microemulsion phase in equilibrium with a phase of excess oil. At higher temperatures, the system undergoes phase inversion and a water-in-oil (w/o) microemulsion (Winsor II) is produced in equilibrium with an excess water phase. Intermediate temperatures give a three phase system comprising of a surfactant rich middle phase (Winsor III) coexisting with excess oil and water phases (see chapter 1 for a more in-depth account of surfactant phase behaviour). For ionic surfactants,

the effect of temperature on microemulsion phase inversion, and hence on the preferred oil-water monolayer curvature, is opposite to that for non-ionic surfactants[1]. Ionic surfactants undergo the phase sequence Winsor I - III - II with *decreasing* temperature.

With the differences in behaviour in microemulsions between ionic and non-ionic surfactants in mind, it is of interest to determine how the extent of oil adsorption and possible penetration of the surfactant monolayer tailgroup region varies with temperature for both ionic and non-ionic surfactants,[2] and from this, obtain the enthalpies and entropies associated with transferring the alkane oil molecules from pure oil into the mixed surfactant/alkane oil films. All adsorption isotherms produced in this chapter were carried out using the Vapour adsorption train described in section 2.8.

6.2 Deriving enthalpies and entropies of adsorption from adsorption isotherms

The enthalpies and entropies associated with the transfer of alkane oil from pure alkane oil into a mixed film consisting of alkane oil and surfactant can be calculated by studying the temperature dependence of the adsorption isotherms. Two different enthalpy changes can be obtained depending on wether the adsorption is considered to

occur at constant surface pressure (Π) of the adsorbed oil or at constant surface concentration $(\Gamma_{ao})^3$. The isosteric enthalpy of adsorption (ΔH^+_Γ), measured at constant surface concentration is given by,

$$\left(\frac{d \ln a_\Gamma}{d \frac{1}{T}} \right) = \frac{\Delta H^+ \Gamma}{R} \qquad (6.1)$$

where T is the absolute temperature, R is the gas constant and a_Γ is the oil activity required to achieve a particular surface concentration (Γ). The equilibrium partial molar free energy of adsorption (ΔH^+_Π), measured at constant surface pressure is given by,

$$\left(\frac{d \ln a_\Pi}{d \frac{1}{T}} \right) = \frac{\Delta H^+ \Pi}{R} \qquad (6.2)$$

where R is the gas constant, T is the absolute temperature and a_Π is the activity required to achieve a particular surface pressure.

The isosteric and equilibrium enthalpies of adsorption are related by

$$\Delta H^{+}_{\Pi} = \Delta H^{+}_{\Gamma} - \left(\frac{T}{\Gamma}\right)\left(\frac{d\Pi}{dT}\right)_{\Gamma} \qquad (6.3)$$

Hence, the gradient of a plot of ln a_{Π} versus 1/T for various values of the surface pressure yields the equilibrium enthalpy of adsorption. Likewise, the gradient of a plot of ln a_{Γ} versus 1/T for various values of the surface concentration yields the isosteric enthalpy of adsorption.

The corresponding entropies of adsorption are obtained from a combination of equation 6.4 and 6.5.

$$\Delta G^{+}_{\Pi/\Gamma} = \Delta H^{+}_{\Pi/\Gamma} - T\Delta S^{+}_{\Pi/\Gamma} \qquad (6.4)$$

where $\Delta G^{+}_{\Pi/\Gamma}$ is the free energy associated with transfering one mole of alkane from pure alkane to the adsorbed state with surface pressure Π/surface concentration Γ. The quantity $\Delta G^{+}_{\Pi/\Gamma}$ can be derived from equation 6.5.

$$\Delta G^{+}_{\Pi/\Gamma} = RT\ln a_{\Pi/\Gamma} \qquad (6.5)$$

6.3 The adsorption isotherms for dodecane on non-ionic and ionic surfactants

The tension lowering ($\Delta\gamma$) associated with the adsorption of dodecane at a range of activities at various temperatures on $C_{12}E_5$ solutions can be seen in figure 6.1 and the corresponding data for the ionic surfactant DoTAB can be seen in figure 6.2. The changing activity of dodecane was achieved in the same way as in chapter 5. The tension lowering is equal to the surface pressure of the adsorbed dodecane in the surfactant/dodecane film. Figure 6.1 shows that, even though the effect is small, for a particular mole fraction activity, $\Delta\gamma$ increases as the temperature decreases. Conversely, figure 6.2 shows the opposite behaviour for the ionic surfactant. For a particular mole fraction activity, $\Delta\gamma$ values increase as the temperature increases.

Figures 6.3 and 6.4 show the derived adsorption isotherms for $C_{12}E_5$ and DoTAB respectively. These were produced, as in Chapter 5, by differentiating the polynomials which fit the $\Delta\gamma$ versus activity data. This, according to equation 5.8, yields the surface concentration plots shown in figures 6.3 and 6.4. Figure 6.3, showing data obtained for dodecane on $C_{12}E_5$, shows roughly linear adsorption isotherms in the same order, with temperature, as observed for the surface pressure plots. The curve for 31°C gives a much lower value of surface concentration when compared to the other temperatures. This is possibly due to being close to the cloud point of the surfactant

Figure 6.1 **Tension lowering following oil addition versus dodecane activity for the adsorption of dodecane onto 6.4mM $C_{12}E_5$.**

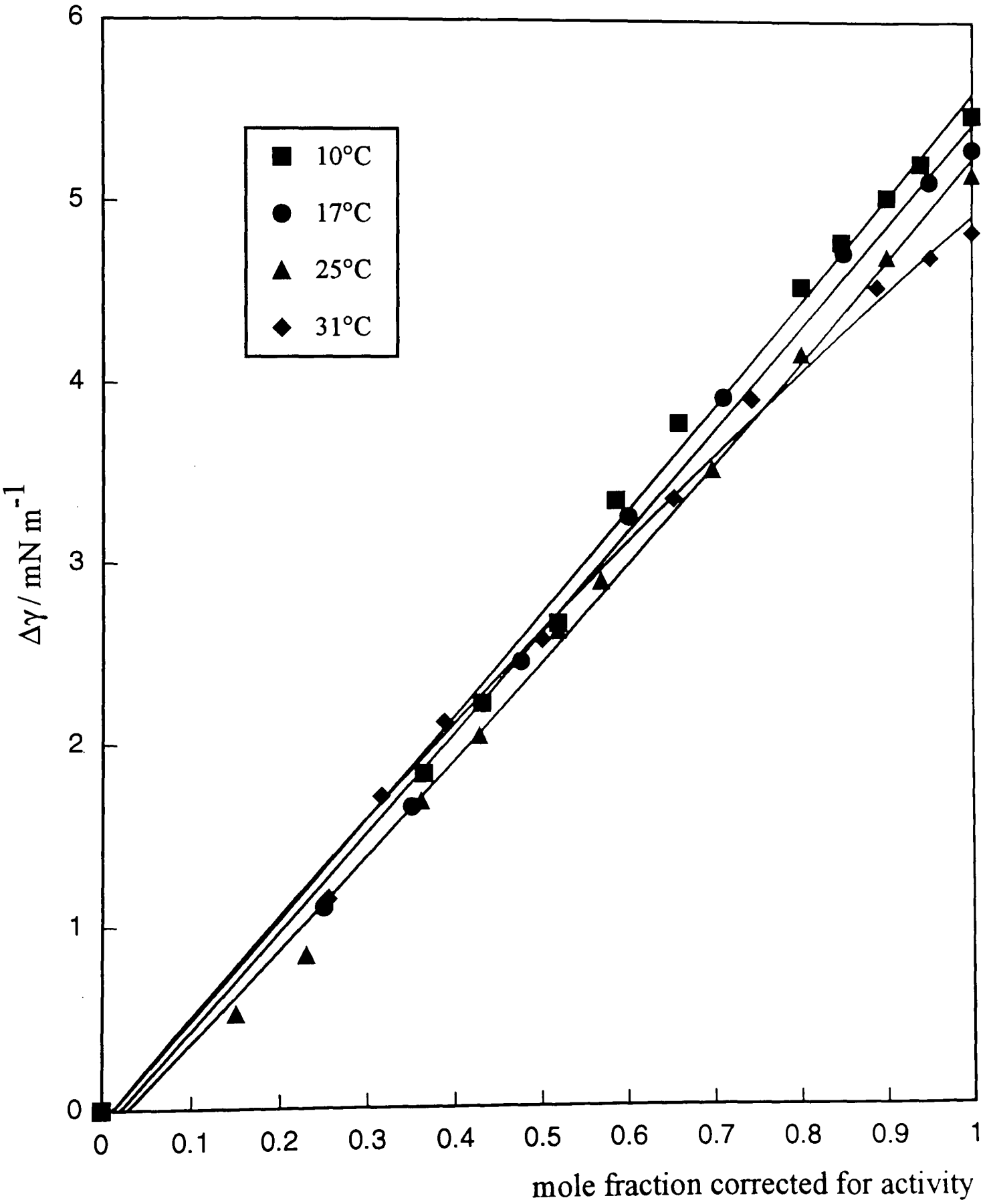

Figure 6.2 **Tension lowering following oil addition versus dodecane activity for the adsorption of dodecane onto 30mM DoTAB.**

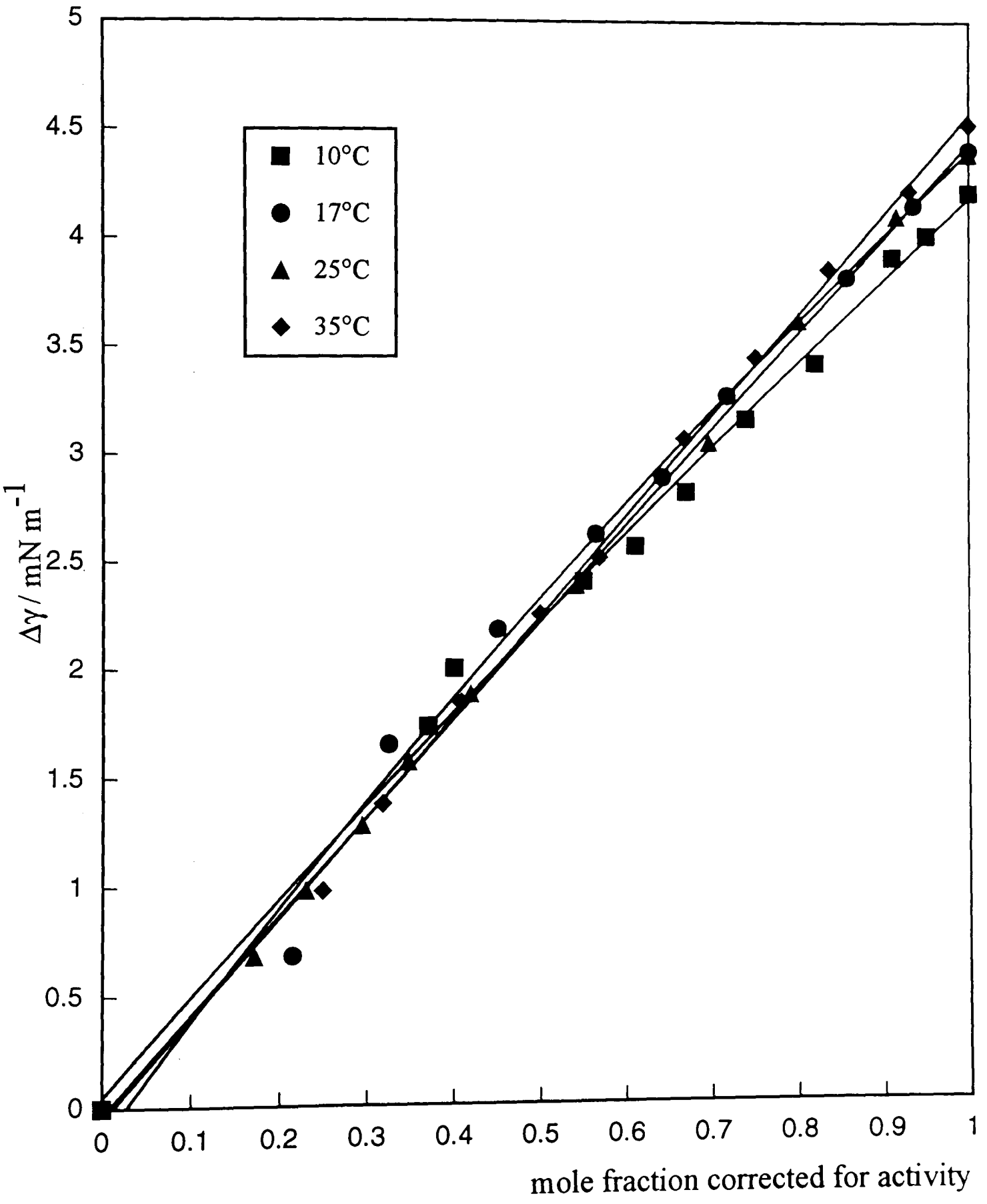

Figure 6.3 **Adsorption isotherms for dodecane onto 6.4mM $C_{12}E_5$ solutions at various temperatures.**

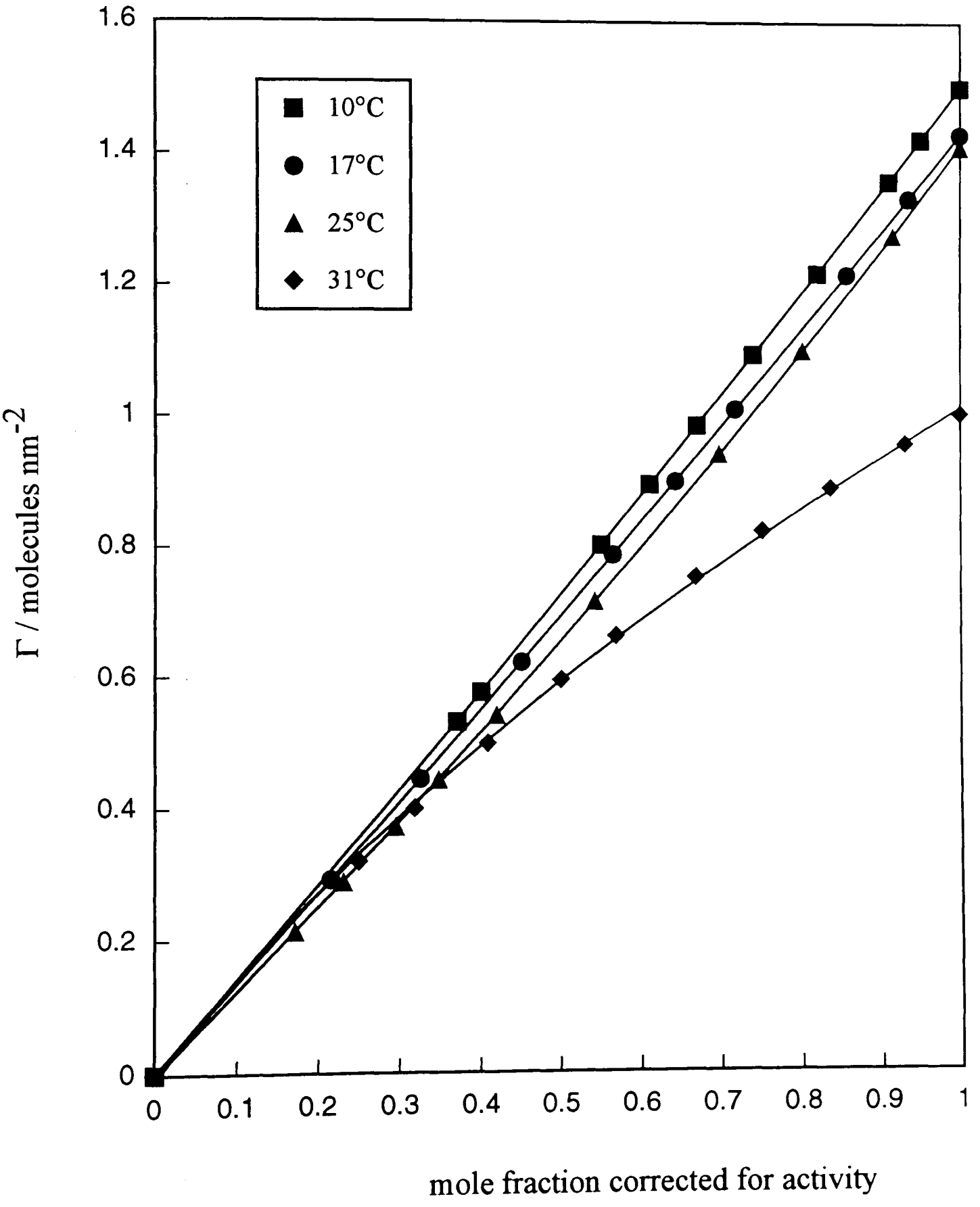

Figure 6.4 **Adsorption isotherms for dodecane onto 30mM DoTAB solutions at various temperatures.**

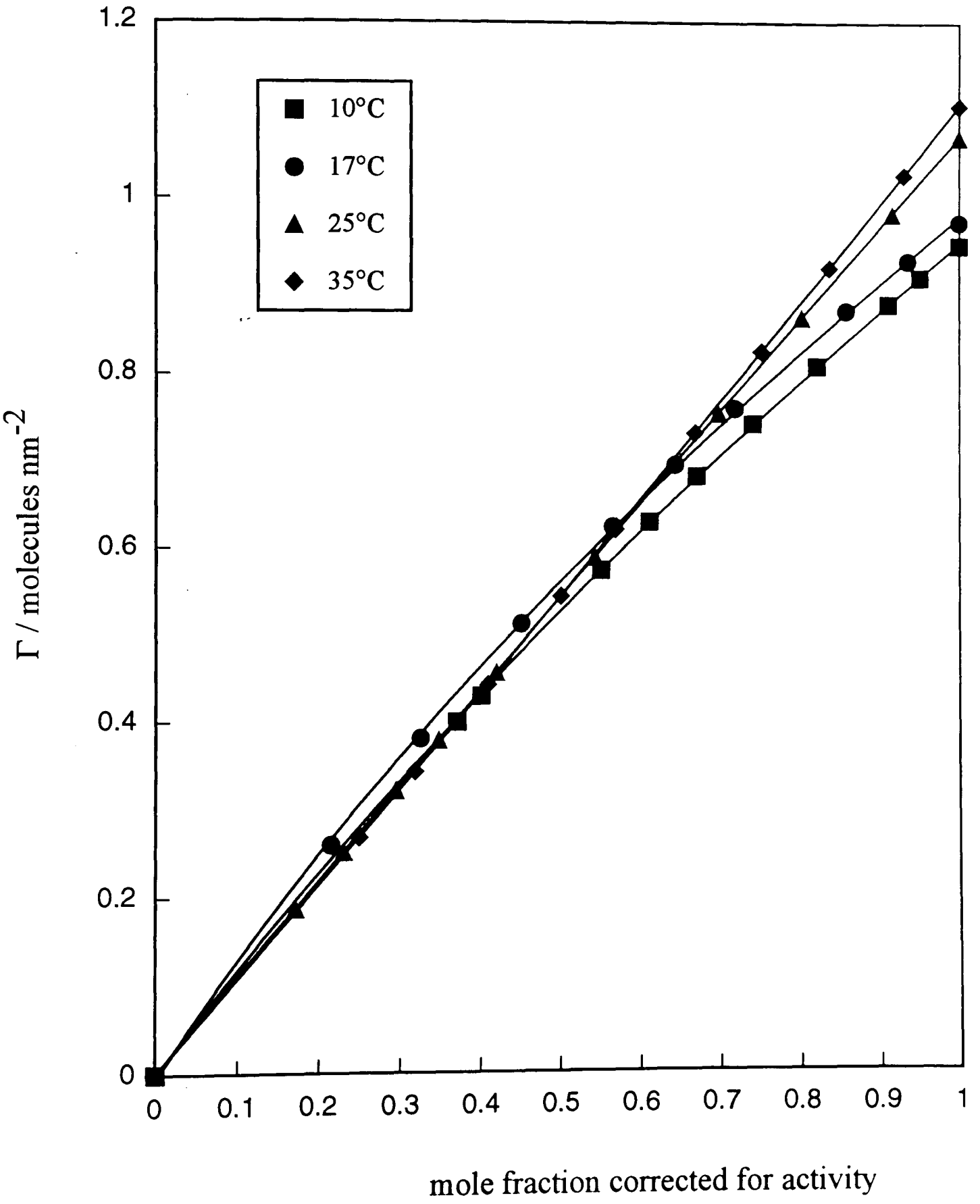

solution. The linearity of the curves suggest that as the activity of the adsorbing oil is increased, the adsorption becomes no more favourable.

Figure 6.4 shows the temperature dependence of the adsorption isotherms of dodecane on DoTAB at an aqueous phase concentration of 30 mM (twice the cmc). Comparison of figures 6.3 and 6.4 show that, for any particular activity, the surface excesses for the two surfactants show a slight opposite temperature dependence.

6.4 Plots derived from the adsorption isotherms

From figures 6.1-6.4, it is possible to derive plots of ln $a_{\Pi/\Gamma}$ versus 1/T for various values of the surface pressure (Π) or surface concentration (Γ). Figure 6.5 shows the plot of ln a_{Π} versus 1/T for dodecane on $C_{12}E_5$ at various surface pressures and figure 6.6 shows the corresponding plot for dodecane on DoTAB. The gradients of the plots shown on these two graphs yield the equilibrium enthalpies of adsorption (see equation 6.2). For $C_{12}E_5$, the gradient (and hence the enthalpy) remains negative at all values of surface pressure, whereas the gradients of the DoTAB plot are initially negative at low surface pressures but become positive at higher surface pressures. Figures 6.7 and 6.8 are the plots of ln a_{Γ} versus 1/T for dodecane on $C_{12}E_5$ and DoTAB respectively. Figure 6.7 shows negative gradients at all surface concentrations but figure 6.8 shows

Figure 6.5 **Variation of ln a_{Π} with 1/T for dodecane adsorption onto $C_{12}E_5$ solutions at different surface pressures of dodecane.**

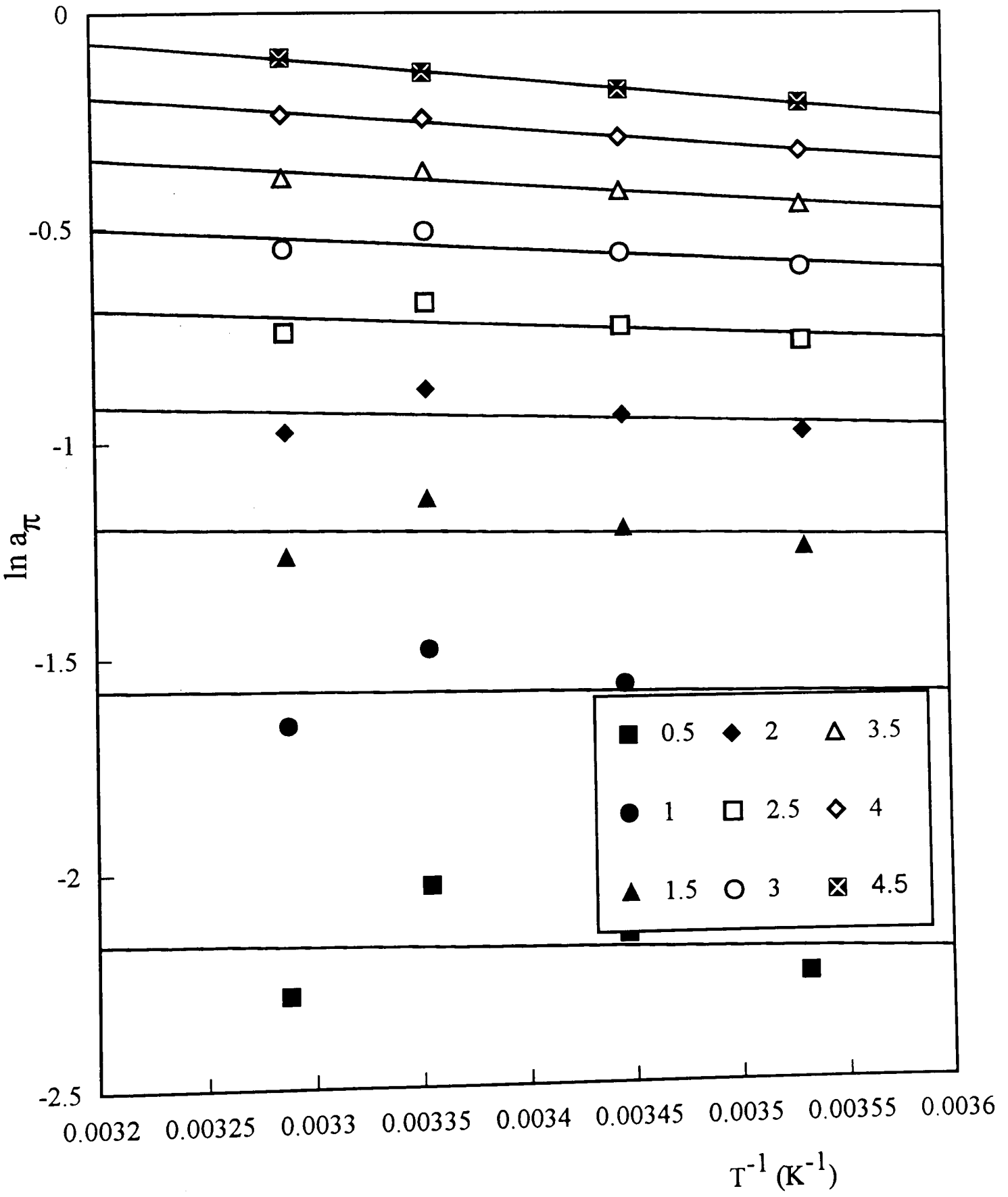

Figure 6.6 **Variation of ln a_{Π} with 1/T for dodecane adsorption onto DoTAB solutions at different surface pressures of dodecane.**

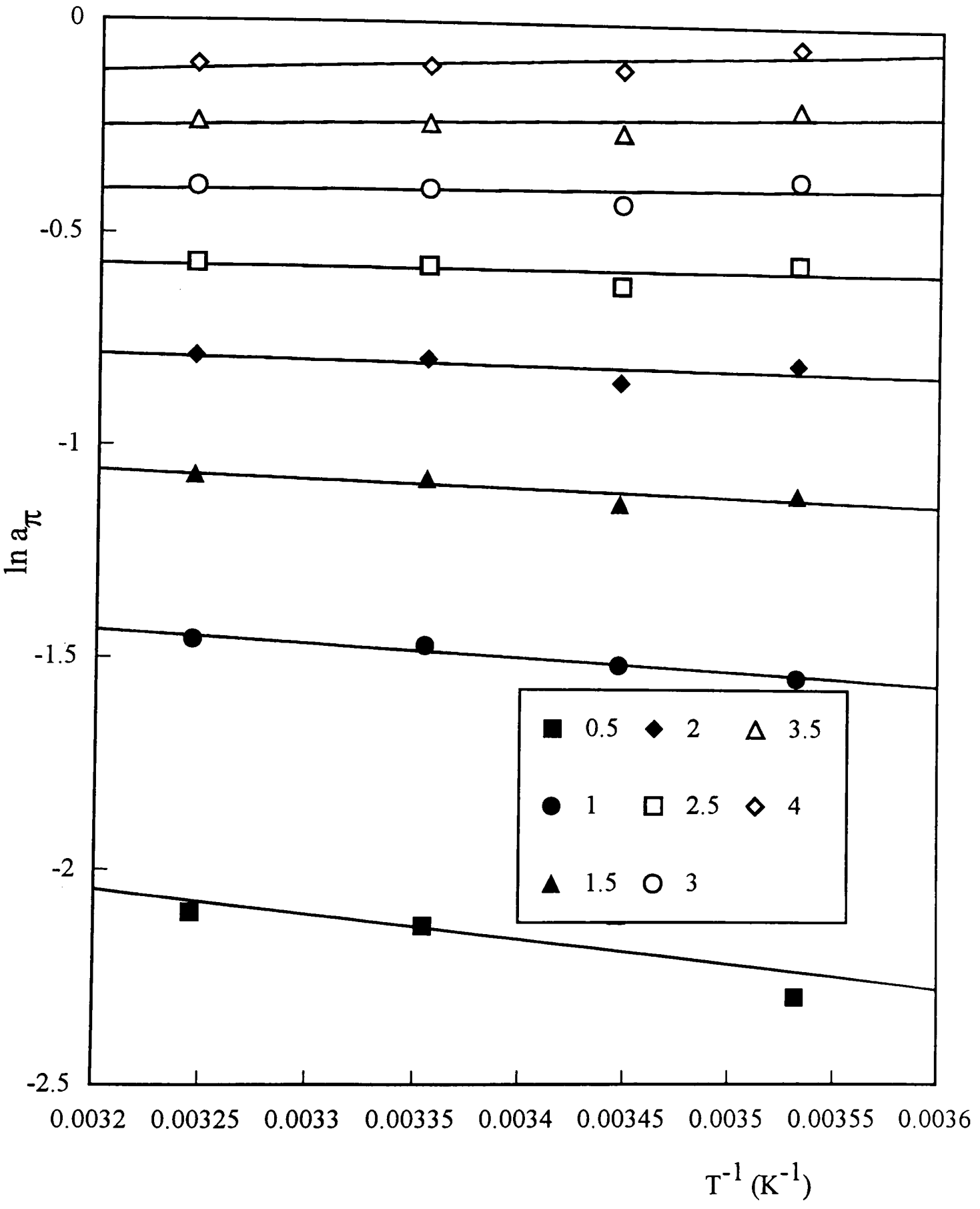

Figure 6.7 **Variation of ln a_Γ with 1/T for dodecane adsorption onto $C_{12}E_5$ solutions at different surface pressures of dodecane**

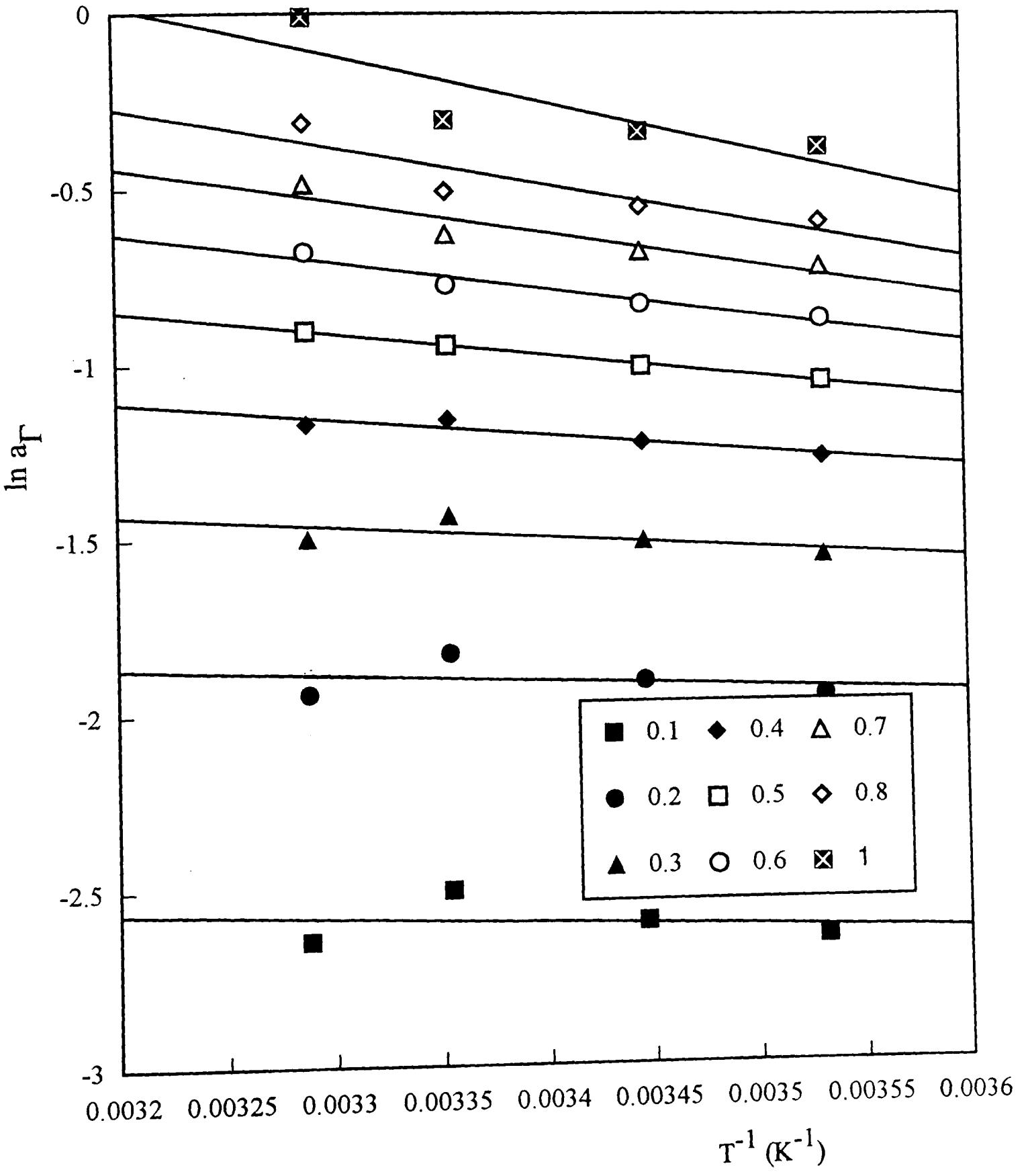

Figure 6.8 **Variation of ln a_Γ with 1/T for dodecane adsorption onto DoTAB solutions at different surface pressures of dodecane**

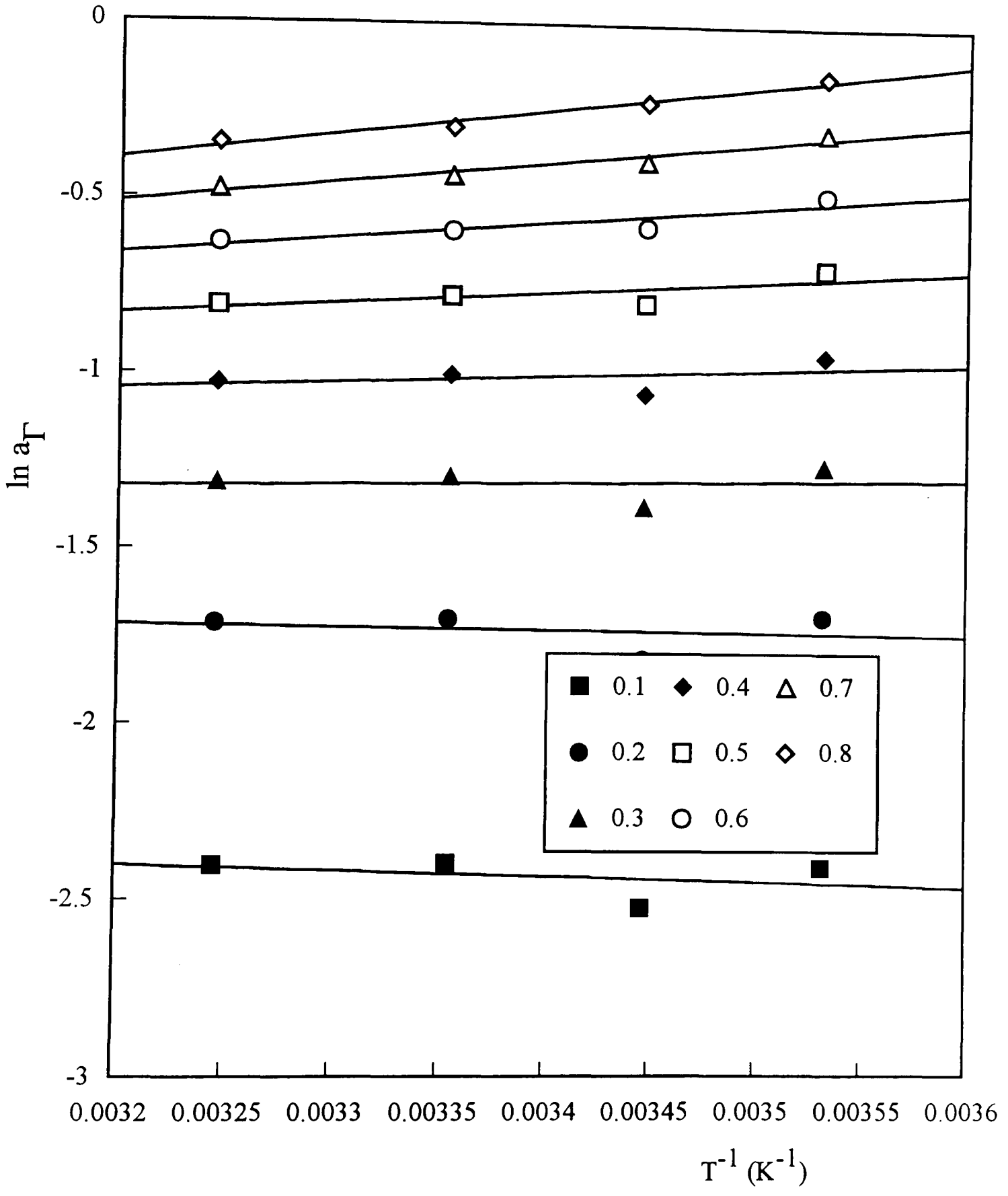

a cross-over from a slightly negative gradient at low surface concentrations to a positive gradient at higher surface concentrations.

6.5 Discussion of the opposite temperature dependence of oil adsorption isotherms of dodecane on non-ionic and ionic surfactants

The opposite temperature dependence of the adsorption isotherms for the non-ionic and the ionic surfactant can be related to the microemulsion phase behaviour and preffered monolayer curvature. It can be seen from figures 6.3 and 6.4 that the maximum oil adsorption into the $C_{12}E_5$ monolayers decreases with increasing temperature whereas the opposite is true for the adsorption into the DoTAB monolayers. With the assumption that increased oil adsorption causes the effective area of the tail region of the surfactant (a_c in equation 1.3) to increase, the directions of the maximum adsorption changes with temperature for the non-ionic and ionic surfactants are not consistent with the behaviour expected in microemulsions. That is to say that, if changes in a_h are ignored, a_c is expected to increase with increasing temperature for non-ionic surfactants (moving towards more negative preferred monolayer curvature) but to decrease for ionic surfactants. Most studies to date relating to temperature effects on preferred monolayer curvature of ionic and non-ionic surfactants have centred on the effects of temperature on the surfactant headgroups.[4] For non-ionics, increasing the temperature is thought to shrink a_h by the dehydration of

the ethoxy headgroups. For ionics, increased temperature may increase a_h by an increased counter ion dissociation, leading to increased electrostatic repulsion between adjacent headgroups in the monolayer (see Chapter 1). The results presented in this chapter indicate that there may be effects of temperature on the tailgroup areas caused by changes in penetration by the oil. Thus, effects of temperature on both a_c and a_h are likely to contribute to the preferred monolayer curvature of a surfactant.

6.6 Discussion of the adsorption enthalpy results

Figures 6.9 and 6.10 show both the equilibrium adsorption enthalpies and the isosteric adsorption enthalpies for dodecane adsorption onto $C_{12}E_5$ and DoTAB. It can be seen that for $C_{12}E_5$, the adsorption enthalpy becomes more negative as either the surface pressure or the surface concentration is increased. The opposite is true for the ionic surfactant which shows more positive values as the surface pressure or surface concentration is increased. It should be noted here that the enthalpies shown in figures 6.9 and 6.10 are small for both types of surfactant given that the estimated uncertainty in the values is ±2 kJ mol^{-1}. If the surfactant tailgroup region was similar in solvent properties to a liquid alkane, mixing of the dodecane into the monolayer would be expected to show approximately zero enthalpy change. Figure 6.10 shows that only at surface concentrations close to the minimum values does this occur. At high surface

Figure 6.9 **Equilibrium adsorption enthalpy versus surface pressure for adsorption of dodecane onto $C_{12}E_5$ and DoTAB**

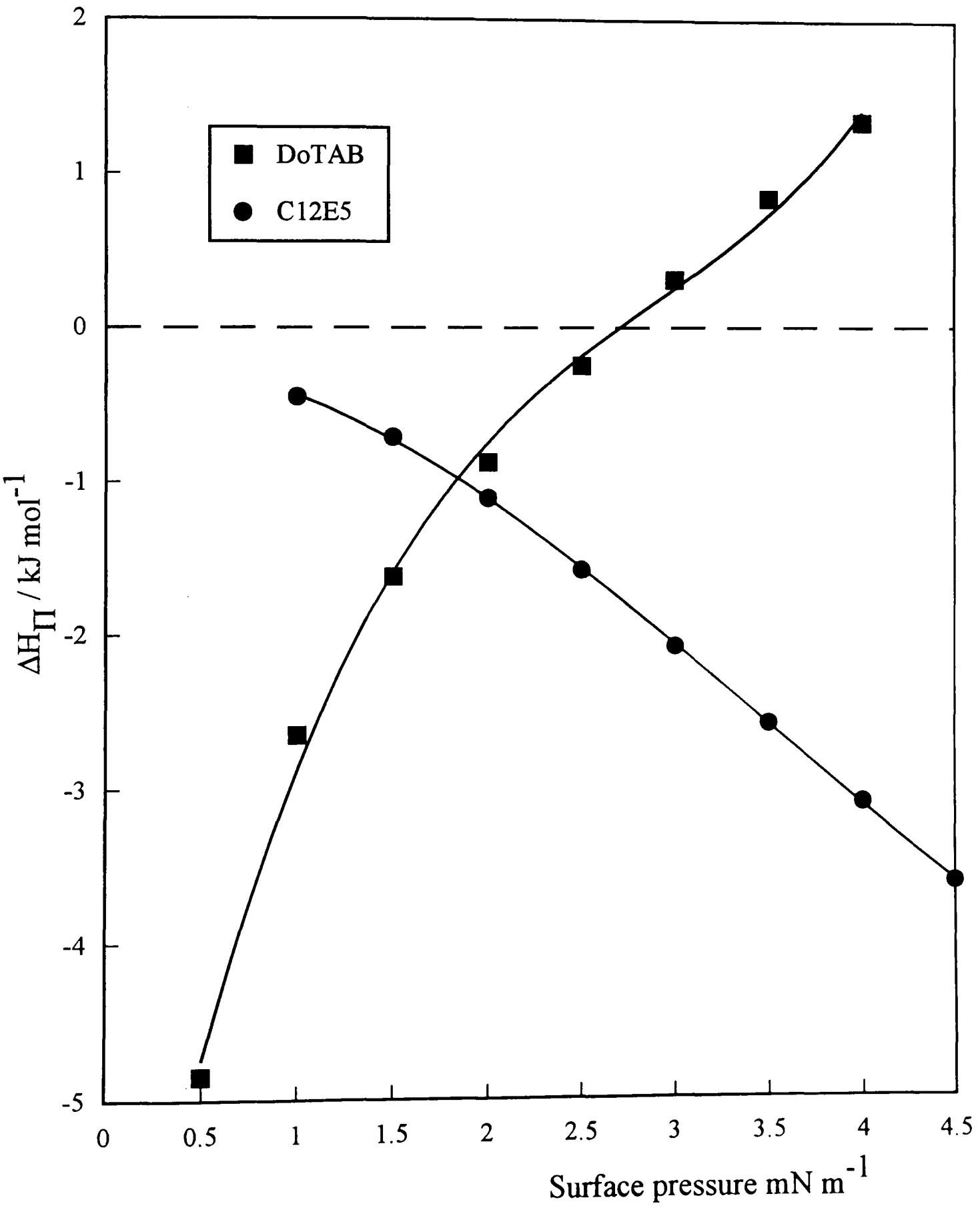

Figure 6.10 **Isosteric adsorption enthalpy versus surface concentration for dodecane adsorption onto $C_{12}E_5$ and DoTAB**

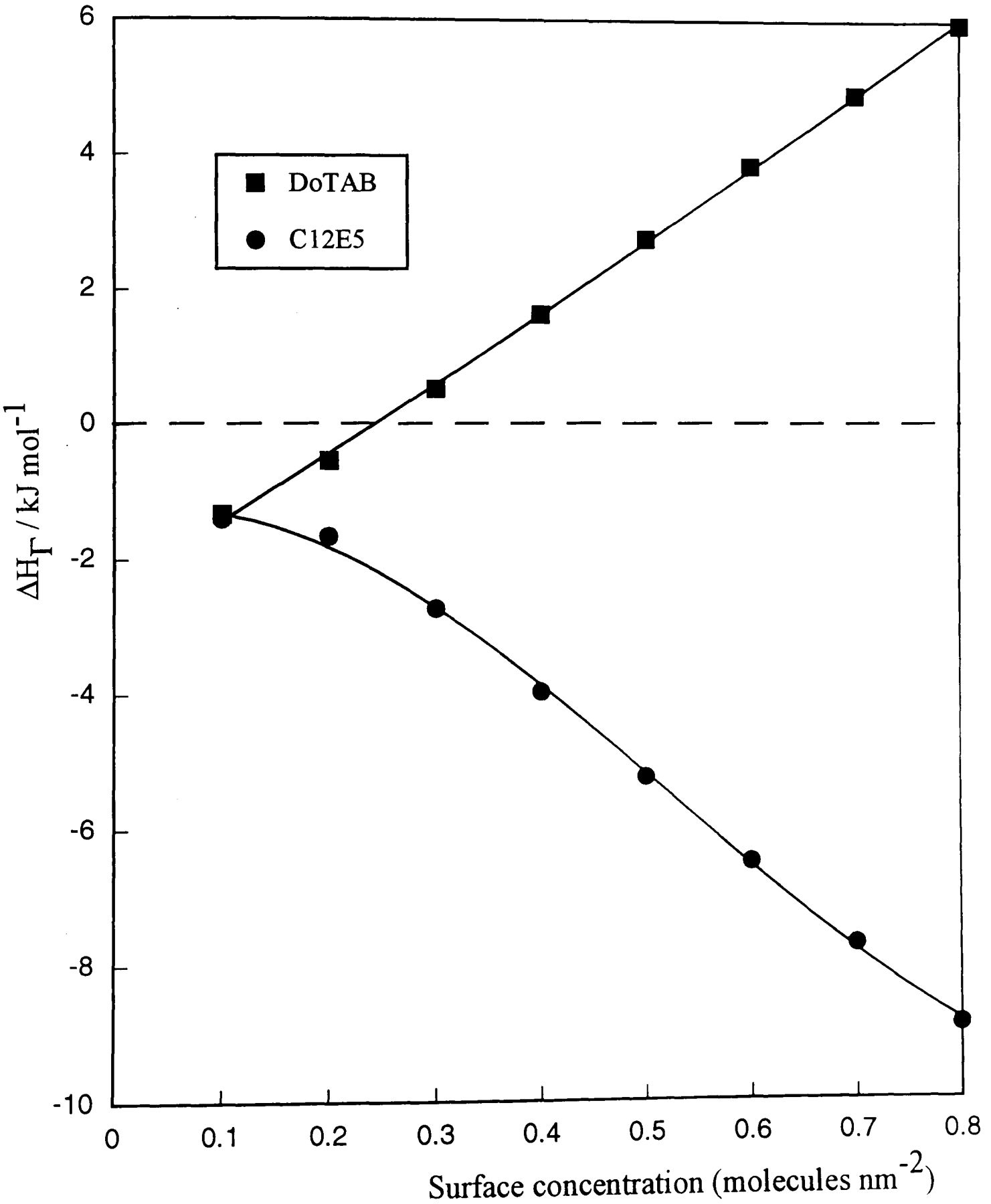

concentrations of adsorpbed dodecane, the magnitude of the enthalpies are relatively high when compared to the error present in these measurements.

As well as the opposite effect on isosteric enthalpy of the surface concentration on the non-ionic and ionic surfactants, it can be seen from figure 6.10 that DoTAB shows a sign reversal with increasing surface concentration of adsorbed dodecane

In attempting to discuss possible contributions to the enthalpies of adsorption, a detailed knowledge of the microstructure of the mixed oil/surfactant film is required. Neutron reflectivity[5,6] has been employed to determine the microstructure of dodecane (at unit activity) adsorbed onto monolayers of various TAB type surfactants (see section 1.4.3). Selective deuteration of the components of the mixed films shows that the dodecane penetrates the monolayers of surfactant to give mixed monolayers down to a depth at which water is present, increases the thickness and area per surfactant only slightly and protrudes slightly beyond the end of the surfactant tails. It can be said that dodecane fills in the spaces within the surfactant chain region, hence increasing the density of the chain region to close to that of bulk alkane. This in turn means that there will be an increase in chain-chain intermolecular attractions upon the transfer of dodecane from bulk liquid to the tail region of the mixed monolayer. This would be expected to give a negative (exothermic) contribution to the adsorption enthalpy. Recently, preliminary neutron reflection work has been carried out on mixed films of dodecane and $C_{12}E_5$[7]. The early results suggest that the behaviour of the

microstructure of the non-ionic system is similar to that of the cationic surfactant system.

There may also be a positive (endothermic) enthalpy contribution from the partial exposure of the dodecane in the mixed film to air. The neutron reflection measurements showed that the dodecane molecules protrude above the cationic surfactant tails for films containing the maximum amount of adsorbed dodecane.[5] Also, there is likely to be an enthalpy change associated with the change in area occupied per surfactant following the addition of the oil. Neutron reflection showed that, for the case of maximum dodecane adsorption on TAB type surfactants, the area per surfactant *increases* by 10-20%. The adsorption of dodecane at activities lower than unity may cause a partial condensation of the tail regions, driven by the gain in chain-chain intermolecular attractions from the increased chain density in the mixed film. This would lead to a *decrease* in the area occupied per surfactant at low amounts of adsorbed oil and would be associated with an enthalpy change of the opposite sign. The derived entropy plots are shown in figures 6.11 and 6.12. Equilibrium adsorption entropy versus surface presure for $C_{12}E_5$ and DoTAB is shown in figure 6.11 and figure 6.12 shows the corresponding isosteric adsorption entropy plot for the same surfactants.

Figure 6.11 **Equilibrium adsorption entropy versus surface pressure for a selection of surfactants.**

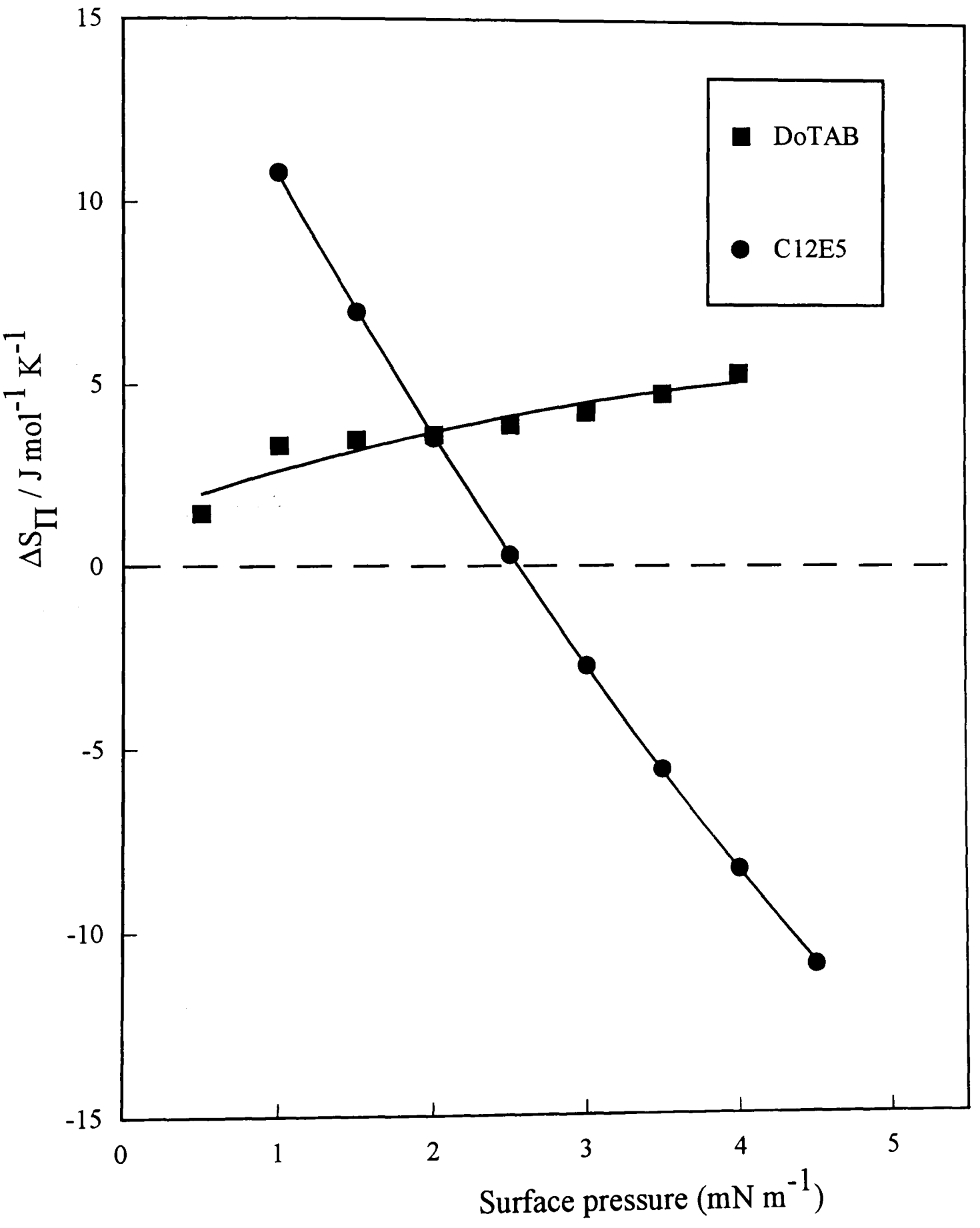

Figure 6.12 **Isosteric adosorption entropy versus surface concentration for a selection of surfactants.**

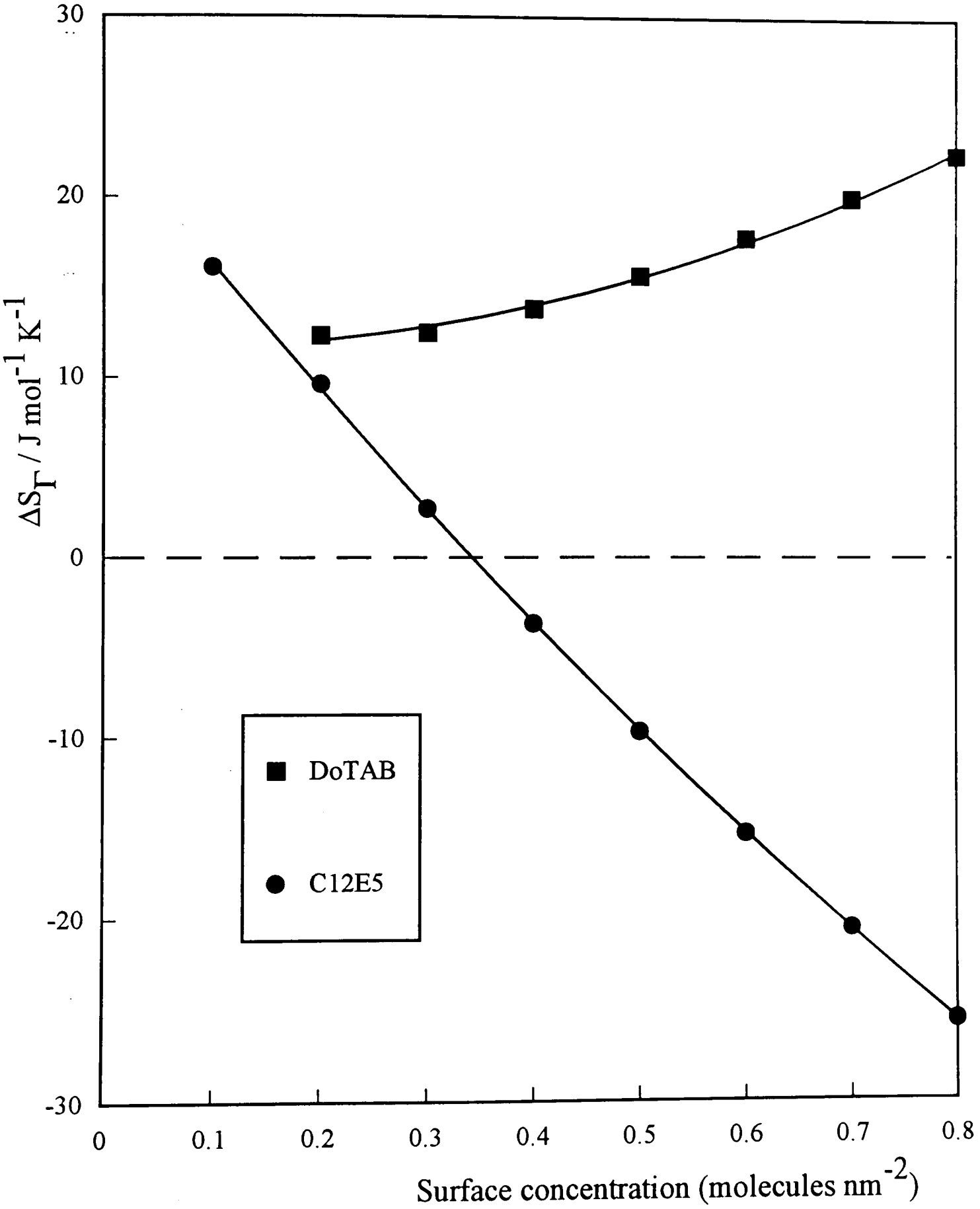

Figure 6.11 shows the values of the equilibrium adsorption entropy for $C_{12}E_5$ become more negative as the surface pressure is increased. The opposite is true for the ionic surfactant. Likewise the same trends are observed in figure 6.12.

6.7 Conclusions

In conclusion of chapter 6, it has been shown that the temperature dependence of the adsorption of dodecane onto surfactant monolayers is slightly sensitive to the nature of the surfactant and shows a moderate opposite temperature dependence for ionic and non-ionic surfactants.

The enthalpies associated with the temperature dependence of the adsorption of dodecane to non-ionic and ionic surfactants may have contributions from changes in the surfactant chain density together with packing densities of the surfactant headgroups. There may also be an enthalpy contribution arising from exposure of the adsorbed oil to air.

A molecular interpretation of the adsorption data requires a knowledge of the detailed microstructure of the mixed films which can be obtained using neutron reflection techniques. At the time of writing, the microstructure of mixed films containing non-ionic surfactants and oil not at unit activity are being studied by the research group at Hull.

6.8 References

[1] M. Kahlweit, R. Strey, R. Schomacker and D. Haase, Langmuir, **5**, 305, 1989.

[2] R. Aveyard, B. P. Binks, P. D. I. Fletcher and J. R. MacNab, Berichte der Bunsen Gesellschaft, 100, 224, 1996.

[3] D. H. Everett, Trans. Faraday Soc., **46**, 453, 1950.

[4] S-H. Chen, S-L. Chang and R. Strey, J. Chem. Phys., **93**, 1907, 1990.

[5] J. R. Lu, R. K. Thomas, R. Aveyard, B. P. Binks, P. Cooper, P. D. I. Fletcher, A. Sokolowski and J. Penfold, J. Phys. Chem., **96**, 10971, 1992.

[6] J. R. Lu, R. K. Thomas, B. P. Binks, P.D. I. Fletcher and J. Penfold, J. Phys. Chem., 99, 4113, 1995.

[7] B. P. Binks, D. Crichton, P. D. I. Fletcher and J. R. MacNab, ISIS Exp. Report, RB 7662, July 1996.

Chapter 7

CHAPTER 7

PRELIMINARY MEASUREMENTS OF PERFUME OIL ADSORPTION AND THE HEADSPACE ANALYSIS TECHNIQUE

7.1 Introduction

The adsorption of the perfume oils studied in this thesis can be measured in the same way as that described previously for apolar oils in chapters 5 and 6. It is important, as before, to determine the c* of the surfactant in the oil phase prior to any $\Delta\gamma$ measurements. The temperature dependence of the $\Delta\gamma$ values for the perfume oils on the various surfactants are all measured at unit activity. In order to obtain a graph of $\Delta\gamma$ versus activity, the activity coefficients of perfume oil/squalane mixtures are required. In theory, these can be measured by using a technique known as headspace analysis.

It is known that the composition of the gas phase above a volatile solution is representative of the composition of the bulk solution which is below it. Thus, analysis

of the vapour phase should give some insight into the relative amounts of individual components existing in the solution.

Headspace analysis is the sampling of the vapour space above a solution for analysis by gas chromatography. The technique is not only useful in analysis, it also has applications in non-analytical areas, such as the thermodynamics of mixed phases[1]. The experimental technique is described in section 2.5. The relative sizes of the peaks obtained for different mole fractions of perfume oil mixed with another oil yields the activity coefficients needed for the $\Delta\gamma$ versus activity graphs.

An overall aim of this project has been to learn more about the interactions of oils with surfactant monolayers with a view to improving and controlling the solubilisation of oils in micellar and microemulsion phases. In chapters 5 and 6 the adsorption of oils into monolayers at the air-water or oil-water interfaces have been discussed. Such adsorption can be envisaged as 2-D solubilisation within flat monolayers. Micellar or microemulsion solubilisation involves curved monolayers. Understanding the effects of monolayer curvature on solubilisation is important since the tendancy of monolayers to curve are expected to depend on whether the solubilisate penetrates the surfactant headgroup or tailgroup regions or if it occupies a central core region of the mixed aggregate without entering the curved monolayer. Headspace analysis can be utilised to measure the solubilisation of an oil as a function of oil activity allowing a comparison to be made with the 2-dimensional adsorption isotherms obtained in

chapter 5. This chapter is divided into three sections. Firstly, the adsorption of perfume oils onto surfactant solutions is studied, followed by an attempt to determine activity coefficients of the perfume oils in squalane mixtures using headspace analysis and finally an attempt to measure full solubilisation isotherms of oil of different activities within surfactant micelles, again, using headspace analysis technique.

7.2 Adsorption data measured for the perfume oils on surfactant solutions

The adsorption of the perfume oil linalool (a branched, unsaturated alcohol) on CTAB solutions (2mM, 2xcmc) was studied. Due to the polar nature of the perfume oil, it is possible that some of the ionic surfactant may transfer from the aqueous solution to the drop of linalool added to the surface. As discussed in chapter 5, this possibility may be tested by recording the tension of the surfactant solution in the presence of oil containing different concentrations of the surfactant. Figure 7.1 presents the data obtained, showing clearly that the equilibrium concentration of CTAB in linalool is approximately 0.8 wt%. This concentration was then used in the oil in all subsequent experiments to avoid artefacts caused by surfactant transfer to the oil.

Figure 7.2 shows the temperature dependence of $\Delta\gamma$ for linalool on CTAB solutions. In contrast to the temperature dependence of alkane adsorption onto ionic surfactants

Figure 7.1 **Surface tension of a CTAB solution ($1.05x10^{-3}$M,1.1xcmc) versus wt% CTAB in a linalool lens.**

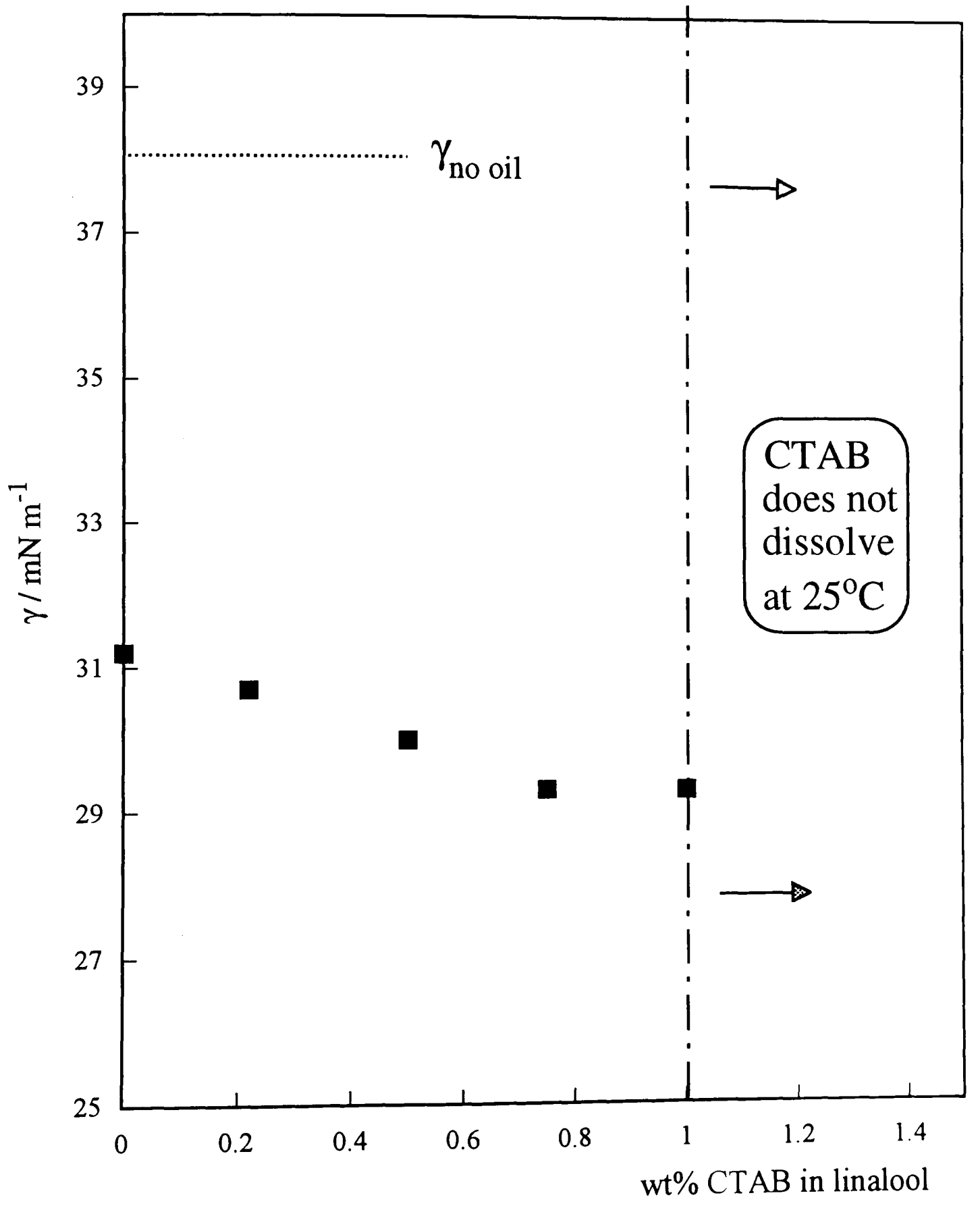

Figure 7.2 $\Delta\gamma$ **of a linalool lens containing 0.8wt% CTAB on CTAB solution ($1.05x10^{-3}$M) versus temperature.**

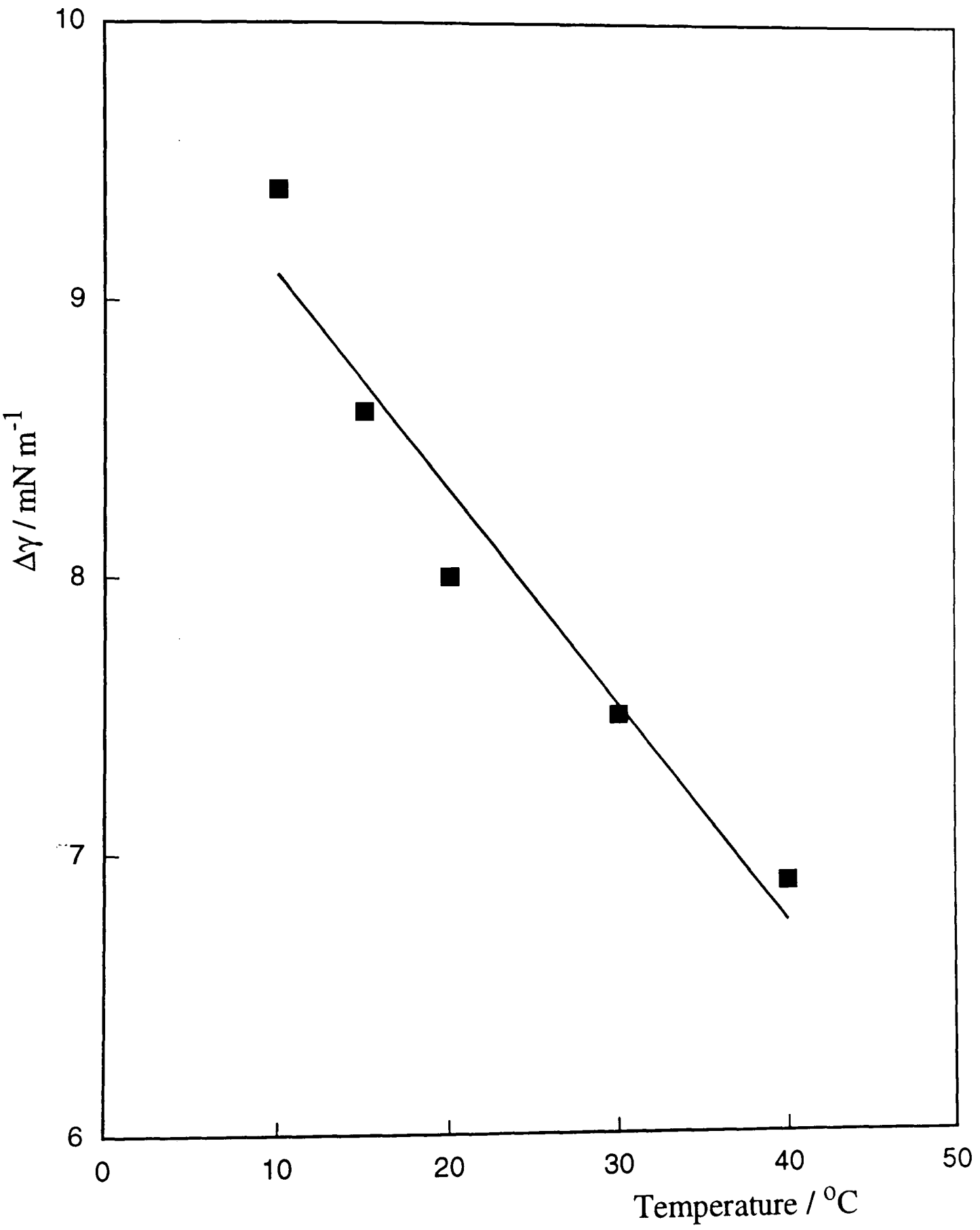

studied in chapter 6, the $\Delta\gamma$ for pure linalool decreases as the temperature is increased. In order to study the temperature dependence further, the activity coefficients of the perfume oils with squalane are required to obtain a full adsorption isotherm as produced for the apolar oils in chapter 6.

7.3 Determination of activity coefficients of perfume oils with diluent oils using headspace analysis

The headspace analysis technique is described in section 2.5. The measured detector peak area should be proportional to the vapour pressure of the component of interest. Peak areas were measured for samples of the pure oil and the oil at various dilutions with diluent oil. The ratio of the peak areas for a diluted oil and the pure oil give the ratios of vapour pressures P/P_o (where P is the vapour pressure of a diluted sample and P_o is the vapour pressure of the pure liquid) which is equal to the activity of the oil in the diluted sample. The activity coefficient is then obtained by comparison of the measured activity with the mole fraction of the diluted sample.

A series of mixtures of dodecane with either squalane or DNP (for which activities are known)[2] were run in order to verify the technique. The dodecane mixtures with DNP and squalane often showed a split peak on the gas chromatograph. The mass spectra of both peaks correspond to that of dodecane and we have no explanation for this.

When splitting occured, the integrated area of the dodecane peak was taken to include both split peaks.

7.3.1 Results for activity coefficients of perfume oils in diluent oils

Table 7.1 summarises the headspace results obtained for dodecane mixtures with either DNP or squalane and the headspace values for the activity of dodecane in the mixtures are compared with the literature values. The headspace results are rather irreproducible and values both above and below the literature values were obtained. This may be due to the incomplete equilibration of the liquid and vapour phases and further work is needed into this application of headspace analysis.

Figure 7.3 shows the preliminary results for activity versus mole fraction for cineole and limonene in mixtures with squalane at 30°C. The data for cineole suggests that this mixture behaves approximately ideally. The limonene data is too scattered for any reliable conclusions to be drawn at this stage. However, it could be possible to measure solubilisation isotherms (i.e. the amount of oil solubilised in micelles in bulk solution) as a function of oil activity with the use of headspace analysis. In this way, comparisons of solubilisation of oils in bulk and at the planar monolayer can be carried out.

Figure 7.3 **Activity from headspace results versus mole fraction in squalane for (a) cineole and (b) limonene at 30^0C**

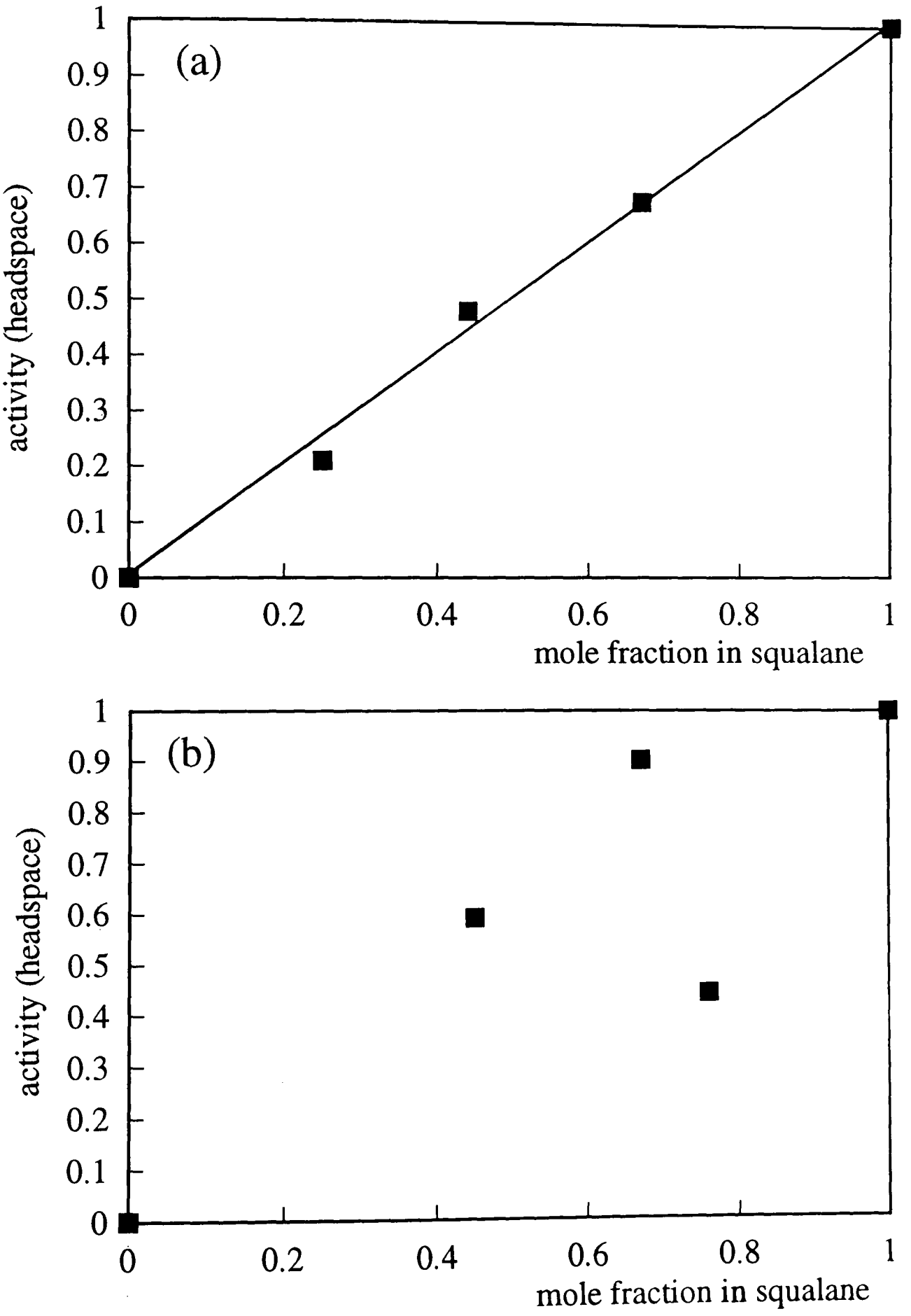

7.4 Solubilisation isotherms measured using headspace analysis

Solubilisation of oils in bulk phase aggregates is typically carried out by measuring the maximum additive concentration (MAC) of the oil into the aggregate before phase separation occurs. Measurement of solubilisation isotherms i.e. the variation in extent of solubilisation with the activity of the solubilisate yields more useful information since the shape of the isotherm may reflect a change in the position of solubilisation within the aggregate. Solubilisation isotherms have been determined by Christian et al[3] and others.[4,5,6]

Solubilisation isotherms are determined by GC-MS headspace analysis by measuring peak areas for samples of the pure oil and for surfactant solutions containing a known concentration of solubilised oil (expressed as the molar ratio of solubilisate:surfactant, R). The measurements yield P/P_o (the activity of the oil) as a function of the mole ratio of solubilisate to surfactant.

7.4.1 Results for solubilisation isotherms for dodecane in a variety of surfactants

Figure 7.4 shows the solubilisation isotherm for dodecane into 0.1M solutions of $C_{12}E_5$ at 30°C. It can be seen that the data obtained for surfactant solutions is more reproducible than that obtained for binary liquid mixtures in section 7.3.1. It is now

Figure 7.4 **R versus activity from headspace for dodecane with $C_{12}E_5$ (0.1M) at 30°C. (■) initial measurements and (●) measurements made one week later with agitiation.**

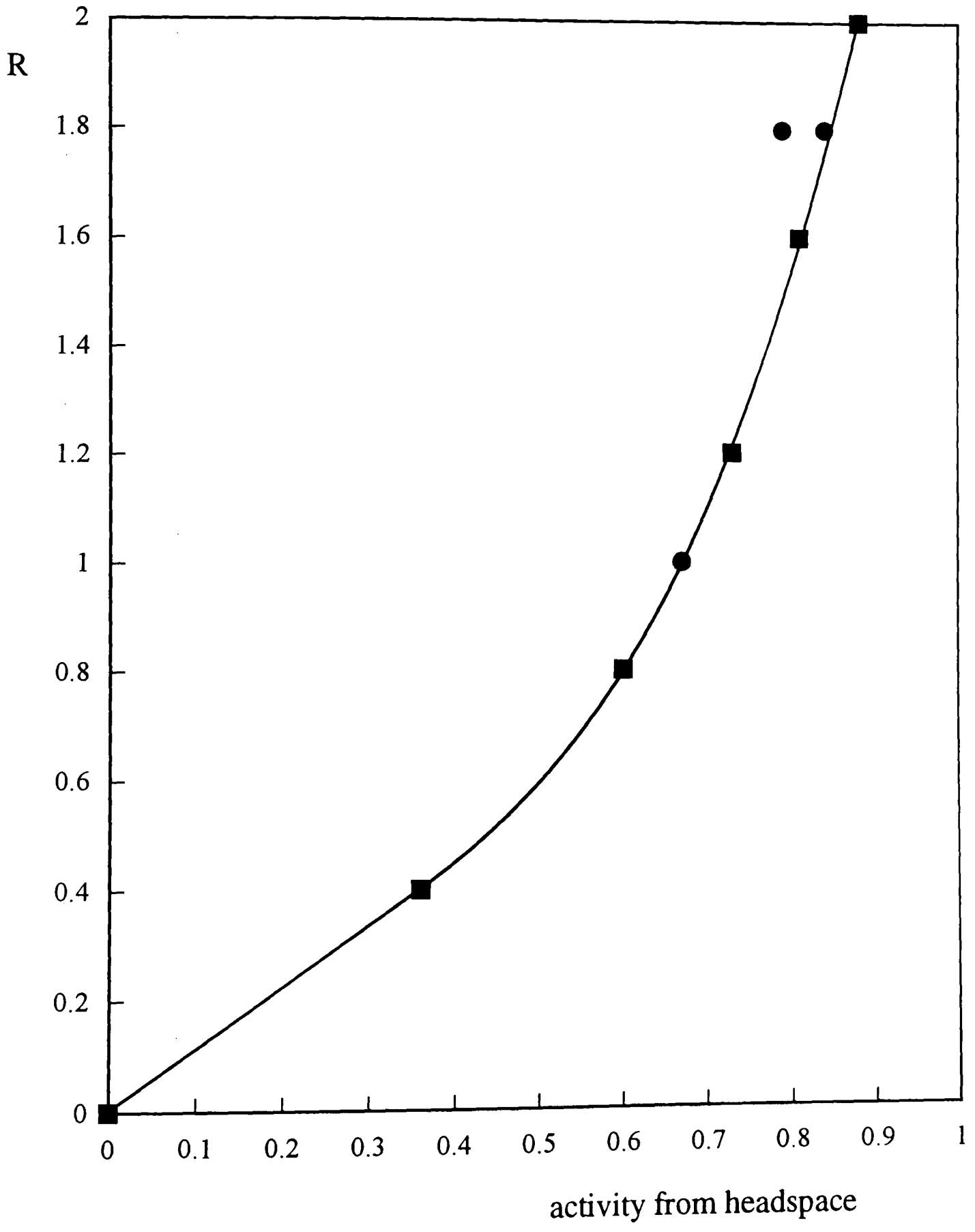

Table 7.1 Summary of headspace GC measurements of binary liquid mixtures containing dodecane

mol% dodecane	peak area	peak no.	activity (GC)	activity (lit)
Squalane mixtures, no agitation, left overnight before running, 30°C				
100% dodecane	41.6	1	1.0	1.0
69 mol%	23.0	1	0.55	0.67
36 mol%	9.6	1	0.22	0.32
DNP mixtures, agitation for 10 mins., left overnight before running, 30°C				
74 mol%	28.7	1	0.69	0.80
32 mol%	12.5	1	0.30	0.45
Squalane mixtures, no agitation, left overnight before running, 35°C				
100% dodecane	38.9	1	1.0	1.0
69 mol%	19.9	1	0.51	0.67
36 mol%	9.3	1	0.24	0.32
DNP mixtures, agitation for 10 mins., left overnight before running, 45°C				
100% dodecane	153.0	2	1.0	1.0
88 mol%	134.6	2	0.87	0.90
74 mol%	112.2	2	0.73	0.80
56 mol%	102.6	2	0.67	0.68
32 mol%	89.7	2	0.59	0.45
DNP mixtures, agitation for 20 mins., left overnight before running, 45°C				
88 mol%	140.6	2	0.92	0.90
74 mol%	98.4	2	0.64	0.80
32 mol%	85.7	2	0.56	0.45

possible to compare the data obtained for solubilisation into micellar solutions with that obtained at the air-water interface. This comparison is shown in figure 7.5. In this figure, the extent of solubilisation, R, was converted into mole fraction in the micelle ($X = 1/(1 + 1/R)$). In order to compare the solubilisation isotherm with the adsorption isotherms for the planar monolayer (measured previously in Chapter 5), the adsorption extent for monolayer adsorption was expressed as a mole fraction in the planar monolayer ($X = \Gamma_{dodecane}/(\Gamma_{dodecane} + \Gamma_{C12E5})$. This assumes that Γ_{C12E5} remains constant at 1.7 molecules nm^{-2}. Figure 7.5 shows that the dodecane molecules seem to have more affinity for the curved monolayer than for the flat air-water surface although the packing of dodecane molecules in the tail region of the curved monolayers in the $C_{12}E_5$ aggregates might be expected to be unfavourable relative to the flat monolayer. This is offset by the fact that solubilisation in solution may not be restricted to the monolayer region but may also form a core of oil.

Figure 7.6 shows the solubilisation isotherms for dodecane into TTAB micelles at two different temperatures. It can be seen that the solubilisation amounts into TTAB are much less than those seen for $C_{12}E_5$. Oil solubilisation extent, for a given oil activity, increases with increasing temperature. This was the case for ionic surfactants at the air-water interface as seen in chapter 6. The isotherms associated with TTAB resemble Type I isotherms in the BET classification system whereas the isotherm for $C_{12}E_5$ resembles a Type III. This suggests that solubilisation becomes less favourable with increasing oil content for TTAB whereas it becomes more favourable for $C_{12}E_5$.

Figure 7.5 **Mole fraction of dodecane in (■) micelles and (●) the monolayer versus activity of dodecane with $C_{12}E_5$ at 30°C.**

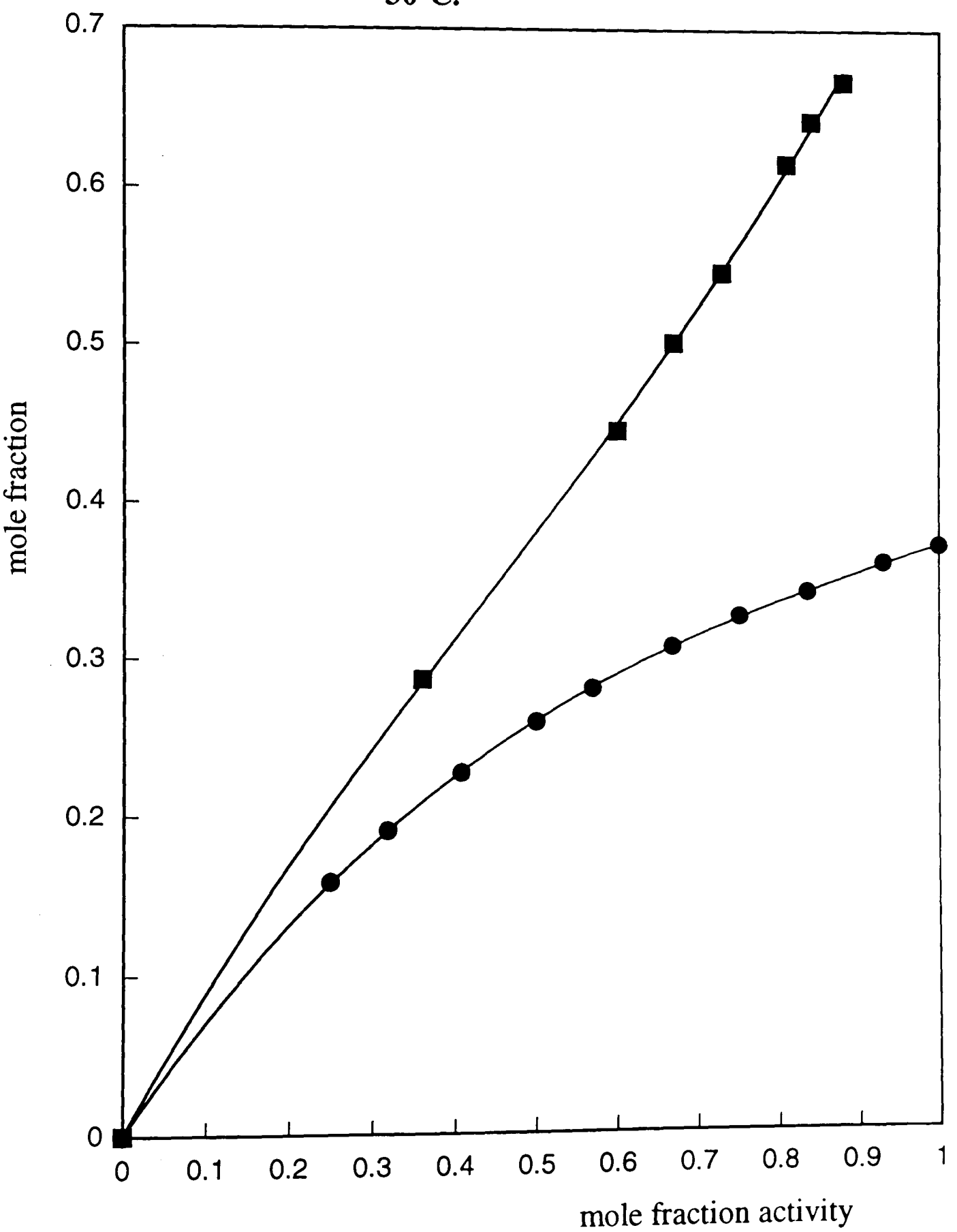

Figure 7.6 **R versus activity from headspace for dodecane in TTAB (0.1M) at (■) 35°C and at (●) 40°C.**

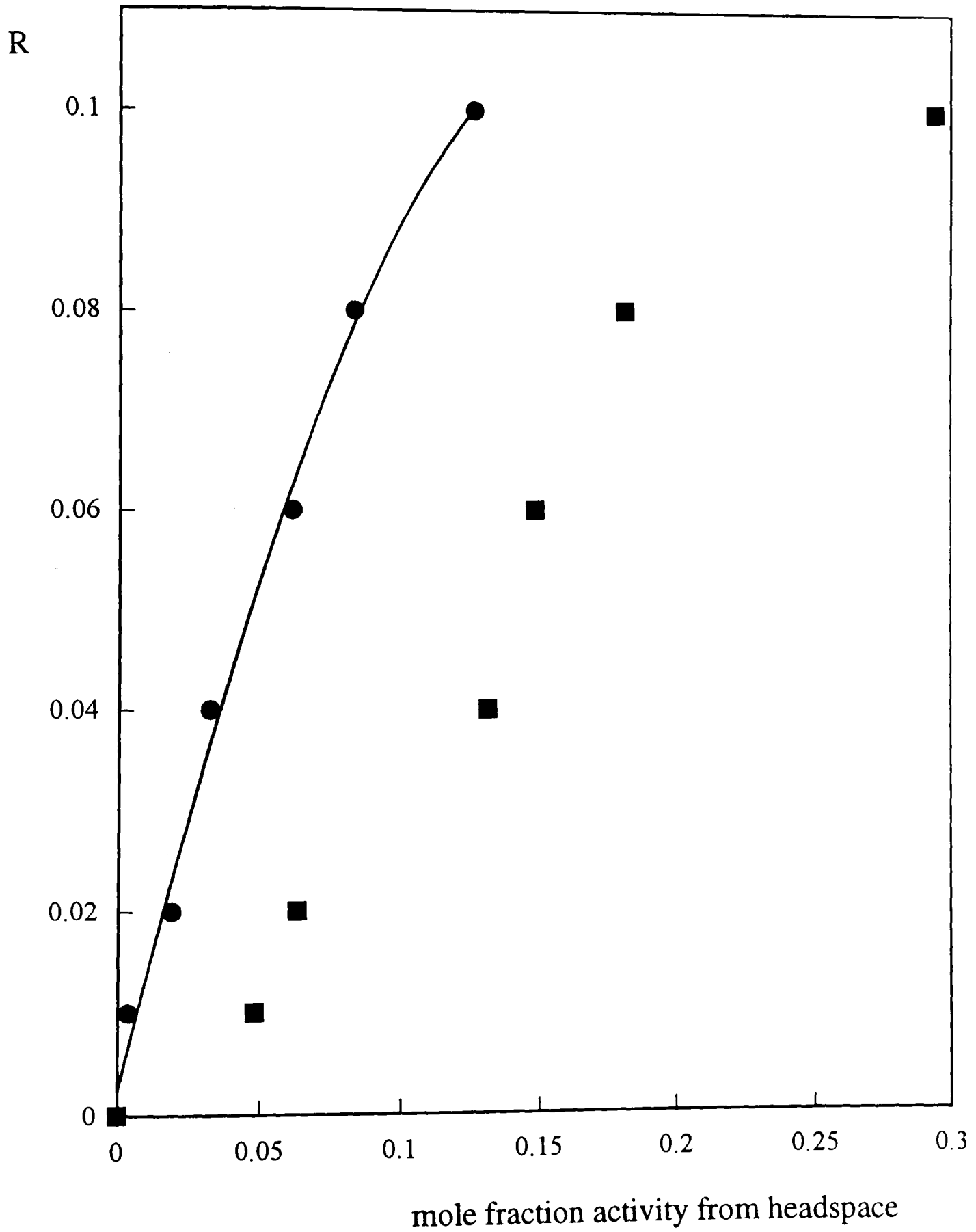

This phenomena may be explained by the solubilised dodecane in TTAB micelles occupying the surfactant tail region whereas it may create a separate oil core in $C_{12}E_5$ aggregates.

7.5 Conclusions

Although the results obtained and discussed in this chapter are preliminary and require further work, they indicate some interesting avenues for investigation in the future. The headspace analysis technique seems to give better results for some systems than for others but a more thorough study of the numerous aspects of headspace analysis should solve many of the initial problems.

1. The value of $\Delta\gamma$ for linalool on CTAB solutions decreases as the temperature is increased. This is in contrast to the temperature dependence observed for alkane adsorption on ionic surfactants.

2. Attempts to determine activities in binary liquid mixtures containing alkanes or perfume oils using GC headspace analysis showed the measurements to be irreproducible. Further work is needed to optimise the method, particularly with regard to the equilibration of the liquid and vapour phases.

3. Preliminary GC headspace results for solubilisation isotherms showed greater reproducibility. Solubilisation and adsorption isotherms could be compared directly.

7.6 References

[1] Chapter 1 in "Applied Headspace Gas Chromatography", Ed. B. Kolb, Heydon & Son, Bristol, 1980.

[2] A. J. Ashworth and D. H. Everett, Faraday Society Trans., **56**, 1609, 1960.

[3] G. A. Smith, S. D. Christian, E. A. Tucker and J. F. Scamehorn, J. Colloid Interface Sci., **130**, 254, 1989.

[4] E. B. Abuin, E. Valenzuela and E. A. Lissi, J. Colloid Interface Sci., **101**, 401, 1984.

[5] J. N. Labows, J. Amer. Oil Chem. Soc., **69**, 34, 1992.

[6] F. Gadelle, W. J. Koros and R. S. Schecter, J. Colloid Interface Sci., **170**, 57, 1995.

Overall conclusions of the thesis

Overall Conclusions of the thesis

This thesis was concerned with the study of the interactions of oils with surfactants. Many of the objectives initially described in the aims of the thesis have been resolved. The main conclusions of the work are listed below.

1. Very little was known about the perfume oils which have been studied in this thesis so it was initially necessary to obtain information about their polarity and adsorption at interfaces. It was found, by measuring the work of adhesion of the perfume oils with various polar phases, that the three perfume oils studied (linalool, eugenol and cineole) showed liquid adhesion properties which are fairly typical of moderately polar oils. When the work of adhesion is broken down into enthalpy and entropy contributions, the enthalpy of adhesion for linalool with water is consistent with typical values for the enthalpy of hydration of the hydroxyl group when the surface area occupied per linalool molecule is taken into account.

2. It was found that linalool and eugenol show reasonably high surface activity at the heptane-water interface. This finding becomes important when the perfume oils

are incorporated into systems containing conventional surfactants. This result shows that in such systems, the perfume oils may act as co-surfactants. This work also concluded that linalool (but not eugenol) partitions to a significant extent into water from heptane.

3. There was very little information in the literature concerning the addition of these perfume oils to surfactant + water + alkane oil microemulsion systems. It was concluded in this thesis that all three of the perfume oils studied reduce the phase inversion temperature of microemulsion systems containing non-ionic surfactants (C_8E_5 and C_8E_3) and alkane oils. As the concentration of perfume oil contained within the oil phase is increased, the phase inversion temperature of the system is further reduced, suggesting that the perfume oils penetrate and swell the tailgroups of the surfactant to a greater extent than the alkane oil.

4. When the phase behaviour of these perfume oil containing microemulsions were studied, it was seen that linalool reduces the size of the three phase region observed for a water + octane + C_8E_5 microemulsion system, reduces its extent on the temperature scale and reduces $\bar{\gamma}$ (see figure 4.5 for an explanation of the symbols used). The addition of perfume oil to the system also increased the critical aggregation concentration in a manner which is consistent with the

approach to a tri-critical point. However, the tri-critical point for this system was never reached as it lies at a temperature below 0°C.

5. From the work carried out concerning the adsorption of oils onto planar surfactant monolayers, it was concluded that the surface tension changes associated with the addition of an oil lens to the surface of a surfactant solution of non-ionic surfactant can be measured reliably as long as proper allowance is made for the partitioning of surfactant into the added oil.

6. When the transition from spreading to non-spreading alkane oils on surfactant solutions above the cmc was studied with respect to alkane chain length, it was found that the transition occurs at different chain lengths depending on the surfactant used.

7. It was found that the equilibrium spreading coefficients for all systems investigated are all roughly zero. This is true for systems which have been judged both spreading and non-spreading.

8. The total alkane adsorption increases with decreasing alkane chain length for all surfactants. The adsorption isotherms show slightly more curvature for the shorter

alkanes signifying that the adsorption becomes more favourable as more alkane is added to the mixed surfactant/alkane film.

9. The adsorption isotherms for oils which are judged to spread on the surfactant solution when visually studied, yield information about the amount of 'surface perturbed' oil associated with the oil-water interface region.

10. The adsorption of the alkanes onto the non-ionic surfactant monolayers studied fit the Aranovich adsortion isotherms, yielding a_m and d values which both decrease with increasing alkane chain length.

11. The study of the alkane oils adsorption to the oil-water interface yielded significant adsorption of the diluting oils (squalane and DNP) in contrast to their lack of adsorption at the air-water interface. Therefore, only relative adsorption of mixed oils can be determined at the oil-water interface.

12. The adsorption isotherms of dodecane on non-ionic and ionic surfactants show an opposite temperature dependence. Van't Hoff plots derived from the temperature dependent isotherms show that the enthalpies associated with the temperature dependence may have contributions from changes in the surfactant chain density

together with packing densities of the surfactant headgrous. The exposure of the adsorbed oil to air above the surfactant monolayer, which has been shown to be the case for dodecane on ionic surfactants, may also contribute to the enthalpy of adsorption.

13. The adsorption of pure linalool to an ionic surfactant (CTAB 2mM, 2x cmc) gives an opposite temperature dependence of surface pressure to that of alkane oil adsorption.

14. Attempts to determine activities in binary liquid mixtures containing alkanes or perfume oils using GC headspace analysis showed the measurements to be irreproducible. A possible avenue of future work would be to optimise the headspace analyser for this field of study, particularly with regard to the equilibration of the liquid and vapour phases.

15. The preliminary GC headspace results for solubilisation isotherms showed greater reproducibility, allowing a direct comparison between solubilisation and adsorption isotherms.

Appendices

Appendix 1

Polynomial fits to data

Table i.i **Polynomial equations used to fit the data of $\Delta\gamma$ versus adsorbing mole fraction activity (a) for various oils on various surfactants.**

surfactant	oil chain length	fitting equation
$C_{12}E_7$	8	$\Delta\gamma = 7.8971a^3 - 1.5402a^2 + 1.0535a + 2.9931$
	16	$\Delta\gamma = 1.3134a^2 + 0.8407a + 2.1052$
$C_{12}E_5$	8	$\Delta\gamma = 0.221a^3 + 0.813a^2 + 6.414a + 0.087$
	10	$\Delta\gamma = -4.437a^3 + 8.614a^2 + 2.013a + 0.0635$
	12	$\Delta\gamma = -3.492a^3 + 5.891a^2 + 2.675a + 0.0531$
	14	$\Delta\gamma = -4.063a^3 + 5.822a^2 + 1.312a + 0.104$
	16	$\Delta\gamma = -0.978a^2 + 3.354a + 0.027$
$C_{10}E_7$	8	$\Delta\gamma = 2.995a^3 - 1.321a^2 + 7.866a - 0.0152$
	10	$\Delta\gamma = 2.861a^2 + 4.418a + 0.0003$
	12	$\Delta\gamma = 0.895a^2 + 4.964a - 0.079$
	14	$\Delta\gamma = 0.0291a^2 + 3.327a - 0.064$

Table i.ii **Polynomial equations used to fit the data of $\Delta\gamma$ versus adsorbing mole fraction activity (a) for dodecane on $C_{12}E_5$ and DoTAB.**

surfactant	temperature	fitting equation
$C_{12}E_5$	10	$\Delta\gamma = 0.194a^2 + 5.469a - 0.0678$
	17	$\Delta\gamma = 0.178a^2 + 5.361a - 0.0113$
	25	$\Delta\gamma = 0.415a^2 + 4.967a - 0.145$
	31	$\Delta\gamma = -0.793a^2 + 5.784a - 0.0721$
DoTAB	10	$\Delta\gamma = -0.418a^2 + 4.523a + 0.0591$
	17	$\Delta\gamma = -0.597a^2 + 5.082a - 0.0876$
	25	$\Delta\gamma = -0.0656a^2 + 4.528a - 0.0519$
	35	$\Delta\gamma = 0.082a^2 + 4.534a - 0.0519$

Table i.iii **Polynomial equations used to fit the data of Γ (surface concentration) versus adsorbing mole fraction activity (a) for dodecane on $C_{12}E_5$ and DoTAB.**

surfactant	temperature	fitting equation
$C_{12}E_5$	10	$\Gamma = 0.0995a^2 + 1.4001a$
	17	$\Gamma = 0.0889a^2 + 1.339a$
	25	$\Gamma = 0.2017a^2 + 1.207a$
	31	$\Gamma = -0.378a^2 + 1.378a$
DoTAB	10	$\Gamma = -0.214a^2 + 1.157a$
	17	$\Gamma = -0.298a^2 + 1.269a$
	25	$\Gamma = -0.0318a^2 + 1.1a$
	35	$\Gamma = 0.0387a^2 + 1.066a$

Appendix 2

Data tables

Table ii.i **Work of adhesion and interfacial tension for various oils with glycerol and water.**

polar phase	oil	Interfacial tension ($mN\ m^{-1}$)	Work of adhesion ($mJ\ m^{-2}$)
water	dodecane	52.5	44.4
	toluene	36.0	65.0
	methyl myristate	24.0	76.7
	cineole	16.9	82.9
	linalool	11.3	87.5
	decanol	9.2	90.5
	eugenol	9.0	99.1
glycerol	dodecane	29.0	57.8
	chloro-octane	23.3	66.6
	methyl myristate	21.0	69.0
	toluene	20.0	70.9
	decanol	5.2	84.8

Table ii.ii **Work of adhesion and interfacial tension for various polar phases with dodecane and toluene.**

oil	polar phase	Interfacial tension ($mN\ m^{-1}$)	Work of adhesion ($mJ\ m^{-2}$)
dodecane	dimethyl formamide	4.3	57.1
	n-methyl formamide	10.0	54.3
	dimethyl sulfoxide	11.2	56.7
	ethylene diol	18.6	55.6
	formamide	28.1	55.0
	glycerol	29.0	57.8
	water	52.5	44.4
toluene	ethylene diol	8.8	66.5
	formamide	14.2	72.0
	glycerol	20.1	70.9
	water	36.0	65.0

Table ii.iii **Interfacial tensions of heptane with water at various oil/water volume ratios containingconstant initial concentrations of eugenol and linalool in the oil phase.**

oil	oil/water volume ratios	Interfacial tension (mN m^{-1})
linalool	0.5	45.25
	1	44.11
	5	42.36
	10	42.11
	20	42.23
eugenol	1	45.89
	5	45.85
	10	45.63
	20	45.84

Table ii.iv **Interfacial tensions of heptane with water with various concentrations of linalool in the oil phase at two different oil/water volume ratios.**

oil/water volume ratio	ln [linalool/M]	Interfacial tension ($mN\ m^{-1}$)
20:1	-3.91	34.88
	-4.60	38.11
	-5.30	42.11
	-5.52	42.97
	-6.21	44.99
	-6.91	46.29
	-7.13	46.79
	-8.11	48.56
	-9.21	49.48
	-9.90	49.72
	-10.82	50.10
1:1	-3.91	38.09
	-4.60	41.67
	-5.30	44.54
	-5.52	45.58
	-6.91	48.60
	-8.11	49.73
	-9.21	49.87
	-9.90	50.30
	-10.82	50.35

Table ii.v **Interfacial tensions of heptane with water with various concentrations of eugenol in the oil phase.**

ln [eugenol/M]	Interfacial tension ($mN\ m^{-1}$)
-3.91	37.90
-4.60	42.10
-5.30	45.53
-5.52	46.00
-6.21	47.41
-6.91	48.91
-7.13	49.08
-7.60	49.47
-8.11	49.50
-8.52	49.52
-9.21	49.70

Table ii.vi **Surface tension of a $C_{12}E_7$ solution at various aqueous concentrations of $C_{12}E_7$ in the absence of oil, with the addition of pure dodecane oil and with the addition of dodecane containing 0.15 wt% $C_{12}E_7$.**

$\ln [C_{12}E_7/M]_{aq}$	Surface tension ($mN\ m^{-1}$)		
	with no dodecane	with pure dodecane	with dodecane containing 0.15 wt% $C_{12}E_7$
-4.0	32.5	26.7	25.7
-4.9	32.5	27.0	25.6
-5.6	32.7		25.9
-7.2	32.9	28.2	26.0
-8.5	33.4		26.5
-9.5	33.7	33.1	

Table ii.vii **Surface tension reduction of surfactant solutions upon the addition of pure alkane oils of different chain lengths.**

	Surface tension reduction ($\Delta\gamma$) (mN m^{-1})			
oil chain length	$C_{12}E_5$	$C_{12}E_7$	DoTAB	Sodium dodecyl sulphate
8	7.58	10.48		
9				
10	6.31	7.91	7.2	6.8
11			6.2	5.9
12	5.15	6.25	5.4	4.5
13			4.3	3.9
14	3.18	4.94	3.5	2.9
15			2.7	
16	2.35		2.3	2.1

Table ii.viii **Surface tension reduction of surfactant solutions upon the addition of pure alkane oils of different chain lengths.**

	Surface tension reduction ($\Delta\gamma$) (mN m^{-1})			
oil chain length	$C_{10}E_7$	$C_{12}E_7$	DTAB	DoTAB
8	9.57	10.48		
9				
10	7.22	7.91	5.9	7.2
11			4.9	6.2
12	5.67	6.25	3.8	5.4
13			2.9	4.3
14	3.21	4.94	2.2	3.5
15			1.6	2.7
16			1.2	2.3

Table ii.ix **Surface tension reduction of $C_{12}E_7$ surfactant solution upon the addition of alkane oils of different activities diluted by squalane.**

oil	activity	Surface tension reduction ($mN\ m^{-1}$)
octane	0	2.1
	0.38	3.6
	0.73	6.0
	0.84	7.5
	0.92	9.0
	0.96	9.6
	1	10.4
hexadecane	0	2.1
	0.29	2.5
	0.45	2.7
	0.63	3.2
	0.94	4.0
	1	4.3

Table ii.x **Surface tension reduction of $C_{12}E_5$ surfactant solution upon the addition of alkane oils of different activities by Vapour adsorption train.**

oil	activity	Surface tension reduction ($mN\ m^{-1}$)
octane	0	0
	0.18	1.25
	0.27	1.88
	0.36	2.59
	0.47	3.27
	0.55	3.94
	0.74	5.4
	0.842	6.14
	0.912	6.73
	1	7.58
decane	0	0
	0.196	0.75
	0.256	0.9
	0.321	1.49
	0.409	2.08
	0.527	2.98
	0.643	3.79
	0.714	4.23
	0.786	4.71
	0.93	5.79
	1	6.31
dodecane	0	0
	0.15	0.52
	0.23	0.84
	0.36	1.68
	0.427	2.04
	0.518	2.62
	0.697	3.51
	0.8	4.15
	0.9	4.69
	1	5.15

Table ii.xi **Surface tension reduction of $C_{10}E_7$ surfactant solution upon the addition of alkane oils of different activities by vapour adsorption train.**

oil	activity	Surface tension reduction ($mN\ m^{-1}$)
octane	0	0
	0.246	1.82
	0.318	2.47
	0.45	3.56
	0.543	4.32
	0.625	5.16
	0.693	5.85
	0.822	7.14
	0.912	8.3
	1	9.57
decane	0.229	1.25
	0.326	1.71
	0.406	2.13
	0.519	3.07
	0.65	4.15
	0.75	4.95
	0.91	6.41
	0.95	6.8
	1	7.22
dodecane	0	0
	0.279	1.28
	0.354	1.69
	0.5	2.58
	0.601	3.29
	0.703	3.96
	0.807	4.6
	0.867	4.92
	0.948	5.42
	1	5.67

Table ii.xii **Interfacial oil-water tension versus activity of dodecane in the oil phase diluted by squalane and DNP. Aqueous phase contains $C_{12}E_5$ (6.4 mM)**

diluent oil	activity of dodecane	Interfacial tension ($mN\ m^{-1}$)
squalane	0	1.10
	0.25	1.00
	0.5	0.85
	0.75	0.68
	1	0.40
DNP	0	0.71
	0.25	0.60
	0.5	0.50
	0.75	0.45
	1	0.40

Table ii.xiii **Interfacial oil-water tension versus activity of octane in the oil phase diluted by squalane and DNP. Aqueous phase contains $C_{10}E_7$ (9.5 mM)**

diluent oil	activity of octane	Interfacial tension ($mN\ m^{-1}$)
squalane	0	3.20
	0.25	3.00
	0.50	2.70
	0.85	2.40
	1	2.15
DNP	0	1.30
	0.25	1.50
	0.5	1.80
	0.85	2.00
	1	2.15

Table ii.xiv **Tension lowering following oil addition at various dodecane activities onto 6.4mM $C_{12}E_5$ at different temperatures.**

activity	10°C	activity	17°C	activity	25°C	activity	31°C
0	0	0	0	0	0	0	0
0.363	1.83	0.25	1.1	0.15	0.52	0.255	1.15
0.43	2.22	0.35	1.65	0.23	0.84	0.315	1.71
0.518	2.66	0.475	2.45	0.36	1.68	0.387	2.12
0.585	3.34	0.6	3.25	0.427	2.04	0.5	2.57
0.658	3.77	0.71	3.91	0.518	2.62	0.652	3.35
0.8	4.52	0.85	4.71	0.568	2.89	0.743	3.9
0.847	4.77	0.95	5.11	0.697	3.51	0.889	4.52
0.9	5.02	1	5.29	0.8	4.15	0.951	4.69
0.94	5.21			0.9	4.69	1	4.83
1	5.48			1	5.15		

Table ii.xv **Tension lowering following oil addition at various dodecane activities onto 30mM DoTAB at different temperatures.**

activity	10°C	activity	17°C	activity	25°C	activity	35°C
0	0	0	0	0	0	0	0
0.37	1.73	0.215	0.68	0.17	0.68	0.249	0.98
0.40	2.0	0.325	1.65	0.23	0.98	0.318	1.38
0.55	2.4	0.451	2.18	0.29	1.28	0.408	1.84
0.611	2.56	0.565	2.62	0.347	1.57	0.5	2.25
0.67	2.81	0.643	2.88	0.419	1.88	0.569	2.51
0.74	3.15	0.718	3.26	0.542	2.38	0.668	3.06
0.82	3.41	0.857	3.81	0.697	3.04	0.751	3.44
0.91	3.9	0.935	4.14	0.801	3.61	0.836	3.85
0.95	4	1	4.4	0.915	4.09	0.93	4.21
1	4.2			1	4.38	1	4.52